NTNU
Norwegian University of Science and Technology
Department of Marine Technology

M.Sc.THESIS

Title:	**Delivered:**
DYNAMIC RESPONSE ANALYSIS OF A TENSION-LEG FLOATING WIND TURBINE	21.06.2011
	Availability: Open
Student: Jon Erik Lønøy Lygren	**Number of pages:** 175

Abstract:

Offshore wind energy has a significant potential and for increasing water depths it may be most cost effective to exploit this potential by using floating wind turbines. Many concepts have been suggested but it is not yet possible to decide which type of concept is the best. This report investigates a tension-leg platform (TLP) type of concept.

A computer model has been established and time domain simulations have been performed using the computer codes GeniE, HydroD (WADAM) and DeepC (SIMO, RIFLEX, TDHMILL3D). Wind and wave forces are included in the analysis and some theory on how these forces are calculated is given. How the computer model was established is also explained. The mooring system is modeled as a finite element model. The water depth is 200m.

TLPs have a stiff mooring system and high heave, roll and pitch natural frequencies. The second-order sum-frequency wave forces are calculated to see how sensitive the TLP considered is to these forces (springing). This is done using HydroD with a finite element model of the free surface. A simple sensitivity study is performed to investigate how small the element size and how large the radius of the free surface have to be in order to give reliable results. The effect of including the sum-frequency forces in the time domain simulations is seen to be small and the rest of the simulations are performed with only first-order and slowly varying forces included.

The effect of having a control system designed to prevent negative damping contributions from the wind turbine at wind speeds above rated is also investigated. Without the control system (simple notch filter) activated, the pitch response of the TLP is actually unstable due to a large negative damping contribution when the wind speed is close to rated. For wind speeds not very close to the rated speed the unstable behavior is not a problem, and the effect of having the filter is smaller.

The effect of reducing the water depth from 200 m to 120 m is investigated. The TLP performs better at the reduced water depth.

The TLP is also compared with a spar buoy and a semi-submersible concept designed to support the same 5.2 MW wind turbine as the TLP. The TLP has the smallest dynamic heave, roll and pitch motions. The semi-sub has the smallest nacelle accelerations and the spar seems to have the best mooring line characteristics. The comparison given in this study is not extensive enough to decide on which concept is the best. More work is needed in the future.

Keyword:

Floating wind turbine

TLP

Advisor:

Professor Torgeir Moan

Address:
NTNU
Department of Marine Technology
N-7491 Trondheim

Location
Marinteknisk Senter
O. Nielsens vei 10

Tel. +47 73 595501
Fax +47 73 595697

MSC THESIS IN MARINE TECHNOLOGY

SPRING 2011

FOR

STUD.TECHN. Jon Erik Lønøy Lygren

DYNAMIC RESPONSE ANALYSIS OF A TENSION-LEG FLOATING WIND TURBINE
(Dynamisk responsanalyse av en flytende strekk-stag vindturbin)

Background

There is a significant potential for offshore wind energy. In deeper water it may be most cost effective to exploit this potential by using floating wind turbines. Various floating wind turbine concepts have been suggested. However it is currently not possible to demonstrate which is the best concept. Moreover the relevant concept would depend upon the water depth and environmental conditions.

The purpose of this project work is therefore to contribute information about a specific concept and contribute to a comparative study made by fellow M.Sc. candidates in order to shed light on the relative performance of various floating wind turbine concepts.

Project tasks

The aim of this project is generally to establish a dynamic model of a wind turbine for assessing the energy production and responses relevant for assessing the structural integrity of the turbine.

1. **Introductory literature study of wind turbines**
   Review relevant literature including methods to determine the response of the wind turbine subjected to wind and wave loads; including relevant second-order sum-or difference-frequency wave loads. The software system Simo/Riflex serves as basis for the analysis.

2. **Establishing the dynamic model and load model**
   A dynamic model involving buoyancy, mass, mooring system etc should be established based on a reference model.

   The mooring system may be modeled by Riflex and integrated in the Simo model for coupled mooring analysis. Alternatively simple springs may be used to model the mooring system.

   The wave and wind induced loads should be modelled. A dll version of Simo should be used to model the wind force as function of wind speed at the nacelle.

3. Validation or verification of the model

The natural frequencies of the relevant modes of the concept should be estimated and compared with those of the reference model. Possible discrepancies should be explained. If necessary, the model should be adjusted.

Other simple checks of the model based on idealized load cases should be carried out.

4. Case study

Based on some relevant operational and survival load cases analyses should be carried out.

Since these load cases should serve as basis for comparison of the three concepts the same cases should be considered and decided in a "project" meeting.

A sensitivity study should be performed to study e.g. the effect of statistical uncertainty inherent in the sampling of stochastic loads, water depth, and possible other parameters.

5. Conclude and recommend further work.

The work scope could be larger than anticipated. Subject to approval from the supervisor, topics may be deleted from the list above or reduced in extent.

In the thesis the candidate shall present his personal contribution to the resolution of problem within the scope of the thesis work.

Theories and conclusions should be based on mathematical derivations and/or logic reasoning identifying the various steps in the deduction.

The candidate should utilize the existing possibilities for obtaining relevant literature.

The thesis should be organized in a rational manner to give a clear exposition of results, assessments, and conclusions. The text should be brief and to the point, with a clear language. Telegraphic language should be avoided.

The thesis shall contain the following elements: A text defining the scope, preface, list of contents, summary, main body of thesis, conclusions with recommendations for further work, list of symbols and acronyms, reference and (optional) appendices. All figures, tables and equations shall be numerated.

The supervisor may require that the candidate, in an early stage of the work, present a written plan for the completion of the work. The plan should include a budget for the use of computer and laboratory resources that will be charged to the department. Overruns shall be reported to the supervisor.

The original contribution of the candidate and material taken from other sources shall be clearly defined. Work from other sources shall be properly referenced using an acknowledged referencing system.

The thesis shall be submitted in two copies:

- Signed by the candidate
- The text defining the scope included
- In bound volume(s)
- Drawings and/or computer prints which cannot be bound should be organized in a separate folder.

Prof. Torgeir Moan

Supervisor at NTNU

Dr.Bjørn Skaare

Supervisor at Statoil

Tor David Hanson

Supervisor at Statoil

In addition Dr. Zhen Gao and Dr. Madjid Karimirad serve as co-supervisors.

Deadline: June 21. 2011

Preface

This report constitutes the final work with my master thesis in marine hydrodynamics at the Norwegian University of Science and Technology (NTNU) in Trondheim. The work has been carried out in the spring of 2011 at the Statoil research center in Bergen.

The thesis investigates the dynamic behavior of a tension-leg wind turbine. Forces from wind and waves are included in the analysis and the main focus will be on the rigid body motions of the structure together with forces in the mooring system. Much effort is devoted to describing the theoretical basis of the analysis and how the computer model was established. Many different concepts for floating wind power exist, and this project is intended to contribute more information about the TLP concept. The results obtained will also be included in a comparative study with a spar buoy and a semi-submersible type of concept.

Many people have contributed to the work. Firstly I would like to thank my main supervisor at NTNU, Professor Torgeir Moan and my supervisors at Statoil, Tor David Hanson and Dr. Bjørn Skaare for their cooperation and contributions during the thesis work. I would also like to thank my co-supervisors Dr. Zhen Gao and Dr. Madjid Karimirad. Special thanks to Dr. Zhen Gao for his help with the analysis tools and discussions during the semester. Gratitude is also given to Finn Gunnar Nielsen at the Statoil research center in Bergen for his contributions.

Jon Erik Lygren

Bergen, June 21. 2011

Abstract

Offshore wind energy has a significant potential and for increasing water depths it may be most cost effective to exploit this potential by using floating wind turbines. Many concepts have been suggested but it is not yet possible to decide which type of concept is the best. This report investigates a tension-leg platform (TLP) type of concept.

A computer model has been established and time domain simulations have been performed using the computer codes GeniE, HydroD (WADAM) and DeepC (SIMO, RIFLEX, TDHMILL3D). Wind and wave forces are included in the analysis and some theory on how these forces are calculated is given. How the computer model was established is also explained. The mooring system is modeled as a finite element model. The water depth is 200m.

TLPs have a stiff mooring system and high heave, roll and pitch natural frequencies. The second-order sum-frequency wave forces are calculated to see how sensitive the TLP considered is to these forces (springing). This is done using HydroD with a finite element model of the free surface. A simple sensitivity study is performed to investigate how small the element size and how large the radius of the free surface have to be in order to give reliable results. The effect of including the sum-frequency forces in the time domain simulations is seen to be small and the rest of the simulations are performed with only first-order and slowly varying forces included.

The effect of having a control system designed to prevent negative damping contributions from the wind turbine at wind speeds above rated is also investigated. Without the control system (simple notch filter) activated, the pitch response of the TLP is actually unstable due to a large negative damping contribution when the wind speed is close to rated. For wind speeds not very close to the rated speed the unstable behavior is not a problem, and the effect of having the filter is smaller.

The effect of reducing the water depth from 200 m to 120 m is investigated. The TLP performs better at the reduced water depth.

The TLP is also compared with a spar buoy and a semi-submersible concept designed to support the same 5.2 MW wind turbine as the TLP. The TLP has the smallest dynamic heave, roll and pitch motions. The semi-sub has the smallest nacelle accelerations and the spar seems to have the best mooring line characteristics. The comparison given in this study is not extensive enough to decide on which concept is the best. More work is needed in the future.

List of contents

List of figures

List of tables

List of symbols

Symbol	Description
ρ	Mass density of seawater
ρ_a	Mass density of air
ω	Angular frequency
ω_d	Damped natural angular frequency
ω_o	Undamped natural angular frequency
λ	Damping ratio or wave length depending on use
∇	Displaced volume or del operator depending on use
δ	Logarithmic decrement
η_{2A}	Motion amplitude, sway direction
η_j	Motion in degree of freedom j
ϕ_j	Radiation potential
ϕ_D	Diffraction potential
ϕ_0	Incident wave potential
ϕ	Total velocity potential
$\phi^{(1)}\,(\phi_L)$	First-order (linear) velocity potential
$\phi^{(2)}\,(\phi_Q)$	Second-order (quadratic) velocity potential
ζ_A	Wave amplitude
A_{ij}	Added mass
B_{ij}	Damping
C_{jk}	Stiffness
F	Force
F_j	Complex amplitudes of the exiting forces and moments

T	Thrust force or time (period) depending on use
C_T	Thrust coefficient
C_{T0}	Thrust coefficient at the mean wind speed
g	Gravitational acceleration constant
Hs	Significant wave height
I	Mass moment or area moment of inertia depending on use
I_{CM}	Mass moment of inertia about the center of mass
$\mathbf{i}, \mathbf{j}, \mathbf{k}$	Unit vectors
$\mathbf{n}$	Normal vector
k	Wave number
l	Submerged length of the substructure
M	Mass of the entire structure
P	Pressure
ΔP	Change in pressure
r	Radius of the substructure
Re	Reynolds number
$R_{X, Y \text{ or } Z}$	Radius of gyration
T_0	Undamped natural period
T_d	Damped natural period
T_n	Period of cycle number n in decay test
x_n	Motion amplitude of cycle number n in decay test
Tp	Peak period
u, v, w	Velocity in x, y and z – direction.
U_{hub}	Mean wind speed at hub height
U_{rel}	Relative wind speed
U_{dyn}	Dynamic variation of the wind speed

U_w	Wind speed
K_{CT}	Slope of thrust coefficient, used to determine wind turbine damping
$\sigma_{\tilde{u}}$	Standard deviation of wind speed
I_{Turb}	Turbulence intensity
L_K	Integral length scale
$\dot{m}$	Mass flow rate
a	Axial induction factor or wave amplitude depending on use
ε	Perturbation coefficient
$H^{(2)}$	Second-order force transfer function
$b1, b2$	Linear and quadratic damping coefficient divided by mass
b_e	Equivalent linear damping coefficient
B_C	Critical damping
α_1	Mass proportional Rayleigh damping coefficient
α_2	Stiffness proportional Rayleigh damping coefficient
γ_1	Skewness
μ_3	Third central moment
γ_2'	Kurtosis
μ_4	Fourth central moment

List of acronyms and abbreviations

BM	Distance from the center of buoyancy to the metacenter
CB	Center of buoyancy
CM	Center of mass
DNS	Direct numerical simulation
FEM	Finite element method
GM	Metacentric height
KB	Distance from the center of buoyancy to the keel
KG	Distance from the center of gravity to the keel
LC0-X	Load case with wind and waves coming from 0 degrees
LC30-X	Load case with wind coming from 0 and waves coming from 30 degrees
LC90-X	Load case with wind coming from 0 and waves coming from 90 degrees
MIT	Massachusetts Institute of Technology
NREL	National Renewable Energy Laboratory
BEM	Blade Element Momentum theory
STD	Standard deviation
TLP	Tension leg platform
WADAM	Wave Analysis by Diffraction and Morison theory
WAMIT	Wave Analysis at MIT
SIMO	Simulation of Marine Operations
DNV	Det Norske Veritas
JONSWAP	Joint North Sea Wave Project
DLL	Dynamic Linked Library

1. Introduction

1.1 Motivation

As the demand for energy is increasing and focus is shifted towards non-polluting renewable energy sources, wind energy has emerged as a good alternative. Wind energy has been utilized for power production for decades and for agricultural purposes for centuries. Offshore wind energy has a large potential in terms of space, larger average wind speeds and less turbulence than onshore. Currently, most offshore wind turbines use bottom fixed substructures, which limits them to shallow water depths. For larger water depths floating wind turbines might be the most cost effective solution Floating wind turbines is a new technology and it is not yet possible to decide which type of concept is the best. Land based turbines on the other hand are a proven technology but have met a lot of resistance because of their aesthetics and impact on nature. Offshore wind turbines do not have the same problem, but reducing the costs to a reasonable level is a challenge. Important for the future success of floating offshore wind turbines is the development of a reliable and viable substructure that can support the wind turbine and its tower. The tension leg platform or TLP is one of the concepts that have been proposed.

1.2 TLP concept

A tension leg platform is not a new type of concept. TLPs have been in use for offshore oil and gas production for decades and the first production TLP was the Conoco Hutton built early in the 1980s. A TLP is recognized by low natural periods in heave, roll and pitch due to a stiff mooring system. These natural periods will in most cases stay below the energetic wave period range. The TLP can therefore be seen as an opposite design philosophy compared with for example spar buoys and semi-submersibles. Large pretensions in the mooring system are obtained by the buoyancy of the structure. The volume of the submerged parts of the structure will therefore need to be quite large to ensure sufficient pretension. An important design parameter for a TLP is that the lines (tethers) remain taught at all time or at least that the consequence of slack lines is investigated.

The TLP considered was originally designed at the Massachusetts Institute of Technology (MIT). Modifications have later been performed by D. Matha [1] in order to overcome problems with the original design. The TLP is designed to support a 5.2 MW wind turbine. Matha used the time-domain simulation tool FAST with AeroDyn and HydroDyn to create a model of the TLP [1]. In this thesis work the same TLP will be considered but different computer programs will be used to establish the dynamic model. Excitation forces from waves and wind are included and the effect of having a turbine control system designed for floating wind turbines is investigated. The effect of including second-order sum frequency wave forces is also looked into. The TLP will be compared up against a spar buoy and a semi-submersible concept supporting the same 5.2 MW wind turbine.

2. Description of the TLP

The TLP consists of a mooring system, substructure and a tower with a wind turbine on top. The design water depth is 200 m but a shallower water depth of 120 m will also be considered. The mooring system consists of eight lines (tethers) mounted in pairs of two at the end of spokes mounted at the bottom of the substructure. The angle between the spokes is 90 degrees and the lines go straight down to attachment points on the sea floor. The stiff mooring system gives natural frequencies in heave, roll and pitch that most of the time is well outside of the energetic wave frequency range. The substructure is providing the buoyancy force needed to provide the required pretension. Concrete ballast is used at the bottom of the substructure to ensure stability in moderate sea states when the mooring system is not attached. This is important during installation (stable flout-out of the entire system is the chosen installation procedure). The concept is shown in figure 2.1.

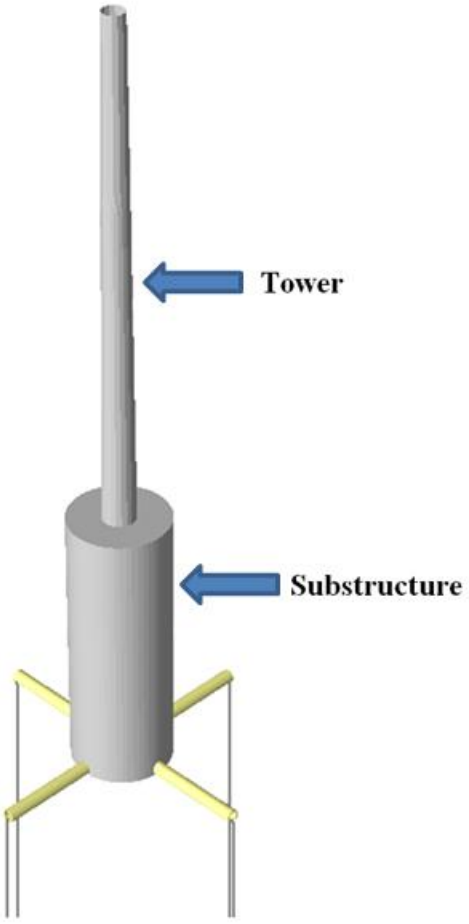

Figure 2.1: TLP concept

The global coordinate system has its origin in the still water level. The rigid-body translatory motions are referred to as surge, sway and heave and the angular motions are referred to as roll, pitch and yaw. The motions are shown in figure 2.2.

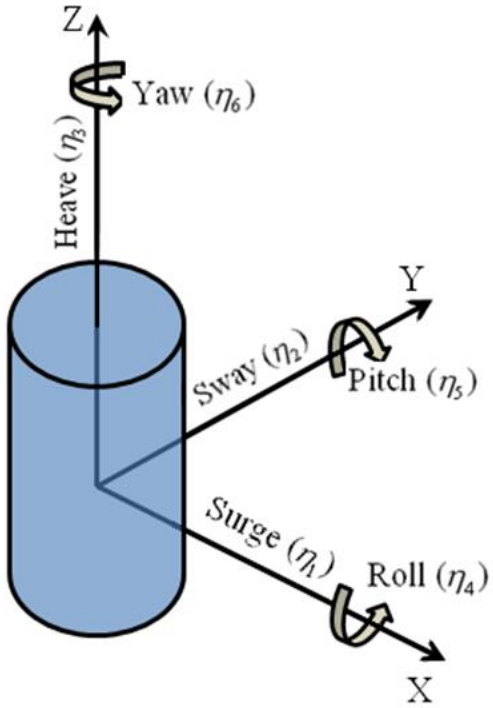

Figure 2.2: Translatory and angular motions

The main dimensions, mass data and mooring details are taken from Jonkman [2] and Matha [1] and are given in the following sections.

2.1 Wind turbine and tower

The wind turbine used is known as the "NREL offshore 5-MW baseline wind turbine." It is a three-bladed upwind turbine. The turbine has a cut-in wind speed of 3m/s which is the wind speed required to start power production. The maximum wind speed for power production is 25 m/s. This is the cut out wind speed and the blades are pitched to produce minimum lift and stops rotating. This is done in order to reduce the loads on the structure in extreme wind conditions. The rated wind speed is 11.4 m/s and at this speed the thrust force is at its maximum when the turbine is running. The power production and rotor speed is kept constant between rated and cut-out wind speed while the thrust force is decreasing in this interval. The thrust force and power curves are given in figure 2.4 and 2.3.

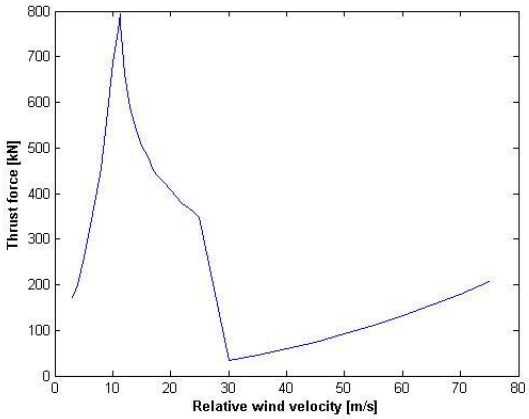

Figure 2.4: Thrust force curve

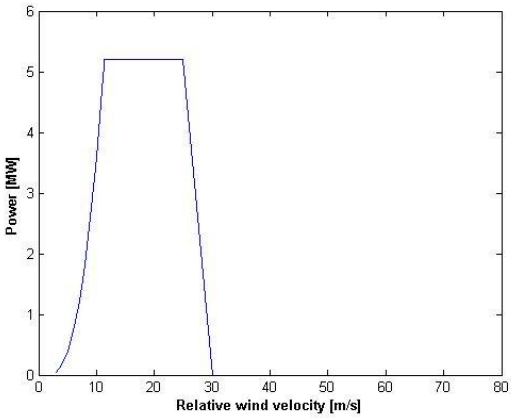

Figure 2.3: Power curve

Further details on the wind turbine can be found in Jonkman [3].

The rotor and nacelle specifications are given in table 2.1.

Hub height	90 m
Tower base diameter	6 m
Tower top diameter	3.87 m
Rotor radius	63 m
Center of mass (CM)	-0.134 m 0.0 m 64 m
Tower mass	110000 kg
Nacelle Mass	240000 kg
Rotor mass	347460kg
Mass moment of inertia about tower bottom, roll [19]	3642052000 kgm^2
Mass moment of inertia about tower bottom, pitch [19]	3628304000 kgm^2
Mass moment of inertia about tower bottom, yaw [19]	23808000 kgm^2
Rated power	5.2 MW
Rotor orientation	Upwind
Cut-in wind speed	3 m/s
Cut-in rotor speed	6.9 rpm
Rated wind speed	11.4 m/s
Rated rotor speed	12.1 rpm
Cut-out wind speed	25 m/s

Table 2.1: Tower, rotor and nacelle

2.2 Substructure

The substructure is made out of steel with concrete ballast. The main dimensions of the substructure are listed in table 2.2.

Radius	9 m
Draft	47.89 m
Ballast	8216000 kg
Total mass	8600000 kg
Center of buoyancy (CB) below still water level	23.95 m
Center of mass (CM) below still water level	40.61 m
Mass moment of inertia about CM, pitch and roll	571600000 kgm^2
Mass moment of inertia about CM, yaw	361400000 kgm^2
Displacement	12187 m^3

Table 2.2: Substructure

2.3 Mooring system

The eight lines (tethers) are mounted in pairs of two and the fairlead radius is 27 meters. The mooring system supplies most of the TLPs restoring forces.

Properties of the mooring system are given in table 2.3.

Unstretched mooring-line length	151.73 m
Line diameter	0.127 m
Line mass per unit length	116.03 kg/m
Line extensional stiffness	1500000000 N
Number of mooring lines	8
Radius to fairlead	27 m
Depth to fairleads	47.89 m
Static tension	3917kN

Table 2.3: Mooring system

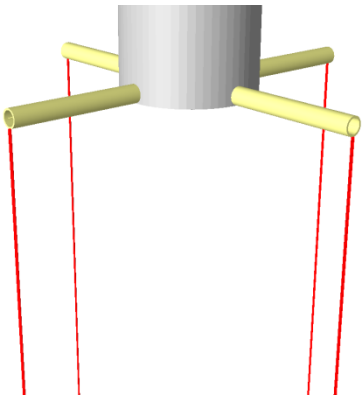

Figure 2.5: Mooring system

2.4 Entire structure

So far we have looked at the properties of each part of the TLP separately. The mass moments of inertia were defined about the tower bottom (XZ) and the center of mass of the substructure (CM_s). The parallel-axis theorem is used to calculate the mass moments of inertia of the entire structure about a coordinate system with origin in the total center of mass (CM_{total}). The coordinate system is shown in figure 2.6 and is noted X´Z´.

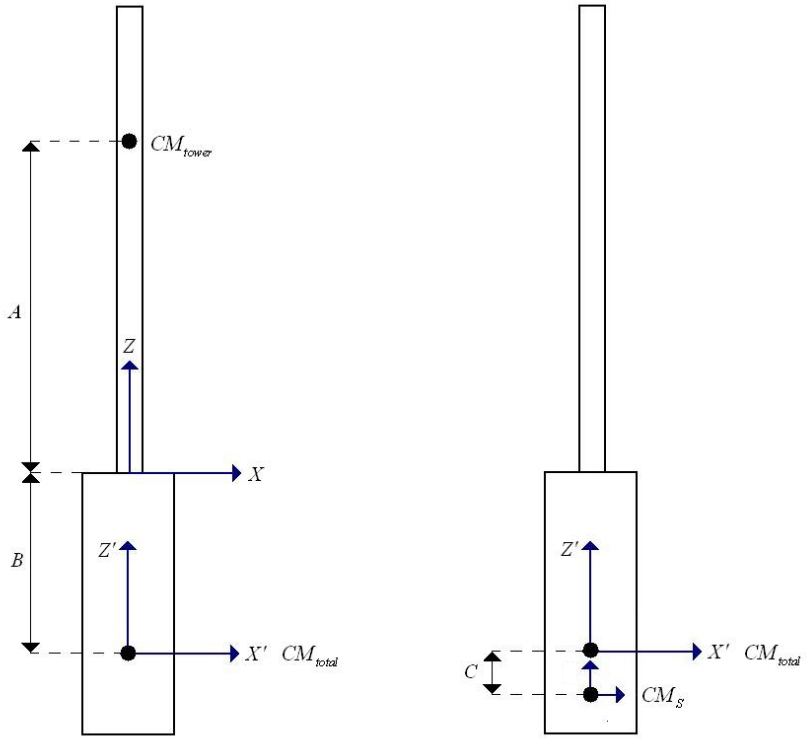

Figure 2.6: Center of mass of tower, substructure and entire structure

The distance B in the figure has been calculated to be 34.7 m and is the center of mass of the entire structure in a coordinate system with origin at the tower bottom. A in the figure is 64.21m and C is 8.02m.

The parallel-axis theorem relates the moment of inertia about an axis trough the center of mass to the moment of inertia about a second, parallel axis [4].

$$I = I_{cm} + Mh^2 \tag{2.1}$$

Here h is the distance between the center of mass of the part we are considering and the new axis we want to calculate the moment of inertia about (X´Z´).

When the mass moment of inertia is calculated, the radius of gyration can be obtained by taking the square root of the moment of inertia divided by the total mass of the TLP.

$$R_{X'} = \sqrt{\frac{I_{X'}}{M}},\ R_{Y'} = \sqrt{\frac{I_{Y'}}{M}},\ R_{Z'} = \sqrt{\frac{I_{Z'}}{M}} \tag{2.2}$$

The total mass, M, is 9297000 kg.

The mass moments of inertia and corresponding radius of gyration are given in table 2.4.

Ix´ [kgm^2]	8711445422
Iy´ [kgm^2]	8697696484
Iz´ [kgm^2]	385207062
R$_{X'}$ [m]	30.611
R$_{Y'}$ [m]	30.587
R$_{Z'}$ [m]	6.437

Table 2.4: Mass moment of inertia and radius of gyration

2.5 Stability without the mooring system installed

The center of mass of the TLP is located 32.59 m below the still water level and the center of buoyancy is located 23.95 m below the still water level. In other words, the center of mass is well below the center of buoyancy and this will make the TLP stable even without the mooring system installed.

To check the initial stability of the TLP without the mooring system installed, the metacentric height, the GM value, is calculated:

The area moment of inertia in the waterline is given by:

$$I = \frac{\pi \cdot r^4}{4} = \frac{\pi \cdot 9^4}{4} = 5153\ m^4 \tag{2.3}$$

Displaced volume of the submerged part of the substructure:

$$\nabla = \pi \cdot r^2 \cdot l = \pi \cdot 9^2 \cdot 47.89 = 12187\ m^3 \tag{2.4}$$

BM value:

$$BM = \frac{I}{\nabla} = \frac{5153 m^4}{12187 m^3} = 0.423\ m \tag{2.5}$$

Distance from the “keel” to the center of buoyancy, KB = 23.94 m.

Distance from the “keel” to the center of mass, KG = 15.3 m.

The GM value can then be calculated:

$$\mathrm{GM} = \mathrm{KB} + \mathrm{BM} - \mathrm{KG} = 23.94 + 0.423 - 15.3 = 9.1\ \mathrm{m} \tag{2.6}$$

As expected, the GM value is positive and the structure is stable. The TLP will therefore remain stable in moderate sea states even without the mooring system installed, and this was one of the

requirements MIT had to the original design. This makes it possible to assemble the entire structure in calm waters near land and then tow it out to the installation site. During installation the TLP thus resembles a spar buoy with its roll and pitch restoring forces supplied by a low center of gravity. When installed however, most of the restoring is supplied by the mooring system. The drawback of doing things this way is the large amount of concrete ballast needed in the bottom of the substructure (8216 tons). Without the concrete ballast the pretension in the mooring system could be increased, or the substructure could have been made smaller. Removing the ballast would require a different installation procedure. Perhaps it is possible to use water ballast instead and then remove some of it when the mooring system is installed. This will not be investigated further.

3. Potential theory

To describe the flow around the structure and calculate the forces, we will mainly rely on potential theory. This is a simplification of the "real" problem and we assume the fluid to be incompressible, irrotational and inviscid. This means that we don't get any effect from viscosity using potential theory. Viscous effect need to be calculated in other ways, for example by using Morison's equation. This chapter is taken from the report written in connection with the pre-studies for this thesis, J. Lygren [5].

One could of course use the full momentum equation (Navier-Stokes equations, DNS) to describe the fluid, but good methods for doing this accurately is difficult and require a lot of computer power. To illustrate this we can look at the ratio between the largest (integral) and smallest (Kolmogorov) turbulence scales in a turbulent flow. The ratio is Re^3/4, meaning that for a three dimensional problem the required grid number would be in the order of Re^9/4. For more details see H.Tennekes [6] and White [7]. For normal full scale Reynolds numbers, this is not practically possible with today's computer technology, and we need turbulence modeling to reduce the problem. We will not look into this, but use potential theory. It is expected that potential theory combined with adding viscous forces by using Morison's equation, will give satisfactory results for our problem.

We assume the water to be incompressible and inviscid, and that the fluid motion is irrotational. The fluid velocity vector can then be described by a velocity potential in the following way:

$$\mathbf{V} = \nabla\phi = \mathbf{i}\frac{\partial\phi}{\partial x} + \mathbf{j}\frac{\partial\phi}{\partial y} + \mathbf{k}\frac{\partial\phi}{\partial z} = \mathbf{i}u + \mathbf{j}v + \mathbf{k}w \tag{3.1}$$

When we know the velocity potential, we can use Bernoulli's equation to find the pressure. The pressure can then be integrated over the wetted surface up to the mean water level to find the forces. For a linear analysis, the second order terms in Bernoulli's equation are neglected and the pressure (dynamic pressure) can be obtained from:

$$P = -\rho\frac{\partial\phi}{\partial t} \tag{3.2}$$

The force is then:

$$F = -\iint_S P\mathbf{n}dS \tag{3.3}$$

The main issue is to find the total velocity potential. It will be the sum of the incoming wave potential, diffraction potential and the radiation potentials associated with the rigid body motions. We are considering an inelastic structure so there will be no radiation potentials associated with elastic modes.

The total velocity potential:

$$\phi = \phi_0 + \phi_D + \sum_{j=1}^{6}\phi_j \tag{3.4}$$

ϕ_0 is the incident wave potential:

$$\phi_0 = \frac{g\zeta_A \cosh(kh+hz)}{\omega \cosh(kh)} \sin(kx-\omega t) \tag{3.5}$$

Where k is the wave number, $k = \frac{2\pi}{\lambda}$.

The diffraction potential is the potential due to diffracted waves. To find this potential we need to solve a boundary value problem. The diffraction potential need to satisfy the following conditions:

- Laplace equation in the fluid:

$$\nabla^2 \phi = 0 \tag{3.6}$$

  This is the continuity equation.

- Free surface condition (linearized):

$$\frac{\partial^2 \phi}{\partial t^2} + g\frac{\partial \phi}{\partial z} = 0 \quad \text{on} \quad Z = 0 \tag{3.7}$$

  This condition is a combination of the dynamic and kinematic free surface condition. It means that the water pressure is equal to the atmospheric pressure on the free surface and that a fluid particle on the free surface stays on the free surface.

- Body boundary condition:

$$\frac{\partial \phi_D}{\partial n} = \frac{\partial \phi_0}{\partial n} \tag{3.8}$$

  Meaning no water flow through the hull. The structure is fixed with incoming waves.

- Condition on seabed:

$$\frac{\partial \phi_D}{\partial z} = 0 \tag{3.9}$$

  Meaning no water flow through the horizontal seabed.

- There is also a radiation requirement, meaning that waves radiates away from the body.

The incident wave potential and the diffraction potential is associated with the excitation forces, the Froude-Kriloff and diffraction forces (and moments) respectively. It is the forces on the structure when it is restrained from oscillating.

The radiation potentials for the six degrees of freedom are found solving a boundary value problem similar to that of the diffraction potential. The main difference is the body boundary condition. The structure is now forced to oscillate with the wave frequencies in still water. The water around the body is then set in motion, and this motion is assumed to be described by the radiation potential. For a harmonic oscillation in sway for instance, with amplitude η_{2A} .The body boundary condition is:

$$\frac{\partial \phi_2}{\partial n} = -\eta_{2A}\omega \sin(\omega t)\mathbf{j}\cdot\mathbf{n} \tag{3.10}$$

Where **n** is a normal vector pointing into the fluid.

Again, this means no water flow through the hull.

The fluid pressure caused by these forced motions can be integrated over the wet surface to give the added mass and damping loads:

$$F_i = -A_{ij}\frac{\partial^2 \eta_j}{\partial t^2} - B_{ij}\frac{\partial \eta_j}{\partial t} \tag{3.11}$$

"ij" meaning force in i-direction due to acceleration/velocity in j-direction.

The problem above is solved using the computer program WADAM (Wave Analysis by Diffraction and Morison Theory) by using a 3D panel model to evaluate the velocity potentials. The potential theory in WADAM is based on the WAMIT program developed by the Massachusetts Institute of Technology, MIT. The program uses plane quadrilateral panels and constant source strength over each panel. For more details, see the WAMIT user manual and Faltinsen [8].

Here we have considered the first-order velocity potential and how the first-order wave forces can be calculated. In order to calculate the second-order wave forces oscillating at the sum-frequency, the second order velocity potential has to be obtained. This will be discussed in section 7.

4. Wind theory

In addition to the wave forces, the wind thrust force is important when calculating the response of the TLP. In this section some theory about wind and calculation of the thrust force is given. The damping contribution from the wind turbine is also investigated.

The wind thrust forces are included in the analysis through the numerical thrust force model TDHMILL3D. A further description of TDHMILL3D is given in section 5.3.3.

4.1 Wind spectrum

The wind velocity $\tilde{u}$ can be split up into a mean and a fluctuating part:

$$\tilde{u} = U + u \tag{4.1}$$

Here u is the fluctuating part and U is the time-mean value or time average of $\tilde{u}$:

$$U = \frac{1}{T}\int_0^T \tilde{u}dt \tag{4.2}$$

T is the averaging time chosen to be larger than any significant period of the fluctuations, H. Tennekes [6]. By definition then the mean of the fluctuating part is zero.

The turbulence intensity is defined as the ratio between the standard deviation of the wind speed and the mean wind speed:

$$I_{Turb} = \frac{\sigma_{\tilde{u}}}{U} \tag{4.3}$$

The wind and how the wind turbulence is distributed between different frequencies can be expressed through a wind spectrum. According to [9], the Harris and Kaimal spectrum is commonly used. In TDHMILL3D the Kaimal model is used to generate the wind time series for different mean wind speeds and turbulence intensities.

The Kaimal wind spectrum is given as [10]:

$$S_K(f) = \frac{4\sigma_{\tilde{u}}^2 \frac{L_K}{U_{hub}}}{(1+\frac{6L_k f}{U_{hub}})^{5/3}} \tag{4.4}$$

Where

$\sigma_{\tilde{u}} = I_{Turb}(0.75U_{hub} + 5.6)$
$L_K = 8.1\lambda$

are the standard deviation and integral length scale.

U_{hub} is the mean wind velocity at hub height and λ is the spectral parameter.

The Kaimal wind spectrum for different mean wind speeds and turbulence intensities is given in figure 4.1 The spectral parameter used is 42.

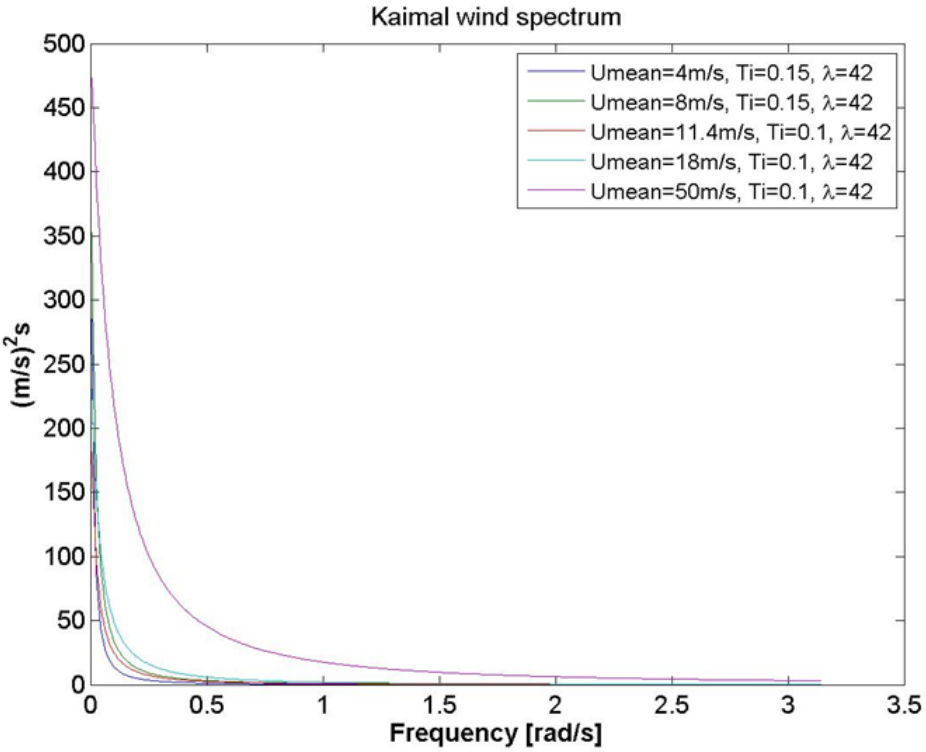

Figure 4.1: Kaimal wind spectra

4.2 Thrust force from 1-D momentum theory

To give some understanding about how the rotor thrust force can be calculated in a simple manner the 1-D momentum theory will be briefly discussed.

The simple 1-D model is shown in figure 4.2. The rotor is considered as an ideal, frictionless disc and the wake behind it is not rotating. The flow is incompressible, steady and inviscid. The pressure far downstream of the rotor is equal to the atmospheric pressure also found far upstream, P_0.

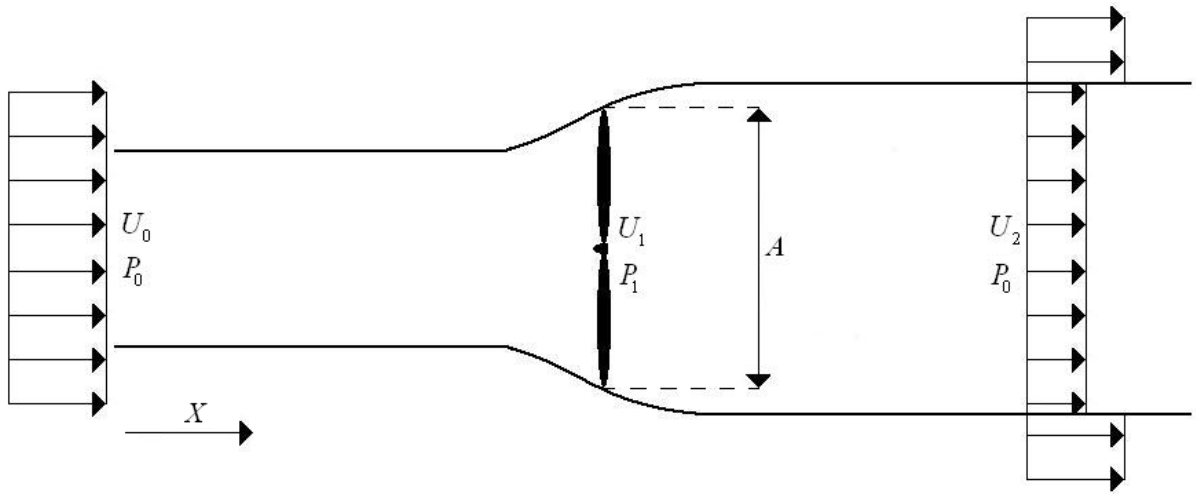

Figure 4.2: 1-D momentum model

There is a pressure drop over the rotor. Using Bernoulli's equation upstream and downstream of the rotor gives the following expression for the change in pressure:

$$\Delta P = \frac{1}{2}\rho_a (U_0^2 - U_2^1) \tag{4.5}$$

Where ρ_a is the mass density of air.

An expression for the thrust force is then obtained by multiplying the pressure drop with the swept rotor area.

$$T = \Delta P A \tag{4.6}$$

To determine the magnitude of the velocity behind the rotor, U_2, the momentum equation will be used together with the conservation of mass. The thrust force can be expressed as:

$$T = -\sum F_x = \dot{m}_0 U_0 - \dot{m}_2 U_2 \tag{4.7}$$

$\dot{m}_0$ and $\dot{m}_2$ is the mass flow rate at location 0 and 2 in the figure. The flow is steady and the conservation of mass then gives:

$$\dot{m}_0 = \dot{m}_2 = \dot{m}_1 = \rho_a U_1 A \tag{4.8}$$

The thrust force then becomes:

$$T = \rho_a U_1 A(U_0 - U_2) \tag{4.9}$$

If equation (4.9) is combined with equation (4.5) and (4.6), the following expression for the velocity at the rotor is obtained:

$$U_1 = \frac{1}{2}(U_0 + U_2) \tag{4.10}$$

The axial induction factor, a, is defined as the ratio of the reduction in fluid velocity between location 0 and 1 and the velocity at location 0:

$$U_1 = (1-a)U_0 \tag{4.11}$$

Inserting this into equation (4.10) gives:

$$U_2 = (1-2a)U_0 \tag{4.12}$$

Inserting equation (4.12) and (4.11) into (4.9) then gives us the final expression for the thrust force:

$$T = 2\rho_a U_0^2 Aa(1-a) = \frac{1}{2}\rho_a U_0^2 AC_T \tag{4.13}$$

Where C_T is defined as a thrust coefficient:

$$C_T = 4a(1-a) \tag{4.14}$$

According to experiments, the momentum theory and the assumptions of an ideal rotor is valid only for an axial induction factor less than 0.4, M. Hansen [11]. The reason for this is that for values of a exceeding this value, the free shear layer at the edge of the wake becomes unstable and starts to transport momentum into the wake.

The axial induction factor is large when the wind speed is low and the wake is broad. This also means that the thrust coefficient is large when the wind speed is low. Further details on this can be found in chapter 4 in [11].

The thrust coefficients used in TDHMILL3D are taken from the NREL report defining the wind turbine considered [3]. In this report the Blade element momentum (BEM) theory was applied to calculate the thrust (and power) coefficients. The computer program FAST/AeroDyn was used. The BEM method also takes into account local events taking place at the blades. The BEM theory will not be reviewed here. Further details on the topic can be found in [11].

4.3 Negative damping from the wind turbine

Floating wind turbines equipped with a control system designed for conventional land based turbines may for wind speeds above the rated speed experience large resonant motions. The wind forces may amplify the wave motions and this can be considered as a negative damping effect. Above the rated wind speed of 11,4m/s the power output is kept constant by controlling the blade pitch, see figure (4.4). From the corresponding thrust force curve in figure (4.3), we see that the thrust force decreases for wind speeds above rated. This can explain the negative damping effect. Consider a case with wind speed above rated. If the turbine is surging/pitching towards the wind, the relative wind speed will increase and the thrust force according to figure (4.3) will decrease, leading to a smaller force against the movement. If the turbine is moving away from the wind the opposite will happen.

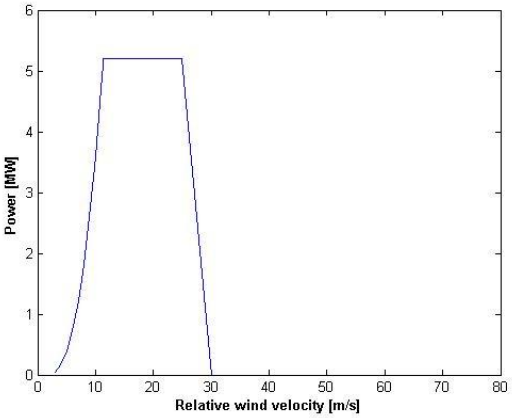

Figure 4.4: Power curve

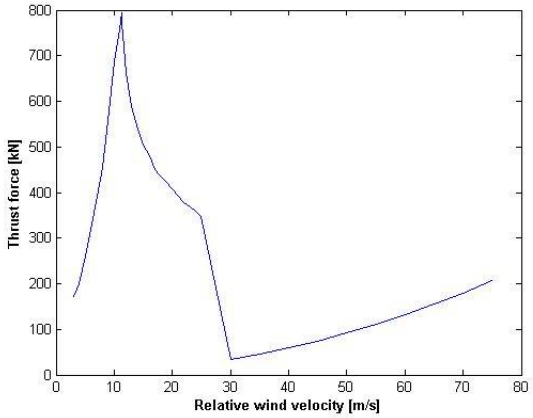

Figure 4.3: Thrust force curve

Especially for floating wind turbines of the spar/semi-sub type this is a problem because the pitch motions are large and the wind contains significant energy around the typical pitch natural frequencies. In section 9.2 it will be seen that this is also a problem for the TLP around the rated wind speed. For floating wind turbines it is therefore necessary to have a wind turbine control system designed to overcome this issue.

In the following a theoretical approach to show the negative damping effect will be given. The derivations are based on the design brief by F. G. Nielsen [12].

A non-constant thrust coefficient C_T is considered and is assumed to vary linearly with the relative wind velocity, U_{rel}. The thrust coefficient can be written:

$$C_T(U_{rel}) = C_{T0}(1 + k_{CT}\frac{U_{dyn}}{U_w}) \tag{4.15}$$

U_w is the mean wind speed, C_{T0} is the thrust coefficient at the mean wind speed, k_{CT} is the slope of the thrust coefficient and is assumed to be frequency independent and without phase shift. U_{dyn} is the dynamic variation of the wind speed:

$$U_{dyn} = U_{rel} - U_w \tag{4.16}$$

The thrust force then becomes:

$$T = \frac{1}{2}\rho_a U_{rel}^2 A C_{T0}(1 + k_{CT}\frac{U_{dyn}}{U_w}) \tag{4.17}$$

An expression for the linearized damping is then obtained by computing the dissipated energy over one cycle of oscillation. It is also assumed that the dynamic variations in the wind speed are much smaller than the mean wind speed [12].

$$Damping = \frac{1}{2}\rho_a U_w A C_{T0}(1 + \frac{k_{CT}}{2}) \tag{4.18}$$

According to the expression above we see that there will be a negative damping (excitation) contribution for values of k_{CT} less than -2.

To get an expression for k_{CT}, equation (4.17) is divided by U_{rel}^2 and differentiated with respect to U_{rel}:

$$\frac{d(\frac{T}{U_{rel}^2})}{dU_{rel}} = \frac{d}{dU_{rel}}\left(\frac{1}{2}\rho_a A C_{T0}(1 + k_{CT}\frac{U_{rel} - U_w}{U_w})\right) = \frac{1}{2}\rho_a A C_{T0}\frac{K_{CT}}{U_w} \tag{4.19}$$

We then solve for k_{CT}:

$$K_{CT} = \frac{2U_w}{\rho_a A C_{T0}}\frac{d(\frac{T}{U_{rel}^2})}{dU_{rel}} \tag{4.20}$$

The thrust coefficients of the wind turbine used on the TLP are known for different relative wind speeds. It is then straight forward to calculate k_{CT} for our wind-turbine. k_{CT} as a function of wind speed is plotted in figure 4.5.

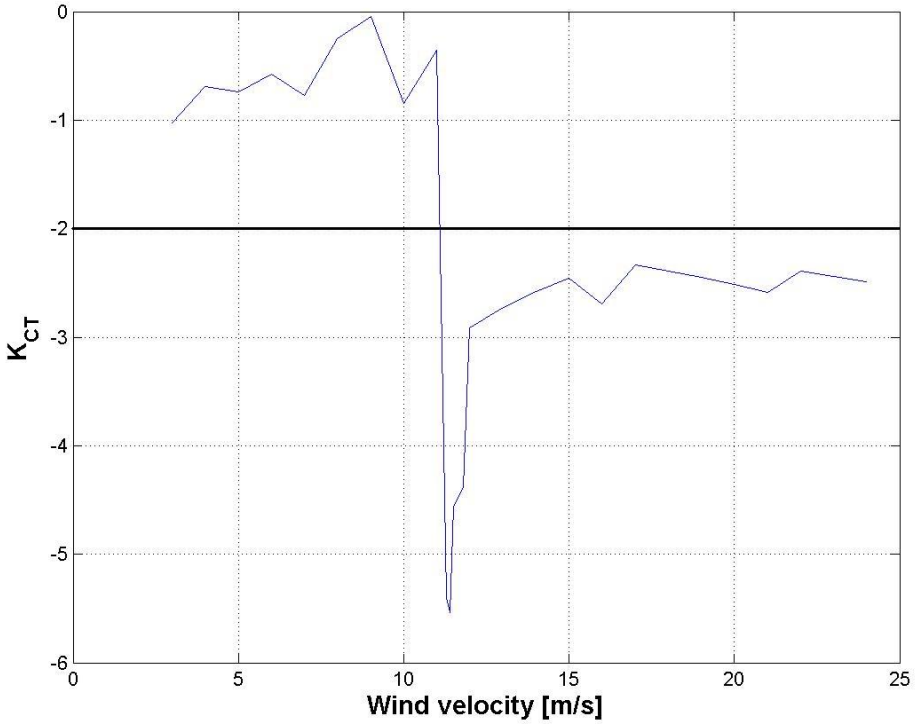

Figure 4.5: K_{CT} value

At wind speeds below rated (11.4 m/s), k_{CT} is larger than -2 and the damping contribution due to the wind turbine given in equation (4.18) is positive. Above rated wind speed the k_{CT} value is below -2 and especially at and close to the rated wind speed there is a large negative damping contribution. If this will result in a dynamic unstable system or not, depends on whether or not this damping contribution is the dominating contribution for the entire system including all the other damping contributions, see section 8. In section 9 it will be shown that the system is indeed dynamically unstable when exposed to the rated wind without the control system (notch filter) activated.

5. Computer modeling

The computer analysis is carried out using the user interfaces GeniE, HydroD and DeepC developed by Det Norske Veritas (DNV). In the following a short description of the different computer programs and how they were used will be given. The following chapter is based on the pre-studies for this master thesis, J. Lygren [5], where much of the work with establishing the computer model was done.

5.1 Panel model – GeniE

GeniE was used to make the panel model that is needed in the hydrodynamic calculations. After some sensitivity studies, an element size of 1 meter was chosen. This gave 3052 wet elements for the full structure. The spokes were modeled as Morison elements, and are needed as attachment points for the tension legs in HydroD. The panel model is exported into HydroD where the hydrodynamic calculations are performed. The GeniE model is shown in figure 5.1.

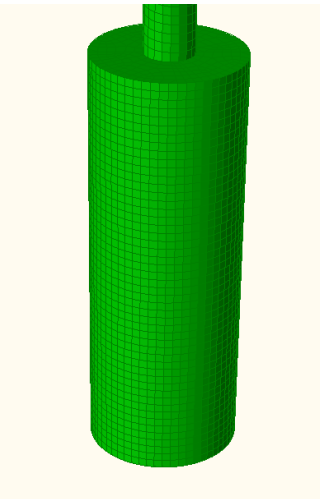

Figure 5.1: Panel model

More details about GeniE are given in the user manual [13].

5.2 Hydrodynamic calculations - HydroD

The WADAM module in HydroD is used. WADAM stands for "Wave analysis by diffraction and Morison theory)" and can use Morison and 3D potential theory in the wave load calculations. For the TLP we will only use potential theory part of the program (panel model). Drag forces on the spokes and substructure are added in DeepC. The WADAM calculations are performed in the frequency domain. At this stage only the first order wave forces are calculated. More details about the programs are given in the manuals [14] and [15].

The hydrodynamic model is a combination of a panel model and a Morison model that don't cover the same parts of the structure (substructure and spokes). This type of model is called a

“composite model”. As stated earlier, we will not use HydroD to calculate the forces on the spokes. The reason for this is that it is not recommended to include Morison forces in HydroD when we are going to use the results to perform a coupled line/vessel analysis in DeepC. The forces on the spokes will be calculated using DeepC. The Morison elements are needed in HydroD only as attachment points for the tension legs. To make sure that no forces are calculated on them, the drag and added mass coefficients is set equal to zero. It is not believed that the forces on the spokes will be significant since they are fairly slender and located about 48 meters below the free surface

From HydroD we are interested in the frequency dependent added mass and potential damping, the restoring forces (not including contributions from the mooring system) and the wave force transfer functions. We will not use the RAOs calculated by HydroD. The calculations of the first-order wave forces do not require an accurate mass distribution. The only requirement is that the submergence is correct. Calculations of second-order forces on the other hand, require that the mass distribution is correct. To achieve this, the tension legs are modeled with the correct stiffness and tension. The calculation of second-order sum-frequency wave forces also requires a finite element model of the free surface, and how to do this using HydroD/WADAM is discussed in section 7. The restoring forces from the tension-legs will not be transferred to DeepC.

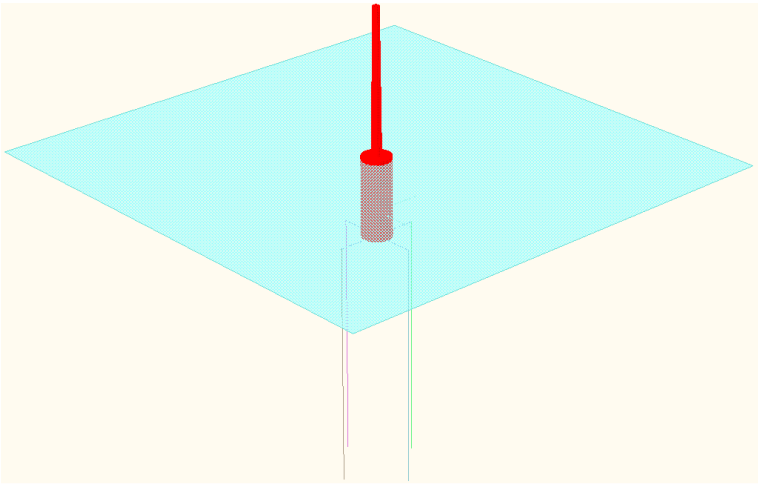

Figure 5.2: HydroD model

5.2.2 Drift forces

The slowly varying drift forces can be found based on the linear velocity potentials using Newman´s approximation. This is done by HydroD (WADAM). The high frequency (sum-frequency) wave loads however, require a nonlinear free surface model and cannot be calculated by this simplified approach. Further details are provided by Faltinsen [8].

The slowly varying forces are important for the surge and sway motions. The heave motions are also affected because of the coupling with surge and sway, the so called set-down effect caused by the tension legs.

5.3 Time domain simulations - DeepC

DeepC [16] is a modern graphical user interface which employs the MARINTEK developed programs SIMO and RIFLEX to perform time domain simulations. Input to DeepC is the frequency depended added mass and potential damping, restoring forces and excitation forces calculated in HydroD. The thrust force on the wind turbine is calculated using TDHMILL3D. TDHMILL3D is a DLL developed by MARINTEK and Statoil, and it communicates with SIMO.

The panel model generated in GeniE is used for graphical purposes; no new calculations are performed on the panel model. The DeepC model is shown in figure 5.3.

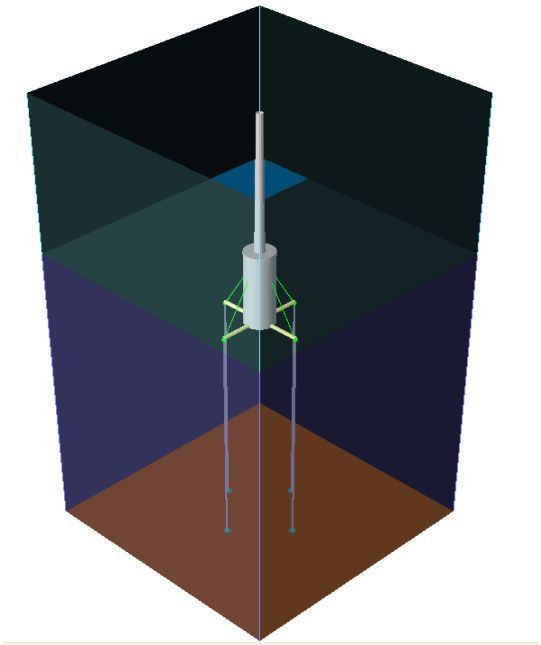

Figure 5.3: DeepC model

5.3.1 SIMO

SIMO – Simulation of Marine Operations is a time domain simulation program for multi body systems. SIMO models all structures as rigid, meaning that only the rigid body motions and no elastic modes are included. For the TLP this mean that we will get the motions in the six degrees of freedom; surge, sway, heave, roll, pitch and yaw. In that sense, the SIMO model can be looked upon as a point exposed to forces and moments from the mooring system (RIFLEX) and the environment (results from HydroD).

More details about the program can be found in the SIMO theory manual [17].

5.3.2 RIFLEX

RIFLEX is a nonlinear finite element method program for static and dynamic analysis of slender marine structures. RIFLEX is used to model the mooring system.

More details about the program can be found in the RIFLEX user manual [18] and theory manual [19].

5.3.3 TDHMILL3D

TDHMILL3D is used to calculate the wind thrust force on the wind turbine. Pre defined thrust coefficients for the wind turbine are included in the input files to the program. Wind time series are generated internally in the program by using the Kaimal wind spectrum as mentioned in section 4.1. By using the relative wind velocity at the nacelle, the thrust force is then calculated:

$$T(t) = \frac{1}{2}\pi\rho_a R^2 C_T(U_{rel})U_{rel}^2(t) \tag{5.1}$$

R is the rotor radius and C_T is the thrust coefficient given as a function of the relative wind speed. The translational and angular velocity at a time step is computed by SIMO before the thrust force to be used for advancing to the next time step is computed. These velocities are then transformed into the TDHMILL3D local coordinate system and the relative wind velocity at the nacelle is calculated.

The program also includes a notch filter that filters the motion induced velocities at the nacelle over a given frequency band. The purpose of this is to in a very simplistic way model a control system which strives to prevent the negative damping contributions from the wind turbine at wind speeds above rated. The negative damping contributions were explained in section 4.3. The effect of having the notch filter is examined in section 9.2 and 9.5.

Gyro moments are also introduced if the rotor is running and the rotor plane is altered when the structure moves. This is explained in the user manual [10].

TDHMILL3D is included in the analysis as a dynamic linked library (DLL) called by SIMO.

5.3.4 Brief description of the modeling in DeepC

The first thing that is done in DeepC is to define the location, meaning that parameters such as properties of the seabed, water depth, water density, kinematic viscosity and so on are specified. For the waves we use a 3 parameter JONSWAP spectrum. Peakness parameter, peak period and significant wave height is used to define the different sea states that we want to investigate. The mean wind velocity and turbulence intensity is specified in a separate TDHMLL3D input file.

The mooring system consists of eight lines mounted in pairs of two at the end of the spokes mounted at the bottom of the platform, see figure 5.3. The fairlead points are specified in DeepC and we add cylindrical sections (the spokes) between the fairlead points and the substructure. No information about the diameter of the spokes is available in the reports by Jonkman [2] and Matha [1]. A cross section with an outer radius of 1.2 m is therefore used. This cross section is chosen under the requirement that the maximum stress in the spokes need to be below the yielding stress of the material used (steel). A more refined analysis also including fatigue can be performed later, but it is not believed that this parameter will be very significant in terms of the global forces and motions. DeepC is used to calculate the forces on the spokes (Morison elements). Each 18 m long spoke is divided into 6 strips and wave forces are calculated based on the wave particle kinematics at the centre of each strip. Both drag and inertia forces are included and we use a quadratic drag coefficient of 0.7 in the transverse directions and 0.07 in the

longitudinal direction. The added mass is set to be equal to the weight of the displaced water in the transverse directions (cylinder) and one tenth of the displaced volume in the longitudinal direction.

The mooring lines (tension-leg tethers) are added between the fairleads and support points on the sea floor. The line characteristics are defined in accordance with table 2.3. The element length used is five meters. Wave kinematics is computed for the lines, and we use a drag coefficient of 0.7 in the transverse direction and 0.07 in the longitudinal direction of the lines.

We also include viscous forces (Morison elements, drag force) on the substructure. This is necessary since we only have calculated forces from potential theory in HydroD. We use drag coefficients of 0.7 and 0.07 in the transverse and longitudinal direction respectively.

In order to get the required pretension of 3917 kN in each of the mooring lines, we need to specify a constant force in the vertical direction. This force is equal to the buoyancy force minus the weight of the structure. The same technique of specifying a constant force is used later when decay tests are performed.

6. Hydrodynamic results

According to Faltinsen [8], the equations of rigid body motions for steady-state sinusoidal motions can be expressed as:

$$\sum_{k=1}^{6}\left[(M_{jk}+A_{jk})\ddot{\eta}_k+B_{jk}\dot{\eta}_k+C_{jk}\eta_k\right]=F_j e^{(-i\omega_0 t)}, \qquad (j=1, 2, 3, 4, 5, 6) \tag{6.1}$$

M_{jk} are the components of the mass matrix for the structure. It contains the structural mass and mass moment of inertia, see [8] for more details. A_{jk} are the components of the added mass matrix, B_{jk} are the components of the damping matrix and C_{jk} are the components of the restoring matrix. The restoring matrix can be split into a hydrostatic and a mooring part. The total restoring matrix is given as the sum of these parts. For a TLP the restoring effects due to hydrostatic effects are small in comparison with the restoring from the mooring system. F_j are the complex amplitudes of the exiting forces and moments. The force and moment components are given by the real part of $F_j e^{(-i\omega_0 t)}$.

In the following sections, the added mass, potential damping and excitation forces obtained from the hydrodynamic analysis will be presented.

6.1 Added mass

The frequency dependent added mass obtained from the HydroD (WADAM) analysis is shown in figure 6.1 and 6.2. There are a total of 36 coefficients in a full added mass matrix.

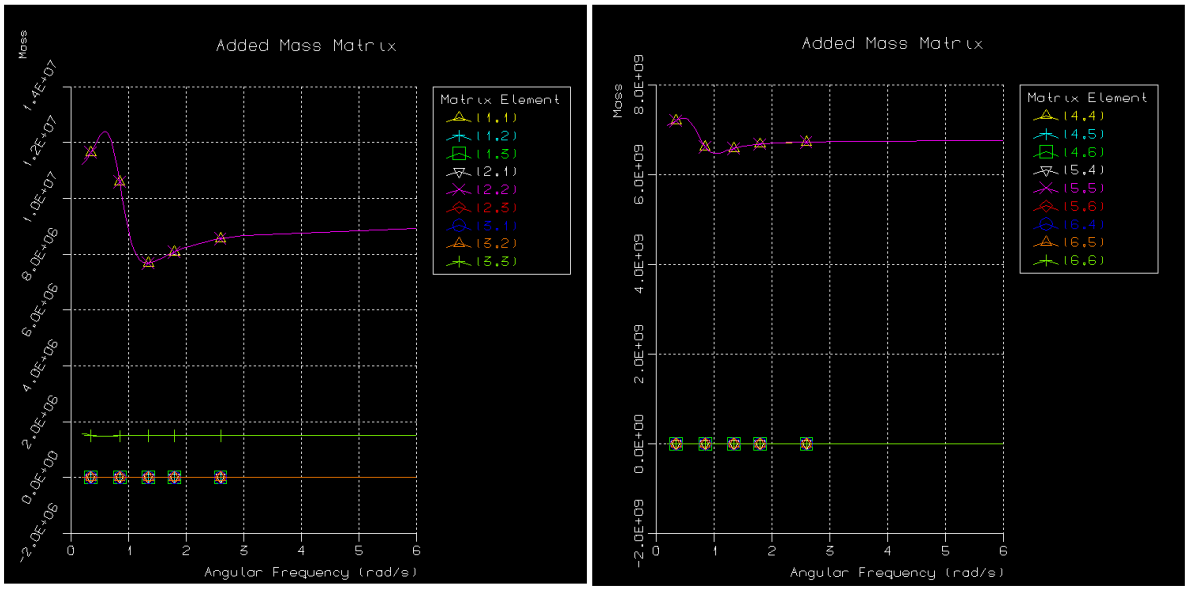

Figure 6.1: Addes mass; Force translation and moment rotation modes

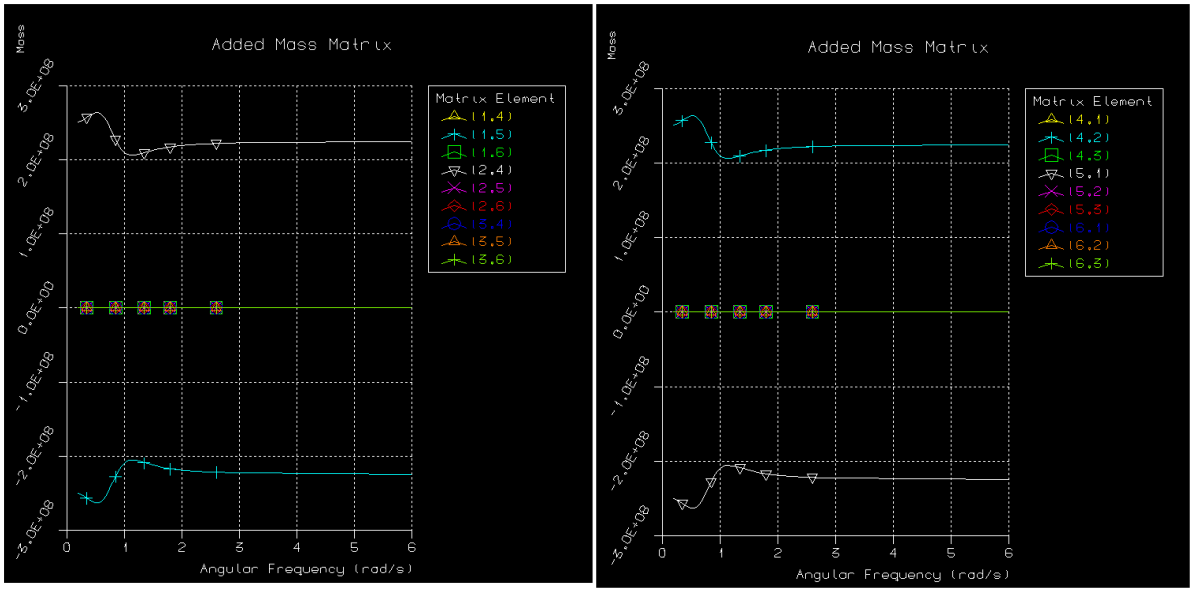

Figure 6.2: Added mass; Force rotation and moment translation modes

It is seen that many of the terms are zero, or at least close to zero. This is due to the fact that the substructure is symmetric about the XZ and YZ plane, has zero forward speed and no current is present [8] . For the force translation case, left part of figure 6.1, we see that A_{11}, A_{22} and A_{33} are nonzero. A_{11} and A_{22} (surge and sway) are of course equal and A_{33} is the smallest because the "wetted area" from motion in heave direction is the smallest. If we look at the right part of figure 6.1, moment rotation, we see that A_{55} and A_{44} are nonzero and equal. A_{66} is zero because the substructure is a cylinder and no added mass force in yaw direction is generated because of motions in yaw direction. If we look at the left part of figure 6.2, moment translation, we see that A_{24} and A_{15} are nonzero, equal in magnitude but with opposite signs. In the right part of figure 6.2, moment translation, we see that only A_{42} and A_{51} have significant values, again this is due to symmetry.

The nonzero terms in the added mass matrix are summarized below:

$$\mathbf{A} = \begin{bmatrix} A_{11} & 0 & 0 & 0 & A_{15} & 0 \\ 0 & A_{22} & 0 & A_{24} & 0 & 0 \\ 0 & 0 & A_{33} & 0 & 0 & 0 \\ 0 & A_{42} & 0 & A_{44} & 0 & 0 \\ A_{51} & 0 & 0 & 0 & A_{55} & 0 \\ 0 & 0 & 0 & 0 & 0 & 0 \end{bmatrix} \tag{6.2}$$

6.2 Potential damping

The frequency dependent potential damping contributions obtained from the HydroD (WADAM) analysis are shown in figure 6.3.

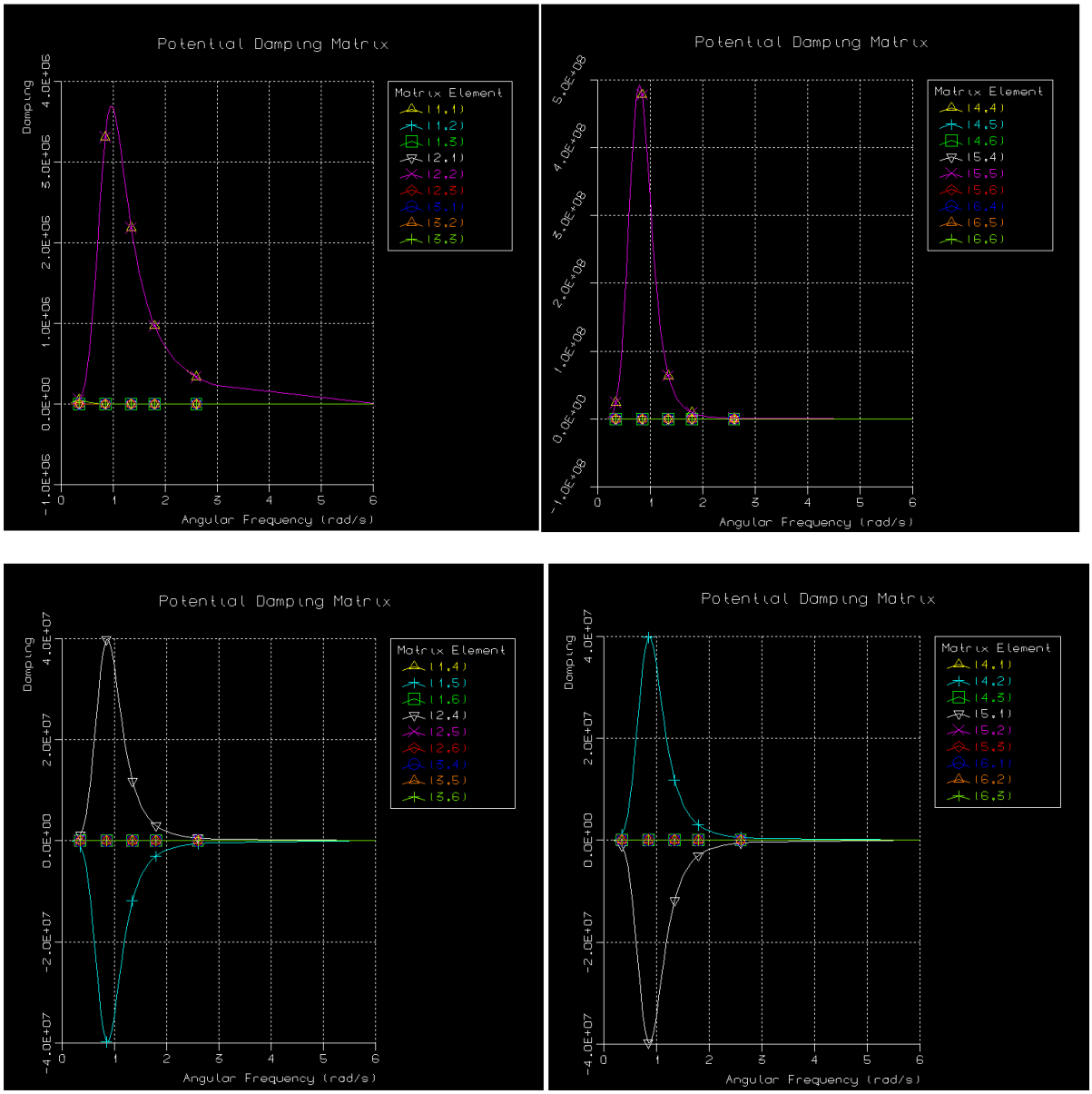

Figure 6.3: Potential damping; Force translation, moment rotation, force rotation and moment translation modes

We see that we have the same nonzero terms as we did in the added mass case in the previous section. We see that the potential damping approaches zero in the low and high frequency limits. Here only the potential damping is presented. Viscous forces are added to the analysis by using Morison elements as described in section 5.3.4. Damping is further discussed in section 8.

6.3 Excitation forces

The excitation force and moment transfer functions obtained from the first-order HydroD (WADAM) analysis are given in figure 6.4.

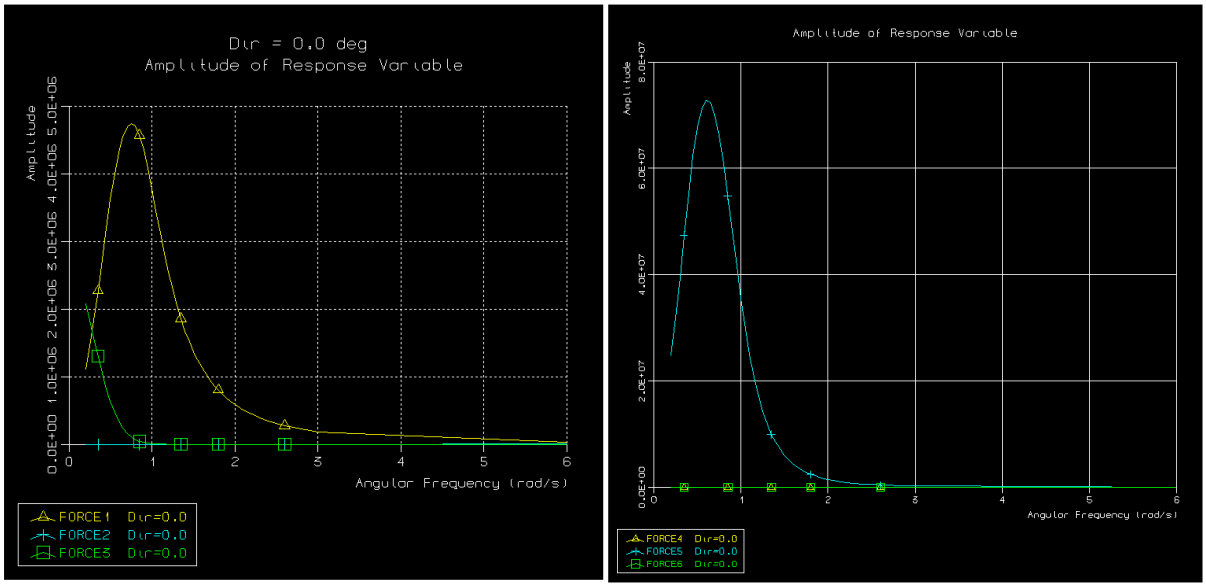

Figure 6.4: Excitation forces and moments from HydroD

The forces are plotted for a wave direction of 0 degrees, meaning along the positive x-axis. If we look at the figure to the left, we see that the force in sway direction (Force2) is zero. If we instead had shown the forces for waves coming along the y-axis (90 degrees), the force in surge direction would have been zero and the force in sway direction would have been identical to the surge force in the figure above. If we look at the figure to the right, we see that the pitch moment is nonzero. If we instead had used a direction of 90 degrees, the pitch moment would have been zero and the roll moment would be identical to the pitch moment in the figure. In either case the yaw moment is zero. We also observe that the forces approaches zero for high frequencies.

To verify the hydrodynamic model, the frequency dependent added mass, potential damping and force transfer functions have been compared with the results of Matha [1]. The agreement is very good both in terms of magnitude and frequency dependency. This is a good indication that the results from the hydrodynamic analysis in HydroD are correct.

7. Second-order forces

Tension-leg platforms typically have natural periods in heave roll and pitch smaller than the normal linear wave loading periods. For this reason, second order (and higher) effects might be important

Springing is normally defined as a steady state resonant response at an elastic mode. We distinguish between linear springing (generated by linear loads from waves) and nonlinear springing (second order effects). Linear springing is most likely to occur in moderate sea states where most of the energy is contained in short waves with small periods. Nonlinear springing however can arise in more severe sea states, where the waves are longer and also contain more energy. The springing effect is expected to reduce the fatigue life time of the mooring system and structure, and is therefore important to investigate. In the following the second-order sum-frequency wave forces on the TLP will be calculated. The effect of including these forces in the time domain simulations is investigated in section 13.

7.1 Theory

Because of the high natural frequencies in heave, roll and pitch of the TLP, the second-order wave forces oscillating at the sum-frequency might be important (springing). Until now we have focused on the first-order wave forces and the drift forces. The drift forces can be obtained from the first-order velocity potential (Newman) and thus do not require the second-order velocity potential. The second-order loads at the double frequencies on the other hand, require the second-order velocity potential to be known.

As were the case for the first-order potential, the second-order potential will also be the sum of an incoming potential, diffraction potential and radiation potentials associated with the rigid body motions.

The total velocity potential can be obtained by a perturbation power series [20].

$$\phi = \sum_{n=1}^{\infty} \varepsilon^n \phi^{(n)} \tag{7.1}$$

The perturbation coefficient ε is the wave slope:

$$\varepsilon = ka = \frac{2\pi}{\lambda} a \tag{7.2}$$

Here a is the wave amplitude and λ is the wave length.

With the first and second-order potential divided into the incoming, diffraction and radiation potentials associated with the 6 rigid body motions, the expression becomes:

$$\phi = \varepsilon(\phi_0^{(1)} + \phi_D^{(1)} + \sum_{j=1}^{6} \phi_j^{(1)}) + \varepsilon^2(\phi_0^{(2)} + \phi_D^{(2)} + \sum_{j=1}^{6} \phi_j^{(2)}) \tag{7.3}$$

For details on the second order boundary value problem and on determining the second-order potentials, see [21] and [22].

In the following we will write the total velocity potential as a sum of a linear (first-order) and a quadratic (second-order) part in the following way:

$$\phi = \phi_L + \phi_Q \tag{7.4}$$

In contrast to the linear analysis (section 3), the second-order terms in Bernoulli's equation is now included and the pressure can be obtained from:

$$P = -\rho g z - \rho \frac{\partial \phi}{\partial t} - \frac{\rho}{2}(\nabla \phi)^2 \tag{7.5}$$

To second order this gives the following expression for the pressure in the fluid:

$$P = -\rho \frac{\partial \phi_L}{\partial t} - \rho g z - \rho \frac{\partial \phi_Q}{\partial t} - \frac{\rho}{2}(\nabla \phi_L)^2 \tag{7.6}$$

The force can then be found by integrating the pressure over the instantaneously wetted surface. In the vertical direction the integration is performed from the bottom of the structure (-D) to the wave elevation (ζ). This is illustrated in the following expression:

$$F = -\iint_S \mathbf{n} P dA = -\int_{-D}^{\zeta} \int \mathbf{n} P dA = -\int_{-D}^{0} \int \mathbf{n} P dA - \int_{0}^{\zeta} \int \mathbf{n} P dA \tag{7.7}$$

To second order:

$$F = \rho \int_{-D}^{0} \int \mathbf{n}\left(\frac{\partial \phi_L}{\partial t} + g z\right) dA + \rho \int_{0}^{\zeta} \int \mathbf{n}\left(\frac{\partial \phi_L}{\partial t} + g z\right) dA + \rho \int_{-D}^{0} \int \mathbf{n} \frac{\partial \phi_Q}{\partial t} dA + \frac{\rho}{2} \int_{-D}^{0} \int \mathbf{n} (\nabla \phi_L)^2 dA \tag{7.8}$$

The first part of the force equation (7.8) is the first order force. This term do not give rise to any sum- or difference-frequency forces and is the force used in a linear analysis.

The remaining terms in equation (7.8) represent the second-order force:

$$F^2 = \rho \int_{0}^{\zeta} \int \mathbf{n}\left(\frac{\partial \phi_L}{\partial t} + g z\right) dA + \rho \int_{-D}^{0} \int \mathbf{n} \frac{\partial \phi_Q}{\partial t} dA + \frac{\rho}{2} \int_{-D}^{0} \int \mathbf{n} (\nabla \phi_L)^2 dA \tag{7.9}$$

From equation (7.9) we see that there are three contributions to the second-order force. The first contribution is that due to the variation in wetted surface, obtained by integrating to the instantaneous free surface. The second contribution is that due to the second-order potential and the third contribution is that due to quadratic products of the linear potential, the velocity squared term in Bernoulli's equation. The second-order force will have contributions both at sum-frequencies and difference-frequencies.

HydroD (WADAM) will be used to calculate the first- and second-order velocity potentials and the forces on the TLP. The results are represented in the form of second-order force transfer functions for the different degrees of freedom. If $H^{(2)}$ is the second-order transfer function, the force in a long-crested sea may be expressed as follows:

$$q^{(2)} = \int_{-\infty}^{\infty}\int_{-\infty}^{\infty} a_i(\omega_i)a_j(\omega_j)H^2(\omega_i,\omega_j)d\omega_i d\omega_j \qquad (7.10)$$

Here a_i and a_j are the amplitudes of waves oscillating with frequency ω_i and ω_j. For short-crested seas the directional dependency of the transfer function and the waves must also be included. For the sum-frequency case, the second-order wave system and associated forces with frequencies $2\omega_i$, $2\omega_j$ and $(\omega_i + \omega_j)$ are what's interesting and might induce springing response in the TLP.

7.2 Modeling in HydroD (WADAM)

As were the case for the first-order wave loads, the second-order sum-frequency wave loads will also be calculated using potential theory. In order to get the second-order velocity potential needed to calculate the second-order forces, it is first necessary to solve the first-order problem to get the motions induced by the first-order forces, [16] and [23]. It is therefore necessary to have the correct mass and mass distribution of the model used in HydroD. The tension legs and their stiffness are also included to give the correct response.

To calculate the second-order forces, a free surface model is also required. This panel model was generated using GeniE, 4 node shell elements is used. The free surface should be a perfect circle and is defined by its radius, R. In the same way as for the TLP we can utilize that we have two symmetry planes and only model one quarter of the surface. This will reduce the number of panels and computing time greatly. A picture of a panel model generated by GeniE is shown in figure 7.1.

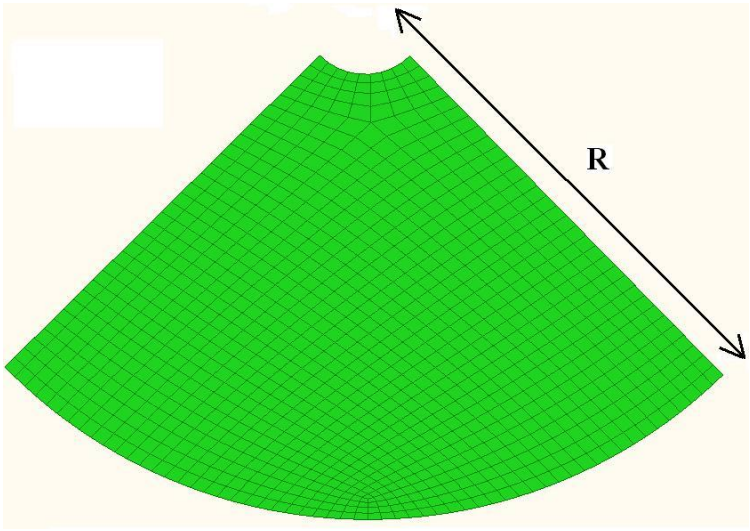

Figure 7.1: Free surface model in GeniE

To get correct results it is important to use a sufficiently large free surface model to model long waves correctly, and a mesh size small enough to account accurately for the shortest waves present. The necessary extent of the surface, R, depends on the decaying rate of local waves. A good approximation is to use R equal to the water depth for shallow water and equal to the longest wave length in the case of deep water [15]. To get a more certain estimate on the required surface size, the results sensitivity to this parameter should be checked.

The required mesh size will depend on the wave frequencies we choose to include in the analysis. According to DNV [24], a rule of thumb is to include on the order of 6 panels per second-order wave length. From this requirement we can derive a simple formula for the required element size. The dispersion relation for deep water waves gives a correlation between the wave length and wave period:

$$\omega^2 = kg \longrightarrow \left(\frac{2\pi}{T}\right)^2 = \frac{2\pi}{\lambda} g \longrightarrow \lambda = \frac{gT^2}{2\pi} \tag{7.11}$$

We then use the requirement of 6 elements per second-order wave length and the fact that the "second-order wave length" is one quarter of the first-order linear wave length to get the required element size:

$$Element \leq \frac{gT^2}{150} \tag{7.12}$$

The TLP has a natural frequency in heave of 2.6 rad/s (2.4 s) and 1.7 rad/s (3.68 s) for pitch and roll. It is important that the sum of two and two of the frequencies included in the hydrodynamic analysis cover these natural frequencies in order to get the correct forces at resonance. A limitation in the version of WADAM that was used is that the free surface can consist of no more than 3000 basic elements. For a frequency of 1.3 rad/s, half the heave natural frequency, the required element size according to equation (7.12) is 1.5 m. If one on the same time is to have free surface radius equal to the water depth (200 m), this will require more than 10000 elements and is therefore not possible. It was therefore necessary to do some investigations on how the results were affected when the element size and surface radius were changed to give different configurations of the panel model that was possible to run.

7.3 Free surface configuration sensitivity study

The second-order sum-frequency force transfer functions obtained by using free surface models with different sizes and mesh densities have been compared to get an indication about how extensive the free surface model needs to be.

We will focus our attention on the heave and pitch transfer functions. The pitch moment is believed to be the most important regarding the TLP response and forces in the tethers.

The wave frequencies used in the hydrodynamic analysis are listed in table 7.1. The frequency set was chosen so that the natural frequencies for heave and pitch motion can be found as the sum of

different pairs of the frequencies. Only waves coming from the same direction is included. The wave direction is 0 degrees, meaning along the positive x-axis.

Frequency number:	***1***	***2***	***3***	***4***	***5***	***6***	***7***	***8***	***9***
Frequency [rad/s]:	0.3	0.48	0.55	0.65	0.7	0.75	0.8	0.85	0.9
Frequency number:	***10***	***11***	***12***	***13***	***14***	***15***	***16***	***17***	***18***
Frequency [rad/s]:	0.95	1.0	1.08	1.15	1.2	1.25	1.3	1.35	1.4

Table 7.1: Frequencies used when calculating second-order forces

7.3.1 Dependency on free surface radius

Some of the different surfaces used to study the effect of the surface radius are listed in table 7.2.

	Radius, R [m]	**Elemet size [m]**	**Number of elements on quarter free surface**
Surface 1	72	3.5	342
Surface 2	126	3.5	1087
Surface 3	207	3.5	2837

Table 7.2: Free surface configurations, changing the radius

The element size used on the TLP itself is 1 m for all the cases. Surface 3 is larger than the water depth and should be able to account for the longest waves included in the analysis. The element size of 3.5 m was chosen so that the number of elements is below the limit of 3000 for the largest surface. The second-order pitch and heave transfer function are given in figure 7.2 and 7.3.

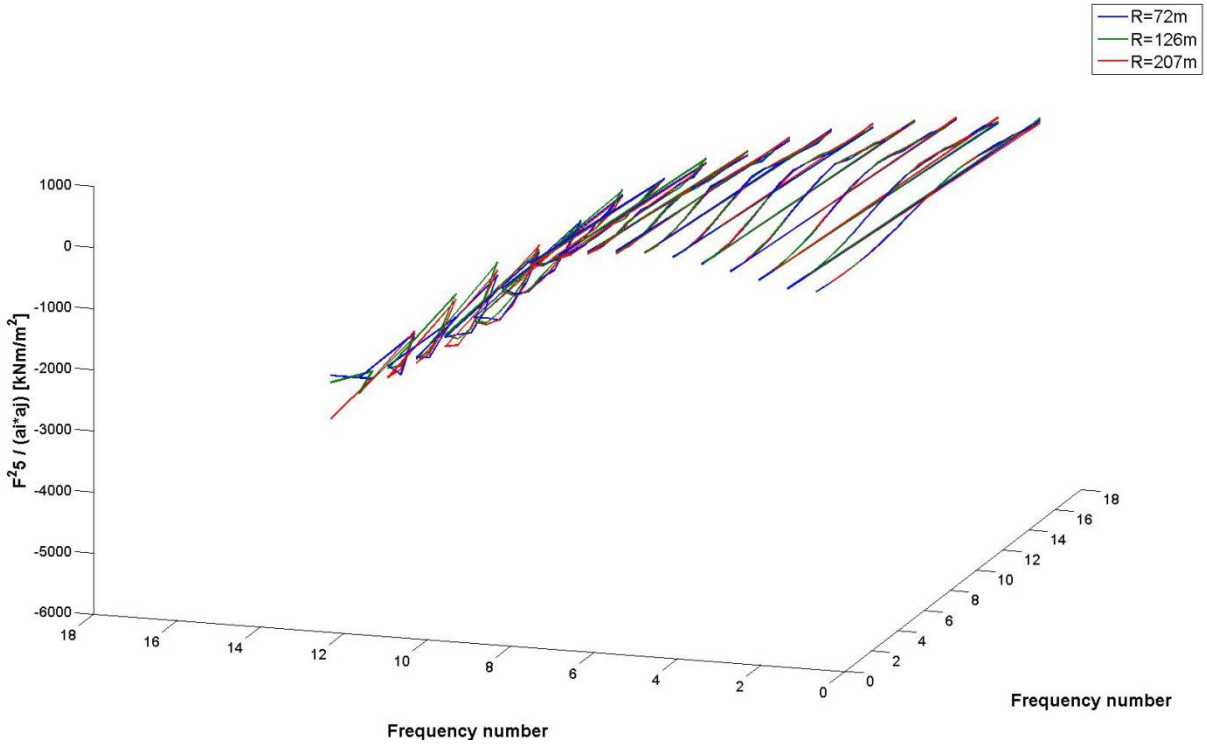

Figure 7.2: Pitch second-order sum-frequency force transfer functions, element size 3.5 m, changing the surface radius

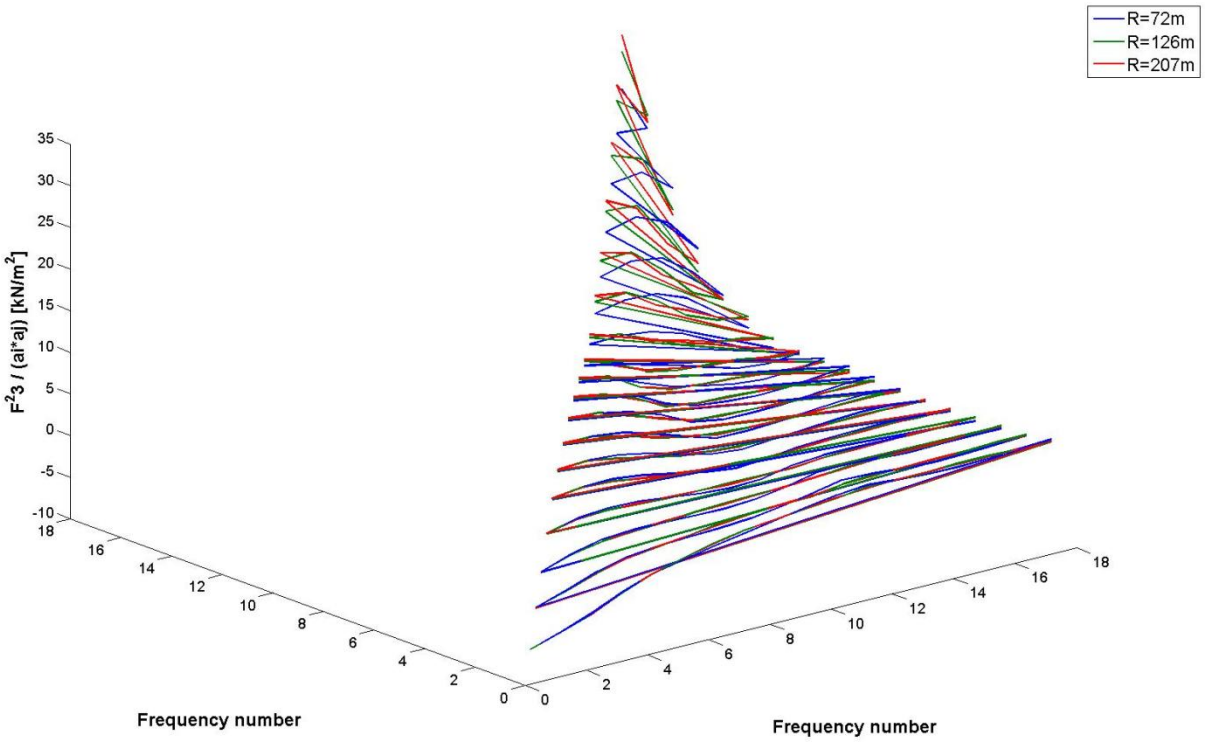

Figure 7.3: Heave second-order sum-frequency force transfer functions, element size 3.5 m, changing the surface radius

In the figures the force transfer function is on the vertical axis and the frequencies, table 7.1, are on the horizontal axis. We can see that the results agree quite well for the lower frequencies and that there are some deviations at high frequencies. The best agreement is between the forces obtained with the medium surface (126 m) and the largest surface (207 m). The surface with radius 126 m will therefore be used in the final analysis, making it possible to also reduce the element size, see next section.

7.3.2 Dependency on element size

In order to get an idea of how fine the free surface discretization needs to be, the results from the following configurations were compared:

	Radius, R [m]	Elemet size [m]	Number of elements on quarter free surface
Surface 1	126	1.3 and 2.7	2901
Surface 2	126	2.1	2856
Surface 3	126	3.5	1054
Surface 4	126	4.5	624
Surface 5	126	5.4	457
Surface 6	126	6.4	337

Table 7.3: Free surface configurations, changing the element size

The element size used on the TLP itself is 1 m. The highest frequency included is 1.4 rad/s. According to the DNV recommendation of 6 elements per second-order wave length, the element size should be 1.32m. In order to have this mesh size close to the TLP and on the same time have

a radius of 126 m, it was necessary to make a surface model with different mesh density at a distance away from the TLP. This resulted in surface 1 which has an element size of 1.3 m the first 36 m of the surface and an element size of 2.7 m between 36 and 126 m. The second-order pitch and heave transfer function calculated with the different surface configurations are given in figure 7.4 and 7.5.

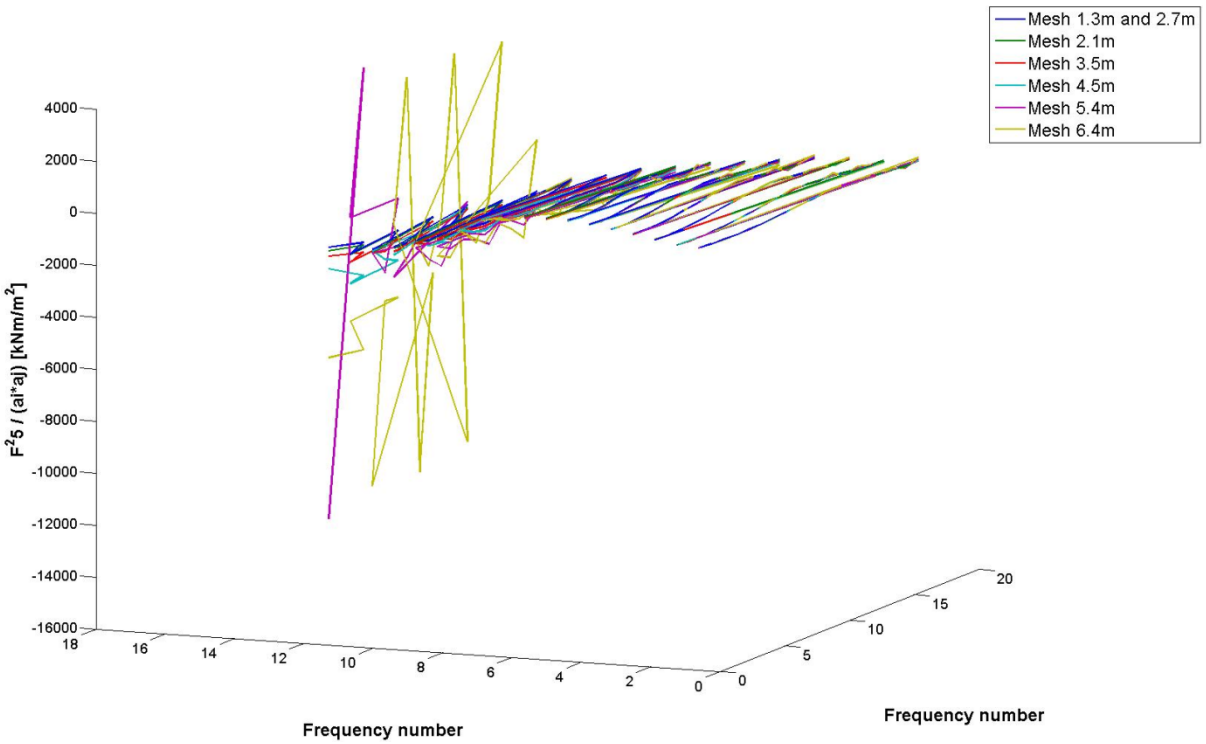

Figure 7.4: Pitch second-order sum-frequency force transfer functions, surface radius 126m, changing the element size

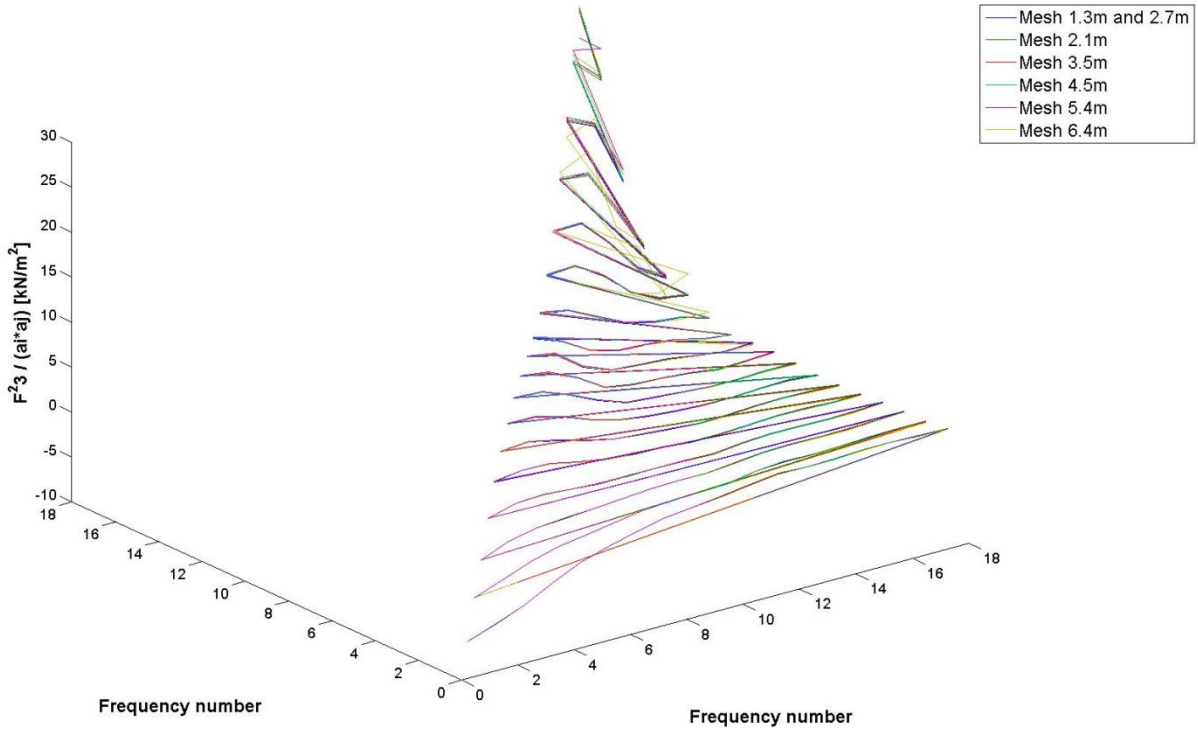

Figure 7.5: Heave second-order sum-frequency force transfer functions, surface radius 126m, changing the element size

From figure 7.4 we clearly see that the coarsest meshes (6.4 and 5.4 m) can't be used for other than the low frequencies and must therefore be discarded. This behavior was expected since it for the shortest "sum-frequency wave" only is about one and a half element describing it. When the wave frequencies are low, the wavelength is long and there are enough elements per wavelength to give a good model of the free surface. From figure 7.5, the heave force transfer function, we see that the results obtained with the coarser mesh don't deviate in the same extent as they did for the pitch case, but the deviations are still significant. The results obtained with the three finest meshes are seen to agree quite well, converging to almost the same values even for the highest frequency combinations.

In the further analysis a mesh size of 2.1 m will be used on a surface with a radius of 126 m as this is seen to give good results. This is a smaller surface with a coarser mesh than what's recommended by the WADAM manual [15] and equation (7.12). A possible explanation to that the surface give good enough results for this application is that we are only interested in the forces on the TLP and not the actual sum-frequency free surface elevation which is expected to need a more comprehensive free surface to be accurately determined [24]. The TLP geometry is also fairly simple with only one column that penetrates the free surface. There is thus no need to model second-order interaction effects between different columns, which according to [25] at least would require a very fine frequency mesh. The surface model together with the TLP is shown in figure 7.6.

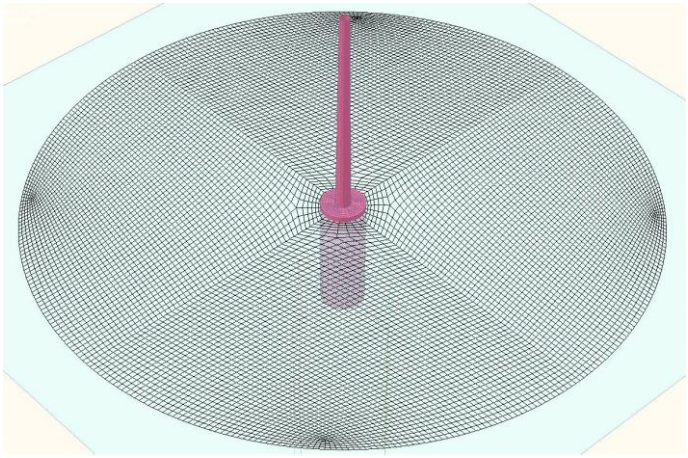

Figure 7.6: Free surface model with a radius of 126 m and an element size of 2.1 m

The effect of including the second order sum-frequency wave forces will be investigated in section 13.

Tension-leg platforms are also known to be susceptible to what's known as ringing response. Ringing is a high frequency transient response and large, steep and asymmetric waves have been shown to give ringing response, Aarsnes [26]. The ringing behavior is typically observed in sea states with peak period 3-5 times the natural periods, meaning third order or higher wave theory is needed to explain this behavior. Slamming forces could also be taken as a possible source for ringing response, but measurements have shown that the ringing response actually use a couple of cycles to "build up", meaning that slamming forces is not the source [26]. This also makes ringing difficult to calculate and is beyond the scope of this thesis.

8. Damping and decay tests

Decay tests (simulations) have been performed to find estimates of the damping and the natural periods of the system. The decay tests will also provide a good check on that the computer model is working properly.

The decay tests were performed by giving the structure a static displacement in the surge, pitch, heave and yaw degrees of freedom. This was done by applying a constant force in the beginning of the simulations. The force is acting the first 10 seconds and is then set equal to zero. The structure will then start to oscillate and we can use the logarithmic decrement to calculate the damping ratio. Contributions from both linear and quadratic damping will be considered. The motions measured in the waterline are considered. There are no wave and wind loads present.

After the force is removed the motion in the degree of freedom considered can be described by:

$$M\ddot{x} + F_{Damp} + kx = 0 \tag{8.1}$$

M is the sum of the structural and added mass, F_{Damp} is the damping force and k is the restoring coefficient.

Important contributions to the damping is the wave radiation damping (potential damping), viscous damping on the submerged parts of the structure, viscous damping on the tower and nacelle due to the relative wind velocity, damping due to the velocity dependent forces on the wind turbine [12] and structural damping. In the motion decay tests there will be no wind forces present and thus no damping from the wind.

8.1 Damping calculations

If we assume that the system will have both linear and quadratic damping the damping force can be written:

$$F_{Damp} = B_1\dot{x} + B_2\dot{x}\left|\dot{x}\right| \tag{8.2}$$

Where B_1 and B_2 are the linear and quadratic damping coefficients and $\dot{x}$ is a velocity either translatory or angular. The linear damping term is mainly related to the body's ability to generate waves, i.e. radiation damping in addition to structural damping. The nonlinear (quadratic) damping is mainly related to the drag from Morison's equation, i.e. viscous damping. The nonlinear damping is proportional to the velocities squared and will increase its importance relative to the linear damping for increasing velocities.

By dividing equation (8.1) by the mass and inserting equation (8.2) we get:

$$\ddot{x} + b_1\dot{x} + b_2\dot{x}\left|\dot{x}\right| + \frac{k}{M}x = 0 \tag{8.3}$$

Where $b1$ and $b2$ are the linear and quadratic damping coefficients divided by the mass.

Nielsen [27] showed that the damping force can be linearized by introducing an equivalent linear damping coefficient b_e:

$$\ddot{x} + b_e \dot{x} + \frac{k}{M} x = 0 \tag{8.4}$$

The requirement to b_e is that the energy dissipated per cycle in the linear model shall be the same as the energy dissipated per cycle by the damping force in equation (8.2).

$$\int_0^{Tn} (b_1 \dot{x} + b_2 \dot{x} |\dot{x}|) dx = \int_0^{Tn} b_e \dot{x} dx \tag{8.5}$$

Performing the integration and solving for be:

$$b_e = b_1 + \frac{16 x_n}{3 T_n} b_2 \tag{8.6}$$

Where x_n and T_n is the motion amplitude and period of cycle n respectively.

The logarithmic decrement can then be used to calculate the damping from the decay time series.

The solution of the freely oscillating system can be written as:

$$u(t) = e^{-\lambda \omega_o t} (A \sin(\omega_d t) + B \cos(\omega_d t)) \tag{8.7}$$

ω_o is the undamped natural frequency, ω_d is the damped natural frequency and A and B depend on the initial conditions. λ is the damping ratio, meaning the ratio between the actual damping and the critical damping:

$$\lambda = \frac{B}{B_C} = \frac{B}{2M\omega_0} \tag{8.8}$$

The logarithmic decrement is defined as the natural log of the ratio between two successive peaks:

$$\delta = \ln \frac{x_t}{x_{t+Td}} = \ln \frac{e^{-\lambda \omega_o t}}{e^{-\lambda \omega_o (t+Td)}} = \lambda \omega_o T_d = \lambda 2\pi \frac{\omega_o}{\omega_d} \tag{8.9}$$

See figure 8.1 for definition of the amplitude values and the damped natural period T_d.

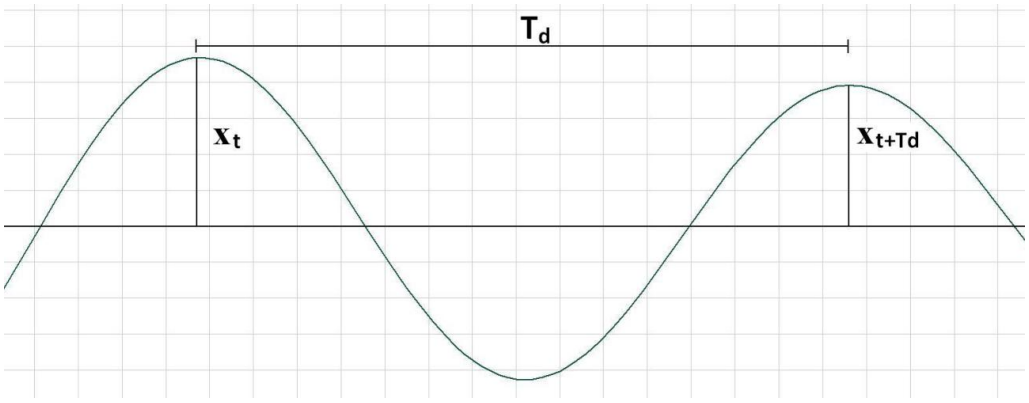

Figure 8.1: Motion decay

The damped natural frequency can be expressed in the following way:

$$\omega_d = \omega_o \sqrt{1-\lambda^2} \tag{8.10}$$

The logarithmic decrement can then be written:

$$\delta = 2\pi \frac{\lambda}{\sqrt{1-\lambda^2}} \tag{8.11}$$

We then solve for the damping ratio:

$$\lambda = \frac{\delta}{\sqrt{4\pi^2 + \delta^2}} \tag{8.12}$$

By inserting the definition of the damping ratio, solving for B_e and dividing by the mass M:

$$b_e = \frac{B_e}{M} = \frac{4\pi}{T_0} \frac{\delta}{\sqrt{4\pi^2 + \delta^2}} \tag{8.13}$$

The measurements of the equivalent linearized damping in equation (8.13) can be fitted to equation (8.6) by linear regression. By plotting b_e with $\frac{16x_n}{3T_n}$ on the x-axis, b_2 is found as the slope and b_1 as the intersection with the y-axis. This means that the linear damping is the value of the linearized damping for zero motion amplitude and a constant slope of b_e means a constant quadratic damping coefficient [27].

8.2 Surge

The decay test simulation for the surge motion was performed by applying a constant force of 1 MN at the bottom of the substructure in the global x-direction, giving a static displacement of approximately 5 meters. After 10 seconds, the force is zero and the TLP is oscillating as shown in figure 8.2. Matlab has been used to calculate the damping characteristics.

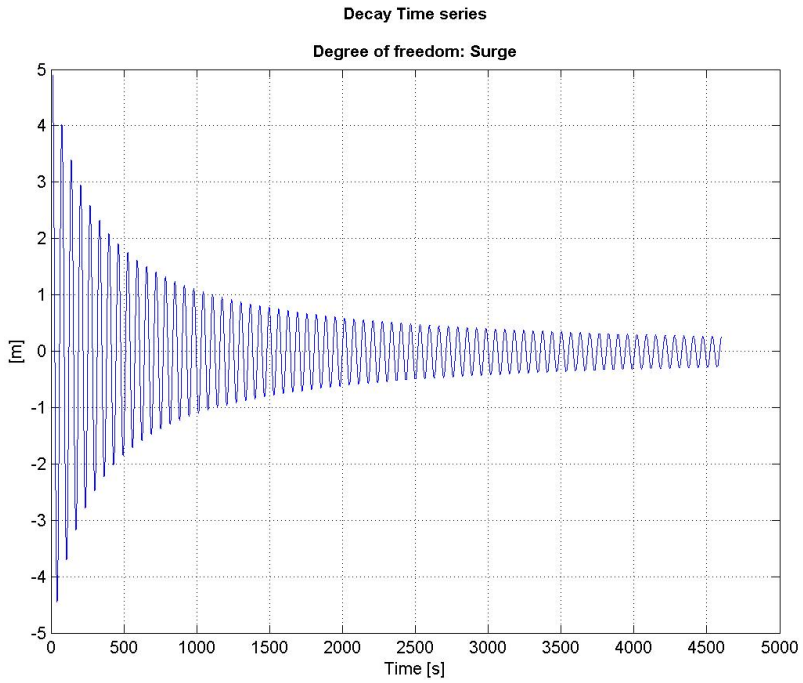

Figure 8.2: Surge decay time series

The damping ratio has then been calculated from the time series above. The ratio is shown in figure 8.3 as a function of the motion amplitude.

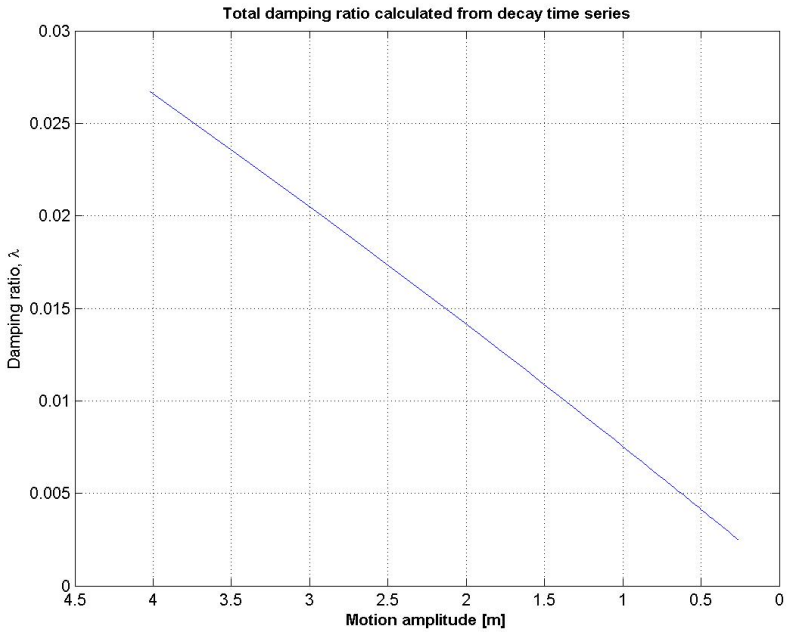

Figure 8.3: Surge damping ratio as function of motion amplitude

The damping ratio is largest when the motion amplitudes are large. The damping ratio is 2.6% for 4 m amplitude and 0.4% when the amplitude is 0.5 m. This is because the contribution from the quadratic damping is large when the velocities (motions) are large.

The damping divided by the mass (b_e) is calculated by using equation (8.13). This is then plotted with $\frac{16x_n}{3T_n}$ on the x-axis in figure 8.4. According to equation (8.6) we then find b1 as the intersection with the y-axis and b2 as the slope of the linear regression line (blue).

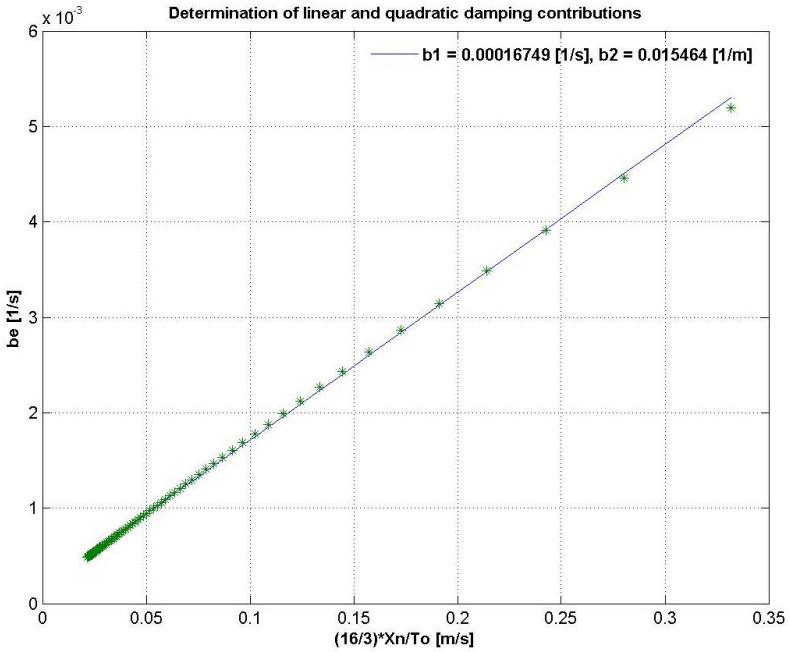

Figure 8.4: Determination of linear and quadratic damping contributions

The result for surge motion is b1=0.000168 [1/s] and b2 = 0.0155 [1/m]. This is the linear and quadratic damping coefficients divided by the mass.

To see what damping mechanisms that are most important, it would be interesting to see how the ratio between the linear and quadratic damping vary with the motion amplitude.

The linear damping contribution to the damping ratio is constant:

$$\lambda_1 = \frac{B_1}{B_C} = \frac{B_1}{2M\omega_0} = \frac{b_1}{2\omega_0} \tag{8.14}$$

The quadratic damping contribution to the equivalent linearized damping ratio is dependent on the motion amplitude and period, see equation (8.6). The period is almost constant here due to small levels of damping.

$$\lambda_{2e} = \frac{B_{2e}}{B_C} = \frac{B_{2e}}{2M\omega_0} = \frac{16x_n}{3T_n}\frac{b_2}{2\omega_0} \tag{8.15}$$

The ratio λ_1 / λ_{2e} is shown in figure 8.5.

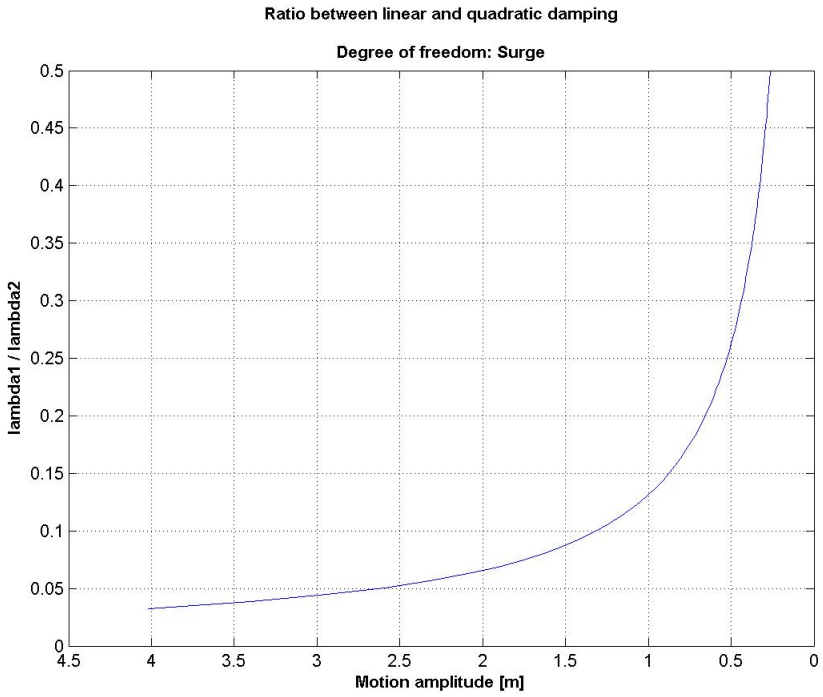

Figure 8.5: Ratio between linear and quadratic damping

The linear damping contributes to less than 5% of the total damping for motion amplitude of 4 meters, but when the motion amplitude is 0.25 meters it contributes to more than 50% of the damping. This shows how important the viscous damping is when the surge motions are large.

8.3 Heave, pitch and yaw

The decay test for the heave motion was performed by applying a constant force of 5 MN at the bottom of the substructure in the positive global z-direction (upwards), giving a static displacement of approximately 0.07 meters. The small displacement is due to the stiff mooring system.

The decay test for the pitch motion was performed by applying two constant forces (3MN), on two of the spokes, 15 m from the center of the substructure. One of the forces acted in the positive z-direction and the other in the negative z-direction. This gave a constant pitch moment and a static rotation of approximately 0.17 degrees.

The decay test for the yaw motion was performed by applying two constant forces (0.5 MN), on two of the spokes, 15 m from the center of the substructure. One of the forces acted in the positive y-direction and the other in the negative y-direction. This gave a constant yaw moment and a static yaw angle of 5.8 degrees.

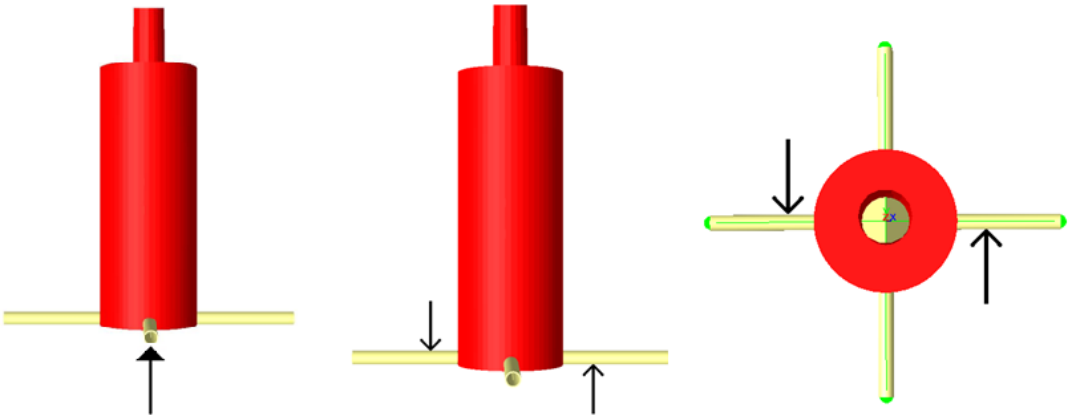

Figure 8.6: Static heave, pitch and yaw excitation

The decay time series are included in appendix A.

As were the case for the surge motion, the yaw motion also have a large contribution from quadratic damping. This can be explained by the limited wave making of the yaw motion, meaning that the damping is mostly caused by viscous forces on the struts at the bottom of the substructure. The damping ratio for the yaw motion is given in figure 8.7. For further details on the yaw damping, see appendix A.

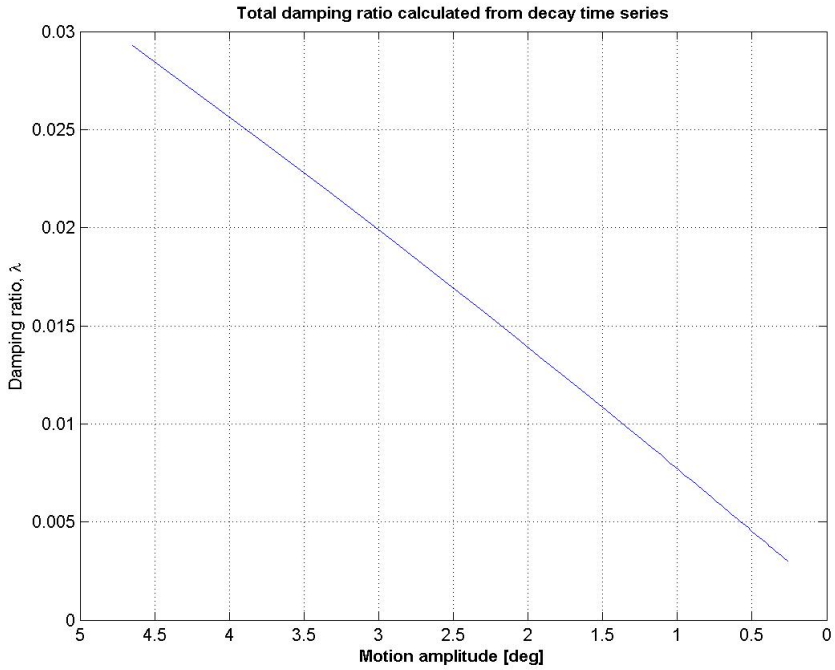

Figure 8.7: Yaw damping ratio as function of motion amplitude

When calculating the damping ratios for the heave and pitch motions, it turned out that the ratio is almost independent of the motion amplitude, indicating that the damping is mostly linear. This is probably due to the small motions and correspondingly small relative water velocity normal to the substructure resulting in negligible viscous damping in the decay tests. The damping ratios were found to be 0.027 for the pitch and 0.0065 for the heave motion.

8.4 Summary and comparison with reference model

The results from the previous sections are summarized in table 8.1. The natural periods estimated from the time series are also included.

	Damping ratio, λ [-]	Damped period, T_d [s]	Undamped period, T_0 [s]	Frequency [rad/s]
Surge	Ranges from 0.027 to 0.0025 in the amplitude range considered, see figure 8.3	65	65	0.097
Heave	0.0065	2.40	2.40	2.62
Pitch	0.027	3.68	3.68	1.71
Yaw	Ranges from 0.029 to 0.003 in the amplitude range considered, see figure 8.7	14.8	14.8	0.43

Table 8.1: TLP natural periods and damping ratios

Due to the symmetry of the structure, the values for roll and sway are equal to the values of pitch and surge respectively. We see that the damping has little or no effect on the oscillation period; this is due to the small levels of damping.

The damping included in the decay tests were the wave radiation, viscous and structural damping. Structural damping is hard to determine and might include material damping, friction in the connections between the spokes and the tension legs and between the tension legs and the supports at the sea floor. Deformation of the sea bottom due to the dynamic tension in the tension legs can also supply some damping. Its however reasonable to assume that this contribution is insignificant and also will change during the lifetime of the structure [28].

The structural damping in the analysis is included as Rayleigh Damping:

$$\mathbf{C} = \alpha_1 \mathbf{M} + \alpha_2 \mathbf{K} \tag{8.16}$$

Here $\mathbf{C}$ is the damping matrix, $\mathbf{M}$ is the structural mass matrix and $\mathbf{K}$ is the structural stiffness matrix. The α_1 parameter is set equal to zero and $\alpha_2 = 0.005$, giving a stiffness proportional structural damping ratio of about 0.4% at the pitch natural frequency [18] [29]. It is believed that this value is somewhat conservative.

Additional damping contributions will arise when the wind forces are included. This was discussed in section 4.3.

The natural periods of the TLP given here have been compared with the results of Matha [1]. The comparison is not straight forward, since the computer model used in this report also accounts for the flexibility of the tower and the blades. Hence, there is a coupling between the platform motions and the flexibility of the structure. In our simulations, the structure is considered rigid and this will give a stiffer system. The comparison is given in table 8.2.

	TLP DeepC	TLP Matha [1]	Difference [s]
Surge [s]	65	61	4
Sway [s]	65	61	4
Heave [s]	2.40	2.29	0.11
Roll [s]	3.68	4.48	-0.8
Pitch [s]	3.68	4.52	-0.84
Yaw [s]	14.8	10.3	4.5

Table 8.2: TLP natural periods, comparison with reference model

The agreement for surge, sway and heave motion is quite good. For pitch and roll the differences are larger, about 20 %. As stated above, this is most likely due to the fact that Matha [1] also included the flexibility of the tower. The impact this have on the final results can be significant. If our model has too small natural periods in pitch and roll, that might result in less resonance response than what's really the case for a given sea state. In our model the mass and the added mass of the spokes are included. Matha on the other hand assumes that the spokes have no mass. This might explain some of the difference between the yaw natural periods.

9. Response analysis

To assess how the TLP performs under different loading conditions, time domain simulations have been performed. The computer programs applied have been discussed in the previous sections. The environmental conditions, herby referred to as load cases will be presented in section 9.1. Response parameters extracted from the computer simulations include platform motions in 6 degrees of freedom in the waterline, nacelle motions, thrust, power, relative wind speed at nacelle and tension in the mooring lines (tethers).

The total simulation length used is 4600 seconds, but the first 1000 seconds of each time series is removed in order to make sure that possible transient start-up effects are ignored when computing envelopes.

The numbering of the eight tension legs is shown in figure 9.1. The tension in each pair is almost identical.

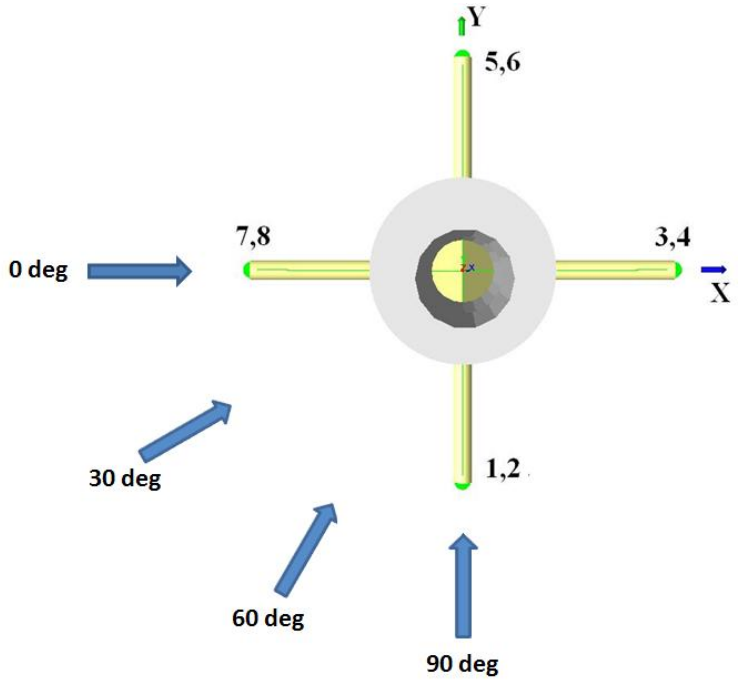

Figure 9.1: Tension leg numbering together with definition of directions

The forces included in the analysis are the thrust force on the wind turbine, the linear wave forces and the slowly varying wave forces (Newman). There are no current present. The second-order (sum-frequency) wave forces calculated in section 7 are not included in the main response analysis, but the effect of including these forces will be investigated in section 13. The water depth is 200 meters. How the TLP performs at a reduced water depth of 120 meters is investigated in section 12.

9.1 Load cases

A total of eleven load cases containing both wind and waves will be considered. The load cases are listed in table 9.1. The wind conditions are defined by their mean wind speed at hub height and turbulence intensity. The sea states are defined by their significant wave height (Hs) and peak period (Tp). Wind/wave directionality is considered by changing the wave directions. Referring to figure 9.1, a wind and wave direction of zero degrees means along the positive x-axis and a rotation towards a positive number means a rotation in the counter clockwise direction. Waves with direction 90 degrees are then travelling along the positive y-axis.

	Vhub (m/sec)	**I (turbulence intensity)**	**Hs (m)**	**Tp (sec)**	**Wind/wave directions (deg)**
LC0-1	4	0.15	1.0	5.0	0 / 0
LC0-2	8	0.15	2.5	9.8	0 / 0
LC0-3	11.4 (rated)	0.1	3.1	10.1	0 / 0
LC0-4	18	0.1	4.4	10.6	0 / 0
LC0-5	50	0.1	12.7	14.1	0 / 0
LC30-3	11.4 (rated)	0.1	3.1	10.1	0 / 30
LC30-4	18	0.1	4.4	10.6	0 / 30
LC30-5	50	0.1	12.7	14.1	0 / 30
LC90-3	11.4 (rated)	0.1	3.1	10.1	0 / 90
LC90-4	18	0.1	4.4	10.6	0 / 90
LC90-5	50	0.1	12.7	14.1	0 / 90

Table 9.1: Definition of load cases

LC0-1 to 5 are the load cases with wind and waves from the same direction. LC0-1 and LC0-2 are load cases with mean wind velocity below rated and small waves. In LC0-3 the mean wind speed is at the rated speed and the thrust from the wind turbine will also be at its maximum in this case. In LC0-4 the wind speed is above rated but still well below the cut out wind speed of 25 m/s. LC0-5 is an extreme load case with a mean wind speed of 50 m/s and significant wave height of 12.7 m. In LC0-5 the wind speed is above the cut out wind speed and the wind turbine is shut down, reducing the forces from the wind to drag forces only. The load cases considering different wind/wave directions, LC30-3 to 5 and LC90-3 to 5, have the same wind and wave conditions as LC0-3 to 5, but the wave direction is 30 and 90 degrees respectively.

The wind is described by a Kaimal wind spectrum. This was discussed in section 4.1. The waves are described by a three-parameter JONSWAP wave spectrum. The three parameters are the significant wave height which is the mean of the 1/3 highest waves, the peak period which is the period where the wave spectrum has its maximum value and a peakness parameter. The JONSWAP spectrum is based on measurements in the southeastern parts of the North Sea. The spectrum is characterized by a sharp peak compared with for example a Pierson-Moskowitz (PM) spectrum. If a JONSWAP and a PM spectrum are used to describe the same sea state, the total energy in the sea state will be the same, but the energy will be distributed differently over the

frequencies. A peakness parameter $\gamma = 3.3$ is used. If $\gamma = 1$, the JONSWAP spectrum is reduced to a PM spectrum [30]. The JONSWAP wave spectrum from LC0-5 is shown in figure 9.2.

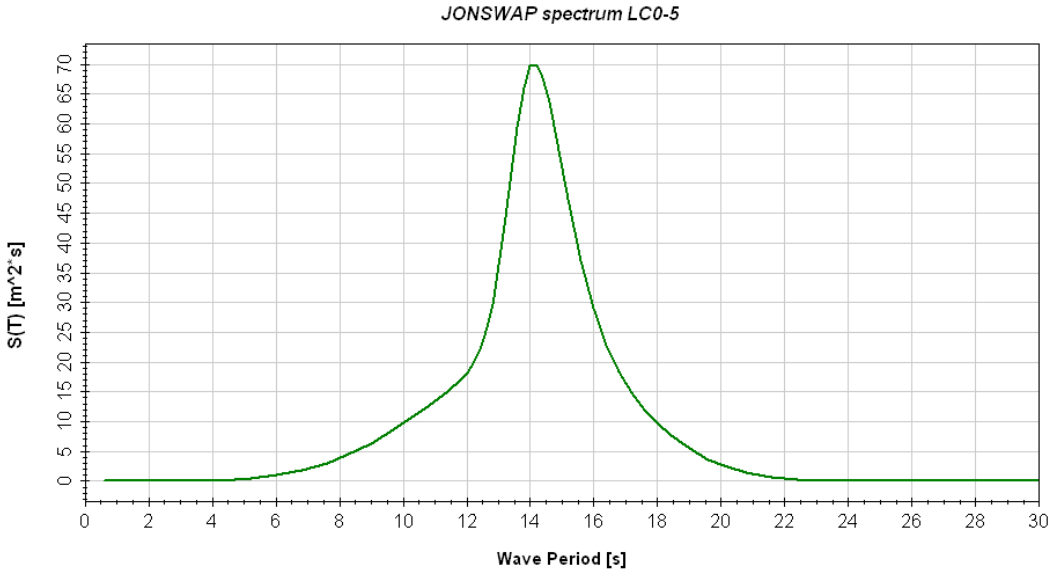

Figure 9.2: JONSWAP wave spectrum, LC0-5

9.2 Notch filter settings

To see how the notch filter included in the wind force dll (TDHMILL3D) affects the motion response of the TLP and how sensitive it is to different settings, it has been tested with LC0-3 and LC0-4. Only the wind force is included to better see the effect. The purpose of the notch filter is to act as a control system which strives for active damping in a very simplistic way. The notch filter is thus included to reduce or eliminate the negative damping effect described in section (4.3). TDHMILL3D works by calculating the velocity vector of the rotor hub and then filter the component perpendicular to the rotor plane. What frequencies that are filtered are determined by the input to the program. This filtered hub velocity is then used to calculate the relative wind velocity used when calculating the thrust force on the wind turbine.

The input parameters to the notch filter are ζ_N, ζ_D and the filtering frequency. The filtering frequency is set equal to the pitch natural frequency because it is the pitch induced velocities at the nacelle we wish to filter. ζ_N and ζ_D determines the steepness and broadness of the "notch". In figure 9.3 eight different notch filter configurations are shown. The figure show how much each configuration filters away. In principle it would be desirable to have a fairly narrow filter around the pitch natural frequency in order to not filter away too much at other frequencies.

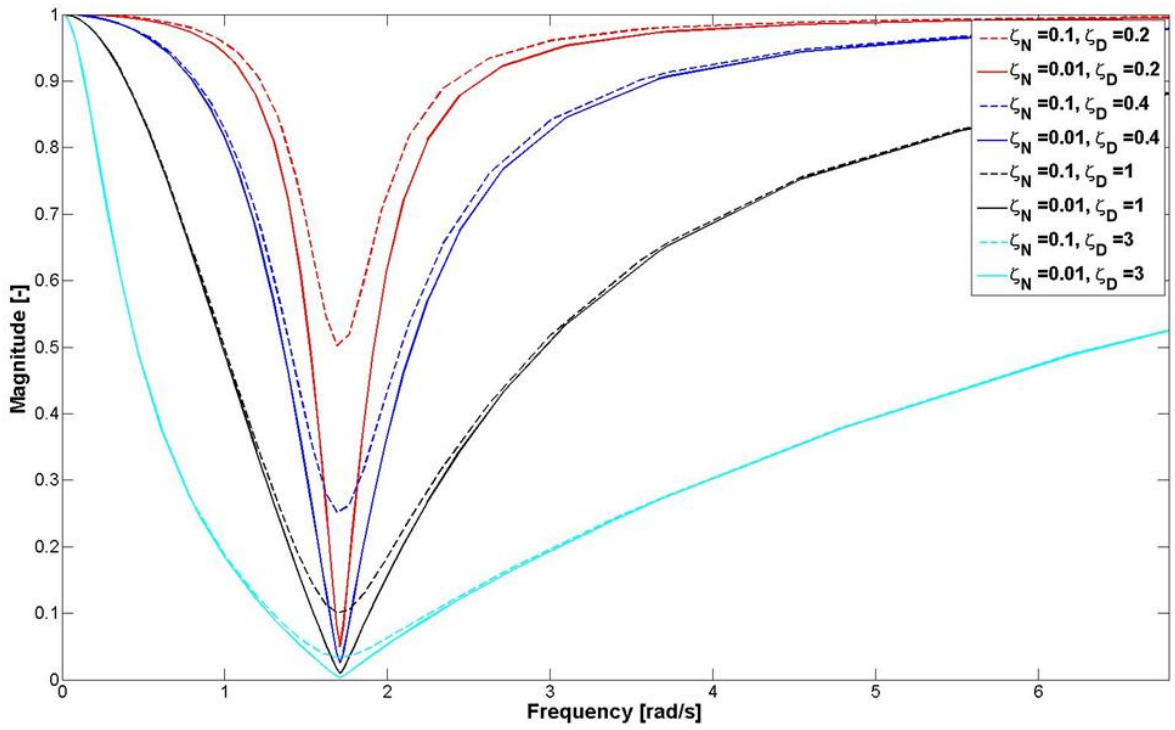

Figure 9.3 Different notch filter settings

In figure 9.4 the mean, standard deviation, maximum and minimum value of the pitch response of the TLP in LC0-4 (above rated wind) are shown for 10 different notch filter settings and without the notch filter.

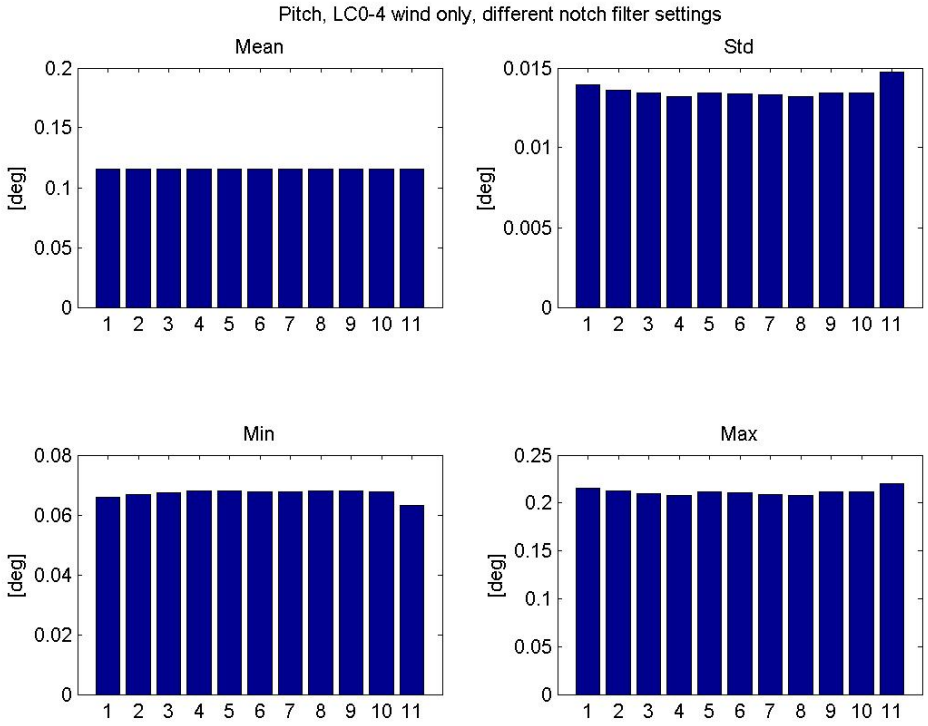

Figure 9.4: Pitch response with different notch filter settings, LC0-4

The different notch filter configurations used in the figure are given in the following table.

Analysis number	Notch period [s]	ζ_N	ζ_D	ζ_D / ζ_N
1	3.68	0.1	0.2	2
2	3.68	0.1	0.4	4
3	3.68	0.1	1	10
4	3.68	0.1	3	30
5	3.68	0.01	0.2	20
6	3.68	0.01	0.4	40
7	3.68	0.01	1	100
8	3.68	0.01	3	300
9	3.78	0.01	0.2	20
10	3.58	0.01	0.2	20
11	**Notch filter OFF**	-	-	-

Table 9.2: Notch filter settings

From figure 9.4 we see that the mean value is not affected by the different notch filter settings. The standard deviation, min and maximum values on the other hand are affected. Analysis 11 and 1 stands a bit out. This is the analysis run without the notch filter and with a filter set up to not filter more than about half of the magnitude in figure 9.3. The effect of having the notch filter in this case is however quite small and for most of the settings the results are quite similar. An explanation to the small effect of the notch filter for this case is that the pitch response is quite small. When comparing the response with and without notch filter for other response variables such as surge, heave and yaw, the change in standard deviation was below 1% and it can be

concluded that these degrees of freedom are not affected by using a notch filter tuned to filter the pitch motions.

In figure 9.5 statistics of the pitch responses in LC0-3 (rated wind) are shown.

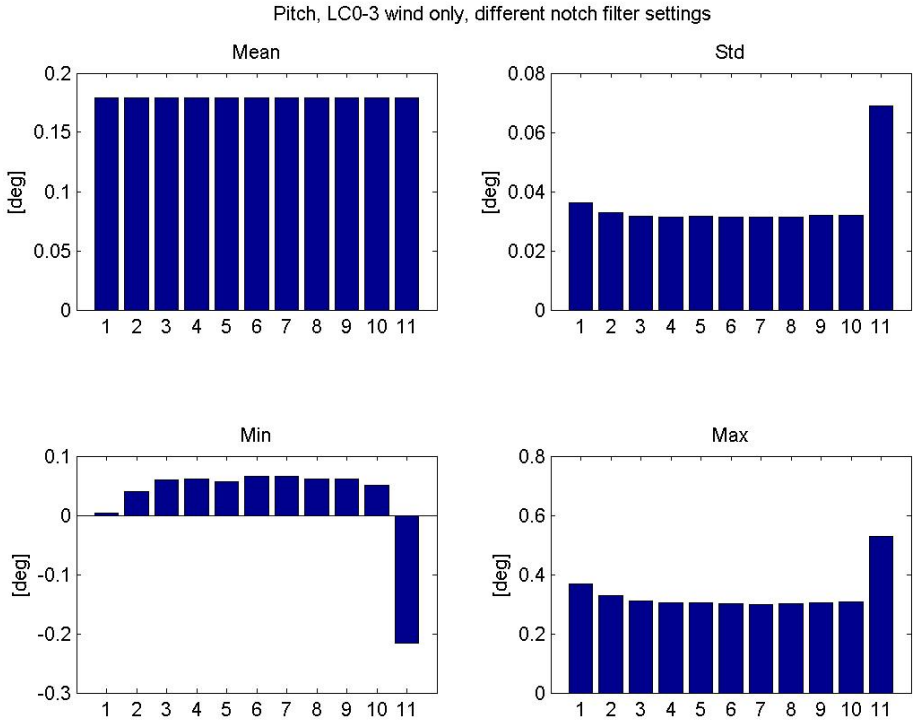

Figure 9.5: Pitch response with different notch filter settings, LC0-3

Again, the mean values are not affected by the notch filter and the response is quite similar for the different notch filter settings as long as the filter is activated. For the analysis without the notch filter activated however, the standard deviation tells us that the dynamic response is significantly larger. To get a clearer picture of what is going on, the pitch time series of the analysis with the notch filter turned off is given in figure 9.6.

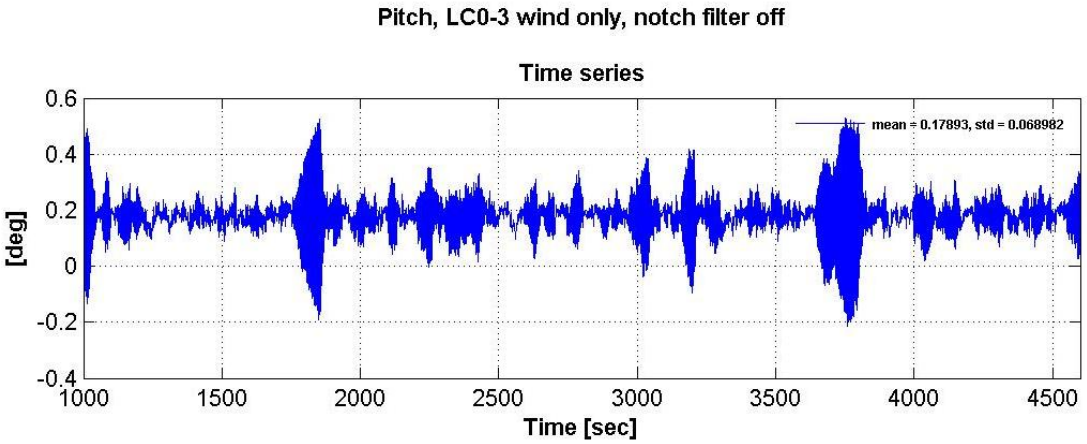

Figure 9.6: Pitch time series in LC0-3 with notch filter off. Unstable behavior

From the time series it can be seen that the system is unstable. The “bursts” seen around 1000s, 1700s and 3700s were eliminated when the notch filter was activated. This explains the large differences in the statistical values in figure 9.5. The explanation to this behavior is that there is a large negative damping contribution from the wind turbine when the wind is at the rated speed (11.4m/s). The damping contribution from the wind turbine was discussed in section 4.3, where it was shown that the k_{CT} value of the turbine has its most negative value at the rated wind speed.

It can be concluded that the notch filter is necessary to have when the wind speed is close to the rated speed in order to avoid having an unstable system. Also at wind speeds above rated the notch filter reduce the dynamic pitch motions. The standard deviation, minimum and maximum values in a one hour simulation is not very dependent on different notch filter settings as long as the notch is not to shallow. It is therefore decided to use a notch filter with input parameters ζ_N = 0.01 and ζ_D = 0.2 in the following analysis. This notch filter is quite narrow and will therefore not filter out over an unnecessarily wide frequency band. This is believed to be the most realistic way to apply the filter.

9.3 Only wind, uniform and turbulent

To give a better understanding of how the wind forces affect the TLP, LC0-1 to 5 have been run without waves present. The load cases were also run without turbulence (uniform wind) to see how the model reacts to that. The notch filter was activated at the pitch natural frequency.

In figure 9.7 the time series and spectra of the surge responses in load case 4 with and without turbulence (LC0-4wT and LC0-4wU) are given. Notice that the time series are shown from zero seconds. In this case the wind speed is 18 m/s.

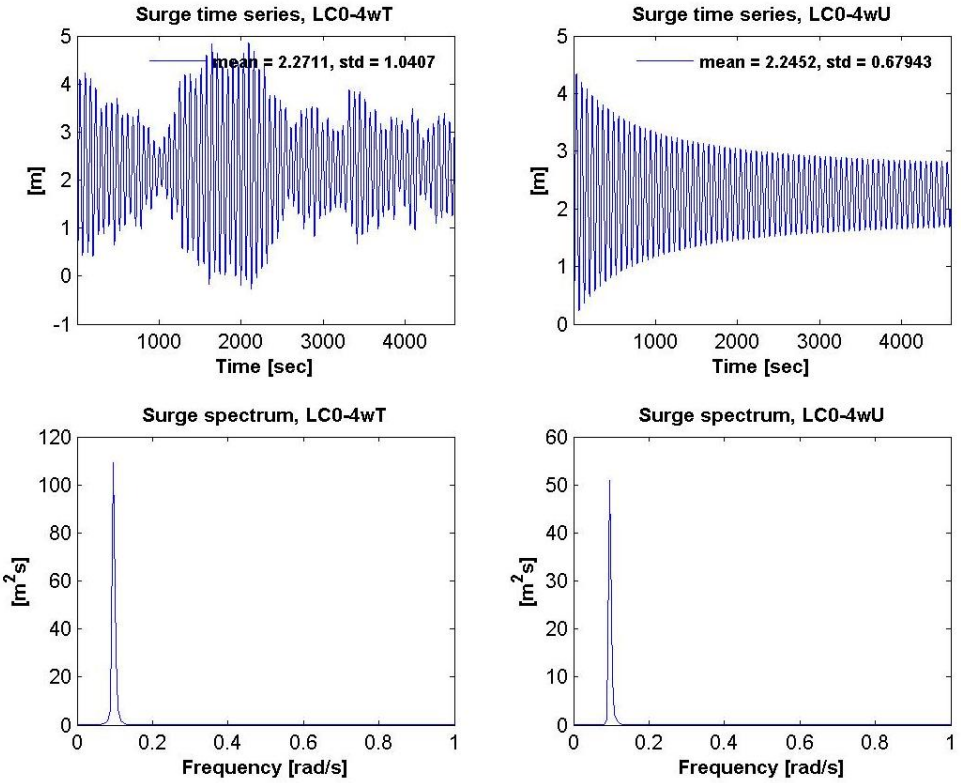

Figure 9.7: Surge response in LC0-4. Turbulent and uniform wind

From the response spectra it is seen that all the response is at the surge natural frequency (0.1 rad/s). In both cases the mean offset is about the same due to similar mean thrust force on the wind turbine (same mean wind speed). With turbulence the TLP moves as expected when exposed to a time dependent loading. In uniform wind the surge response looks like something from a decay test. The explanation to this behavior is that at zero seconds, the wind thrust force is applied directly without any ramp function to smoothen the transient effects. The thrust force then acts as a sudden (impulse) load, giving a large initial displacement.

Comparing the Surge time series in LC0-4wU with the decay time series of surge in section 8.2, we see that the decay in LC0-4wU is slower than in the pure decay test. This can be explained by the negative damping contribution from the wind thrust force at wind speeds above rated. When the TLP is moving against the wind, the relative wind speed is increased. Since the wind speed is above rated this will result in a decrease in the thrust force. When it is moving away from the wind the thrust force will increase. The surge motion is thus exited by the variations in the thrust force caused by different relative wind speeds when the TLP is moving into and away from the

wind. In LC0-3wU (rated wind) the effect was seen even clearer with a near constant surge amplitude during the whole simulation.

Activating the notch filter at the surge natural frequency in LC0-3wU and LC0-4wU reduced the dynamic surge motions substantially. It is however believed that the notch filter is of better use when filtering the pitch induced relative velocity at the nacelle, and was in the previous section indeed shown to be necessary in order to prevent having an unstable system in LC0-3. It should also be noted that having wind with no turbulence is not something that normally occur, and was here simulated mainly to see how the computer model reacts to it.

Turning our attention to the pitch response, figure 9.8, we see that in the case of uniform wind the pitch motion is a result of coupling with surge (slowly varying). In the case of turbulent wind the coupling with surge is also seen, but there is also a contribution at the pitch natural frequency (1.7 rad/s) that is caused by energy in the wind spectra at this frequency. The pitch motion is seen to be quite small.

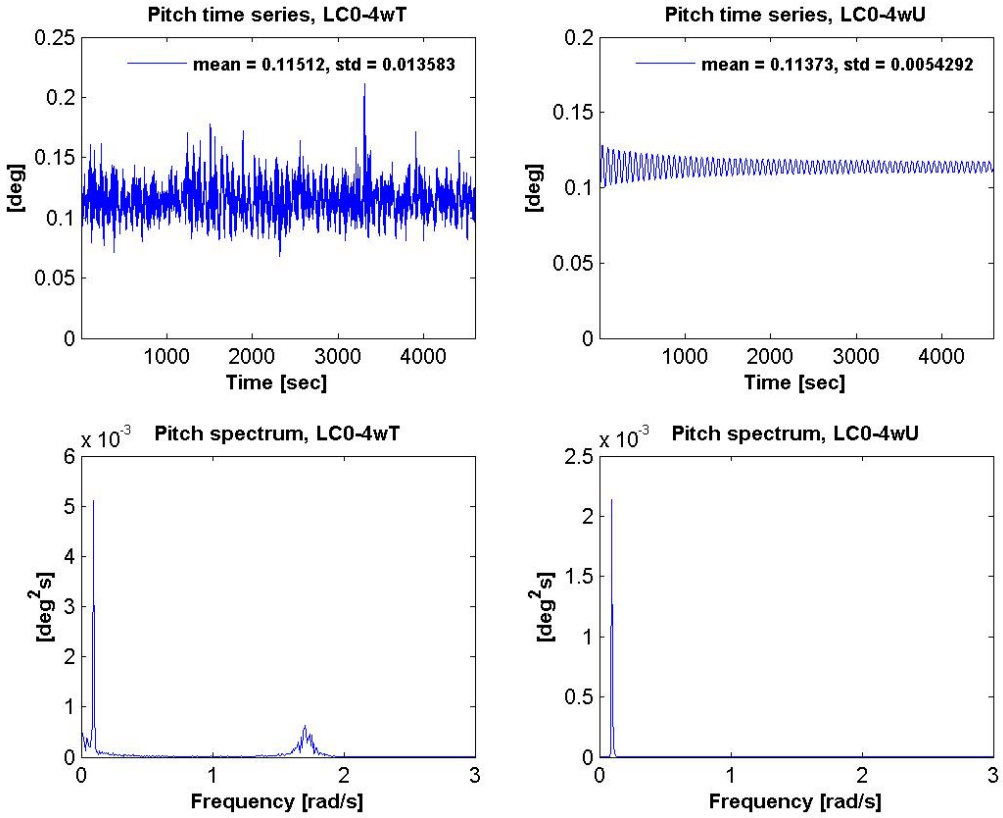

Figure 9.8: Pitch response in LC0-4. Turbulent and uniform wind

In figure 9.9 the time series and spectra of the surge response in LC0-2 with turbulent and uniform wind are given.

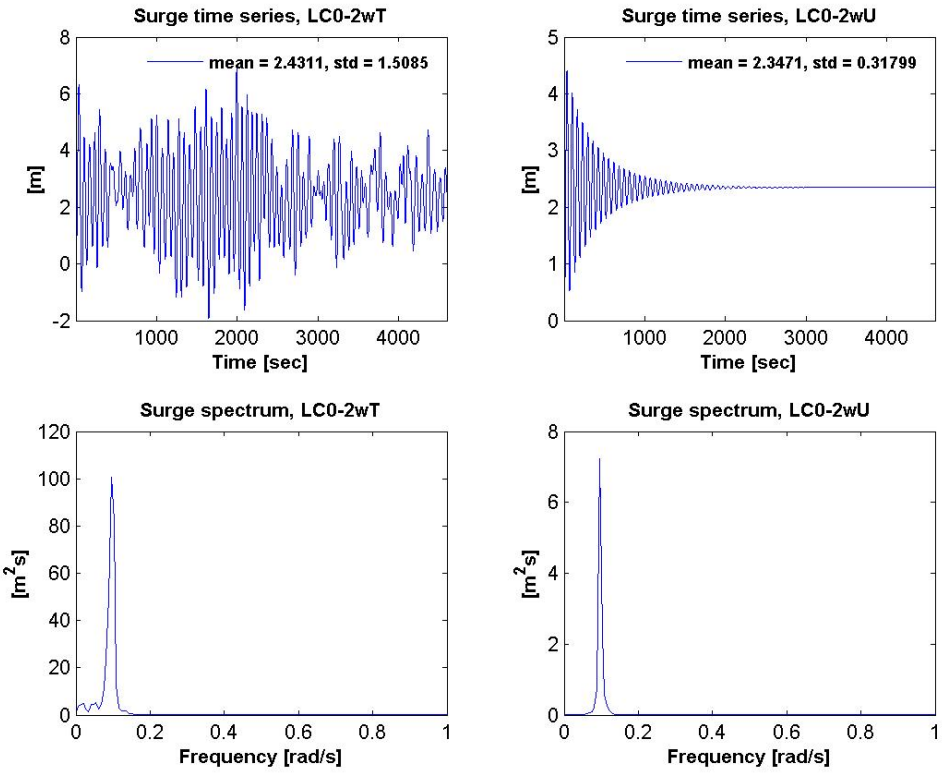

Figure 9.9: Surge response in LC0-2. Turbulent and uniform wind

Again it is seen that the motion is at the surge natural frequency. The wind speed (8m/s) is below rated, meaning that there is no negative damping contribution from the thrust force as were the case for wind speeds above rated. In fact there will be a positive damping contribution from the thrust force. Considering equation (4.18) from section 4.3:

$$Damping = \frac{1}{2}\rho_a U_w A C_{T0}(1+\frac{k_{CT}}{2})$$

The K_{CT} value at a wind speed of 8m/s (figure 4.5) will give a positive value in the bracket and a positive damping contribution. As a result of this the surge motion in the case of uniform wind is seen to decay even faster than in the pure decay test in section 8.2, leaving only a mean surge displacement after about 2000 seconds. A similar behavior was observed in LC0-1 (4m/s wind).

9.4 Combined wind and wave response

In this section the response when both waves and wind are present will be investigated. In section 9.5 the effects of having the notch filter when there are both wind and waves present will be looked into.

9.4.1 Wind and waves from the same direction

In figure 9.10 the response spectra for surge (waterline), heave (waterline), pitch and tension in line (tether) number 7 are shown for load case LC0-1 to 5.

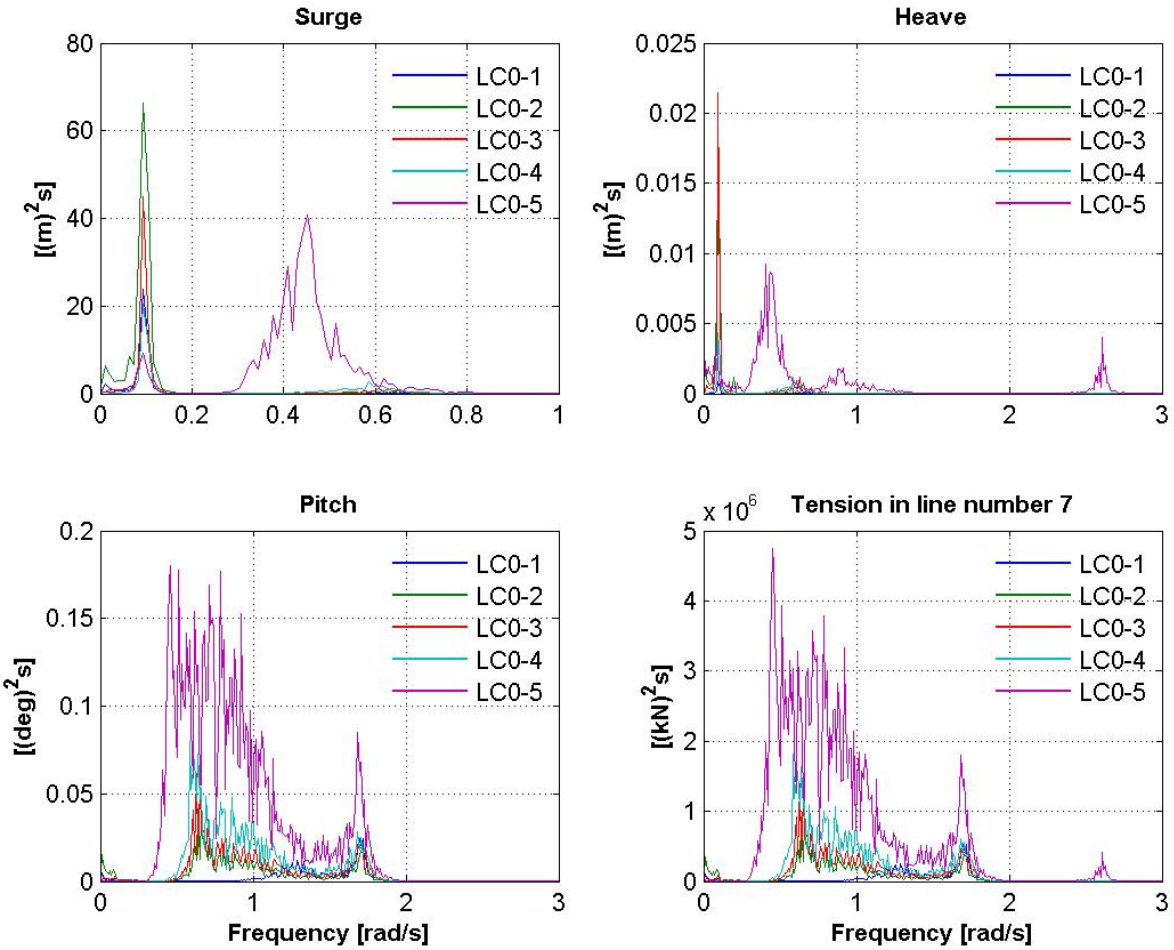

Figure 9.10: Response spectra LC0-1, 2, 3, 4 and 5

In figure 9.11 the wave spectra and thrust force in x-direction on the nacelle are shown to give an idea of at what frequencies the wave and wind forces act.

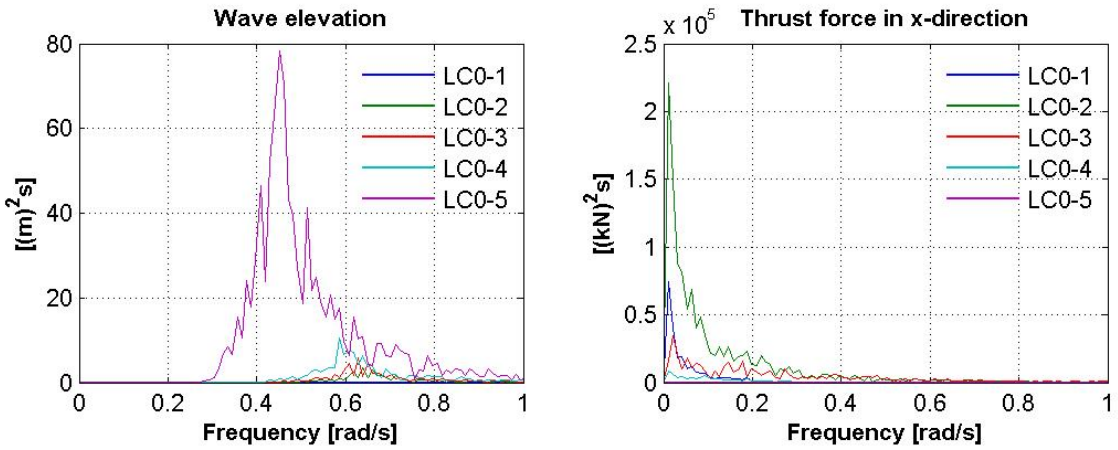

Figure 9.11: Wave and thrust spectra

If we look at the surge motion we see that there is little response in the first order wave frequency range (0.3 – 0.8 rad/s) for all the load cases except load case 5 where the wave frequency range is dominating. In LC0-1 to 4 most of the response is at the surge natural frequency, i.e. slowly varying. The surge response in these cases is mostly dominated by the thrust force on the rotor.

We then turn our attention to the have response. In LC0-1 to 4 most of the response is found around 0.1 rad/s which is the surge natural frequency. This coupling between surge and heave is the so called "set-down effect" or pendulum motion caused by the mooring system. In LC0-5 four contributions to the heave response can be identified; to the left (low frequency) a small peak that is due to the coupling with surge, between 0.3 and 0.8 rad/s response in the energetic wave frequency range and heave resonance at 2.6 rad/s. The peak around 0.9 rad/s is believed to be heave response induced by the pitch wave frequency motion (one periodic pitch motion gives two up and down motions in heave [31]). It should be mentioned that the heave motion is small in all the load cases due to the stiff mooring system, an amplitude of about 0.2 m in LC0-5 was the largest motion observed.

If we look at the pitch response we see that there are contributions around the pitch natural frequency of 1.7 rad/s and at frequencies between 0.3 and 1.5 rad/s. The response between 0.3 and 0.8 rad/s can be explained by being inside the most energetic wave frequency range. Looking at the pitch response transfer function obtained from the HydroD analysis, shows that the TLP is quite sensitive to wave frequencies between 0.8 and 1.5 rad/s, and this explains the large pitch response at these frequencies. The shape of the spectra is similar for all the load cases. The wave frequency part is dominating, indicating that the pitch response is mostly governed by the wave forces. The notch filter was activated, reducing the wind induced pitch resonance in LC0-3 and LC0-4.

By looking at the spectra of the tension in line number 7 and comparing them with the pitch response spectra, we see that the dynamic tension is governed by the pitch motion. In load case 5 a small contribution to the tension at the heave natural frequency is also observed.

Since both wind and waves have the same direction of 0 degrees, the sway, roll and yaw motions are negligible.

9.4.2 Wind/wave directionality

Results from the load cases where the waves are coming from 30 and 90 degrees will now be considered. The results with waves coming from 0 degrees (along the positive x-axis) are also included in the comparison. The wind direction is the same for all the load cases. Response spectra for surge, sway, roll, pitch, yaw and tension in line number 7 (see figure 9.1) are presented in figure 9.12, 9.13 and 9.14.

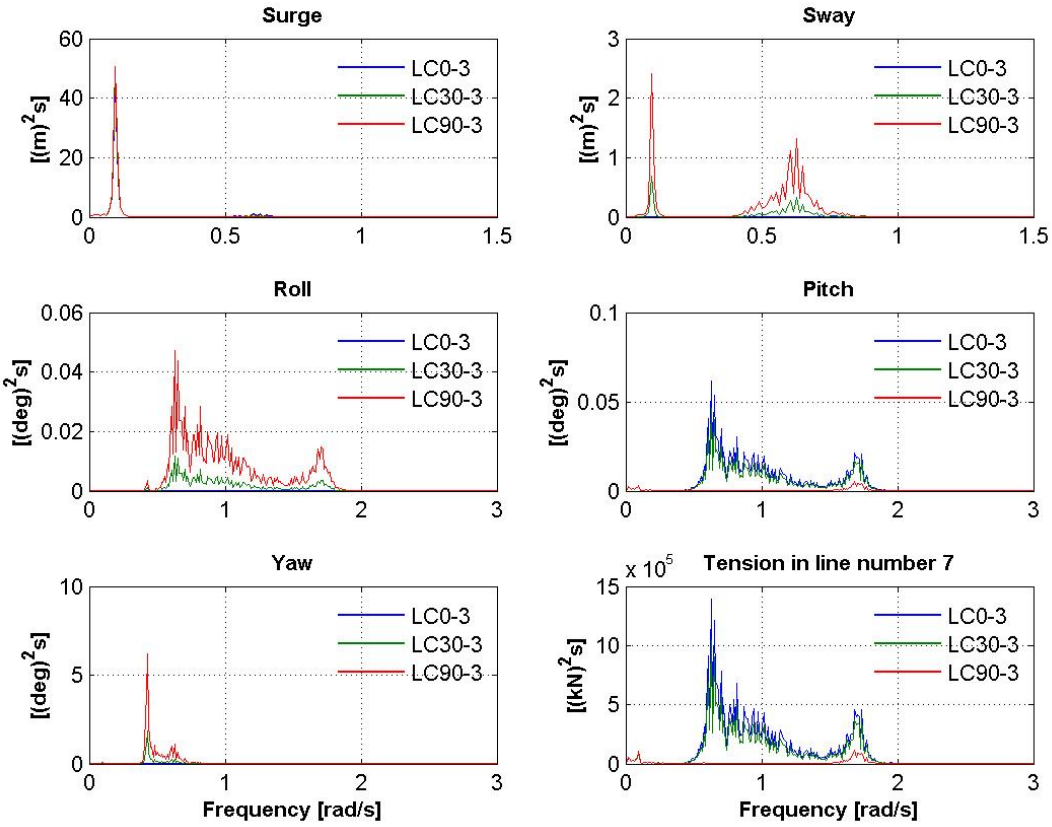

Figure 9.12: Wind and waves from different directions, LC3

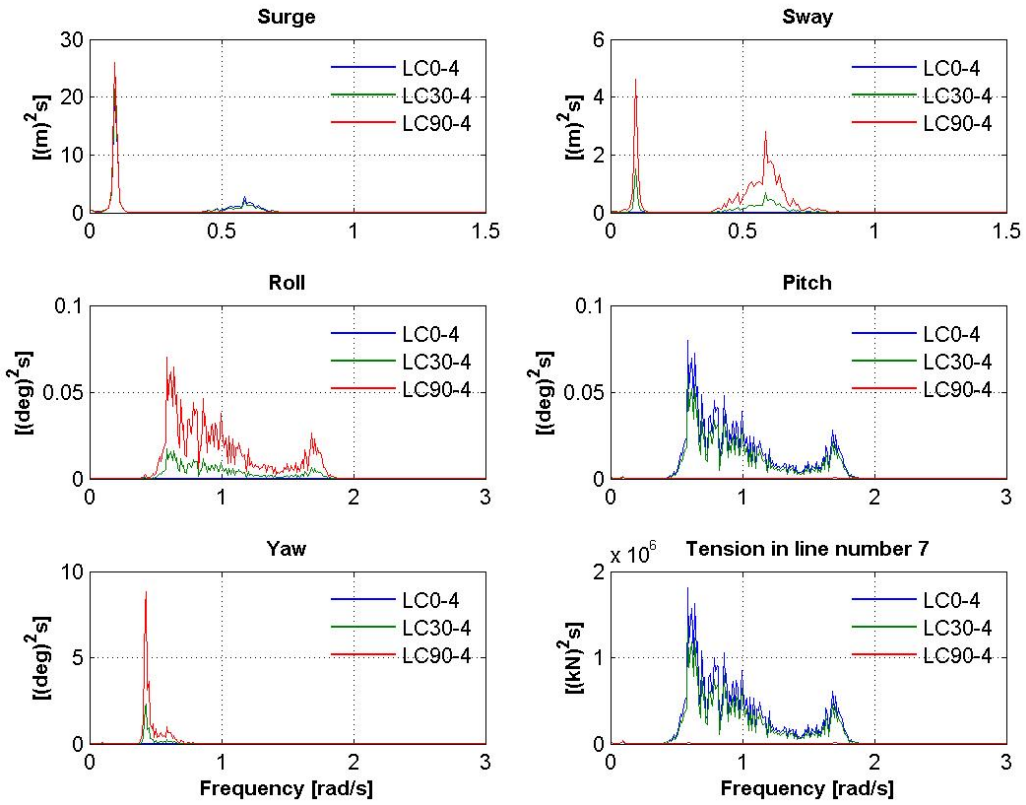

Figure 9.13: Wind and waves from different directions, LC4

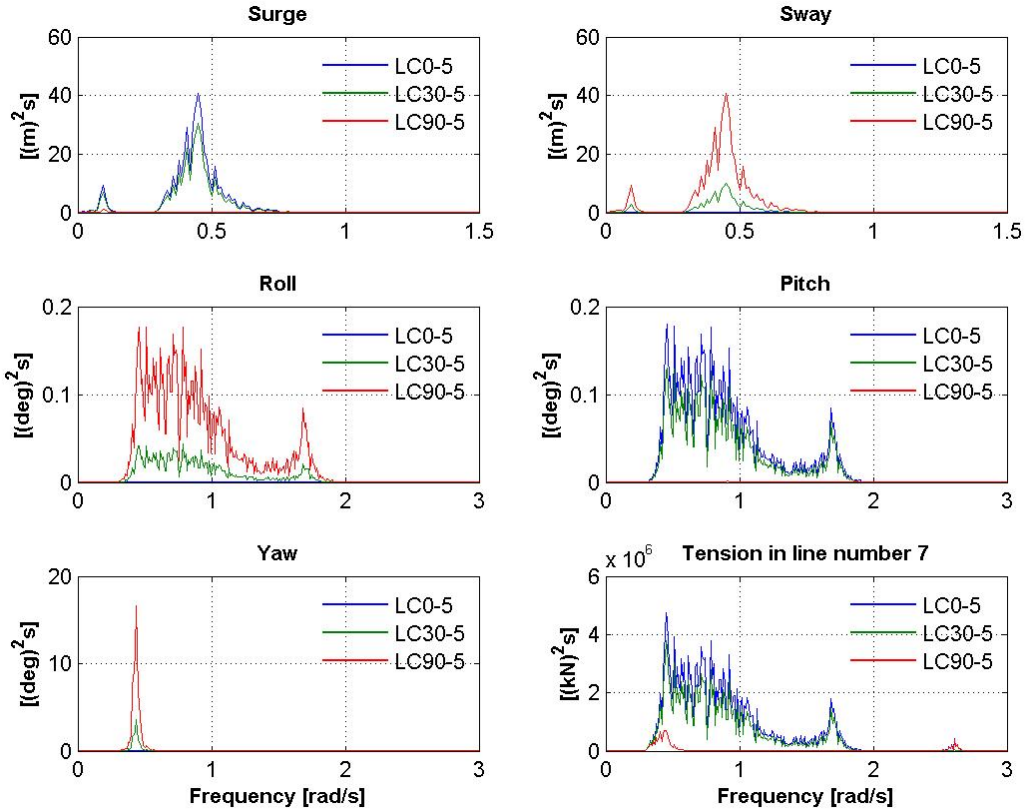

Figure 9.14: Wind and waves from different directions, LC5

The surge motion is not very affected by the change in wave direction under loading conditions 3 and 4. This is because the thrust force on the nacelle dominates the surge response. In load case 5 however, when the rotor is shut down and the waves are large, the surge is dominated by the wave forces and the surge motion is negligible when the waves come from 90 degrees. We then have sway motion instead. The sway motion in load case 3 and 4 is seen to have a contribution in the wave frequency range and a contribution at the sway natural frequency. The latter is caused by the slowly varying (Newman) wave forces. The sway resonance peak is however small compared to the surge resonance peak that is caused by the thrust force at the nacelle in load case 3 and 4.

The roll and pitch motions are mainly caused by the wave forces. This means that the roll response for a wave direction of 90 degrees is similar to the pitch response for wave a direction of 0 degrees. For wave direction 30 degrees the pitch response dominates relative to the roll response, as can be seen from the figures (green line).

The tension in line number 7 is also shown in the figures. The tension spectra are seen to have more or less the same shape as the pitch response spectra. This means that there is little dynamic tension in this line when the waves are coming from 90 degrees. The small peaks seen in LC90-5 are caused by the heave motion (wave frequency range and resonance).

The tension in line number 3 (and 4) is almost the same as in line 7 (and 8), but with a smaller mean value due to the static offset caused by the wind and waves. With a wave direction of 90 degrees the dynamic tension in line 1 and 5 is similar to the dynamic tension in line 7 and 3 with waves coming from 0 degrees. Only the spectra for line 7 are shown in the figures.

There is no yaw motion when the wind and waves come from the same direction (LC0). This is because there is no wave excitation force in yaw due to the cylindrical shape of the substructure. When the wave direction is changed to 30 and 90 degrees, yaw motions are introduced. Also for these directions the wave excitation force in yaw is negligible. The explanation is that for these wave directions the TLP starts to roll. The thrust force that is mainly acting in the global x-direction will then cause a yaw moment. The yaw motion is thus a result of a coupling with roll motion through the thrust force. The yaw natural period is 14.8 s (0.43rad/s). This is within the region of the wave induced roll motions in all the load cases and this explains the yaw resonance peak. Some statistics of the yaw motions are given in figure 9.15.

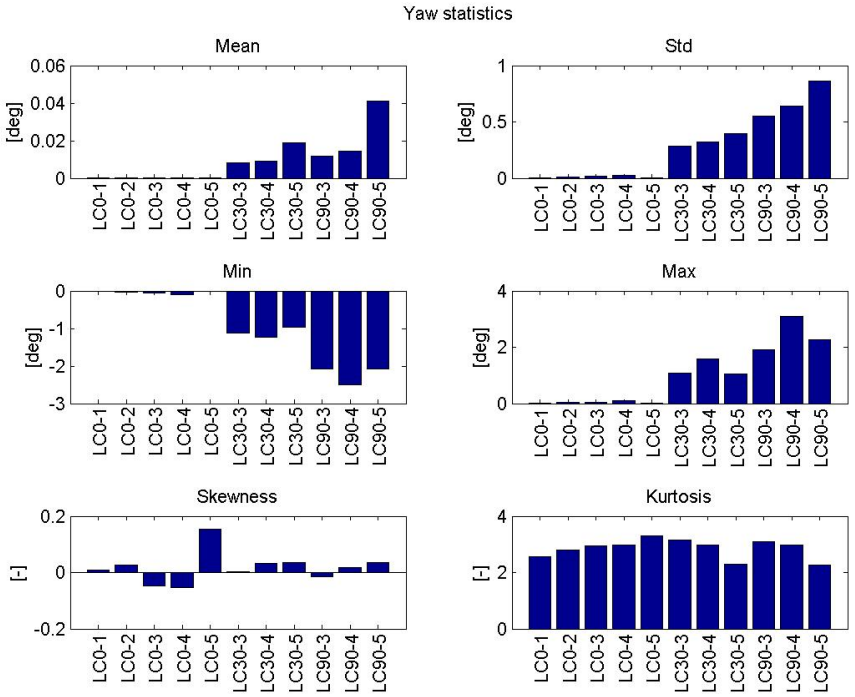

Figure 9.15: Yaw statistics

From this figure we see that there are indeed only yaw motions in the load cases with waves coming from 30 and 90 degrees. The largest yaw amplitude is found in LC90-4 (3.1 degrees). The largest standard deviation is in LC90-5 and this is probably linked with a large standard deviation of the roll motion in this case.

In figure 9.16, 9.17 and 9.18 some statistical values of surge, pitch and tension in line number 7 are summarized for all the 11 load cases.

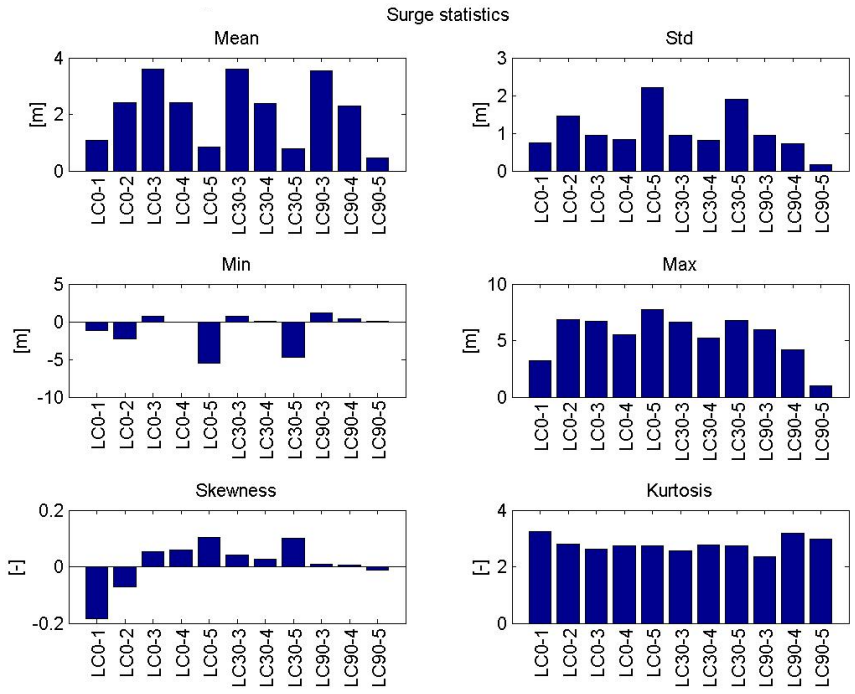

Figure 9.16: Surge statistics

As was seen also in the spectra, the mean surge motion is not very dependent on wave direction since it's mainly the thrust force on the rotor that give this response. The exception is load case 5 where the waves are large. This can be seen by the large standard deviation in LC0-5 compared with LC90-5.

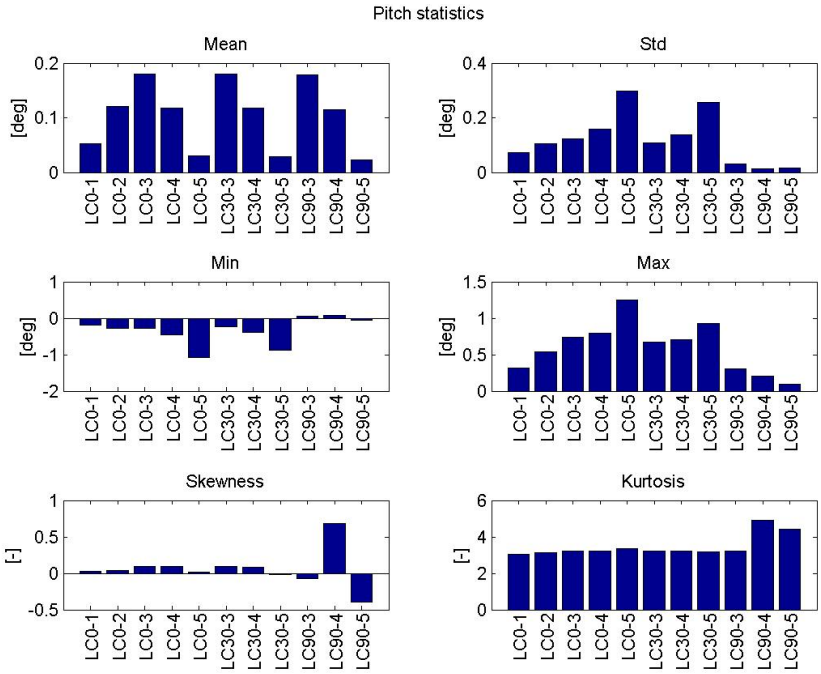

Figure 9.17: Pitch statistics

The mean pitch motion is seen to be independent of wave direction (caused by wind forces). The dynamic pitch motion however is very dependent on wave direction since it is governed by the wave forces as was seen earlier in the spectra.

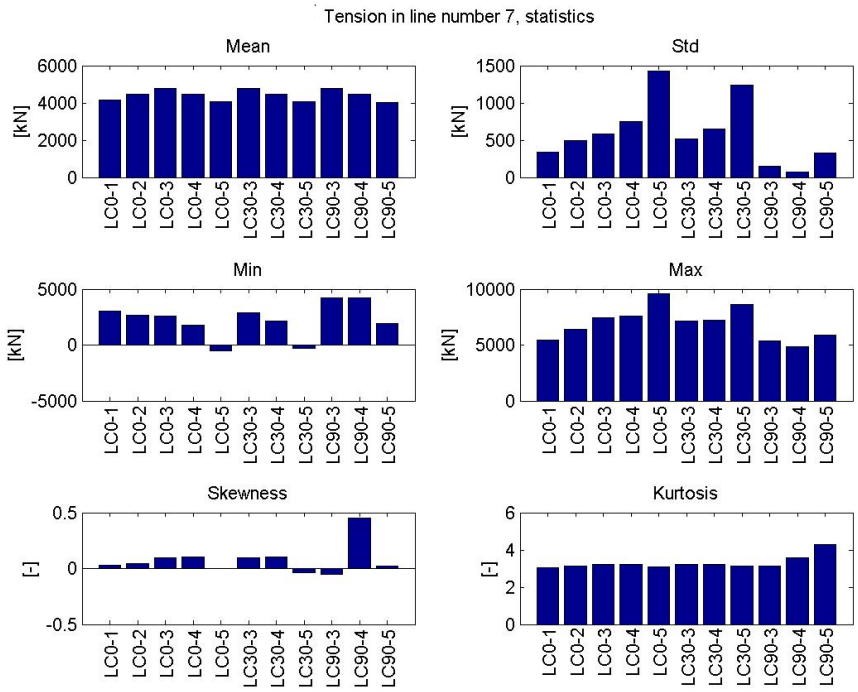

Figure 9.18: Tension in line (tether) number 7, statistics

The Tension in line number 7, which is the windward line, is governed by the pitch motions. The pretension in the line in an unloaded condition is 3917 kN. Due to the mean surge and pitch, this is increased to about 4760 kN in LC0-3, LC30-3 and LC90-3. The maximum tension during the one hour simulation was 9573 kN and the minimum tension was -524 kN, both occurring in LC0-5. The tension thus becomes negative. The problem with negative tension will be discussed in section 9.6.

Statistical values of sway, heave, roll, thrust, power, wave elevation, relative wind speed and tension in line 1, 3 and 5 are given in appendix B. Time series and spectra are given in appendix C.

The skewness and kurtosis are also shown in the figures. In the following a short description of the two parameters will be given. Note that the statistical values in the figures above are obtained from one hour simulations. The statistical uncertainty will be investigated in section 10.

The skewness is the normalized third central moment and is a measure of the degree of asymmetry of a probability distribution:

$$\gamma_1 = \frac{\mu_3}{\sigma^3} \tag{9.1}$$

Where σ is the standard deviation and μ_3 is the third central moment.

A distribution with negative skewness will have a longer left tail and is said to be skewed to the left. A positive skewness means that the right tail is longer and the distribution is then skewed to the right. A probability distribution with the mean equal to the median and zero skewness is symmetric. Positive and negative skewness is illustrated in figure 9.19.

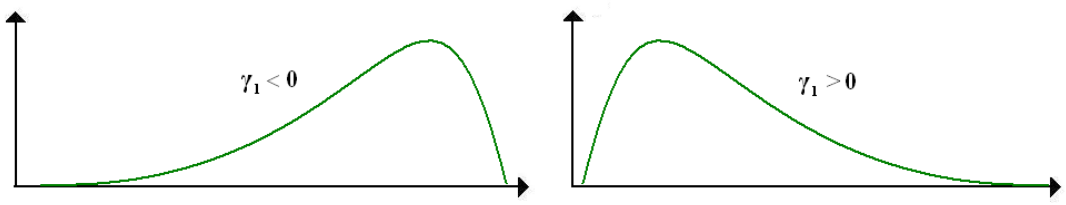

Figure 9.19: Negative and positive skewness

The kurtosis is the normalized fourth central moment:

$$\gamma_2 = \frac{\mu_4}{\sigma^4} \tag{9.2}$$

For a normal distributed variable the kurtosis is 3. A kurtosis larger than 3 indicates that the distribution is peaked relative to the normal distribution and a value smaller than 3 indicates a flat distribution. The kurtosis is therefore the degree of peakedness (or flatness) of a distribution relative to the normal distribution.

9.5 Effect of having notch filter in combined wind and wave loading

The effect of having the notch filter when there is only wind present was examined in section 9.2. The effect was large at the rated wind speed where the system was shown to be unstable without the filter applied. In L0-4 the effect of the filter was also visible, giving a reduction in pitch standard deviations of about 10%. To really asses how the filter performs in more realistic conditions it would be interesting to see how it works in combined wind and wave loadings.

In table 9.3 the mean, standard deviation, minimum and maximum values of the pitch motion is listed for different load cases with and without the notch filter activated. The notch filter is only used in LC3 and LC4 where the mean wind speed is rated and above rated and the rotor is turning.

	Pitch [deg]			
	Mean	**Std**	**Min**	**Max**
LC0-3 Notch on	0.1802	0.1242	-0.2768	0.7381
LC0-3 Notch off	0.1796	0.1470	-0.5109	0.8381
LC0-4 Notch on	0.1178	0.1594	-0.4572	0.7962
LC0-4 Notch off	0.1179	0.1635	-0.4788	0.8110
LC30-3 Notch on	0.1801	0.1088	-0.2229	0.6725
LC30-3 Notch off	0.1795	0.1324	-0.4723	0.7949
LC30-4 Notch on	0.1174	0.1383	-0.3849	0.7035
LC30-4 Notch off	0.1175	0.1418	-0.4037	0.7155
LC90-3 Notch on	0.1790	0.0315	0.0592	0.3038
LC90-3 Notch off	0.1787	0.0663	-0.2000	0.5101
LC90-4 Notch on	0.1153	0.0128	0.0714	0.2097
LC90-4 Notch off	0.1153	0.0141	0.0664	0.2173

Table 9.3: Effect of having notch filter on pitch response

In LC0 and LC30 the pitch motion is significantly larger than it was in section 9.2, where there was only wind present. In LC90 the pitch response is similar to the only wind case since the waves now are propagating along the y-axis and only contribute to the roll motion. The notch filter will only reduce the wind force induced pitch motion, meaning that the percentage decrease in standard deviations in LC0 and LC30 is small since most of the dynamic pitch response is caused by the wave loads. The effect of having the filter is largest in LC3 where the system has an unstable behavior due to the negative damping contribution from the thrust force. In LC0-3 a reduction of 15.5% in the standard deviation is observed. In LC0-4 a reduction of 2.5% in the standard deviation is observed. The decrease in the min/max pitch angle will have a good effect on the min/max tension in the tension legs.

To give a clearer picture of how the notch filter affects the response, the pitch time series, pitch spectra, and thrust spectra in LC0-3 and LC0-4 with and without the notch filter activated is given in figure 9.20.

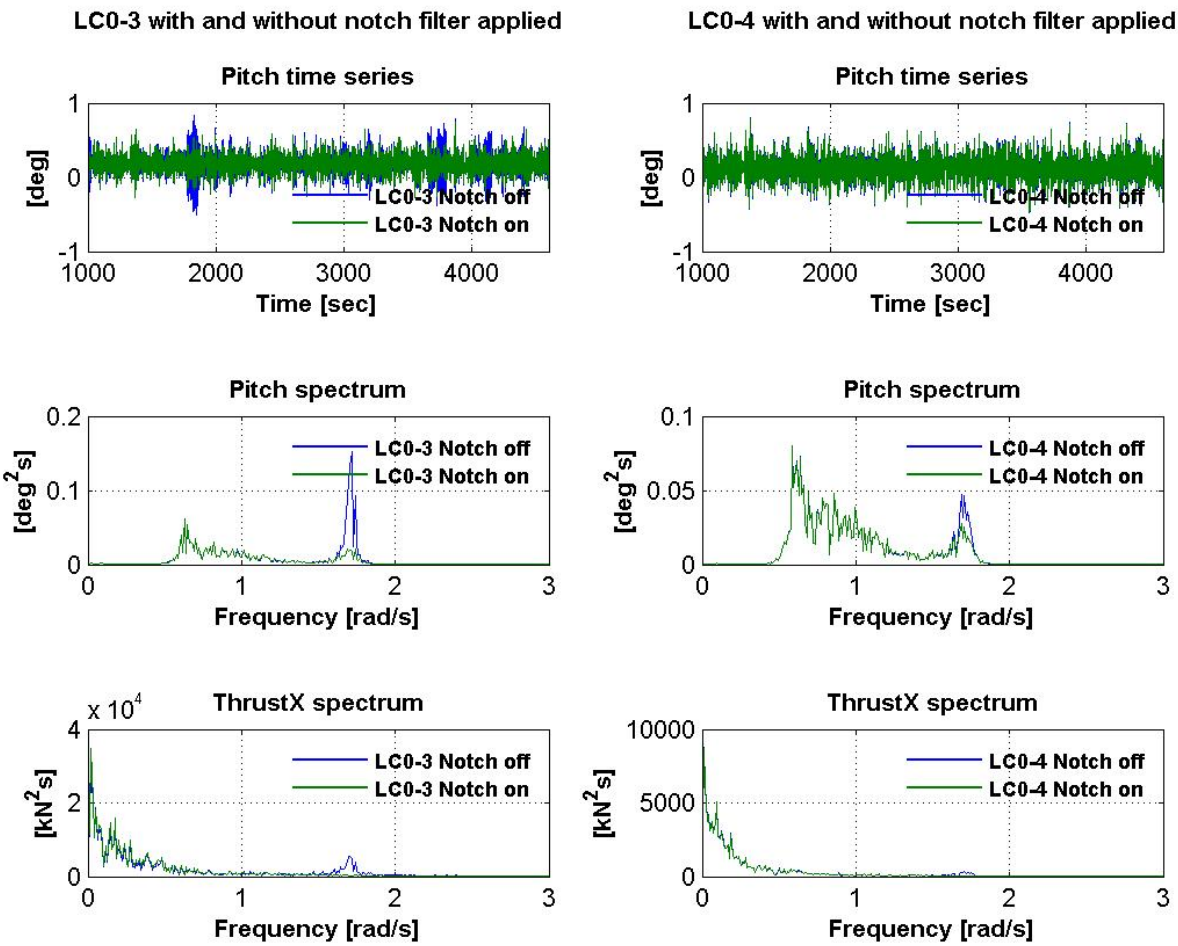

Figure 9.20: Pitch and thrust in LC0-3 and LC0-4 with and without the notch filter activated

From the pitch time series in LC0-3 we see the unstable behavior without the notch filter activated. The reduction of the dynamic response is seen from the pitch spectra to be at the pitch natural frequency (1.7 rad/s). This is because it is the nacelle velocity at this frequency that is filtered. In the spectra of the thrust force it is also possible to see a peak at the pitch natural frequency when the filter is off. The thrust is calculated based on the relative wind speed at the nacelle, and without the filter the pitch motions will give a variation in the thrust force at this frequency.

9.6 Problem with negative tensions in the mooring system

In section 9.4 it was seen in figure 9.18 that the tension in the mooring lines (tethers) becomes negative in the most severe load cases. The line considered in this figure was the windward line, meaning that it gets its mean tension increased by the wind thrust force. The negative tensions are therefore larger in the lines on the opposite side of the structure (line 3 and 4). The fear is that the lines will go slack with subsequent snatch loads that might be detrimental to the mooring system.

In figure 9.21 the time series of the tension in line number 3 in LC0-5 is shown. To the right in the figure a part of the time series is enlarged to better see how the tension varies when it becomes negative.

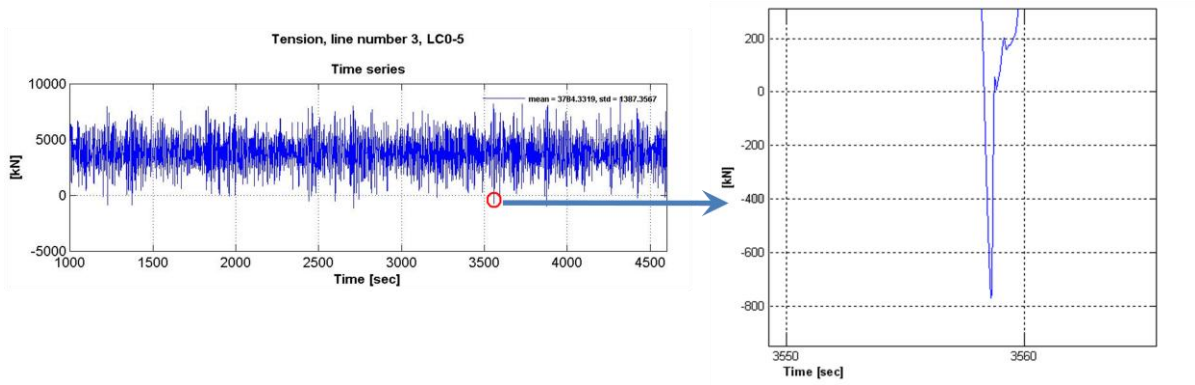

Figure 9.21: Tension time series, line number 3, LC0-5

The value of the negative tension is about -800 kN. What is interesting is that the tension is negative only for about 0.4 seconds. Due to the large inertia of the structure one might therefore argue that the short time the tension is negative isn't enough to cause severe snatch loads. This is something that has to be investigated further.

According to DNV Structural design of TLPs [32], temporary loss in tension is acceptable provided that at least one line per corner of the structure remains non-negative and a comprehensive redundancy analysis is performed to evaluate the effect of loss of tension. The TLP fails the requirement of having at least one line per corner with positive tension. However the standard also states that temporary (high frequency cycle) tension loss might be permitted if a dynamic analysis evaluating the effect on the complete mooring system and supporting structures is conducted. Alternatively model tests may be used. A comprehensive redundancy analysis to demonstrate structural integrity is beyond the scope of this thesis

The best solution would probably be to avoid the negative tensions. One way to overcome the problem is to increase the pretension in the lines to make sure that they never go slack. This can be achieved by increasing the submerged volume of the structure, but that will result in larger wave forces and increased costs. Another possibility is to remove some of the concrete ballast in the bottom of the substructure. This would require a different installation procedure than the stable float-out without the mooring system attached, which the system is designed for at this stage. A different approach is to increase the length of the spokes holding the tethers. Longer spokes will give larger pitch and roll restoring and smaller dynamic tension amplitudes. A combination of the possible solutions mentioned above could also be the best way to do it and many iterations in a design optimization is therefore needed to find an overall better concept.

10. Statistical uncertainty in the simulations

In order to study the statistical variation of the wind/wave simulations and the responses, LC0-3 and 4 have been simulated with different seed numbers for the wind and wave generation. A total of 10 simulations with different seeds have been performed for each load case. As before the simulation length was 4600 seconds, with 1000 seconds cut-off in order to avoid transient effects.

Using different seed numbers will give different realizations of the wind and wave time series and the statistics; mean, standard deviation, min, max, skewness and kurtosis will differ from simulation to simulation. Skewness and kurtosis was explained in section 9.4.

It is common to subtract 3 from the kurtosis in order to make the value for the normal distribution equal to zero. This is called excess kurtosis. A positive excess kurtosis indicates that the distribution is peaked relative to the normal distribution and a negative value indicates a flat distribution. This will be done here in order to increase the readability of the figures.

We will now look at the cumulative averages of the statistical properties mentioned above. LC0-4 is considered. In figure 10.1 the wave elevation, wind at the nacelle, pitch, tension in line number 7, surge motion in the waterline and heave motion in the waterline are considered.

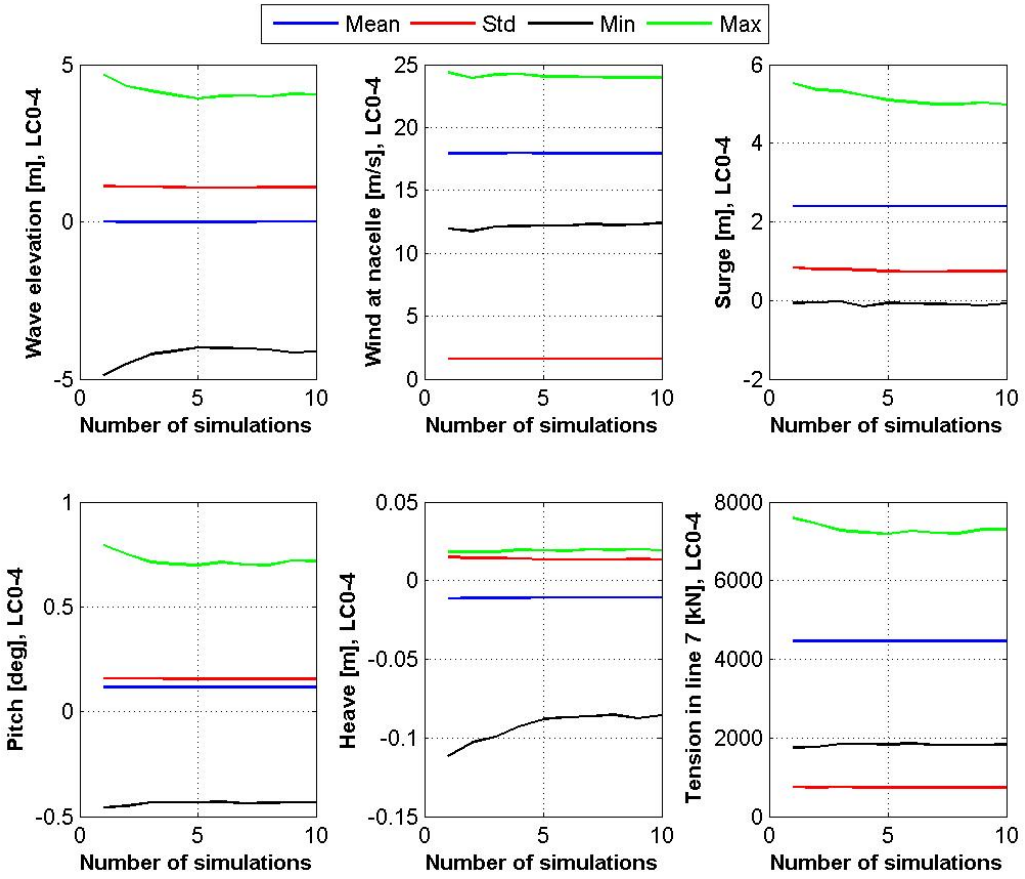

Figure 10.1: Cumulative averages of statistics from LC0-4

The cumulative average is the average off all data up to the current data point, meaning that the value at “Number of simulations” = 5 is the sum of the values in the five first analyses, divided by five. The cumulative averages provide an indication of how many simulations are required for the values to become stable.

From the figure we can see that the values of the mean and standard deviation are affected little by including more simulations. This can be explained by the fact that these values are based on many sample points in the time series. If the simulation length is long enough, the difference between simulations will be small. It can then be concluded that the simulation length of one hour is long enough to obtain the correct values of the mean and standard deviations.

The maximum and minimum value obtained from a simulation is the single largest and smallest peak and valley in the whole one-hour time series. From the figures it is seen that there exists some differences between the different simulations. For the wave elevation, surge and heave the average values stabilizes after about five simulations. The pitch and tension values stabilizes after about three simulations. Running more simulations than this is not going to affect the average maximum values. Instead of running 5 one-hour simulations with different seeds, a single five-hour simulation could be used.

An alternative to calculating the mean of the individual extremes from the set of simulations is to establish an extreme value distribution for the different response parameters [33]. The extreme value distribution will approach a Gumbel distribution for increasing number of maxima obtained. The mean values calculated above will correspond to the expected maximum in such a distribution [33]. We will not go into details about this here.

In figure 10.2 the cumulative averages of the skewness and excess kurtosis of the variables considered are shown.

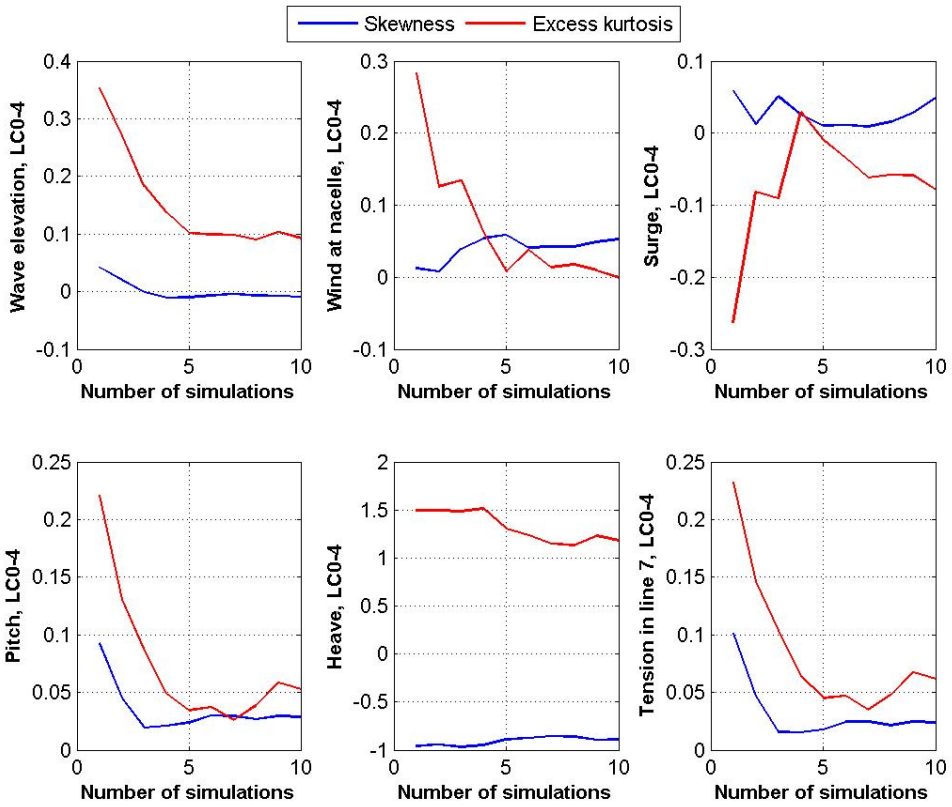

Figure 10.2: Cumulative averages of skewness and excess kurtosis from LC0-4

From the figure it can be seen that the number of simulations necessary to get stable average values is about 5. At least this is the case for the wave elevation, pitch and tension. To give any conclusions regarding the other responses considered, more simulations are needed in order to see what happens. Skewness and kurtosis are known to be difficult to predict and are not very important to us. The mean, standard deviation, max and min discussed earlier are more interesting. Disregarding the heave, we see that the excess kurtosis of the parameters is close to zero. This indicates that they follow a normal distribution. The skewness values are small, but mostly on the positive side indicating a tendency that the right tail of the distributions is the longest.

Important to the convergence of the statistics is the number of cycles in a given time frame. In 10.1 we saw that the slowly varying surge and heave motions required about 5 simulations (5 hours) before stable average maximum and minimum values were obtained. In the case of the pitch and tension, which have a dominant period in the wave frequency range (about 10 s), 3 simulations were enough. The mean and standard deviations were accurately determined after just one simulation. The results discussed in section 9 were obtained from one-hour simulations. It is important to be aware that the min/max values presented there, suffer from the simulation time dependency discussed here. Cumulative averages of the statistics in LC0-3 are given in appendix E.

11. Comparison of TLP, spar and semi-submersible

The TLP will now be compared with a spar buoy and semi-submersible type of concept. The spar and semi-sub is designed to support the same 5.2 MW wind turbine as the TLP. Time domain simulations of the spar have been conducted by Solberg [34] and simulations of the semi-sub have been conducted by Luan [35]. They have used the same versions of DeepC, SIMO and RIFLEX that was used for the TLP. The eleven load cases including both wind and waves that was defined in section 9.1 have been performed for all the concepts. The simulation length of 4600 seconds with 1000 seconds cut-off in the beginning is also the same. This together with the same "random" seed number for wind and wave generation should mean that the different concepts are exposed to the more or less the same environmental loadings. At wind speeds above rated (LC3 and LC4), the notch filter was activated. The notch filter is set to filter at the pitch natural frequency of the different concepts.

11.1 Properties of the spar and semi-sub.

Detailed descriptions of the spar and semi-sub can be found in the master thesis of Solberg [34] and Luan [35] respectively. Here only a brief description will be given. The Spar and semi-sub are shown in figure 11.1.

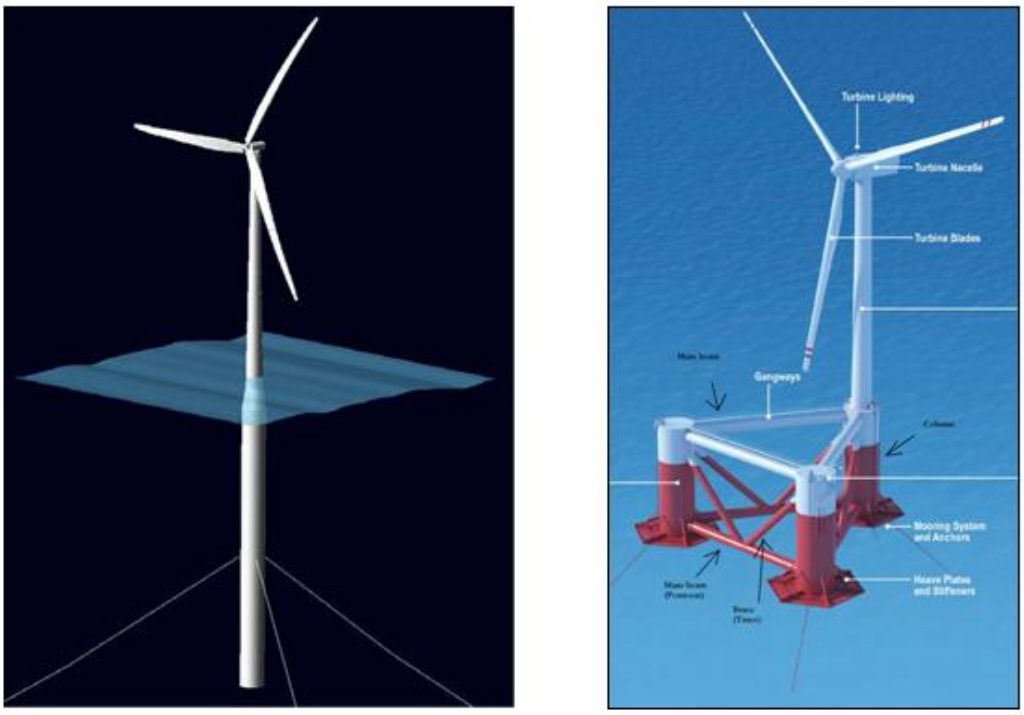

Figure 11.1: Spar [2] and semi-submersible [35]

The spar and semi-sub use catenary mooring systems. The spar has three lines and the semi-sub has four. These mooring systems give them natural periods in heave, roll and pitch that are much larger than the natural periods of the TLP. The spar and semi-sub rely on these natural periods being above the wave period range, whereas the TLP rely on them being below the wave period

range. All three concepts have the mooring system modeled by a finite element model in RIFLEX.

The semi-sub is composed of three main columns that are attached to each other by braces to give sufficient structural stiffness. The columns have a diameter of 10 m and the distance from the center in a column to the center in another is 46 m. Hexagonal heave plates are attached to the bottom of the columns to provide extra damping. The semi-sub is designed to have an active ballast system that transfer water between the columns in order to keep the mean angular motion of the tower vertical. This system was not included in the computer simulations conducted by Luan [35].

The spar buoy consists of a single column with a diameter ranging from 6.5 to 9.4 m (tapered). During installation, before the mooring system is installed, the TLP is designed to work as a spar buoy, obtaining its stability by having a low center of gravity.

In table 11.1 some of the main dimensions of the three concepts are given:

	TLP	**Spar**	**Semi-submersible**
Draft	47.89 m	120 m	17 m
Center of gravity	-32,59 m	-77 m	3,73 m
Mass including ballast	9297 tons	8111 tons	4640 tons
Displacement	12187 m^3	8029 m^3	4540 m^3
Nacelle height	90 m	90 m	89 m
Water depth	200 m	320 m	325 m

Table 11.1: Main dimensions of the three concepts

Notice that they are not placed at the same water depth. The concepts will probably perform differently at other depths. The comparison given here will not address this. How the TLP performs at shallower water depths will be investigated in section 12.

11.2 Natural periods

In table 11.2 the natural periods and frequencies of the three concepts are given.

	TLP		**Spar**		**Semi-submersible**	
	Period [s]	Frequency [rad/s]	Period [s]	Frequency [rad/s]	Period [s]	Frequency [rad/s]
Surge	65	0.097	125.27	0.050	134.7	0.047
Sway	65	0.097	125.20	0.050	147.6	0.043
Heave	2.4	2.618	31.3	0.201	20.5	0.306
Roll	3.68	1.707	31.15	0.202	45.1	0.139
Pitch	3.68	1.707	31.14	0.202	44.3	0.142
Yaw	14.8	0.425	8.22	0.764	63.1	0.100

Table 11.2: Natural periods of TLP, spar and semi-sub

Compared with the TLP the spar and semi-sub have much higher natural periods in heave roll and pitch due to their soft mooring systems. In surge and sway the TLP have a natural period that is about 50% of the natural periods of the other concepts. When it comes to yaw motion, the semi-sub stands out with the highest period.

11.3 Comparing different response parameters

Based on the time domain simulations that have been performed on each concept, statistical values have been calculated and compared for different parameters. The parameters considered is the global surge, sway and heave motions in the waterline, roll, pitch and yaw rotations, surge and sway at the nacelle, accelerations in global x and y-direction at the nacelle, tension in two of the mooring lines, wind velocity, relative wind velocity at the nacelle before and after notch filtering, thrust and power. The mean, standard deviation, maximum value, minimum value, skewness and kurtosis of all these parameters in the eleven load cases are presented in appendix D. The statistics are calculated from one hour simulations and there is believed to be some statistical uncertainty, as was investigated for the TLP in section 10. Especially the correct values of skewness and kurtosis are difficult to obtain from such short samples. Still the values are believed to be accurate enough to make it possible to give a rough comparison between the concepts. In the report we will focus on only a selection of the parameters mentioned above.

11.3.1 Pitch

In figure 11.2 the mean values and standard deviations of the pitch response in the 11 load cases for the three concepts are given. The minimum values, maximum values, skewness and kurtosis can be found in appendix D.

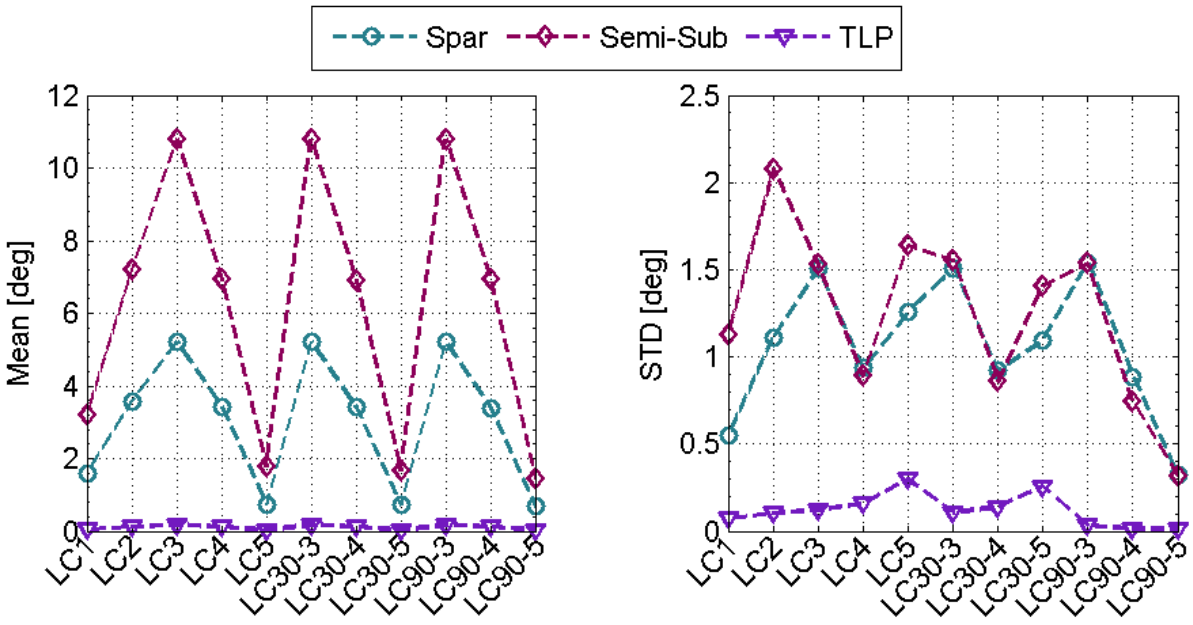

Figure 11.2: Comparison of the pitch response of the three concepts

As expected the TLP has very small pitch response compared with the spar and semi-sub. This is due to the stiff mooing system of the TLP. All the concepts have the largest (max) pitch motion in LC3 (rated) where the mean wind thrust force is at its largest. The semi-sub has quite large mean pitch motions, but this is without the active ballast system activated. If the active ballast system was included in the analysis the mean angular motions would have been reduced. The ballast system will however not try to reduce oscillations in roll and pitch due to wave and turbulent wind excitation. Note that the standard deviation of the pitch motions of the TLP increase with increasing significant wave height. The spar and semi-sub on the other hand have the largest

dynamic pitch motions in LC3 and LC2 respectively, indicating that they are more dependent on the wind loadings than the TLP, which is mostly governed by wave forces. The fact that the semi-sub has the largest pitch standard deviation in LC2, and not in LC3 like the spar, indicates that it's more sensitive to high turbulence intensities in the wind.

The TLP also have small motions in heave and roll compared with the spar and semi-sub. This again is due to the restrictions of the mooring system.

11.3.2 Yaw

The mean values and standard deviations of the yaw motions are given in figure 11.3.

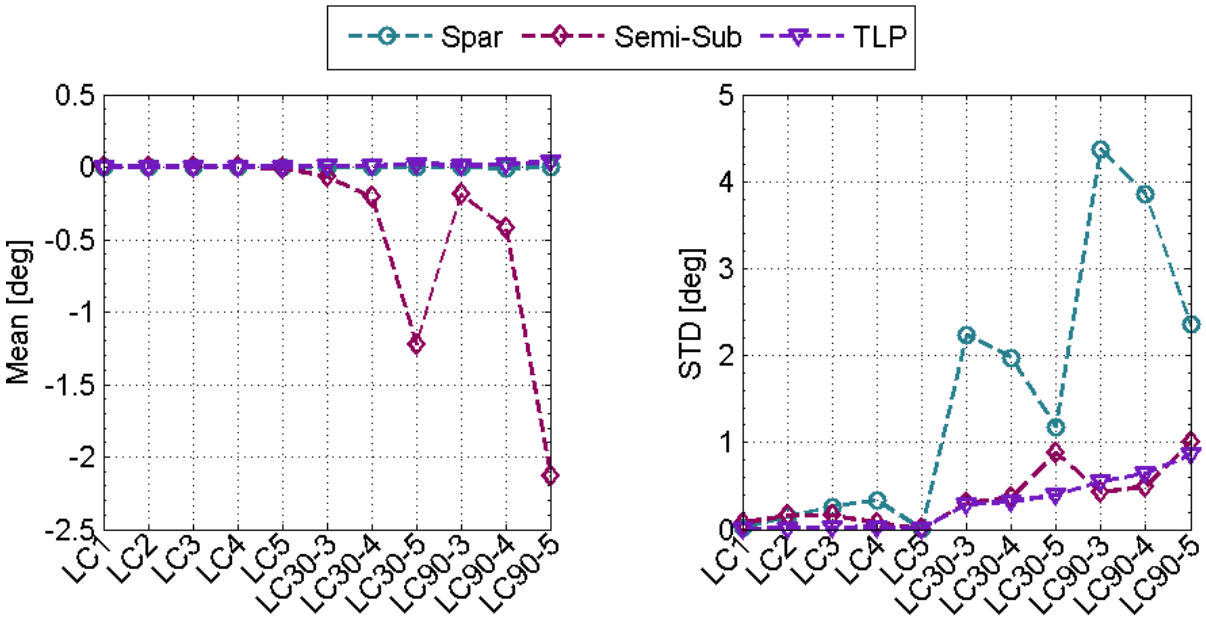

Figure 11.3: Comparison of the yaw response of the three concepts

The semi-sub is seen to have the largest mean yaw rotation of about 2 degrees. This occurs when the wind and waves are coming from different directions in LC90-5. The TLP and spar at least will have no yaw excitation from the waves due to their cylindrically shaped substructures. The yaw moments are a result of a coupling with roll motion through the thrust force. The explanation to the large dynamic yaw motions of the spar is that it has a yaw natural period of 8.22 seconds, and this is well within the wave induced roll motions. The largest yaw angle in the one hour simulation was 17 degrees. Increasing the yaw stiffness of the mooring system will according to Solberg [34] greatly reduce the dynamic yaw motions of the spar.

11.3.3 Wind, power and thrust

The statistics are given in appendix D. As expected there is no observable difference in the statistics calculated from the wind time series used on the different concepts. When it comes to the relative wind speed at the nacelle it is observed that the spar has the largest standard deviations, at least in the load cases where the wind speed is rated or higher. The relative wind speed is a result of the surge and pitch induced motions of the nacelle. The relative wind speed that the wind turbine "reacts" to, the notch filtered wind speed, is however more or less the same for the three concepts indicating that the spar has good use of the notch filter.

Looking at the thrust and power production statistics it is seen that in LC0-2 the TLP have the largest thrust standard deviation and the semi-submersible have the smallest power standard deviation. In the other load cases the standard deviations are quite similar and the mean values are also the same. All in all there is little difference between the concepts when it comes to these parameters.

11.3.4 Mooring line tension

The mean values, standard deviations, minimum and maximum values of the tension in one of the mooring lines of each concept is presented in figure 11.4. The mooring line is named line #2 and for the TLP it is the windward line (tether) number 7, see figure 9.1. For the spar and semi-sub we are also looking at one of the windward lines as can be seen from the increase in mean tension when the wind thrust force increases.

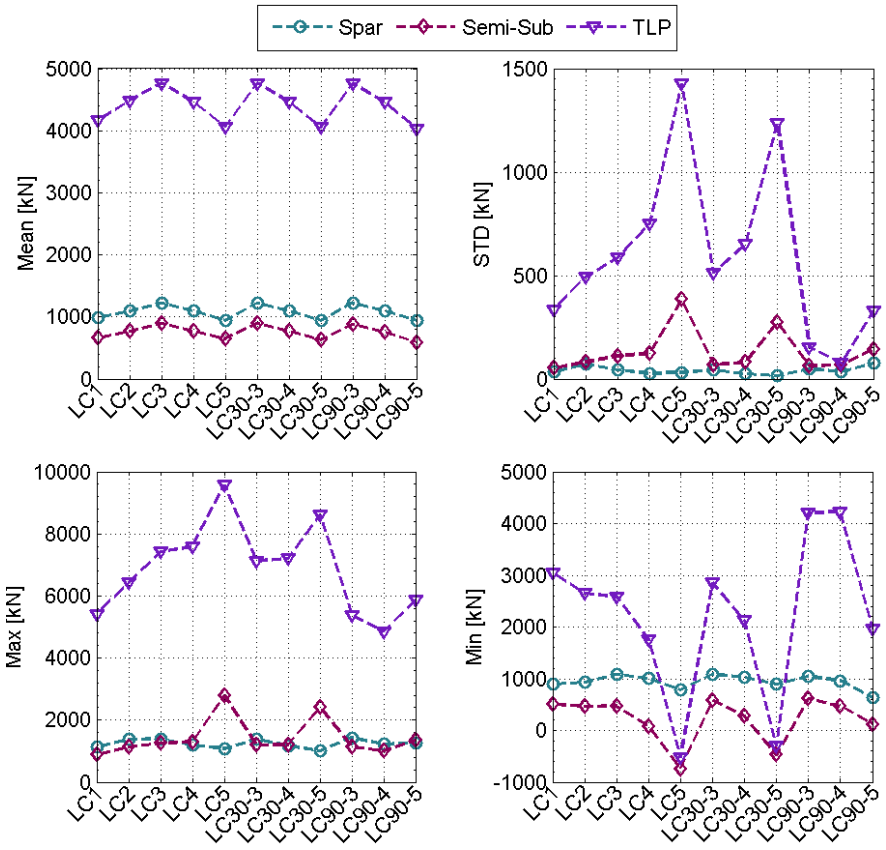

Figure 11.4: Comparison of the windward mooring line tension of the three concepts

The mooring system of the TLP obviously has larger tensions than the catenary mooring systems of the spar and semi-sub. If we consider the spar and semi-sub we see that the semi-sub has the smallest mean tensions and that the standard deviations of the semi-sub are especially large compared with the spar when the waves are large. This is probably due to large wave induced motions of the semi-sub since it has a large structural volume located close to the free surface.

Turning our attention to the minimum values of the tensions obtained from the simulation, we see that in LC0-5 and LC30-5, the TLP tension becomes negative. This might be a serious problem if we get large snatch loads that cause the tether to fail and was discussed in section 9.6. It is more surprising that the semi-sub also experiences negative tensions of up to 850 kN in the same load cases. This should not be possible for a catenary mooring system and indicates that there is a problem with how negative tensions are dealt with in the computer model.

In the future, fatigue life calculations should be performed to better be able to compare the mooring systems of the three concepts. The standard deviations of the tension might offer some indications about fatigue life, but no detailed analysis considering the stress oscillations in the lines have been conducted at this stage.

11.3.5 Nacelle accelerations

A very important parameter in assessing what type of concept that is best suited to be the support structure of the wind turbine is the accelerations at the nacelle. Statistics of the nacelle accelerations in the global x-direction are given in figure 11.5.

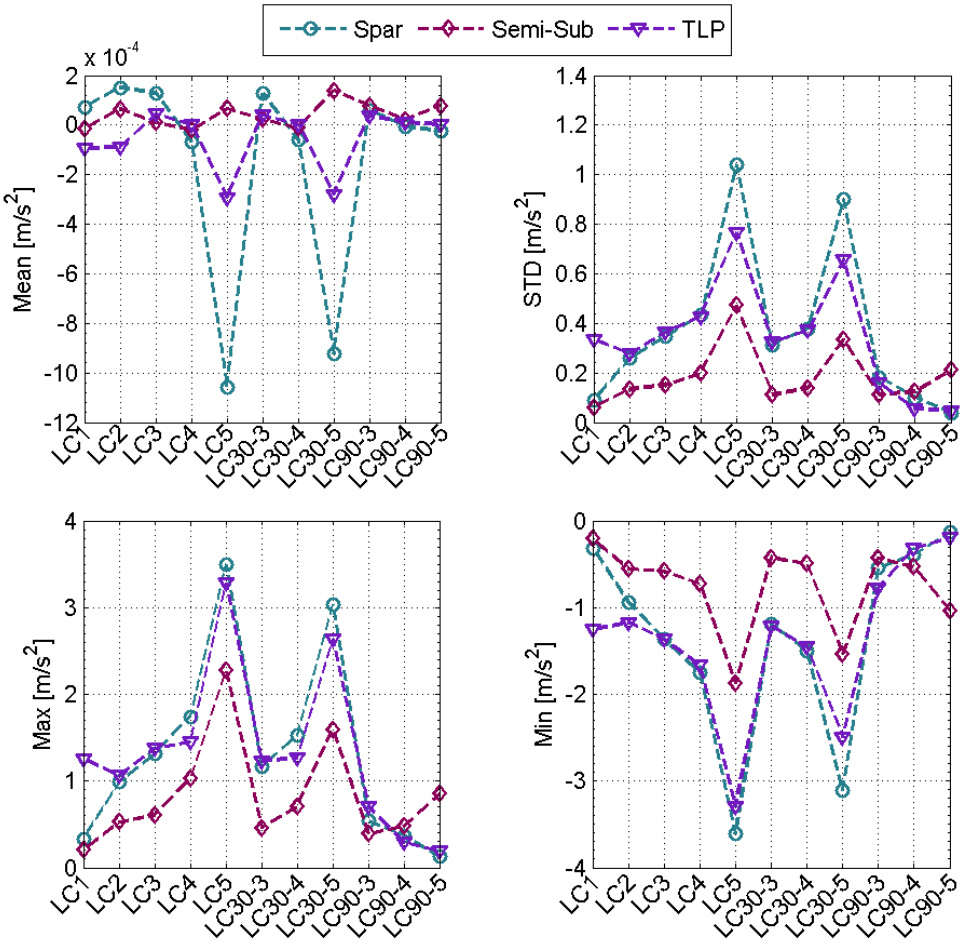

Figure 11.5: Comparison of the nacelle accelerations in x-direction of the three concepts

Note that the mean values of the accelerations are very small; there is a factor of 10^{-4} on the y-axis. By looking at the standard deviations, minimum and maximum values, it is clear that the semi-sub has the smallest nacelle accelerations as long as there is not a very large difference in the wind/wave directions. In LC0-5 and LC30-5 the spar has the largest accelerations, and in LC0-1 the TLP has the largest accelerations. In LC0-1 the peak period is only 5 seconds and the large accelerations of the TLP compared with the other concepts are caused by resonant pitch motions. The accelerations at the nacelle are important to the drive train of the wind turbine and manufactures normally specify maximum recommended nacelle accelerations. The nacelle accelerations are also important when it comes to forces and thereby fatigue life time of the tower structure. The forces in the tower structure arise from three main contributions; the moment caused by the inertia force on the nacelle and rotor rue to nacelle accelerations, moment due to the thrust force and the moment that is caused by the weight of the nacelle and tower when the structure leans to the side due to roll and pitch motions.

Neglecting the yaw motions, the nacelle acceleration in x-direction can be expressed by the surge and pitch acceleration, Faltinsen [8]:

$$\ddot{s} = \ddot{\eta}_1 + z\ddot{\eta}_5 \tag{11.1}$$

Here z is the vertical distance between the rotation center and the nacelle. The spar buoy has a very low center of gravity and will have a large contribution to the surge motions at the nacelle from the pitch motions.

It is somewhat surprising that the semi-sub has the smallest nacelle accelerations. If we look at the response spectra in figure 11.6, we see that in LC0-5 the semi-sub have almost the same dynamic waterline surge motions as the spar and TLP. It also has the largest dynamic pitch motions. It would be reasonable to think that this would lead to large accelerations at the nacelle, but this is not the case and it is seen that the area under the surge motion spectrum and acceleration spectrum at the nacelle is small compared with the spar and TLP. This might be explained by a cancellation effect between the pitch and surge motion.

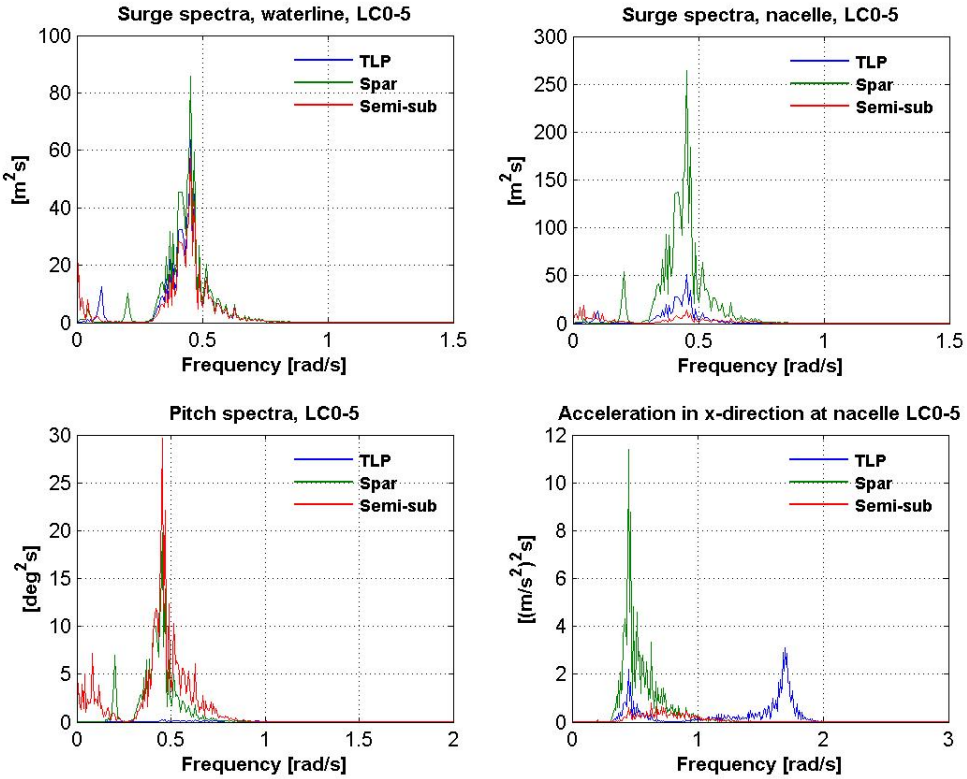

Figure 11.6: Surge, pitch and nacelle acceleration spectra of the three concepts in LC0-5

From the spectra it is also seen that the TLP has very small dynamic pitch motions compared with the other concepts. Still, significant nacelle accelerations of the TLP are observed around the pitch natural frequency of 1.7 rad/s. The explanation is that this high pitch frequency causes large accelerations even though the pitch motion in degrees is quite small.

11.4 Concluding remarks

Due to the large restoring forces from the mooring system, the TLP has the smallest heave, roll and pitch motions. The mean drift due to the wind thrust force is also small. It was seen that there is little difference in power production between the three concepts; at least this is the case with the very simple wind turbine model that is used. The spar experience significant yaw motions when the wind and waves are coming from different directions. According to Solberg [34] this can effectively be solved by increasing the yaw stiffness of the mooring system. The semi-sub has the smallest accelerations at the nacelle, but the nacelle accelerations of the spar and TLP might as well be within acceptable limits.

It is not easy to compare the TLP up against the other two concepts because the design philosophy is very different. A more complete analysis that also includes fatigue life calculations of the mooring systems and structures should be performed. This will require a finite element model of the tower and substructure.

The costs associated with each concept should also be estimated. Reducing the costs is one of the main challenges for the offshore wind industry and this is a very important factor when assessing what concept is best suited for the job. Calculating the costs is outside the scope of this thesis and we do not have enough information about the costs related to each concept at this stage. Still, some general comments will be given. The semi-submersible have the smallest mass of the three concepts but a complicated design and the need for an active ballast system is expected to drive up the costs. The TLP with the current requirement of stability during installation, require more than 8000 tons of concrete ballast in the substructure. The TLP is also expected to have the most expensive mooring system, and significant seabed preparations might be needed prior to installing the tethers. The spar buoy on the other hand is a quite simple construction with the same cylindrical shape as the TLP, but without the expensive mooring system. Due to a large draft the Spar also requires less ballast then the TLP to achieve sufficient stability.

The TLP have the advantage of a small footprint due to the vertically installed tethers. The catenary mooring systems of the Spar and Semi-sub take up much more space, especially at large water depths. If for example the spar loses its windward line, it will probably move quite some distance before the two other lines are able to restrain the movement. Depending on the length of the mooring lines and the distance between the wind turbines in a wind park, this might become a problem. The shallow draft of the semi-sub makes it possible to install it in shallower waters than the TLP and spar.

It is difficult to give a clear recommendation on what is the best concept before more of the above mentioned parameters are investigated in more detail. Simply looking at the rigid body motions, nacelle accelerations and tension in the different mooring systems, is in the author's opinion not enough to support a good conclusion.

12. Effect of reducing the water depth

The effect of reducing the water depth from the original 200 meters to 120 meters will now be investigated. The same type of mooring system that was used in the 200 m case will also be used when the water depth is reduced. The most important mooring characteristics are repeated in table 12.1.

Line extensional stiffness (EA)	1500000 kN
Number of mooring lines	8
Radius to fairlead	27 m
Depth to fairleads	47.89 m
Static tension	3917 kN

Table 12.1: Mooring characteristics

The line (tether) length when exposed to the static pretension is reduced from 152.11m to 72.11m.

The reduced line length will change the restoring coefficients and have a large effect on the natural periods of the system. The restoring coefficient in surge, sway and heave is given by:

$$C_{11} = C_{22} = \frac{F_T}{L},\ C_{33} = \frac{EA}{L} \tag{12.1}$$

Here F_T is the tension in the lines and L is the line length. We see that 1/L is a common factor. The restoring in roll, pitch and yaw will have a similar dependency on the line length. The undamped natural period in degree of freedom i can be written as:

$$T_{ni} = 2\pi\sqrt{\frac{M_{ii} + A_{ii}}{C_{ii}}} \tag{12.2}$$

Where M and A are the mass and added mass. Reducing the length of the mooring lines will result in a stiffer system with lower natural periods. Hydrostatic restoring forces are small compared with the restoring supplied by the mooring system. With stiffness coefficients that are more or less proportional to the inverse of the tether length, this mean that we can derive the following relationship between the natural periods at the different water depths to get an idea of how large the effect is (not taking into account the change in the frequency dependent added mass).

$$T_{n120} \approx T_{n200}\sqrt{\frac{L_{120}}{L_{200}}} = T_{n200} \cdot 0.69 \tag{12.3}$$

HydroD has been used to perform a new hydrodynamic analysis of the TLP at the reduced water depth. The results did not change much from the 200 m case. This is probably due to the fact that at 120 m we are still on “deep water” even for fairly long waves and there are no changes in the geometry of the substructure.

Decay test simulations similar to those in section 8 have been performed to determine the natural periods. The results are given in table 12.2.

	Damped period at 120 m [s]	Damped period at 200 m [s]	Damped period at 120 m using equation (12.3) [s]
Surge	44.3	65	44.9
Heave	1.67	2.42	1.67
Pitch	2.58	3.68	2.54
Yaw	10.0	14.8	10.2

Table 12.2: TLP natural periods at 120 m and 200 m water depths

Due to small levels of damping there will only be a small difference between the damped and undamped periods. The natural periods in sway and roll are equal to the natural periods in surge and pitch respectively. It is also seen that the simple relationship between natural periods and line lengths given in equation (12.3) agrees quite well with the periods estimated from the decay tests.

Time domain simulations have been performed for LC0-1 to 5. The notch filter was activated at the pitch natural frequency. In figure 12.1 the spectra of the surge motion in the waterline and the tension in line number 7 is shown for LC0-3 (rated) and LC0-5 (extreme waves) at the two water depths. Line number 7 (and 8) is the line that is taking the largest loads.

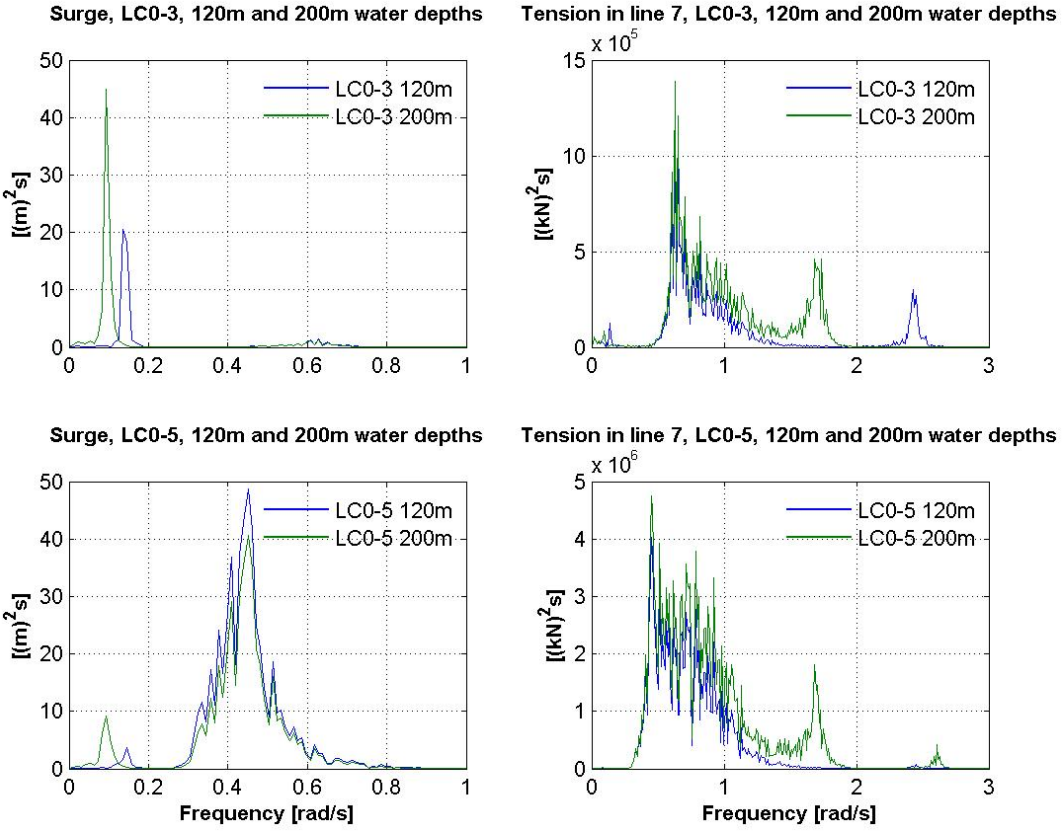

Figure 12.1: Spectra of surge motion and tension in line 7 in LC0-3 and 5 at 120 and 200 m water depths

Looking at the surge spectra it is seen that in LC0-3 most of the response is at the surge natural frequency. The resonance peak of the TLP at 120m water depth is the smallest. In LC0-5 where most of the surge motion is found in the wave frequency range, the dynamic motions are larger in the shallow water case. LC0-5, LC30-5 and LC90-5 are the only load cases where the dynamic

surge motion is largest for the TLP at 120 m, but the difference is not very large. The mean surge displacement at 120 m water depth is less than 50% of the mean surge displacement at 200 m water depth, due to the extra restraint in the mooring system. If the water depth was reduced even more, it is possible that the surge natural frequency could be shifted into the wave frequency range resulting in larger dynamic surge motions. This has not been investigated.

The dynamic tension in the mooring system is mostly governed by the pitch motions. Most of the response is in the wave frequency range for both load cases considered, and in this range we see that the area under the spectra from the simulation at 200 m water depth is a bit larger than the area under the spectra from the simulation at 120 m. In LC0-3 we observe peaks at the pitch resonance frequency of 1.7 rad/s for the TLP at 200 m and at 2.4 rad/s for the TLP at 120m. The latter is the smallest because we now are even further away from the first order wave frequency range, and also the wind excitation is smaller at this frequency. In LC0-5 the wind turbine is shut down and most of the forces come from the waves. From the tension spectra of the TLP at 200 m we see that there are contributions to the tension at the pitch natural frequency (1.7 rad/s) and at the heave natural frequency (2.6 rad/s). The TLP at 120 m water depth do not have any contributions at its pitch and heave natural frequency because these frequencies are outside the range of the wave excitation in this load case.

In figure 12.2 the mean, standard deviation, max and min value of the tensions in LC0-1 to 5 are compared for the two water depths.

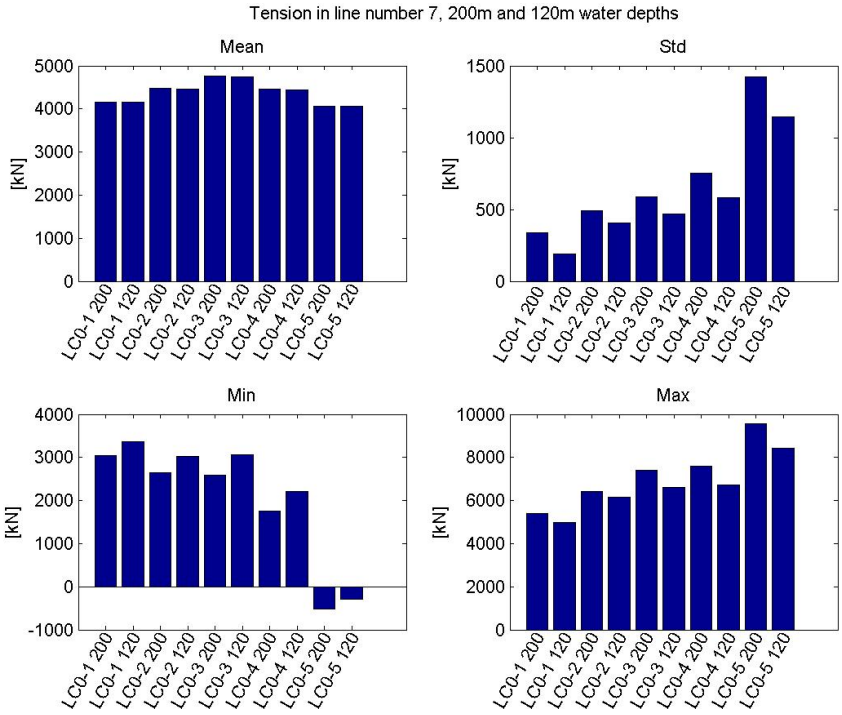

Figure 12.2: Statistics of the tension in mooring line 7 at 120 and 200 m water depths

Changing the water depth from 200m to 120m reduces the maximum tension in LC0-5 by 12%. The standard deviation is reduced by 19.5% and the minimum tension is reduced from -524 kN to -283 kN. It can be concluded that the reduced water depth have a positive effect on the forces in the mooring system.

Another important parameter that can be used to assess how well the TLP performs in the different configurations is the accelerations at the nacelle. Small accelerations will reduce the inertia forces and probably have a good effect on fatigue life of the tower and reduce the wear on the drive train. In figure 12.3 the nacelle accelerations in the global x-direction in LC0-1 to 5 are compared for the two water depths.

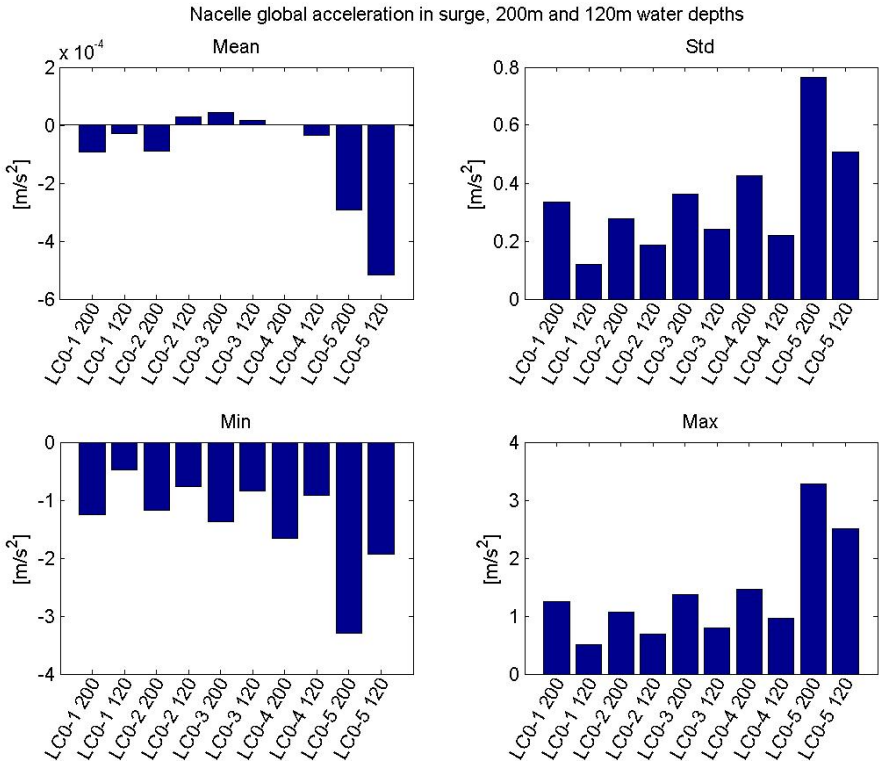

Figure 12.3: Statistics of nacelle accelerations in x-direction at 120 and 200 m water depths

Reducing the water depth reduces the nacelle accelerations significantly. The nacelle accelerations are mostly caused by the pitch motions. With the short lines (tethers) in the 120 m water depth configuration, the pitch motions are greatly reduced due to the limited elongation of these lines and less pith excitation. This reduction in pitch motions overcomes the effect of the reduced oscillation period, and the result is as seen that the nacelle accelerations are smaller.

The statistics of the response in surge, heave, pitch and tension in line number 3 are included in appendix F.

In this analysis only the first order wave forces were included. The effect of including the second order wave forces when the water depth is 200 m will be looked into in section 13. How the second order forces will affect the response at the reduced water depth has not been looked into.

Based on the results presented here it seems that the TLP will perform better at the reduced water depth. The big difference in the response at the two water depths shows how sensitive the concept is to this parameter. Placing the TLP at larger water depths might cause problems with roll and pith natural frequencies coming into the wave frequency range, and it might be necessary to look at different configurations of the mooring system. This will not be investigated in this report.

13. Effect of sum-frequency wave forces on the response

The effect of including the second-order sum-frequency wave forces in the time domain simulations will now be investigated. The first-order force transfer functions (and drift forces) included in the analysis are calculated from a HydroD (WADAM) analysis considering only first-order wave forces. This makes it possible to use a very fine wave frequency distribution when calculating the first-order forces, while a coarser distribution is used when calculating the sum-frequency forces in order to reduce the calculation time. How the sum-frequency forces are calculated using HydroD was explained in section 7. The sum-frequency force transfer functions are then included in the "first-order" SIMO input file and we get an input file for the time domain simulations with both linear and sum-frequency forces.

Four sea states have been considered. The different sea states were first used in simulations where only force transfer functions obtained from the first-order WADAM analysis were used. Then the simulations were performed once more with the second-order sum-frequency force transfer functions included in order to see the difference. There was no wind and current present and a simulation length of 4600 seconds with 1000 seconds cut-off in the beginning was used to remove transient effects.

The focus will be on forces in the line (tether) that is taking the largest load, line 7. The mean, standard deviations, minimum and maximum values obtained from the computer simulations together with the different sea states used are listed in table 13.1. The sea states are defined by their significant wave height (Hs) and peak period (Tp).

Sea state	Second-order forces	Mean [kN]	Std [kN]
Hs=3.1 m, Tp=10.1 s	Included	3918	563
	Not included	3918	560
Hs=3.1 m, Tp=7.36 s	Included	3928	832
	Not included	3928	825
Hs=4.4 m, Tp=10.6 s	Included	3922	748
	Not included	3922	741
Hs=12.7 m, Tp=14.1 s	Included	3951	1500
	Not included	3954	1425

Table 13.1: Tension in line 7 with and without sum-frequency wave forces included

From the table it is seen that the effect of including the sum-frequency forces is quite small in the three first sea states. The standard deviations increase by less than one percent. The sea state with peak period of 7.36 second was chosen because this period is twice the pitch natural period and it was expected that this would cause some extra pitch resonance when the sum-frequency forces were included, but the difference is small. In the most severe sea state however, the effect is larger and the standard deviation is increased by 5 percent (75 kN). To get a better picture of what

is happening, the spectra of the tension in two of the sea states are given in figure 13.1. The sea state with Hs = 3.1 m, Tp = 7.36 s and the sea state with Hs=12.7 m, Tp = 14.1 s (LC5) are considered.

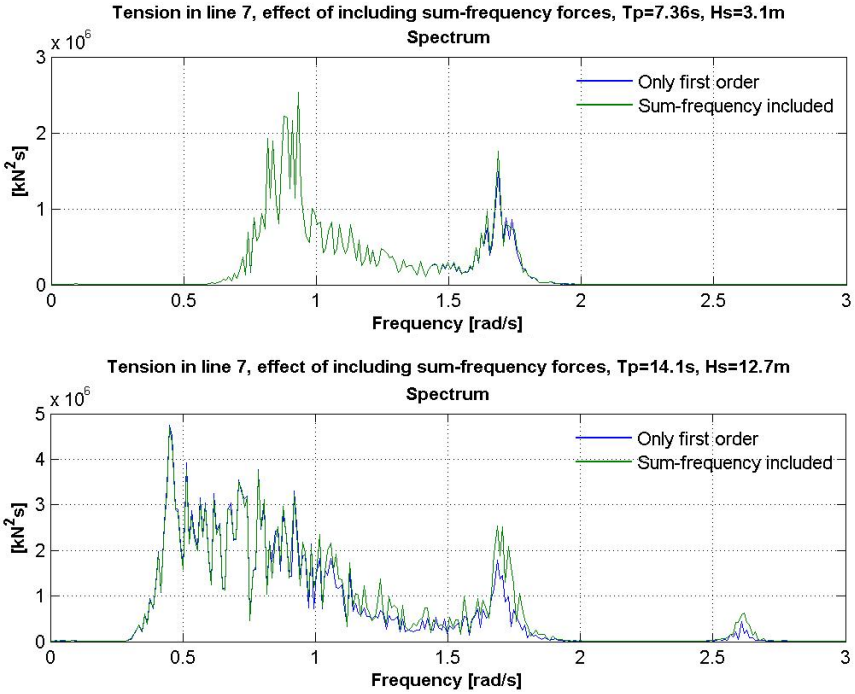

Figure 13.1: Spectra of tension in line 7 with and without the sum-frequency wave forces included

The dynamic tension in the mooring system is mostly governed by the pitch motions and the tension spectra have the same shape as the pitch response spectra. The blue lines are from the simulations with only first-order forces and the green lines are from the simulations where also the sum-frequency forces were included. The two spectra from the simulations with the smallest sea state are almost identical. Only a small difference is visible around the pitch natural frequency of 1.7 rad/s. In the extreme sea state the differences are larger and the pitch resonance peak is noticeable larger when the sum-frequency forces are included. In this sea state there is also a contribution to the dynamic tension from heave resonance at 2.6 rad/s, and also this contribution is increased in the sum-frequency case. Still, the differences are small and as stated above the standard deviation only increased by about 5 percent.

All in all the effect of including the second-order sum-frequency wave forces on the TLP seems to be small. The difference was expected to be larger as TLPs are known to be sensitive to these types of excitations because of their high natural frequencies in heave, roll and pitch (springing). It should be mentioned that the study conducted here is not complete. Before any final conclusions can be made, a more refined hydrodynamic analysis including more wave frequencies and wave directions should be performed in order to make it possible to include waves from different directions in the time domain simulations. A flexible tower and substructure should also be included, since the sum-frequency forces might excite the elastic modes. This will require a finite element model of the structure. The work done here was mainly meant to give an idea of whether the sum-frequency wave forces are very important or not.

14. Conclusion

The purpose of this study has been to establish a computer model able to calculate the dynamic behavior of a tension-leg wind turbine and to contribute information about the concept. The TLP is based on a reference model developed at MIT and modified by Matha [1]. The panel model needed in the hydrodynamic calculations was made using the computer program GeniE. Hydrodynamic calculations were performed using HydroD (WADAM). HydroD uses potential theory and the result from this analysis is the frequency depended added mass and potential damping, restoring forces and transfer functions for the excitation forces. Time domain simulations were performed using DeepC which employs the MARINTEK developed programs SIMO and RIFLEX. Viscous forces were added in DeepC. The thrust force on the wind turbine was included using the dll TDHMILL3D, which is called by SIMO. The mooring system was modeled as a finite element model but the main structure is rigid.

The effect of having a control system designed to prevent negative damping contributions from the wind turbine has been investigated. A simple notch filter that filters the nacelle velocities at the pitch natural frequency was used. Without the notch filter activated the pitch response of the TLP was seen to be unstable for wind speeds close to the rated wind speed of 11.4 m/s. This is due to a large negative damping contribution from the wind turbine at this wind speed, and shows the necessity of having a control system designed to prevent this. Also for wind speeds above rated, there was a reduction in the dynamic pitch motion when the notch filter was activated. The difference was however not very large since the pitch response of the TLP is small and mostly governed by the wave forces.

Due to the high natural frequency in heave roll and pitch of TLPs they are known to be susceptible to springing response. To check whether or not this is a problem for the TLP considered here, the second-order sum-frequency wave forces were calculated. This was done by using HydroD with a finite element model of the free surface. The inclusion of the sum-frequency wave forces in the time domain simulations influenced the response only to a small extent. Perhaps the difference would have been larger if a flexible model of the structure was used.

The TLP was originally designed to operate at a water depth of 200 meters. The effect of reducing the water depth to 120 meters has been investigated. A reduced water depth results in shorter mooring lines (tethers) and a stiffer system. The heave, roll and pitch natural frequencies are then shifted even further away from the energetic wave frequency range and together with the limited elongation of the shorter lines, these motions are reduced. The dynamic tensions in the mooring system and the accelerations at the nacelle were also reduced and it can be concluded that the TLP performs better at the reduced water depth. This also shows how sensitive the concept is to this parameter.

The TLP have been compared with a spar buoy and semi-submersible concept designed to support the same 5.2 MW wind turbine as the TLP. The spar and semi-sub have been analyzed by Solberg [34] and Luan [35] respectively. Due to large restoring forces from the stiff mooring system, the TLP have the smallest heave, roll and pitch natural periods and motions. The TLP also have the smallest mean surge and sway displacements. With the simple wind turbine model used, there is little difference in power production between the concepts. It is not easy to compare the forces in the tension-leg mooring system of the TLP with the forces in the catenary mooring

systems of the spar and semi-sub. Compared with the semi-sub, the spar seems to have the best mooring characteristics. In the most extreme wave conditions the TLP was seen to suffer from negative tensions in the mooring system. This might be a serious problem and design changes might be needed to avoid this. The semi-sub also experienced negative tensions in these load cases. This should not be possible and indicates that there is a problem with how the catenary mooring system was modeled. The semi-sub had the smallest accelerations at the nacelle. Small nacelle accelerations will give small inertial forces and possibly contribute to an increase fatigue life of the tower. Accelerations at the nacelle are also important for the drive train of the wind turbine. All in all it is not easy to compare the TLP up against the other two concepts because the design philosophy is very different. It is therefore difficult to give a clear recommendation on what is the best concept based on the parameters investigated so far. To provide a better basis for decisions, a more detailed comparison must be carried out. Other parameters like the fatigue life time of the mooring systems and structure, building costs, installation costs and decommissioning should then be included. It is also expected that the relative performance of the different concepts will change if different water depths are used in the analysis.

15. Recommendations for further work

A finite element model of the tower and substructure should be included in the computer model. RIFLEX might be used. The responses will then probably be affected by the inclusion of the elasticity of the structure. In particular it would be interesting to investigate if the sum-frequency wave forces play a more important role when the structure is flexible. A finite element model will also make it possible to calculate the stresses and fatigue life time of the structure. This will be an important parameter when deciding on what concept is best suited to support the wind turbine.

The effect of the negative tensions occurring in the lines (tethers) in extreme loading conditions need to be investigated in more detail. The fear is that the lines will go slack with subsequent snatch loads that might be detrimental to the mooring system. The best solution is probably to avoid the negative tensions all together. This might be achieved by increasing the pretension in the lines, or by lengthening the spokes holding the lines. It is expected that many iterations in a design optimization is needed to find an overall better concept.

Accidental limit states (ALS) have not been investigated for any of the concepts in this study. In particular it would be interesting to see what happens if one (or more) of the mooring lines of the TLP fail. If the spar and semi-submersible looses their windward lines they will most likely experience large horizontal offsets. This might be a problem in an offshore wind park with many structures placed close together.

Estimates of the costs related to the different concepts also need to be made in order to give a better basis for deciding what concept is best suited for the task. The relative performance of the different concepts at different water depths should also be investigated.

References

[1] Denis Matha. Model Development and Loads analysis of an Offshore Wind Turbine on a Tension Leg Platform, with a Comparison to Other Floating Turbine Concepts. University of Colorado, 2009.

[2] J. Jonkman and D. Matha. A Quantitative Comparison of the Responses of Three Floating Platforms. National Renewable Energy Laboratory and University of Stuttgart, 2009.

[3] J. Jonkman, S. Butterfield, W. Musial and G.Scott. Definition of a 5-MW Reference Wind Turbine for Offshore System Development. National Renewable Energy Laboratory, February 2009.

[4] Paul A. Tipler and Gene Mosca. Physics for scientists and engineers, fifth edition. W. H Freeman and Company, 2004.

[5] J. Lygren. Dynamic response analysis of a tension-leg wind turbine, project thesis. Department of Marine Technology, NTNU, December 2010.

[6] H. Tennekes and J.L Lumley. A First Course in Turbulence. The MIT Press, 1972.

[7] Frank. M. White. Viscous Fluid Flow, third edition. McGRAW-HILL, 2006.

[8] O. M. Faltinsen. Sea loads on ships and offshore structures. Cambridge university press, 1990.

[9] DNV/Risø. Guidelines for design of wind turbines, second edition. Jydsk Centraltrykkeri, Denmark 2002.

[10] Rune Yttervik. TDHMILL3D User documentation. Statoil internal document, 2009.

[11] Martin O. L. Hansen. Aerodynamics of Wind Turbines, second edition. Earthscan, 2008.

[12] Finn Gunnar Nielsen. Design brief for offshore floating wind-mills. Statoil internal document, 2007.

[13] Det Norske Veritas (DNV). GeniE user manual, 2008.

[14] Det Norske Veritas (DNV). HydroD user manual, 2008.

[15] Det Norske Veritas (DNV). WADAM user manual, 2005.

[16] Det Norske Veritas (DNV). DeepC user manual, 2010.

[17] MARINTEK. SIMO Theory Manual, 2009.

[18] MARINTEK. RIFLEX User´s Manual, 2009.

[19] MARINTEK. RIFLEX Theory Manual, 2008.

[20] K. Herfjord and F.G Nielsen. Non-linear wave forces on a fixed vertical cylinder due to the sum frequency of waves in irregular seas. Applied Ocean Research, 1986.

[21] Yoon R. Choi, Sa Y. Hong, Hang S. Choi. An analysis of second-order wave forces on floating bodies by using a higher-order boundary element method. Korea Research Institute of Ships and Ocean Engineering, 1999.

[22] M. H. Kim. Second-order sum-frequency wave loads on large-volume structures. Department of ocean engineering, Massachusetts Institute of Technology, Cambridge, MA 02139 USA. Applied ocean research, December 1991.

[23] B. Molin and A. Marion. Second-order loads and motions for floating bodies in regular waves. Institut Francais du Petrole, 1986.

[24] Det Norske Veritas (DNV). DNV-RP-F205 Global performance analysis of deepwater floating structures, October 2004.

[25] Det Norske Veritas (DNV). DNV-RP-C205 Environmental conditions and environmental loads, October 2010.

[26] Jan V. Aarsnes. Lecture notes – "Hydroelasticity". NTNU 2010.

[27] Finn Gunnar Nielsen. Lecture notes in marine operations. Department of marine hydrodynamics, NTNU, 2007.

[28] Prof. Torgeir Moan. Personal communication, 2010.

[29] Ivar Langen and Ragnar Sigbjørnsson. Dynamisk analyse av konstruksjoner. SINTEF, Avdeling for konstruksjonsteknikk, Tapir 1979.

[30] Dag Myrhaug. Marin Dynamikk – uregelmessig sjø. Department of Marine Technology, NTNU, 2007.

[31] Dr. Zhen Gao (NTNU). Personal communication, 2010.

[32] Det Norske Veritas (DNV). DNV-OS-C105 Structural design of TLPs (LRFD method). April 2011.

[33] Det Norske Veritas (DNV). DNV-OS-E301 Position Mooring. October 2010.

[34] Thomas Solberg. Dynamic response analysis of a floating spar wind turbine. Master thesis, NTNU, June 2011.

[35] Chenyu Luan. Dynamic response analysis of a semi-submersible floating wind turbine. Master thesis, NTNU, June 2011.

Appendices

Appendix A: Damping

A.1 Heave decay time series

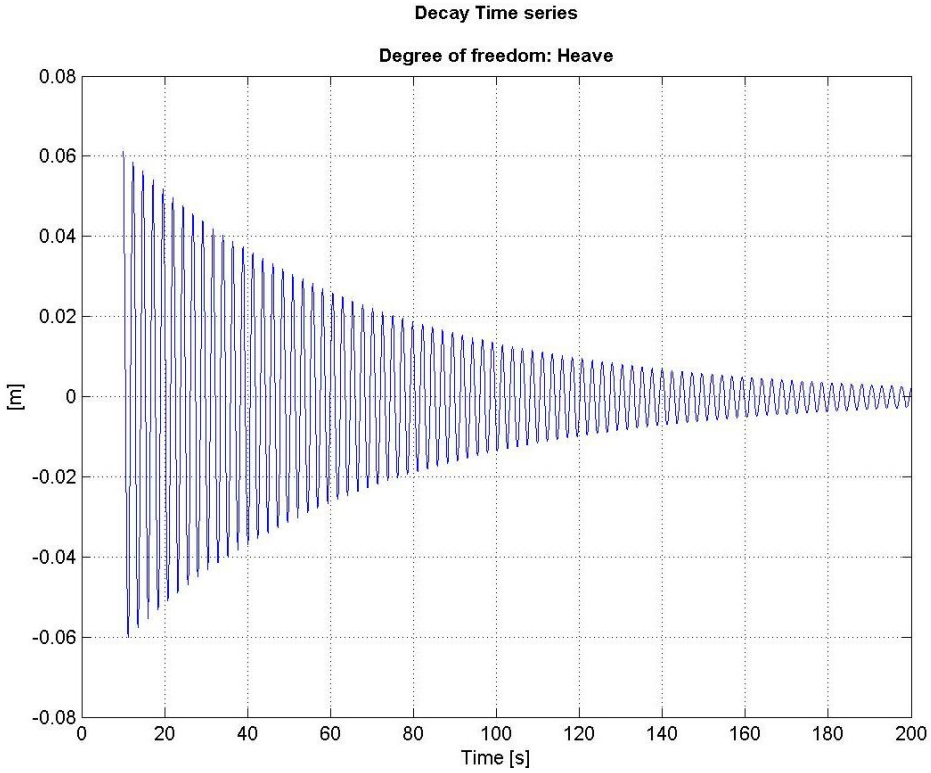

A.2 Pitch decay time series

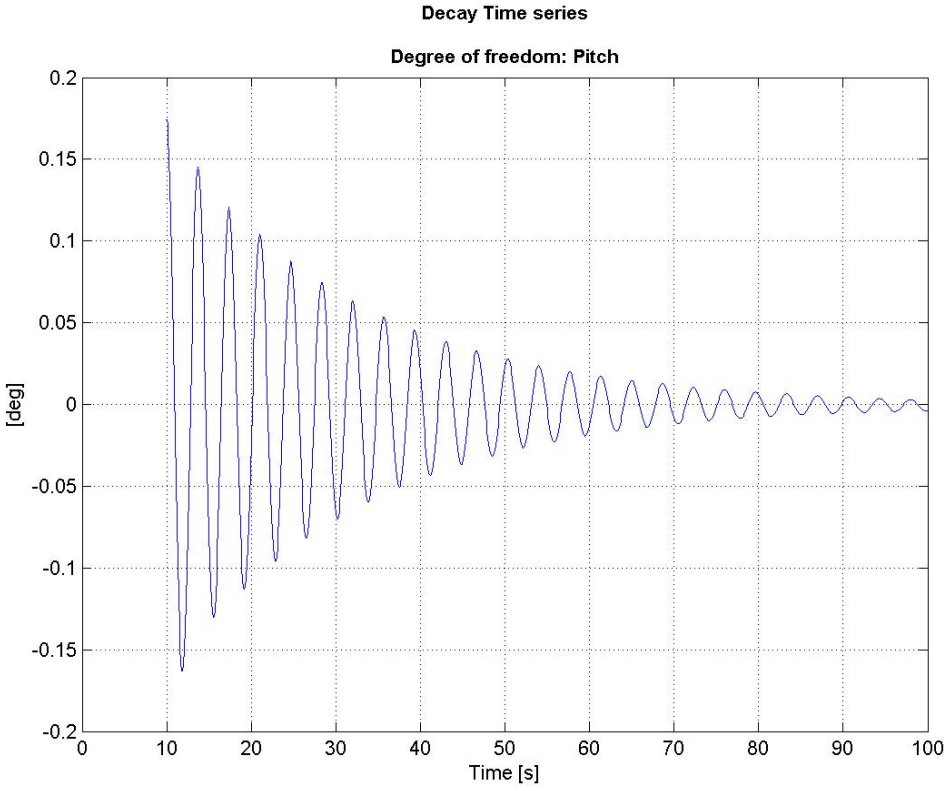

A.3 Yaw damping

Yaw decay time series:

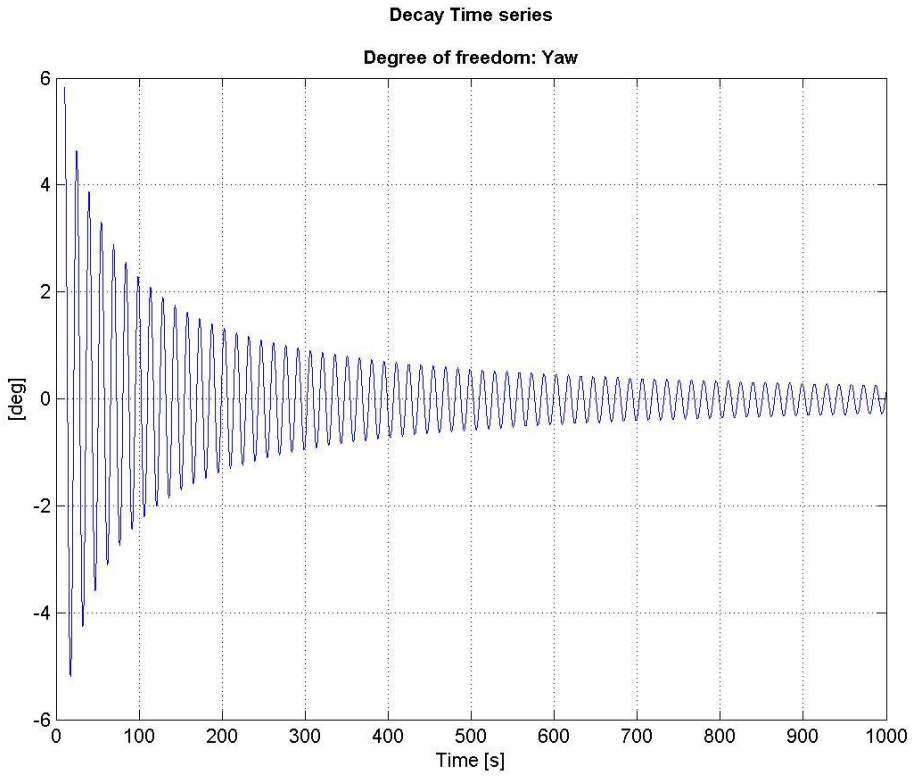

Yaw damping calculated from time series as function of motion amplitude:

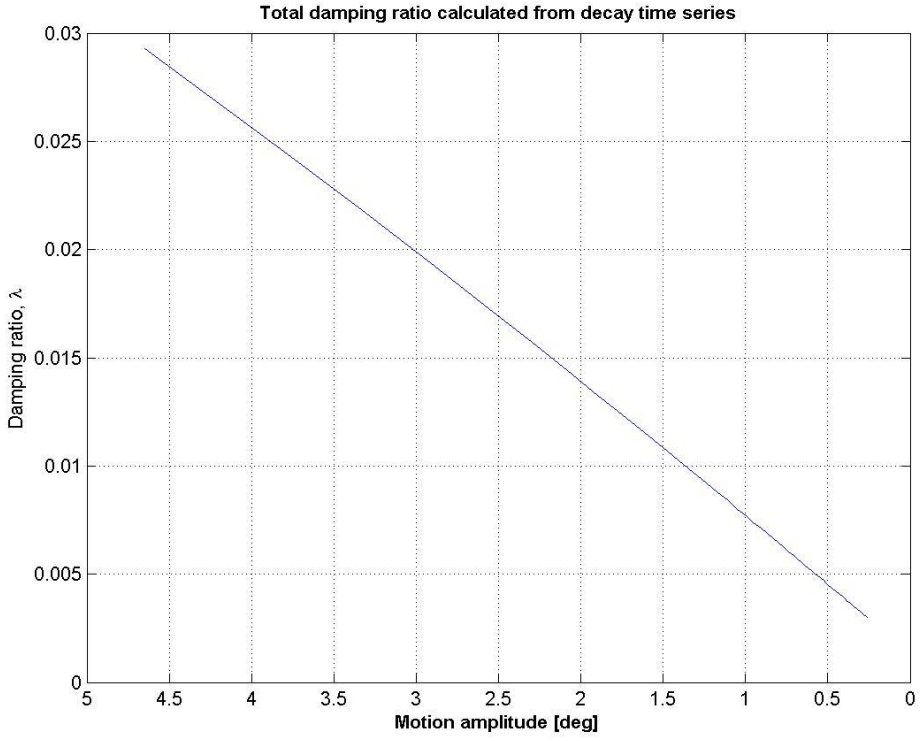

Yaw, determination of linear and quadratic damping contributions:

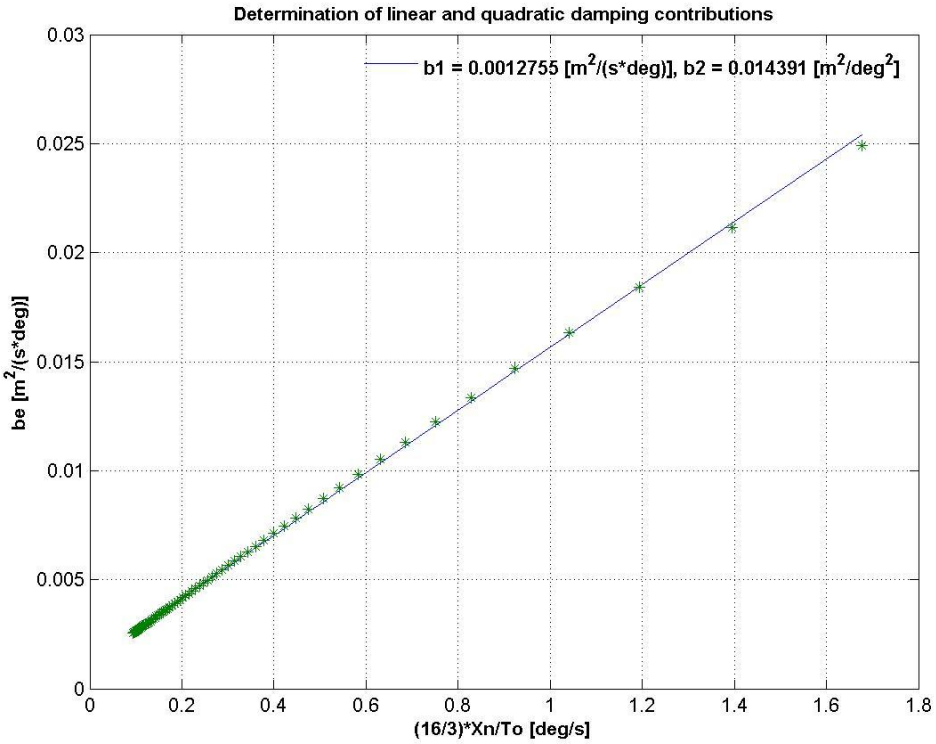

Yaw, ratio between linear and quadratic damping:

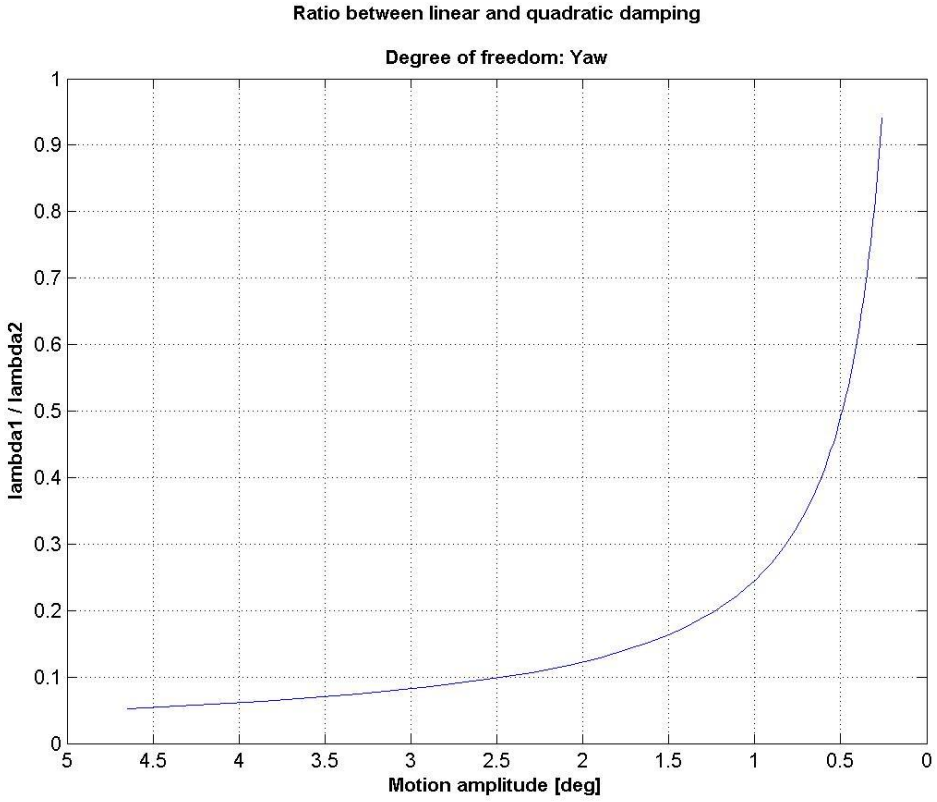

Appendix B: Statistics of the TLP in the eleven load cases

Surge in the waterline:

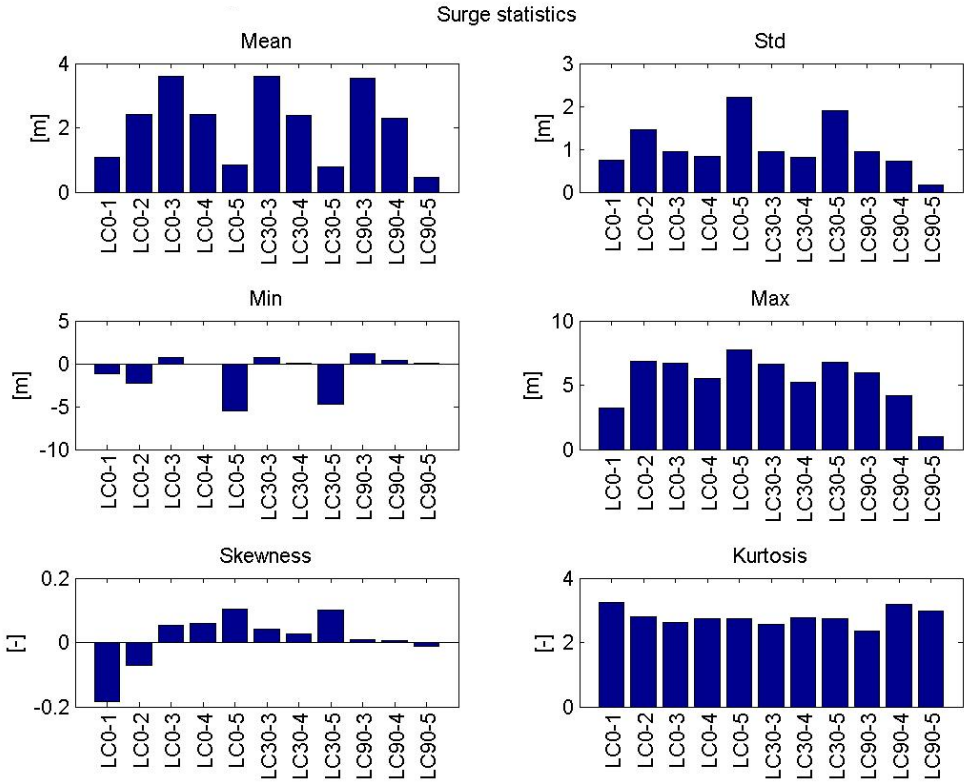

Sway in the waterline:

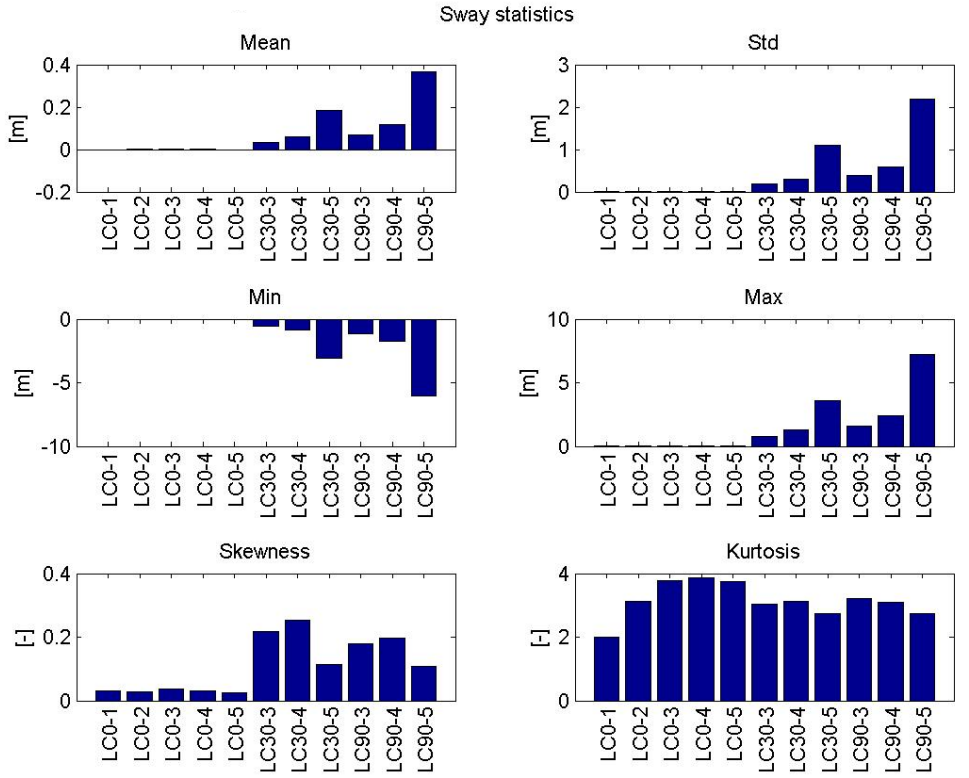

Heave in the waterline:

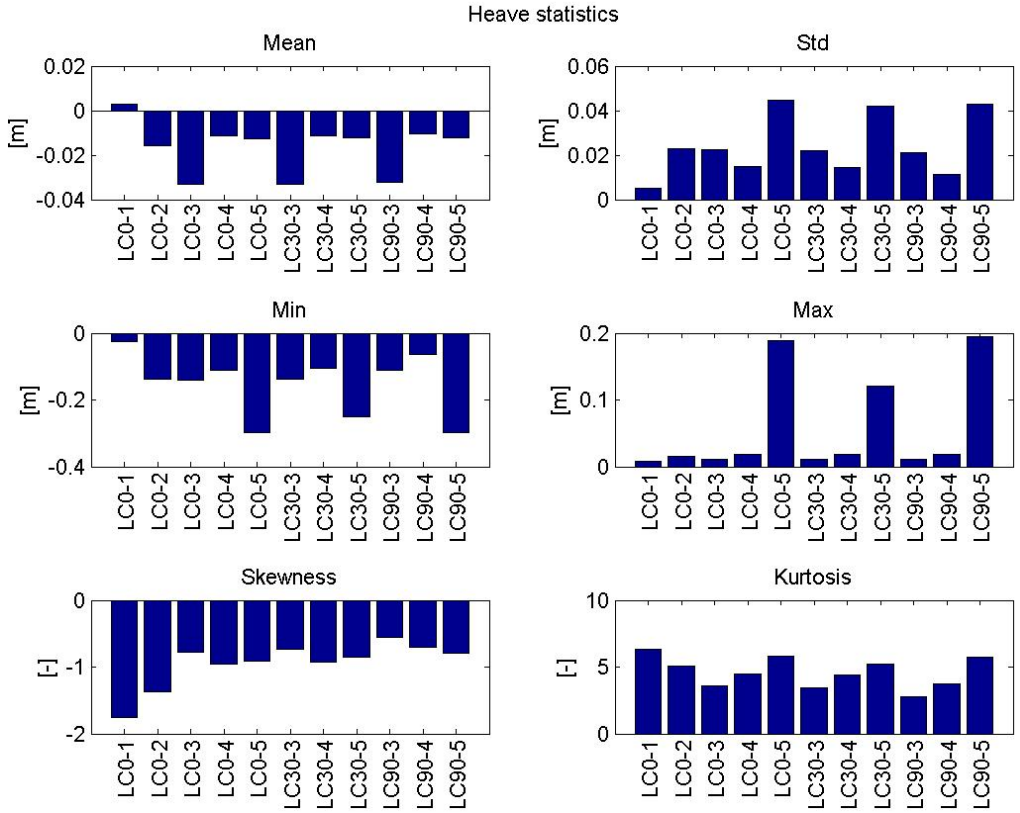

Roll:

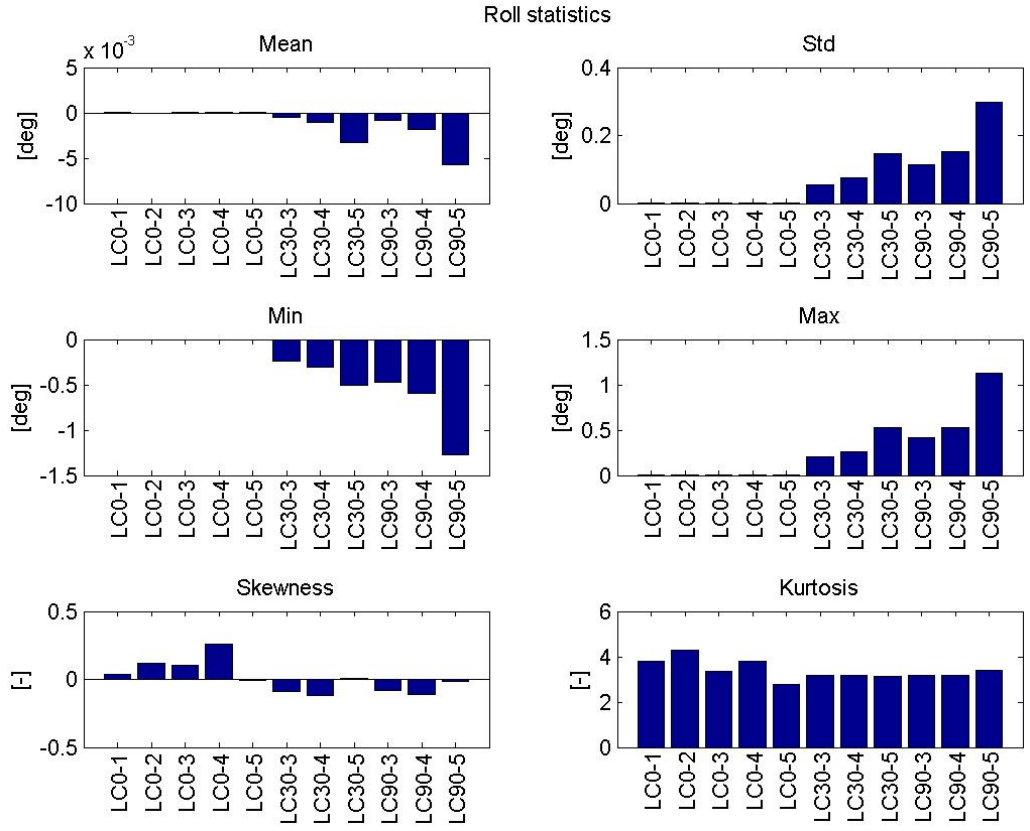

Pitch:

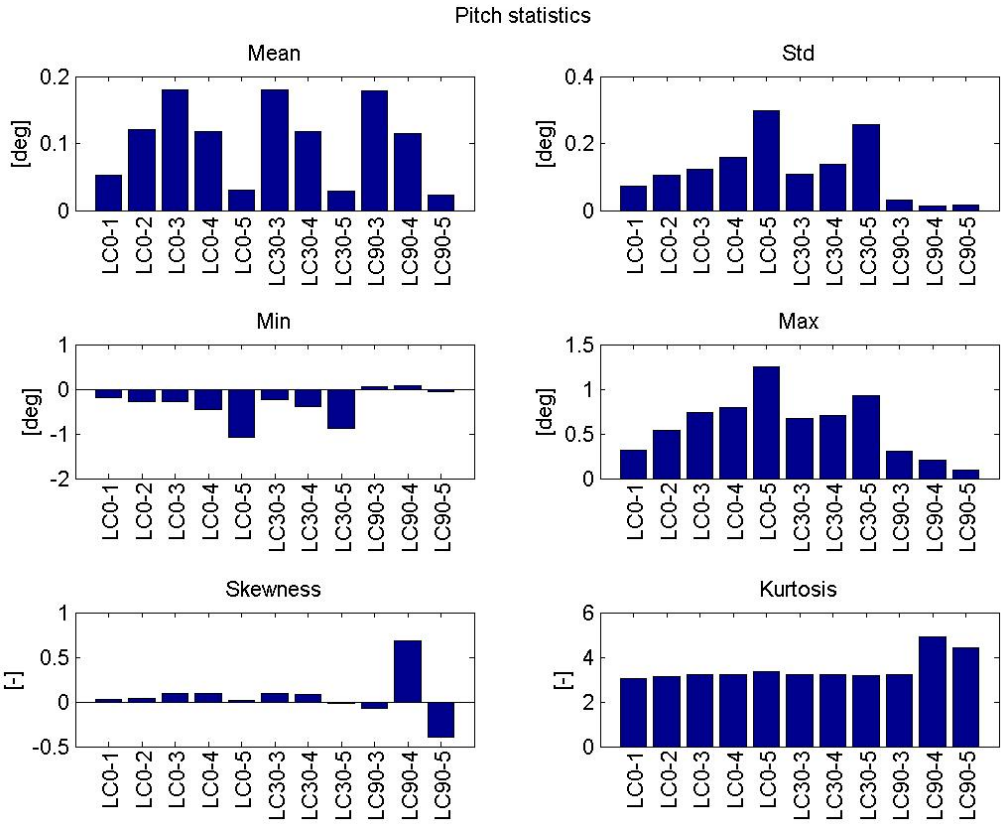
Pitch statistics
Mean
Std
Min
Max
Skewness
Kurtosis
[deg]
[-]
LC0-1
LC0-2
LC0-3
LC0-4
LC0-5
LC30-3
LC30-4
LC30-5
LC90-3
LC90-4
LC90-5

Yaw:

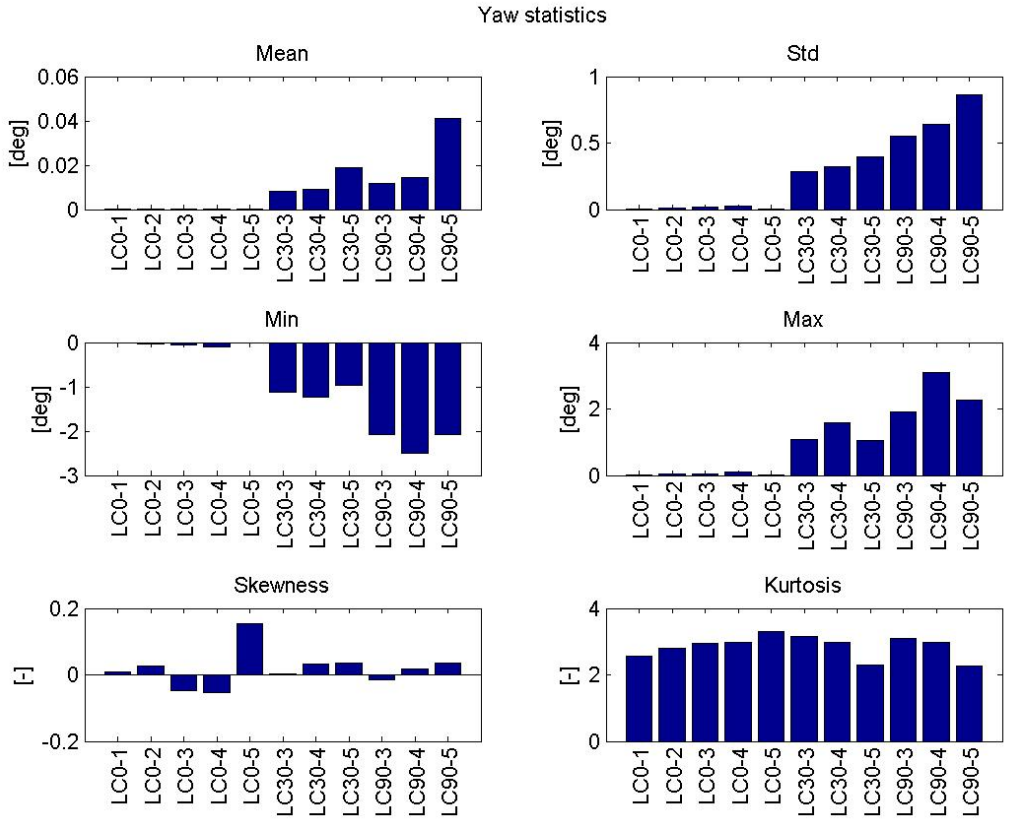
Yaw statistics
Mean
Std
Min
Max
Skewness
Kurtosis
[deg]
[-]
LC0-1
LC0-2
LC0-3
LC0-4
LC0-5
LC30-3
LC30-4
LC30-5
LC90-3
LC90-4
LC90-5

Wave elevation:

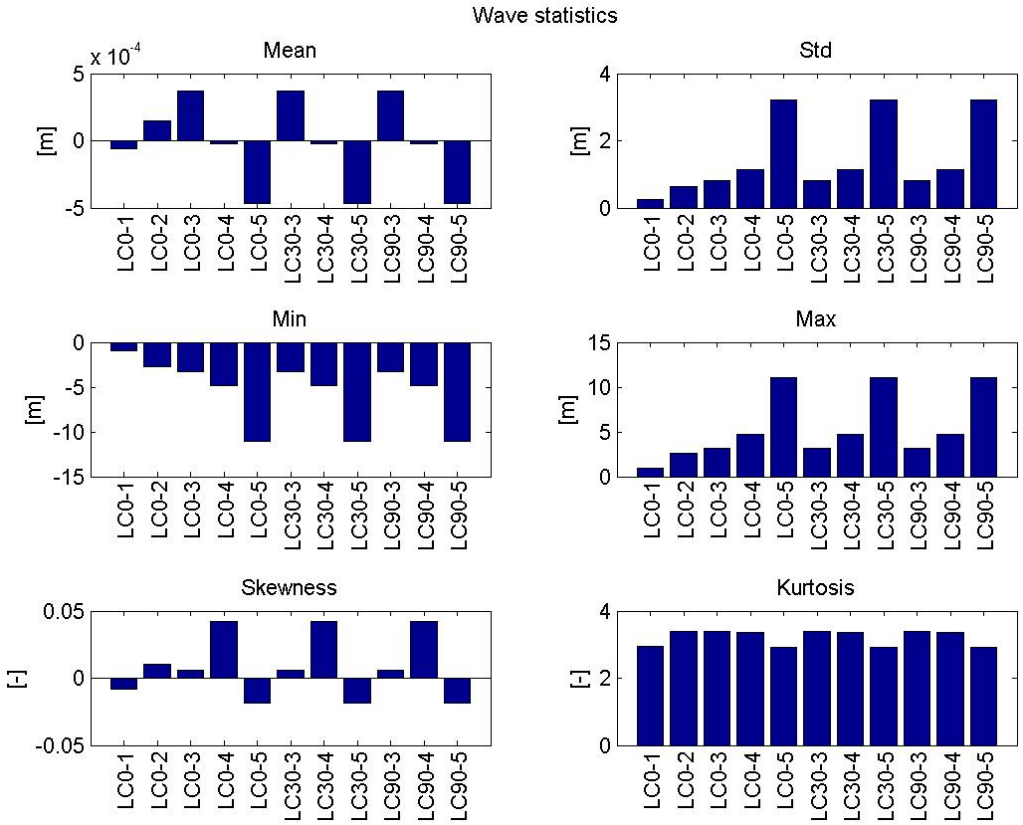

Tension in line (tether) number 1:

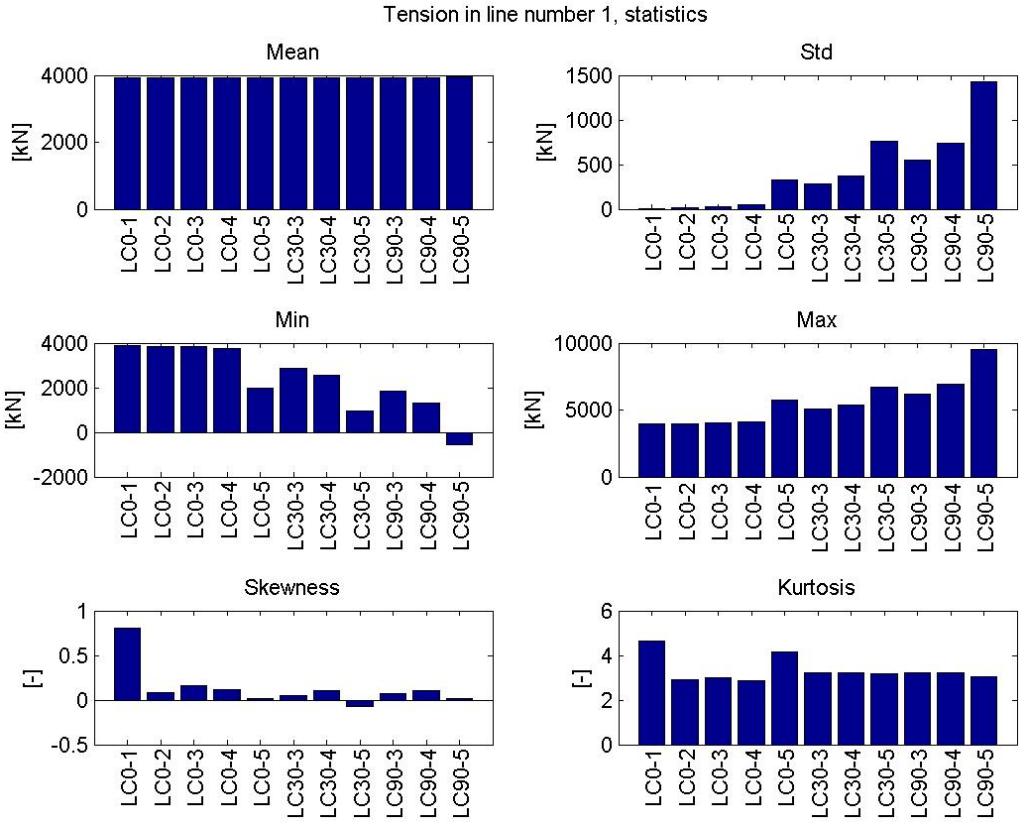

Tension in line (tether) number 3:

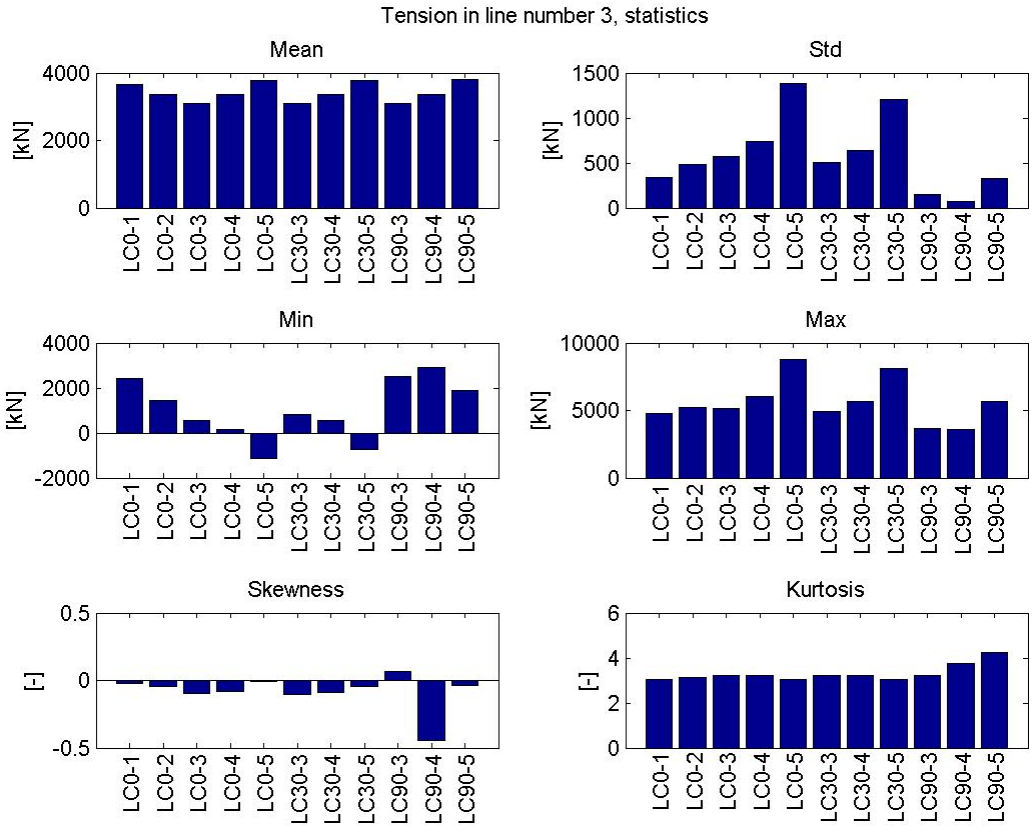

Tension in line (tether) number 5:

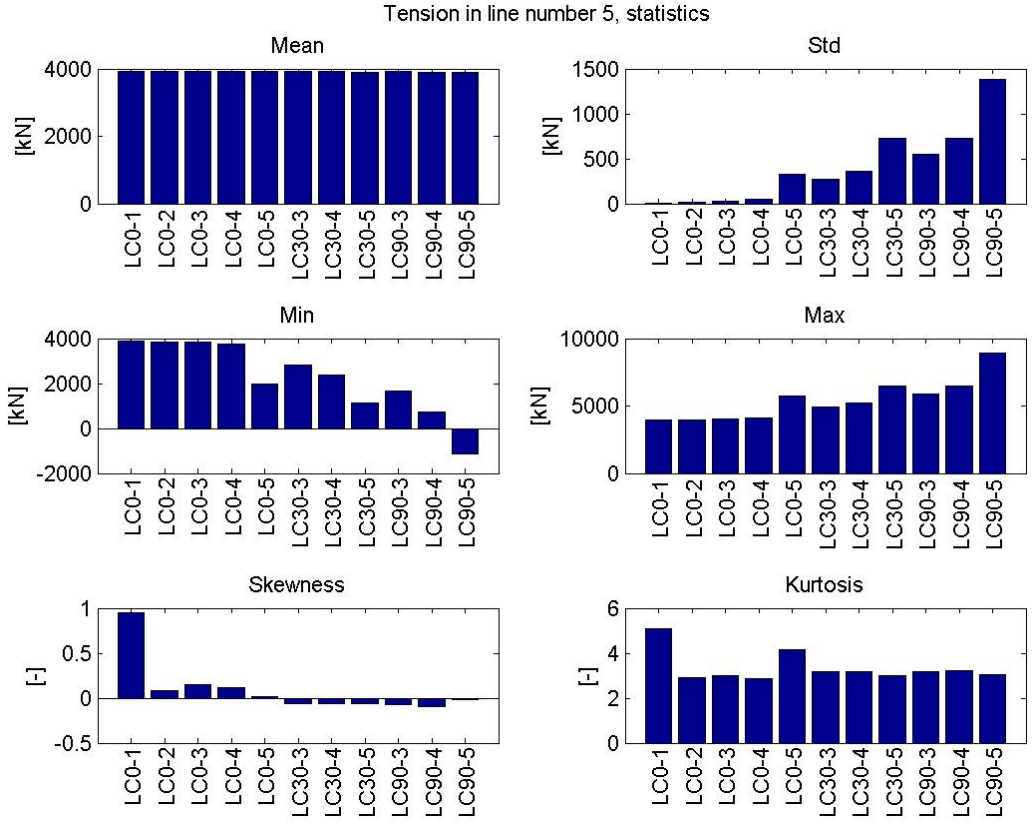

Tension in line (tether) number 7:

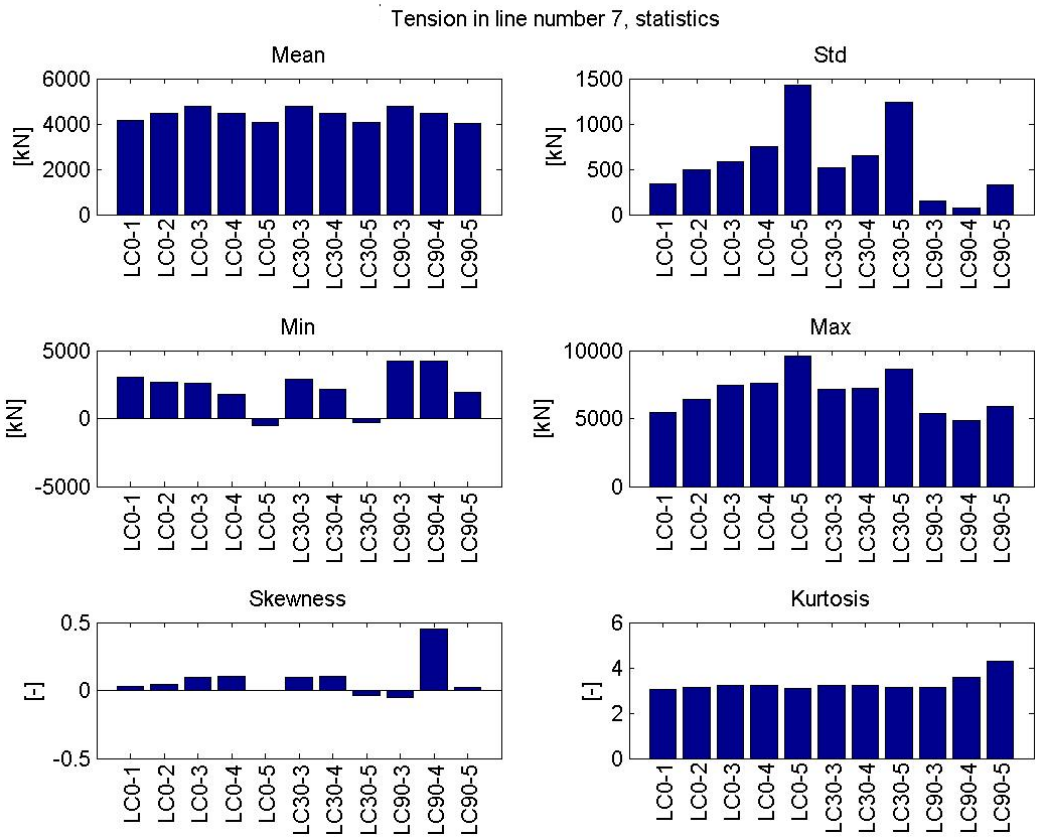

Relative wind speed at nacelle:

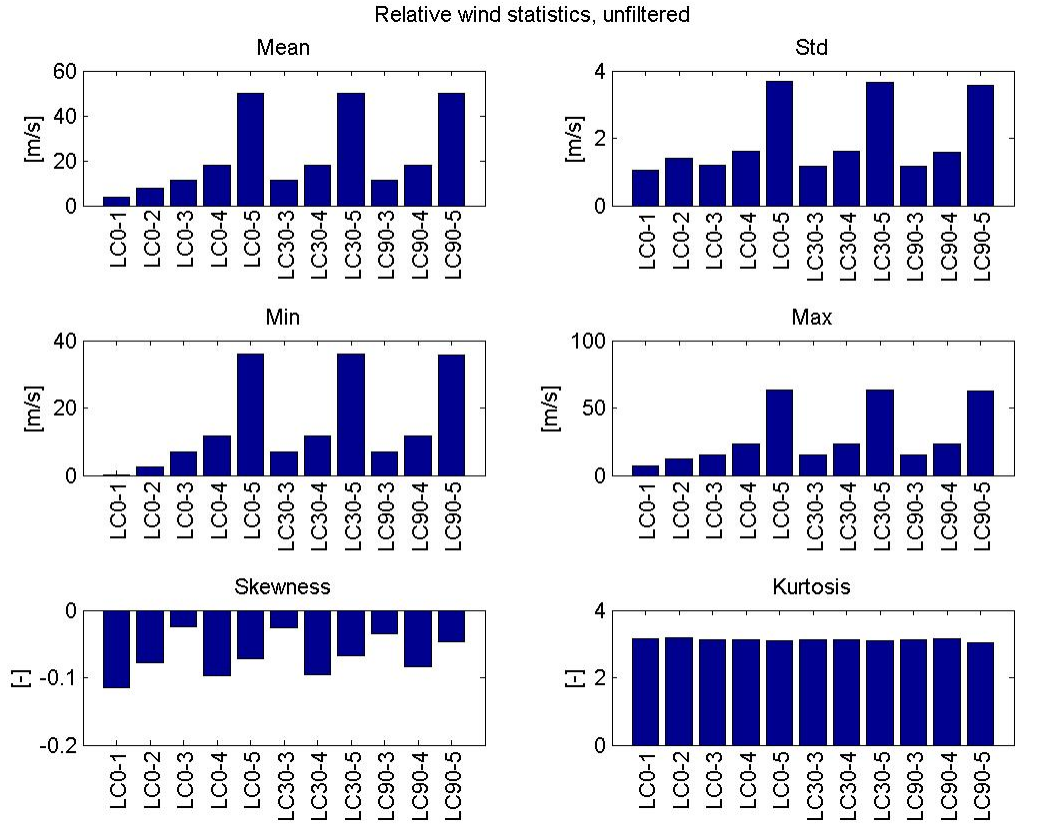

Relative wind speed at nacelle after notch filtering:

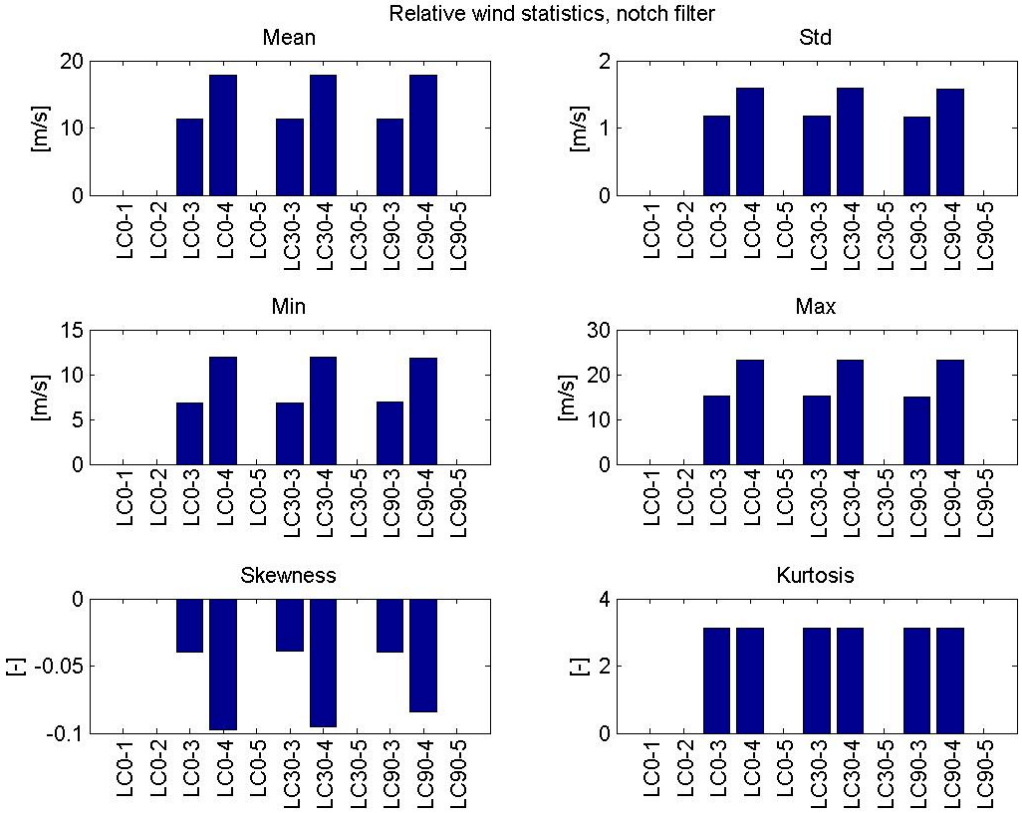

Thrust in x-direction at nacelle:

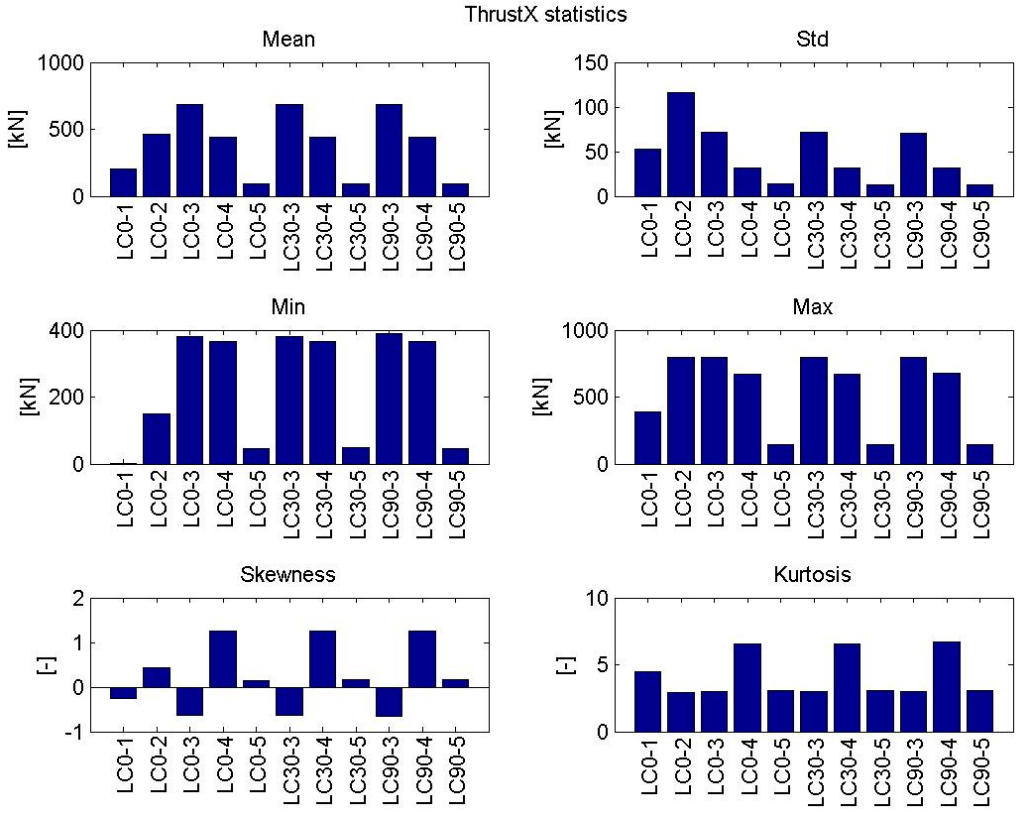

Power based on power coefficients from reference wind turbine:

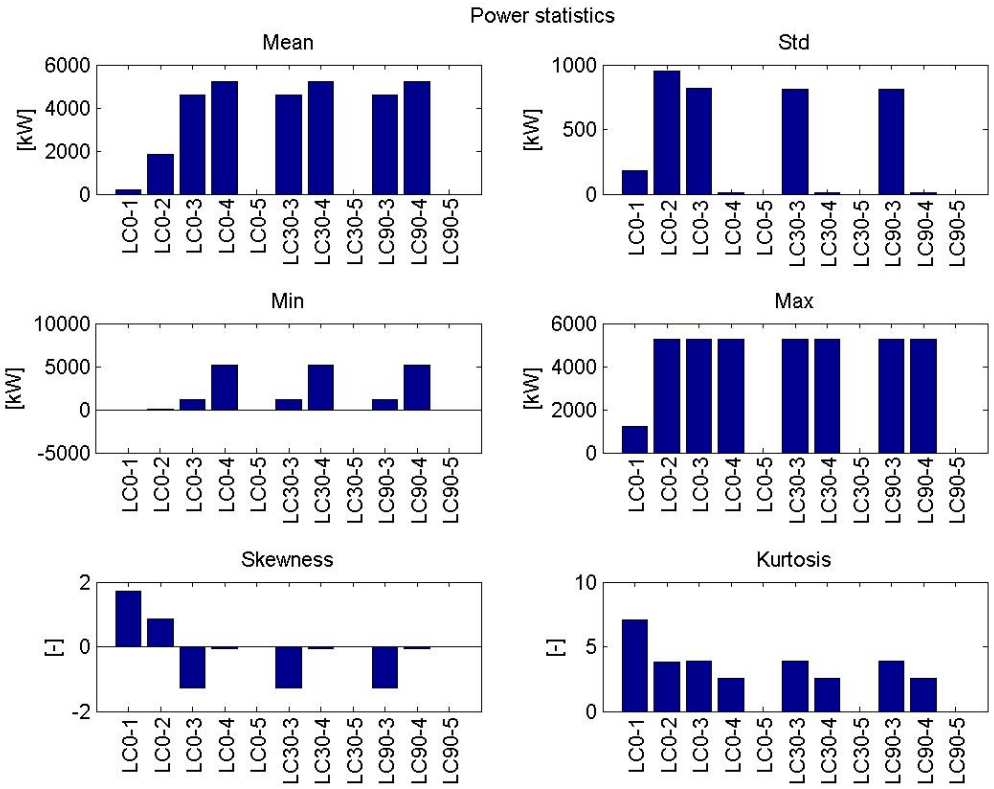

Appendix C: Time series and response spectra of the TLP

Presented here are the time series and spectra of different variables obtained from the time domain simulations of the TLP. Results from LC0-3, LC0-4, LC0-5 and LC30-3 are included (more on CD).

C.1 LC0-3

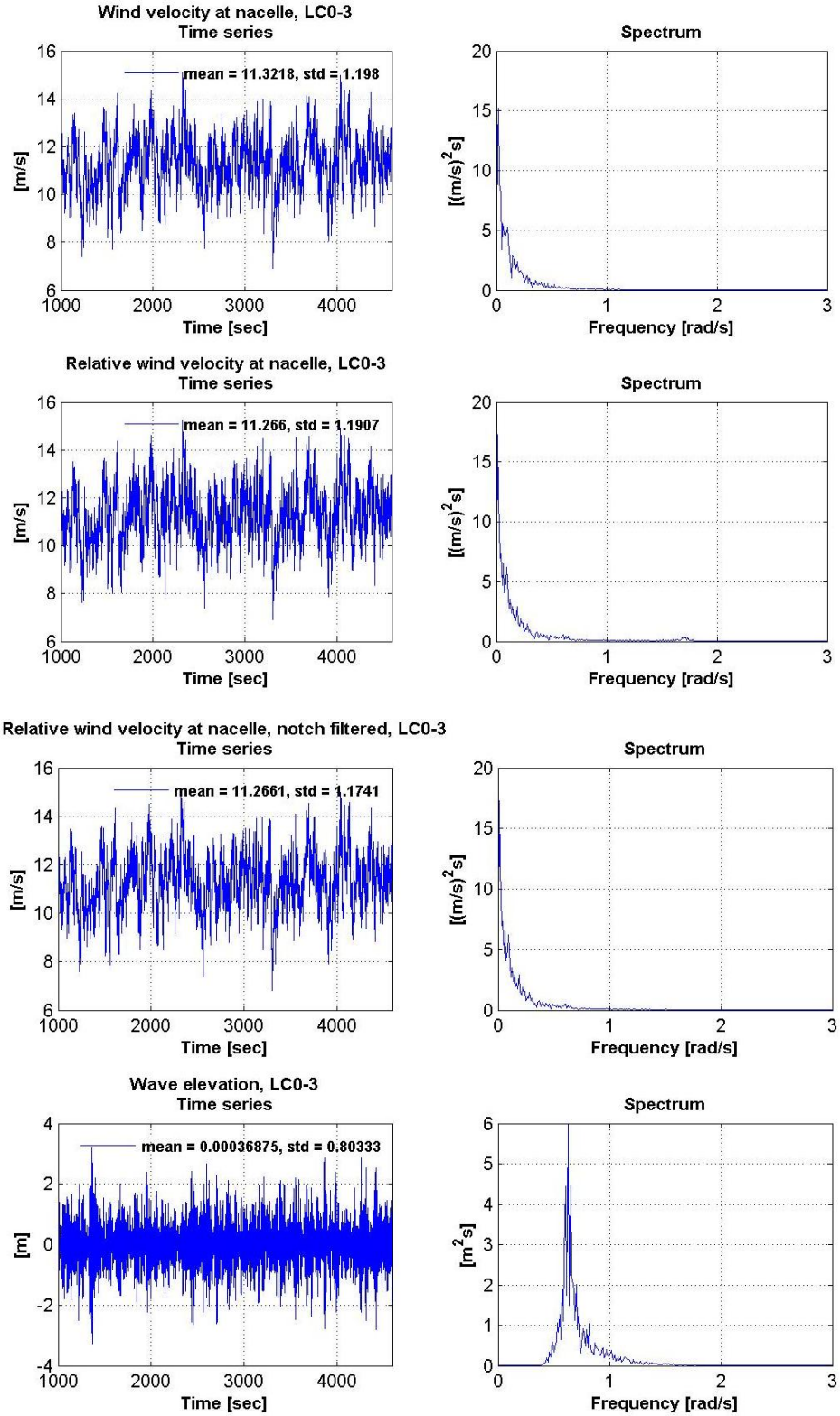

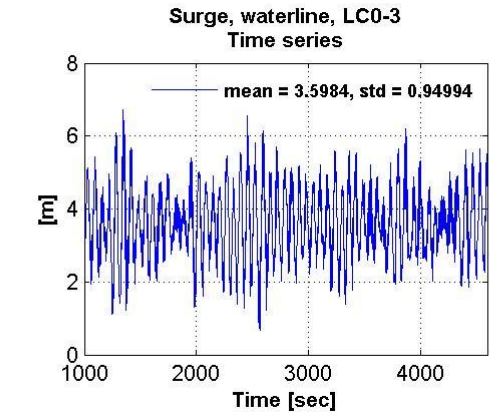
Surge, waterline, LC0-3
Time series
mean = 3.5984, std = 0.94994
[m]
Time [sec]

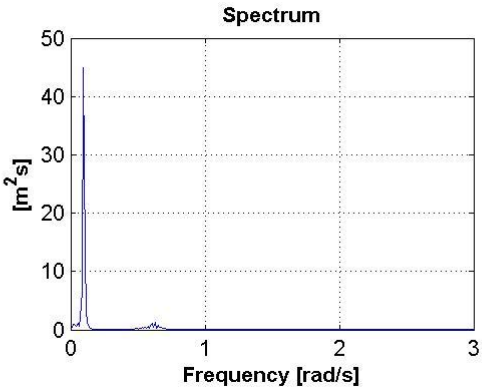
Spectrum
[m²s]
Frequency [rad/s]

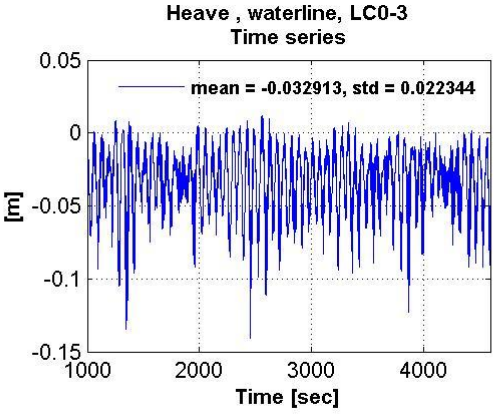
Heave , waterline, LC0-3
Time series
mean = -0.032913, std = 0.022344
[m]
Time [sec]

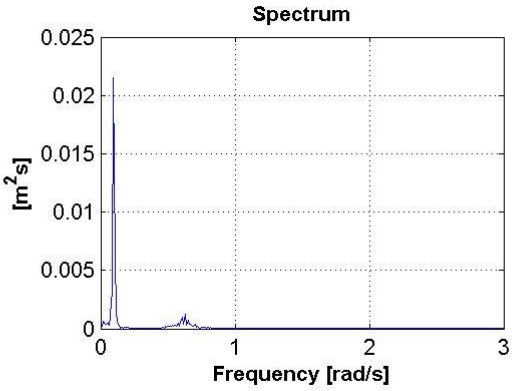
Spectrum
[m²s]
Frequency [rad/s]

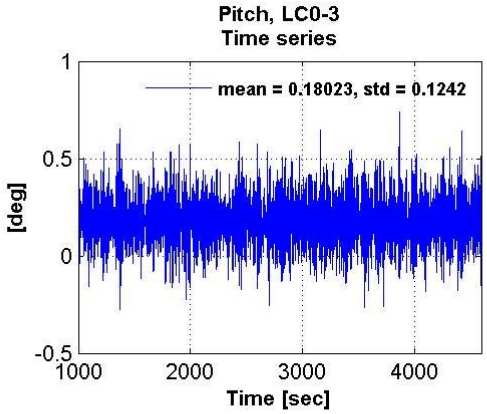
Pitch, LC0-3
Time series
mean = 0.18023, std = 0.1242
[deg]
Time [sec]

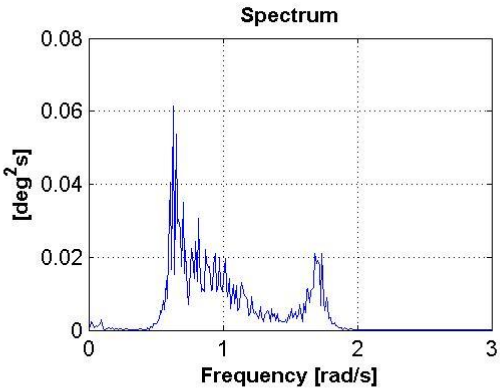
Spectrum
[deg²s]
Frequency [rad/s]

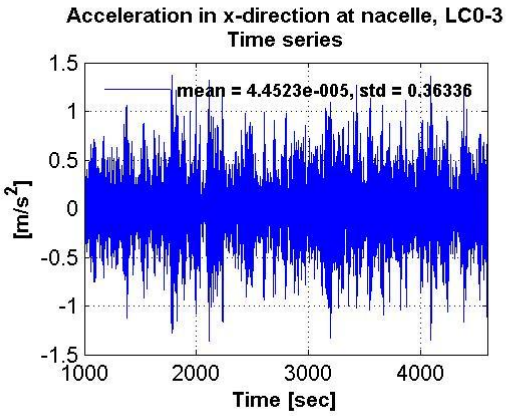
Acceleration in x-direction at nacelle, LC0-3
Time series
mean = 4.4523e-005, std = 0.36336
[m/s²]
Time [sec]

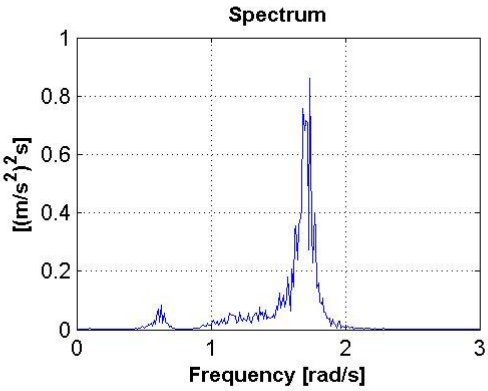
Spectrum
[(m/s²)²s]
Frequency [rad/s]

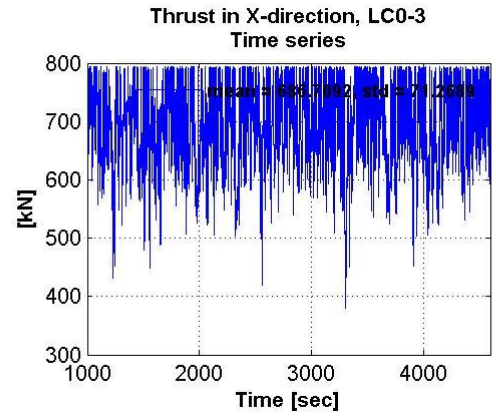
Thrust in X-direction, LC0-3
Time series
mean = 634.7052, std = 71.2609
[kN]
Time [sec]

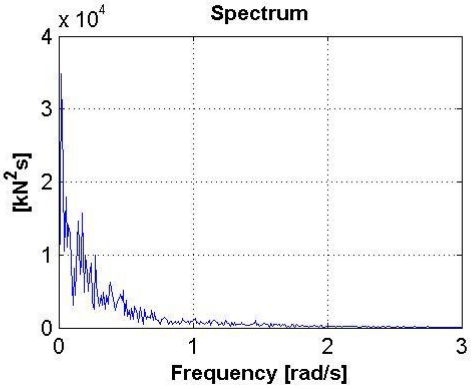
Spectrum
x 10^4
[kN^2s]
Frequency [rad/s]

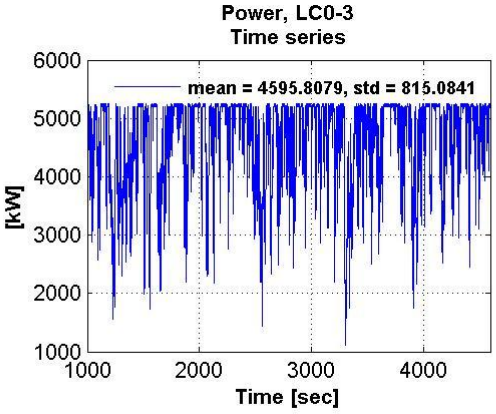
Power, LC0-3
Time series
mean = 4595.8079, std = 815.0841
[kW]
Time [sec]

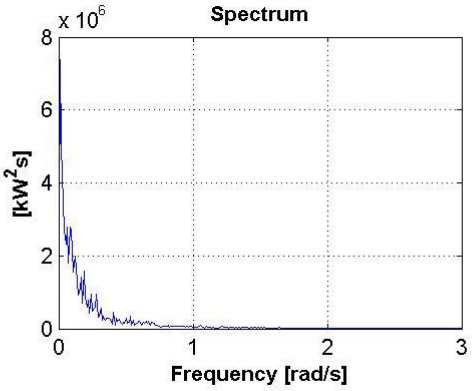
Spectrum
x 10^6
[kW^2s]
Frequency [rad/s]

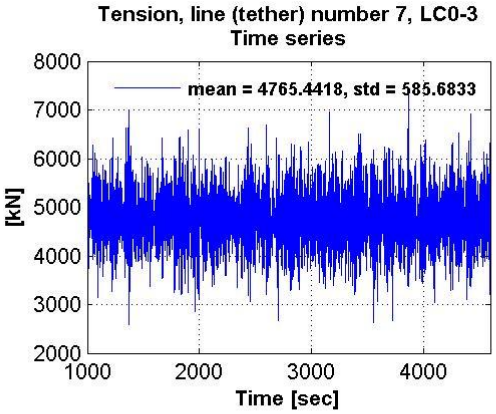
Tension, line (tether) number 7, LC0-3
Time series
mean = 4765.4418, std = 585.6833
[kN]
Time [sec]

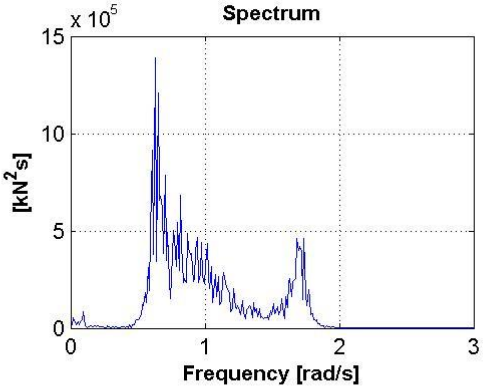
Spectrum
x 10^5
[kN^2s]
Frequency [rad/s]

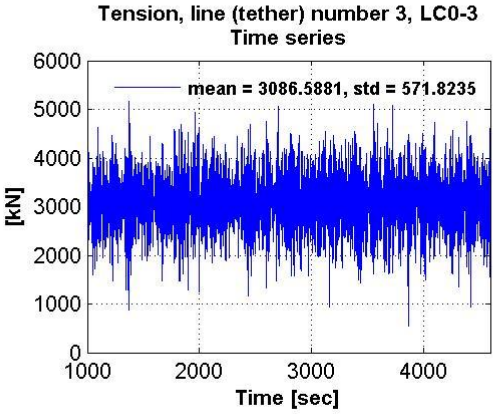
Tension, line (tether) number 3, LC0-3
Time series
mean = 3086.5881, std = 571.8235
[kN]
Time [sec]

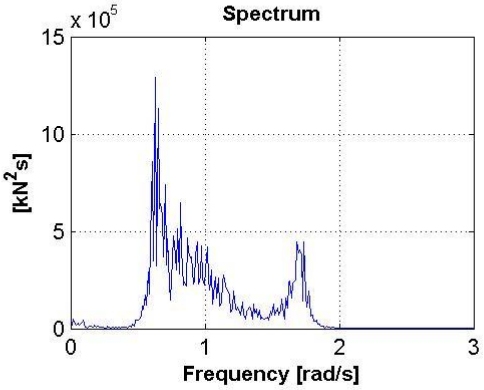
Spectrum
x 10^5
[kN^2s]
Frequency [rad/s]

C.2 LC0-4

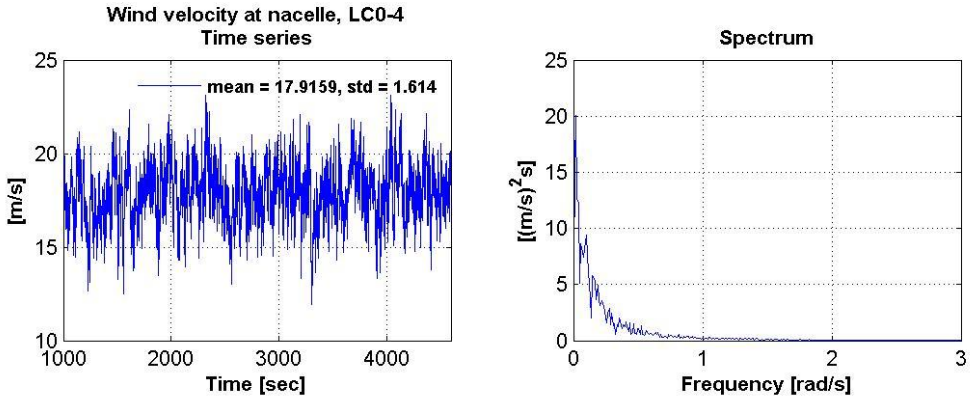
Wind velocity at nacelle, LC0-4
Time series
mean = 17.9159, std = 1.614
[m/s]
Time [sec]
Spectrum
[(m/s)^2s]
Frequency [rad/s]

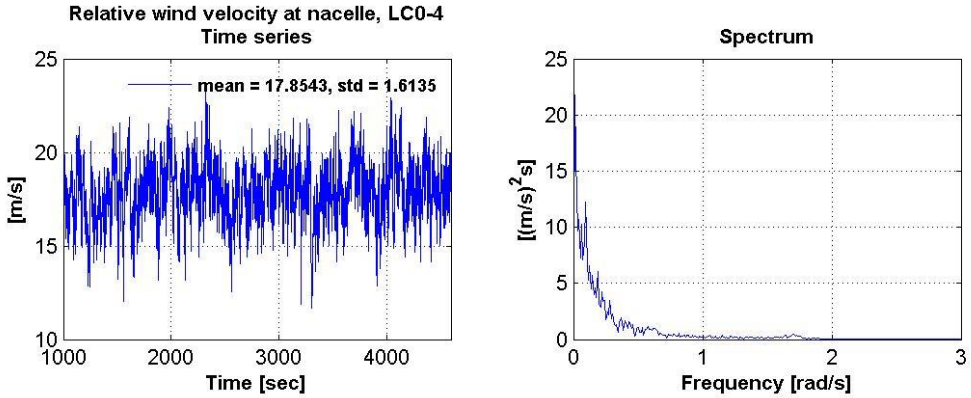
Relative wind velocity at nacelle, LC0-4
Time series
mean = 17.8543, std = 1.6135
[m/s]
Time [sec]
Spectrum
[(m/s)^2s]
Frequency [rad/s]

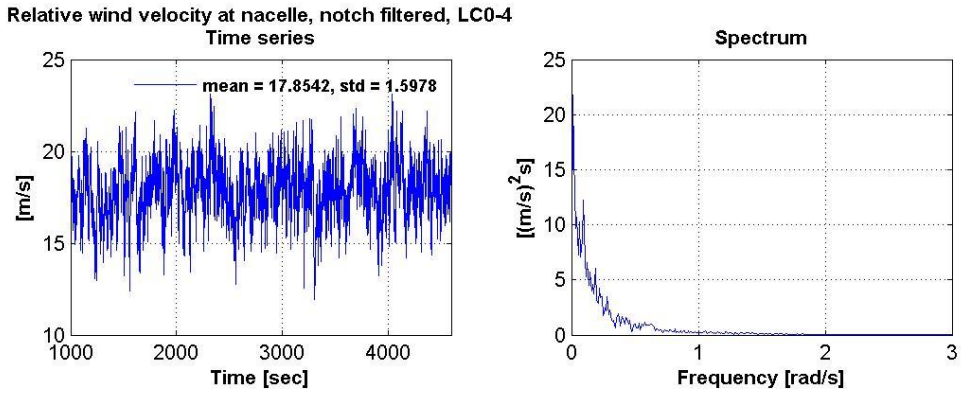
Relative wind velocity at nacelle, notch filtered, LC0-4
Time series
mean = 17.8542, std = 1.5978
[m/s]
Time [sec]
Spectrum
[(m/s)^2s]
Frequency [rad/s]

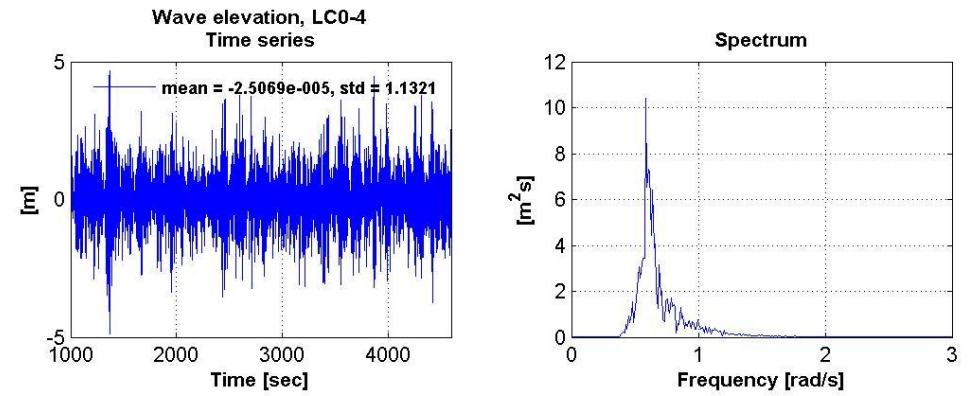
Wave elevation, LC0-4
Time series
mean = -2.5069e-005, std = 1.1321
[m]
Time [sec]
Spectrum
[m^2s]
Frequency [rad/s]

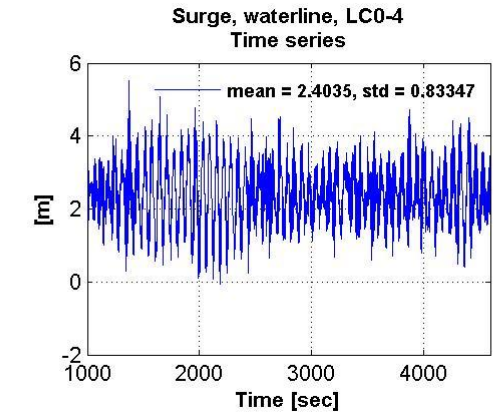
Surge, waterline, LC0-4
Time series
mean = 2.4035, std = 0.83347
[m]
Time [sec]

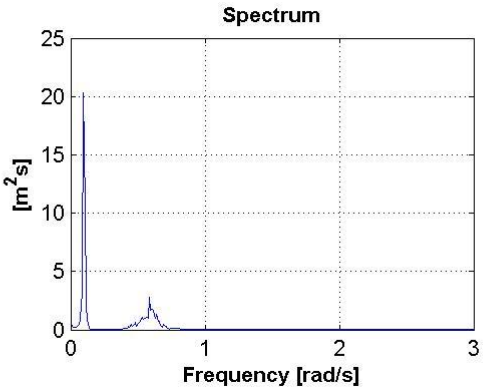
Spectrum
[m²s]
Frequency [rad/s]

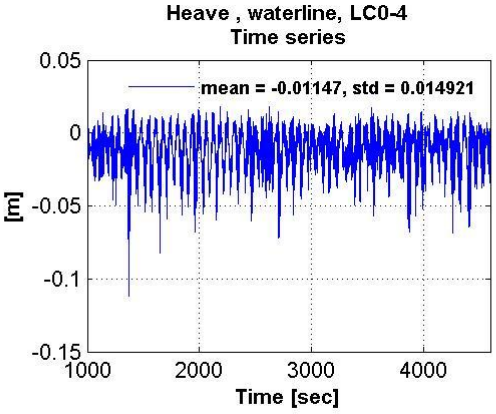
Heave , waterline, LC0-4
Time series
mean = -0.01147, std = 0.014921
[m]
Time [sec]

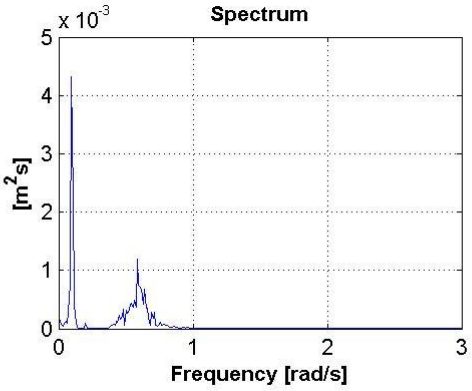
Spectrum
x 10⁻³
[m²s]
Frequency [rad/s]

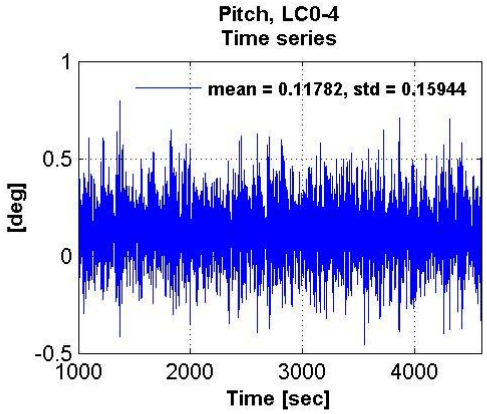
Pitch, LC0-4
Time series
mean = 0.11782, std = 0.15944
[deg]
Time [sec]

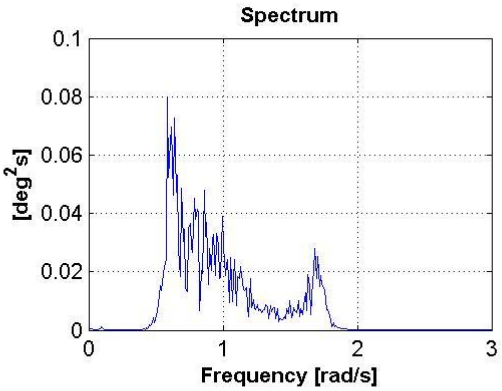
Spectrum
[deg²s]
Frequency [rad/s]

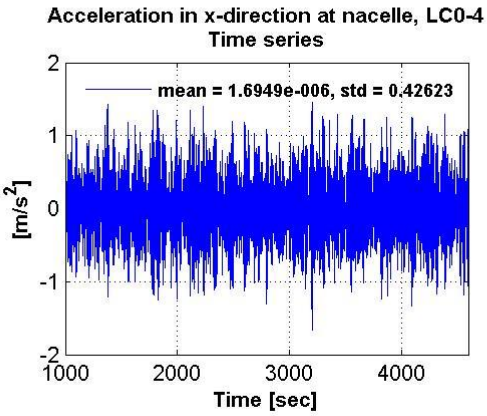
Acceleration in x-direction at nacelle, LC0-4
Time series
mean = 1.6949e-006, std = 0.42623
[m/s²]
Time [sec]

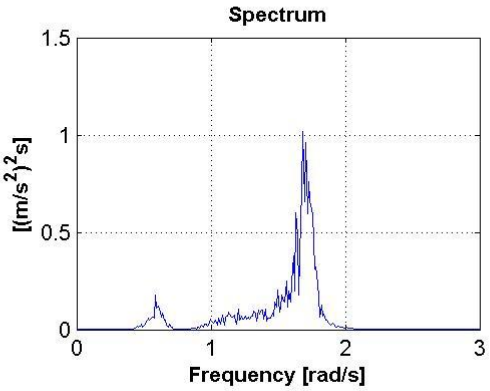
Spectrum
[(m/s²)²s]
Frequency [rad/s]

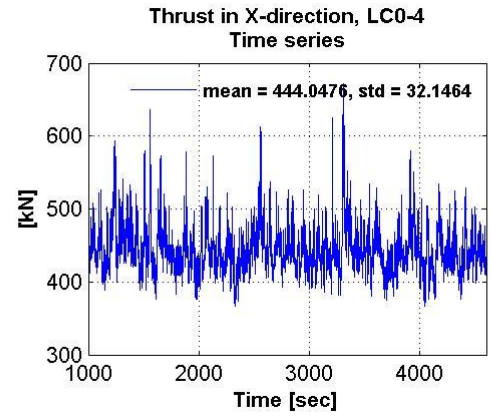
Thrust in X-direction, LC0-4
Time series
mean = 444.0476, std = 32.1464
[kN]
Time [sec]

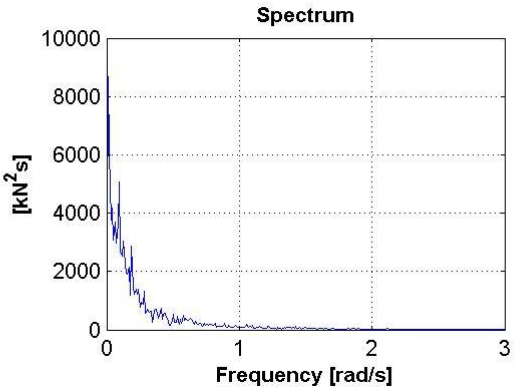
Spectrum
[kN²s]
Frequency [rad/s]

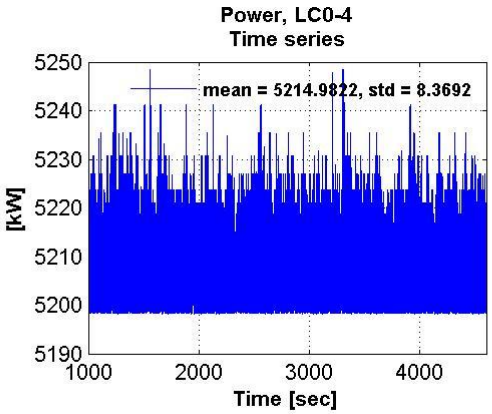
Power, LC0-4
Time series
mean = 5214.9822, std = 8.3692
[kW]
Time [sec]

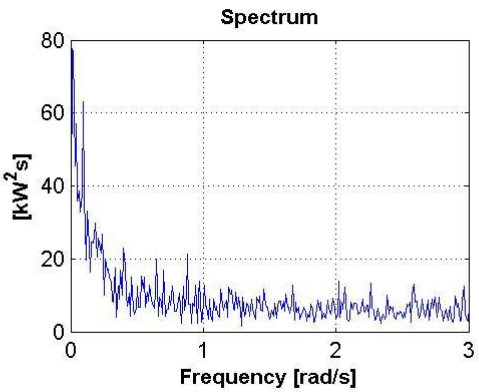
Spectrum
[kW²s]
Frequency [rad/s]

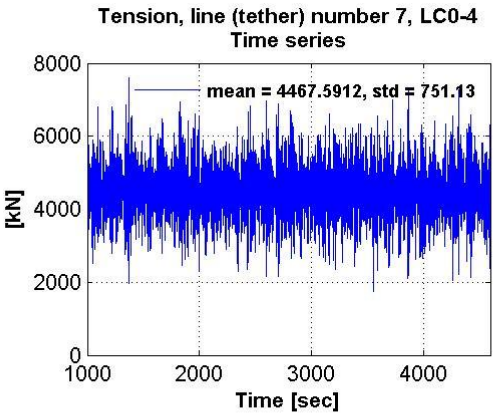
Tension, line (tether) number 7, LC0-4
Time series
mean = 4467.5912, std = 751.13
[kN]
Time [sec]

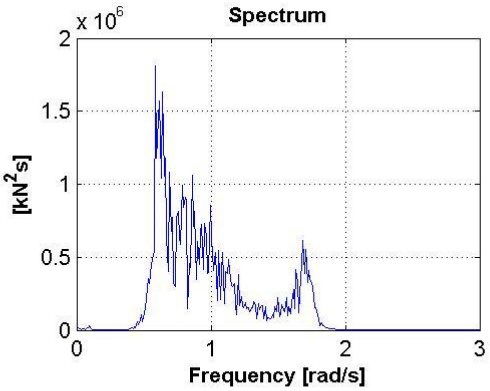
x 10⁶
Spectrum
[kN²s]
Frequency [rad/s]

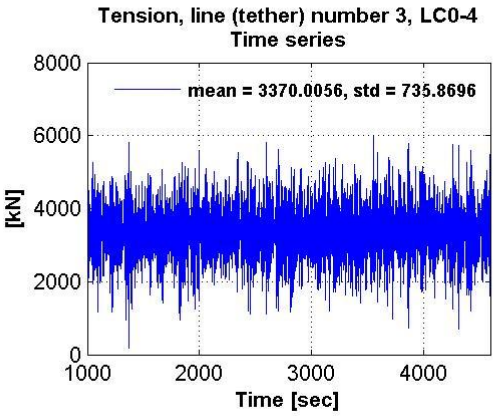
Tension, line (tether) number 3, LC0-4
Time series
mean = 3370.0056, std = 735.8696
[kN]
Time [sec]

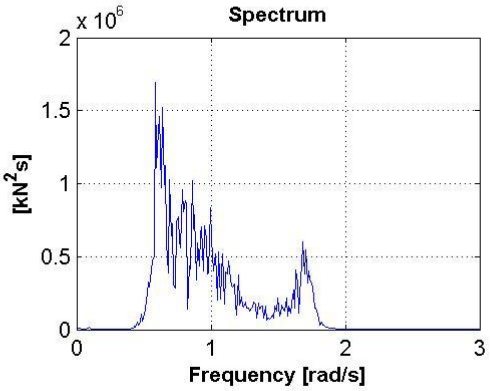
x 10⁶
Spectrum
[kN²s]
Frequency [rad/s]

C.3 LC0-5

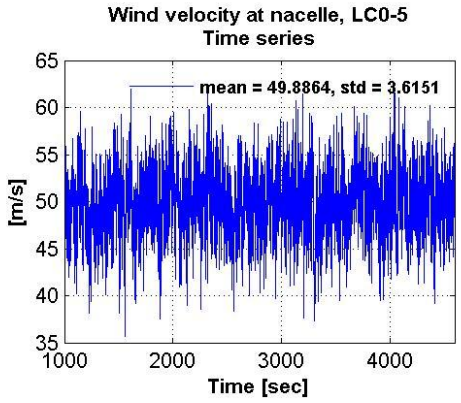
Wind velocity at nacelle, LC0-5
Time series
mean = 49.8864, std = 3.6151
[m/s]
Time [sec]

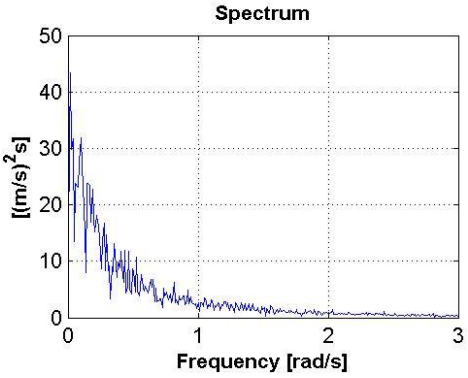
Spectrum
[(m/s)^2 s]
Frequency [rad/s]

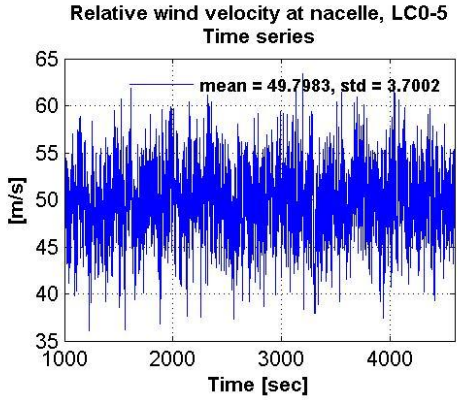
Relative wind velocity at nacelle, LC0-5
Time series
mean = 49.7983, std = 3.7002
[m/s]
Time [sec]

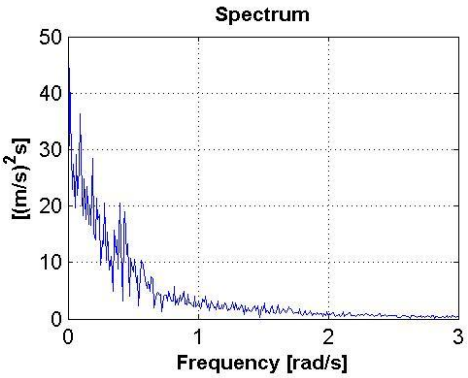
Spectrum
[(m/s)^2 s]
Frequency [rad/s]

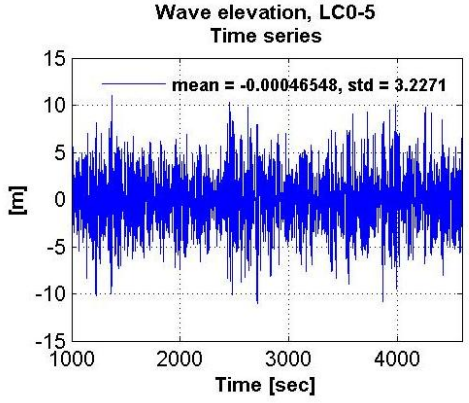
Wave elevation, LC0-5
Time series
mean = -0.00046548, std = 3.2271
[m]
Time [sec]

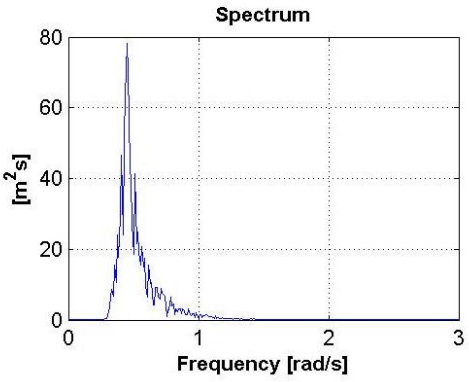
Spectrum
[m^2 s]
Frequency [rad/s]

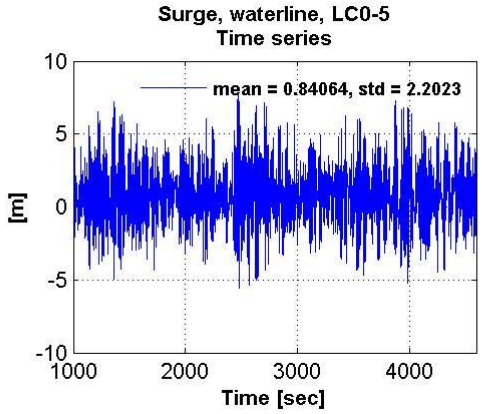
Surge, waterline, LC0-5
Time series
mean = 0.84064, std = 2.2023
[m]
Time [sec]

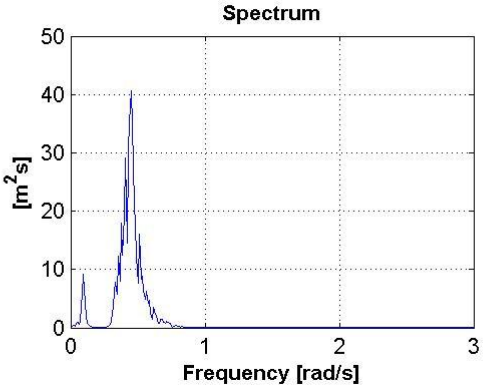
Spectrum
[m²s]
Frequency [rad/s]

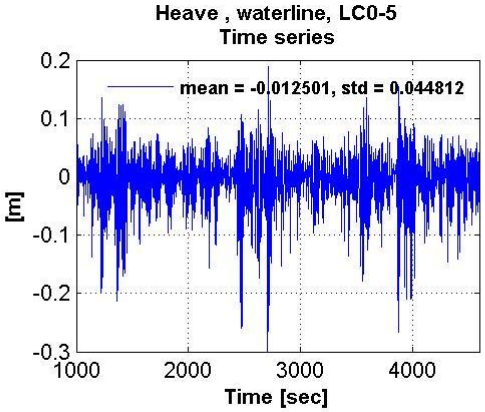
Heave , waterline, LC0-5
Time series
mean = -0.012501, std = 0.044812
[m]
Time [sec]

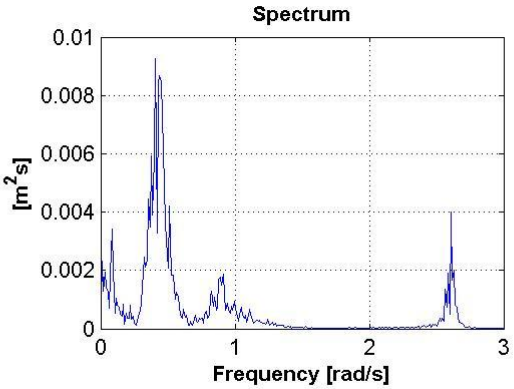
Spectrum
[m²s]
Frequency [rad/s]

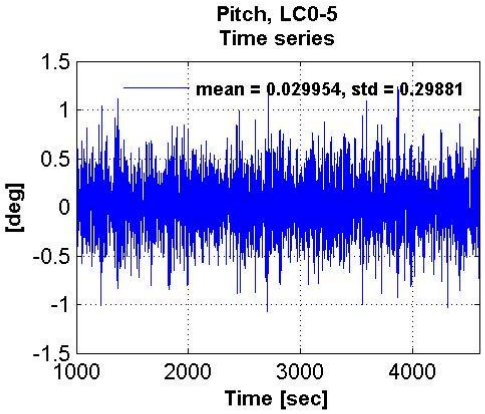
Pitch, LC0-5
Time series
mean = 0.029954, std = 0.29881
[deg]
Time [sec]

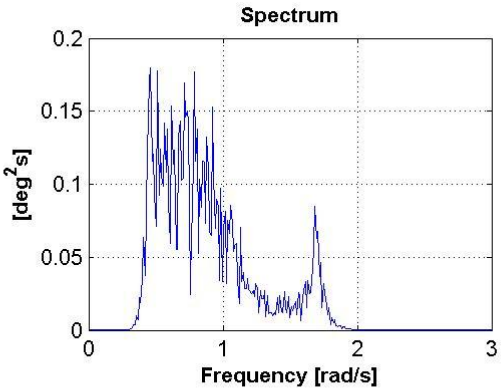
Spectrum
[deg²s]
Frequency [rad/s]

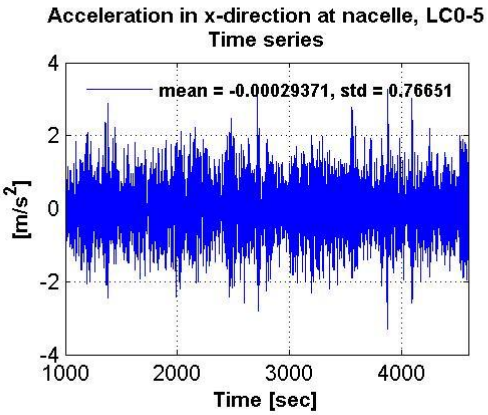
Acceleration in x-direction at nacelle, LC0-5
Time series
mean = -0.00029371, std = 0.76651
[m/s²]
Time [sec]

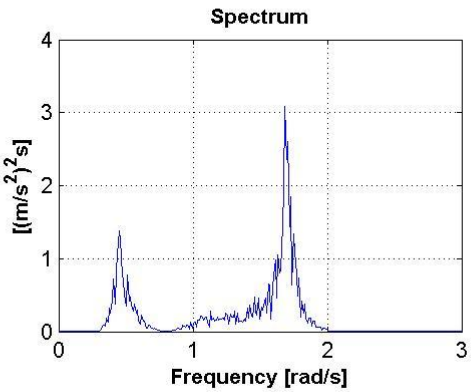
Spectrum
[(m/s²)²s]
Frequency [rad/s]

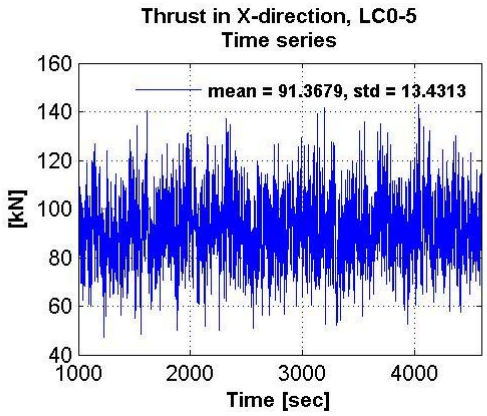
Thrust in X-direction, LC0-5
Time series
mean = 91.3679, std = 13.4313
[kN]
Time [sec]

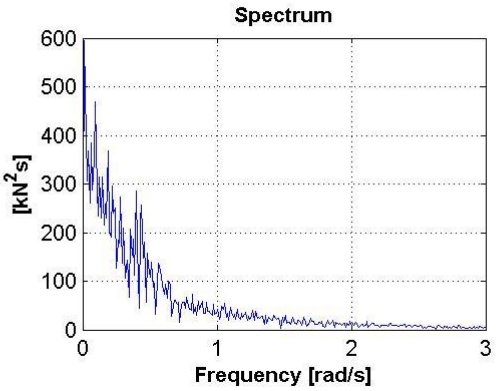
Spectrum
[kN²s]
Frequency [rad/s]

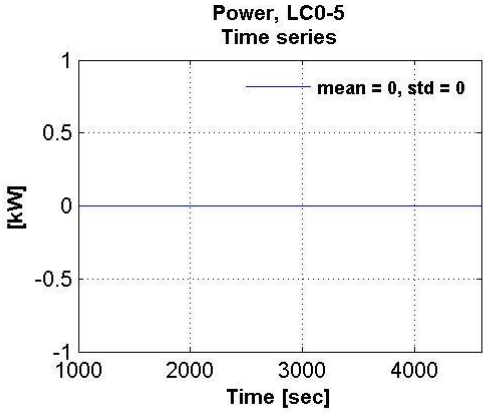
Power, LC0-5
Time series
mean = 0, std = 0
[kW]
Time [sec]

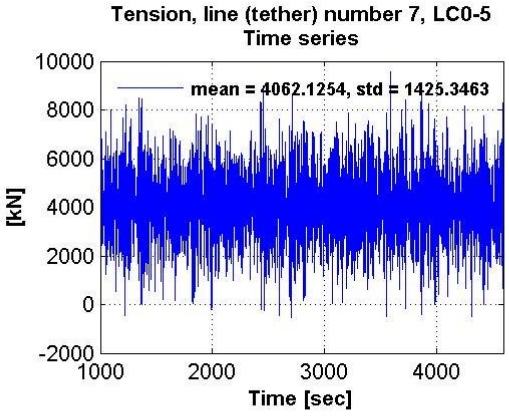
Tension, line (tether) number 7, LC0-5
Time series
mean = 4062.1254, std = 1425.3463
[kN]
Time [sec]

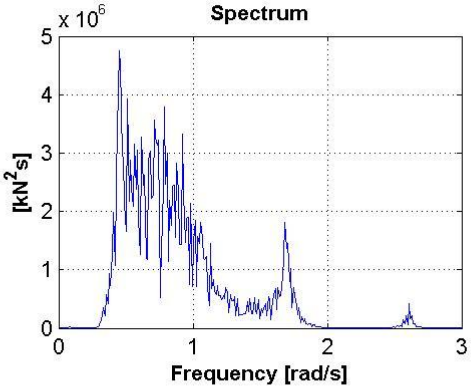
x 10⁶
Spectrum
[kN²s]
Frequency [rad/s]

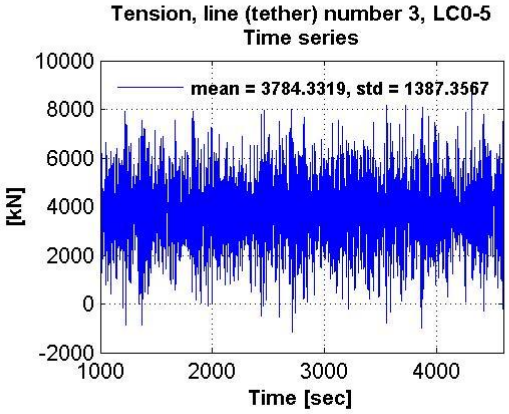
Tension, line (tether) number 3, LC0-5
Time series
mean = 3784.3319, std = 1387.3567
[kN]
Time [sec]

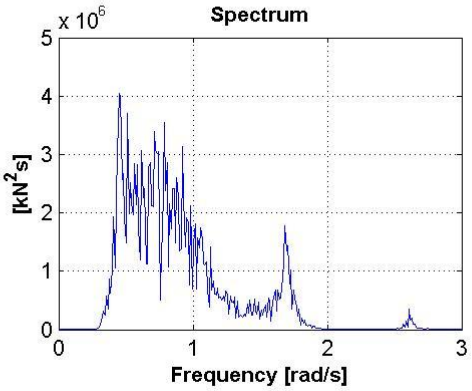
x 10⁶
Spectrum
[kN²s]
Frequency [rad/s]

C.4 LC30-3

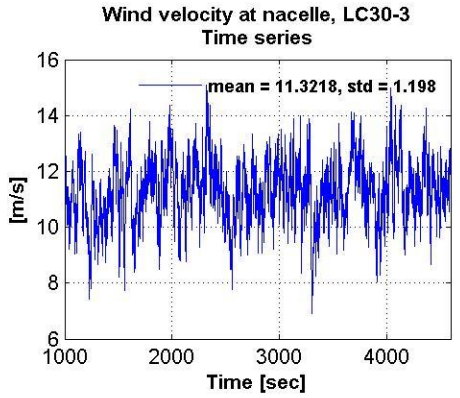
Wind velocity at nacelle, LC30-3
Time series
mean = 11.3218, std = 1.198
[m/s]
Time [sec]

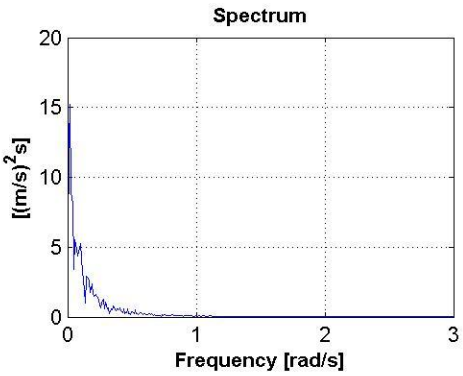
Spectrum
[(m/s)²s]
Frequency [rad/s]

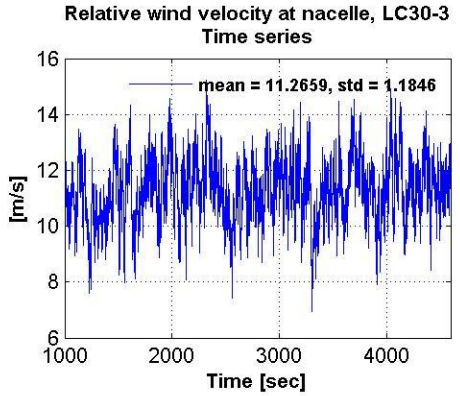
Relative wind velocity at nacelle, LC30-3
Time series
mean = 11.2659, std = 1.1846
[m/s]
Time [sec]

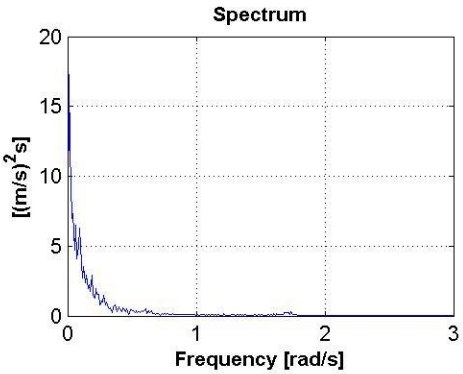
Spectrum
[(m/s)²s]
Frequency [rad/s]

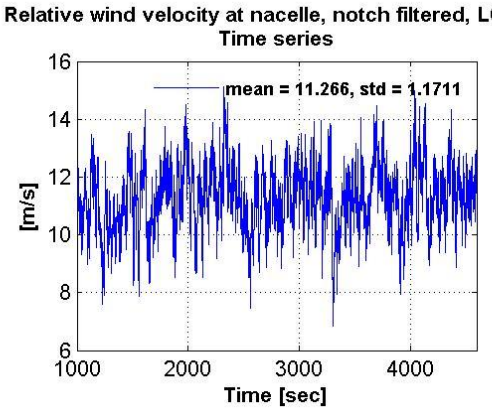
Relative wind velocity at nacelle, notch filtered, LC30-3
Time series
mean = 11.266, std = 1.1711
[m/s]
Time [sec]

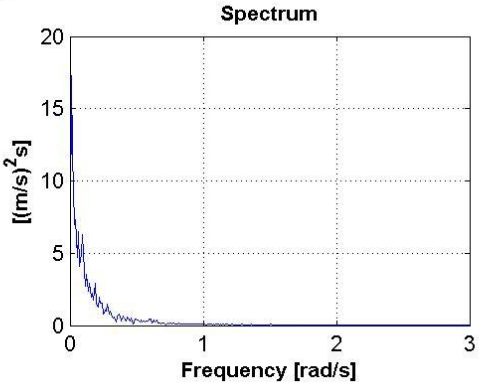
Spectrum
[(m/s)²s]
Frequency [rad/s]

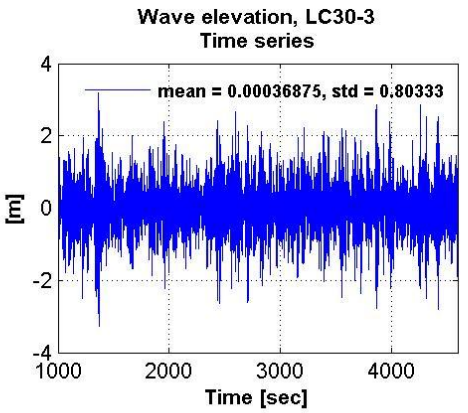
Wave elevation, LC30-3
Time series
mean = 0.00036875, std = 0.80333
[m]
Time [sec]

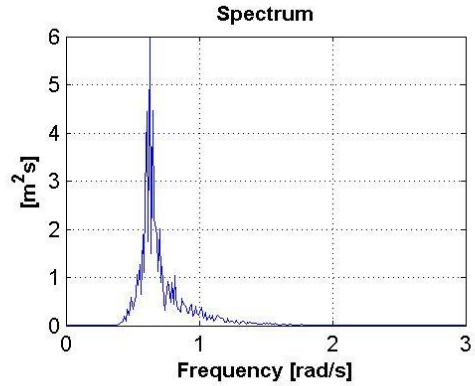
Spectrum
[m²s]
Frequency [rad/s]

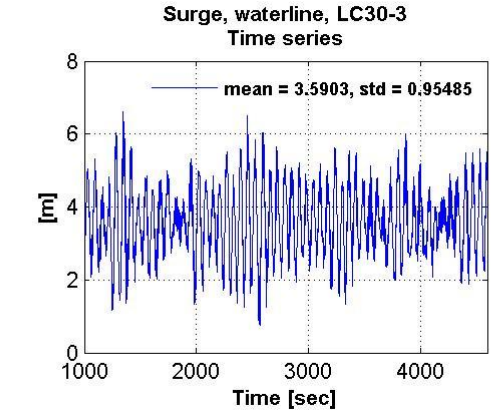
Surge, waterline, LC30-3
Time series
mean = 3.5903, std = 0.95485
[m]
Time [sec]

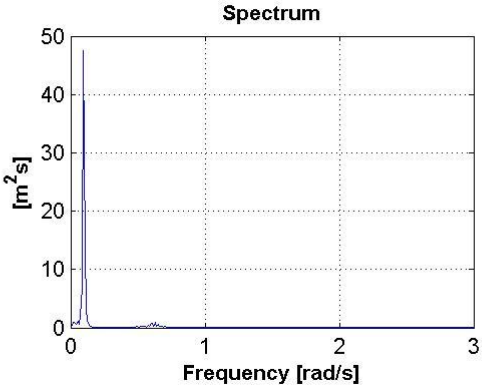
Spectrum
[m²s]
Frequency [rad/s]

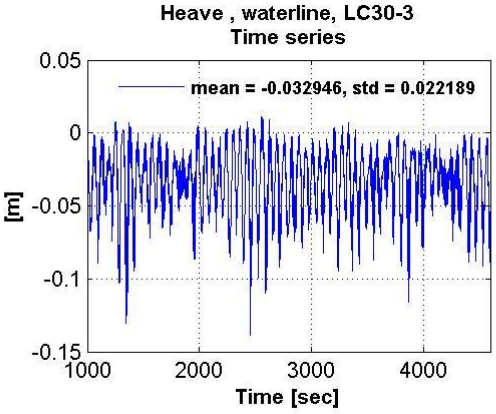
Heave , waterline, LC30-3
Time series
mean = -0.032946, std = 0.022189
[m]
Time [sec]

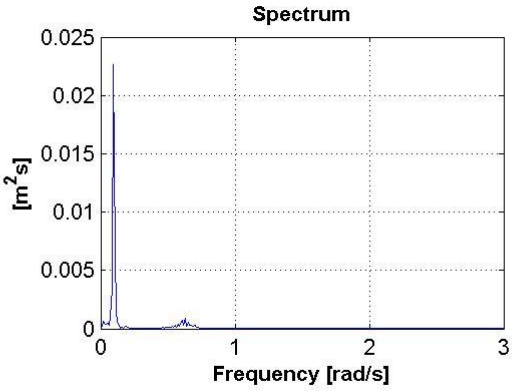
Spectrum
[m²s]
Frequency [rad/s]

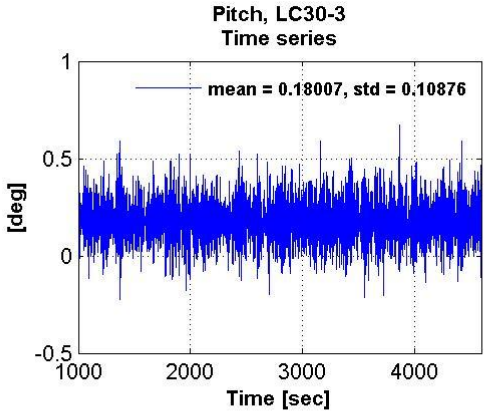
Pitch, LC30-3
Time series
mean = 0.18007, std = 0.10876
[deg]
Time [sec]

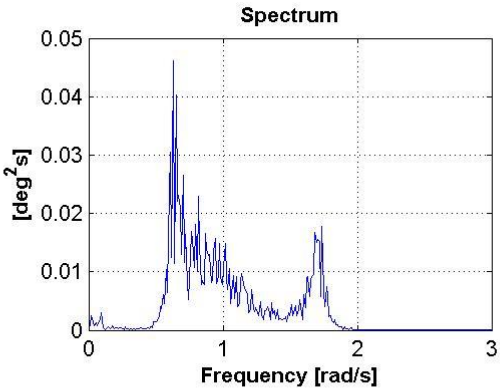
Spectrum
[deg²s]
Frequency [rad/s]

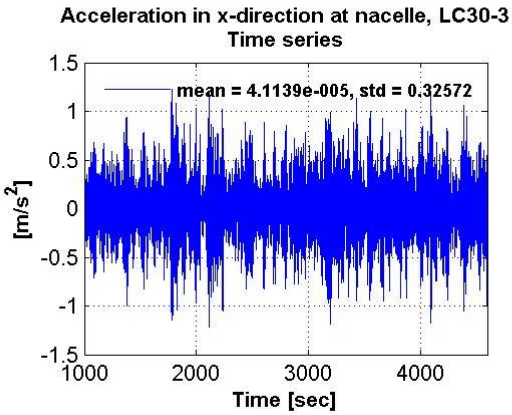
Acceleration in x-direction at nacelle, LC30-3
Time series
mean = 4.1139e-005, std = 0.32572
[m/s²]
Time [sec]

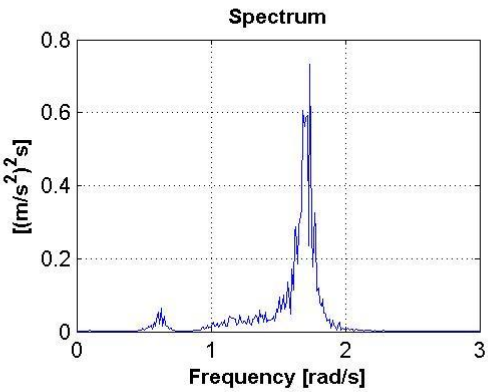
Spectrum
[(m/s²)²s]
Frequency [rad/s]

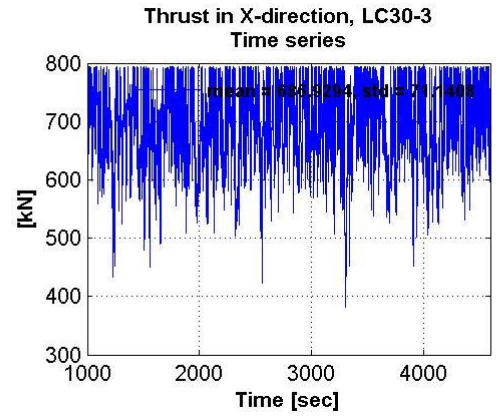
Thrust in X-direction, LC30-3
Time series
mean = 684.9294, std = 79.1408
[kN]
Time [sec]

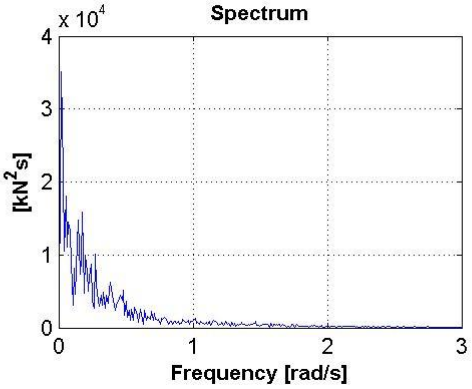
Spectrum
x 10^4
[kN^2s]
Frequency [rad/s]

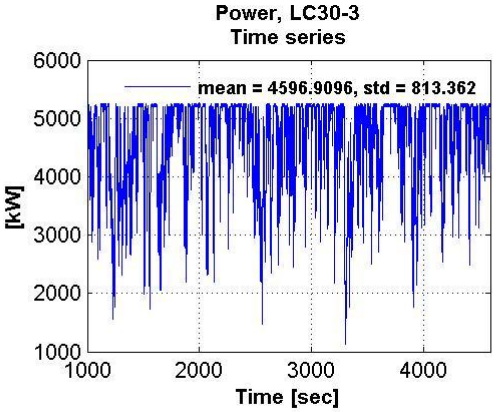
Power, LC30-3
Time series
mean = 4596.9096, std = 813.362
[kW]
Time [sec]

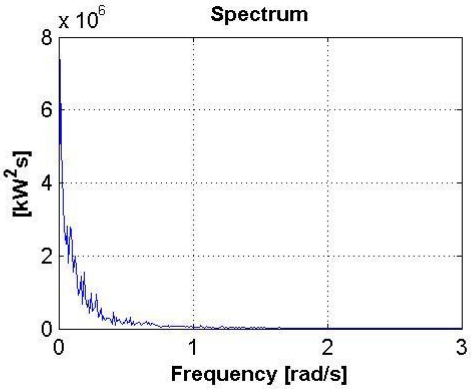
Spectrum
x 10^6
[kW^2s]
Frequency [rad/s]

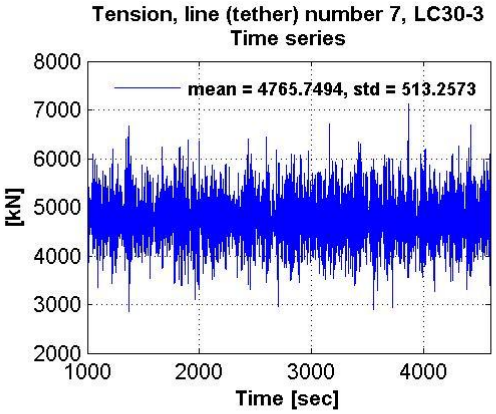
Tension, line (tether) number 7, LC30-3
Time series
mean = 4765.7494, std = 513.2573
[kN]
Time [sec]

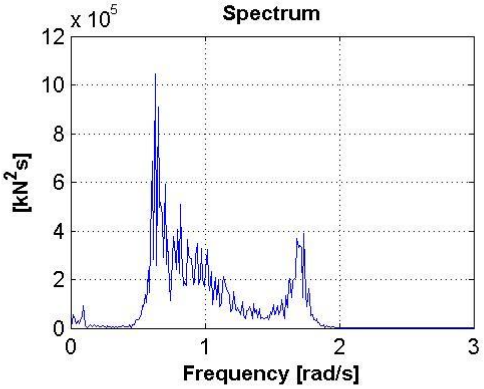
Spectrum
x 10^5
[kN^2s]
Frequency [rad/s]

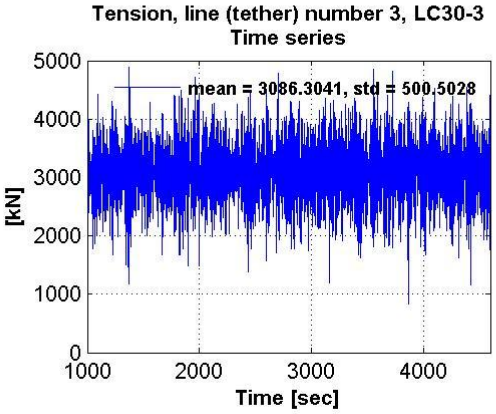
Tension, line (tether) number 3, LC30-3
Time series
mean = 3086.3041, std = 500.5028
[kN]
Time [sec]

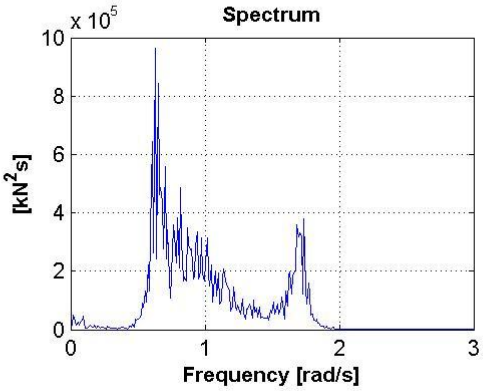
Spectrum
x 10^5
[kN^2s]
Frequency [rad/s]

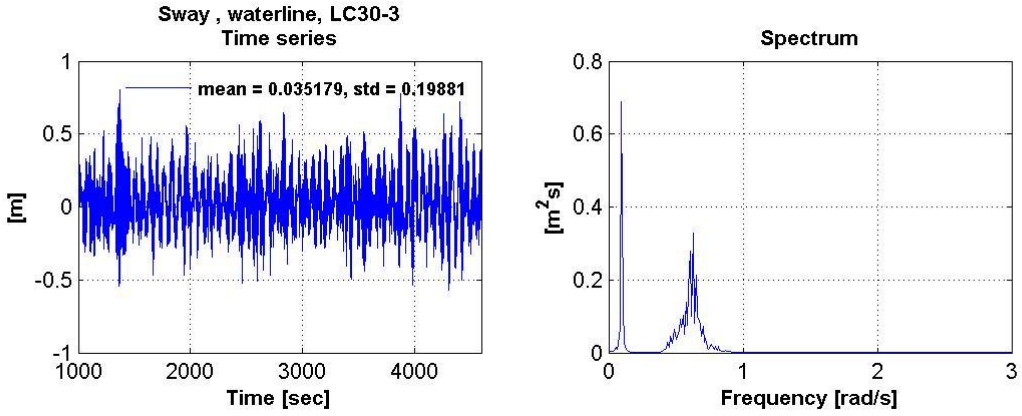
Sway , waterline, LC30-3
Time series
mean = 0.035179, std = 0.19881
[m]
Time [sec]
Spectrum
[m²s]
Frequency [rad/s]

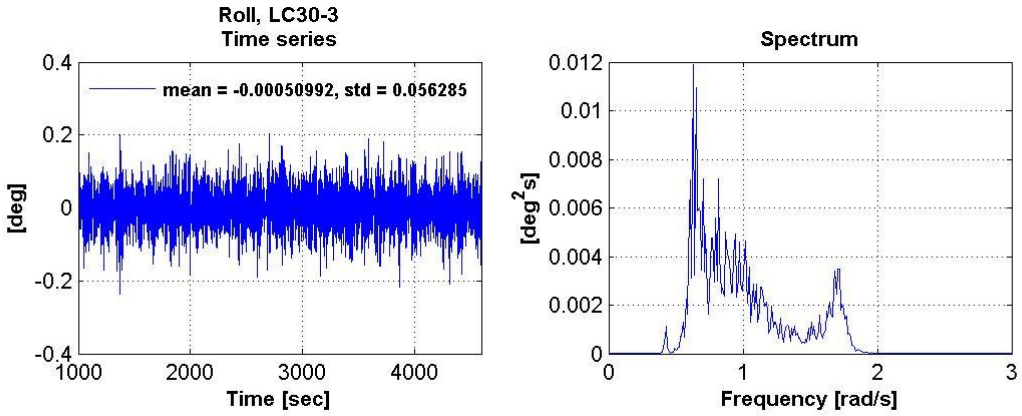
Roll, LC30-3
Time series
mean = -0.00050992, std = 0.056285
[deg]
Time [sec]
Spectrum
[deg²s]
Frequency [rad/s]

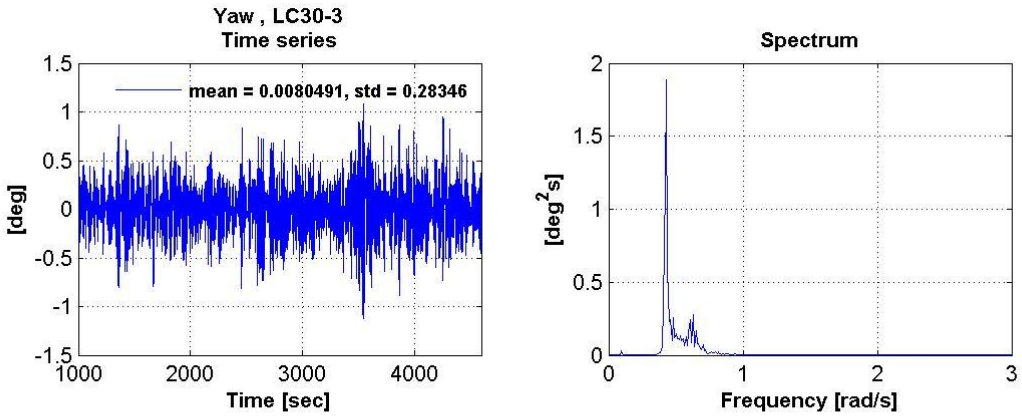
Yaw , LC30-3
Time series
mean = 0.0080491, std = 0.28346
[deg]
Time [sec]
Spectrum
[deg²s]
Frequency [rad/s]

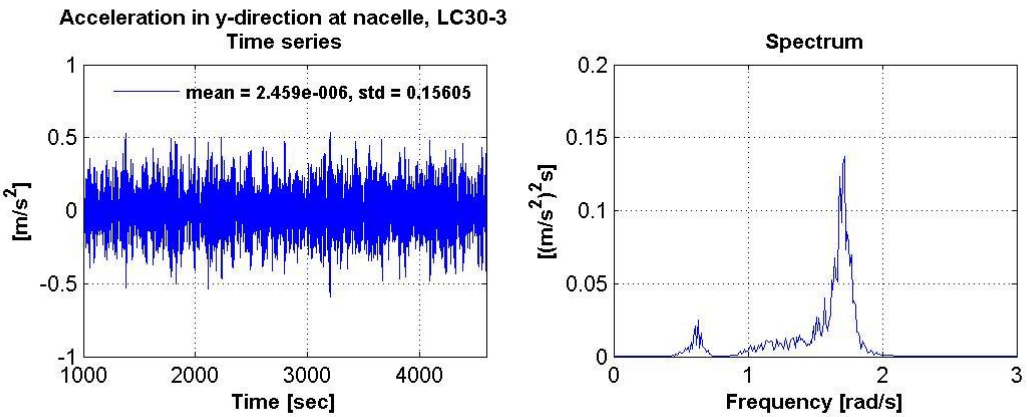
Acceleration in y-direction at nacelle, LC30-3
Time series
mean = 2.459e-006, std = 0.15605
[m/s²]
Time [sec]
Spectrum
[(m/s²)²s]
Frequency [rad/s]

Appendix D: Statistics of TLP, spar and semi-submersible

In the following the statistics (mean, standard deviation, min, max, skewness and kurtosis) of the three concepts are compared in the 11 load cases. 17 response parameters are considered.

Surge in the waterline:

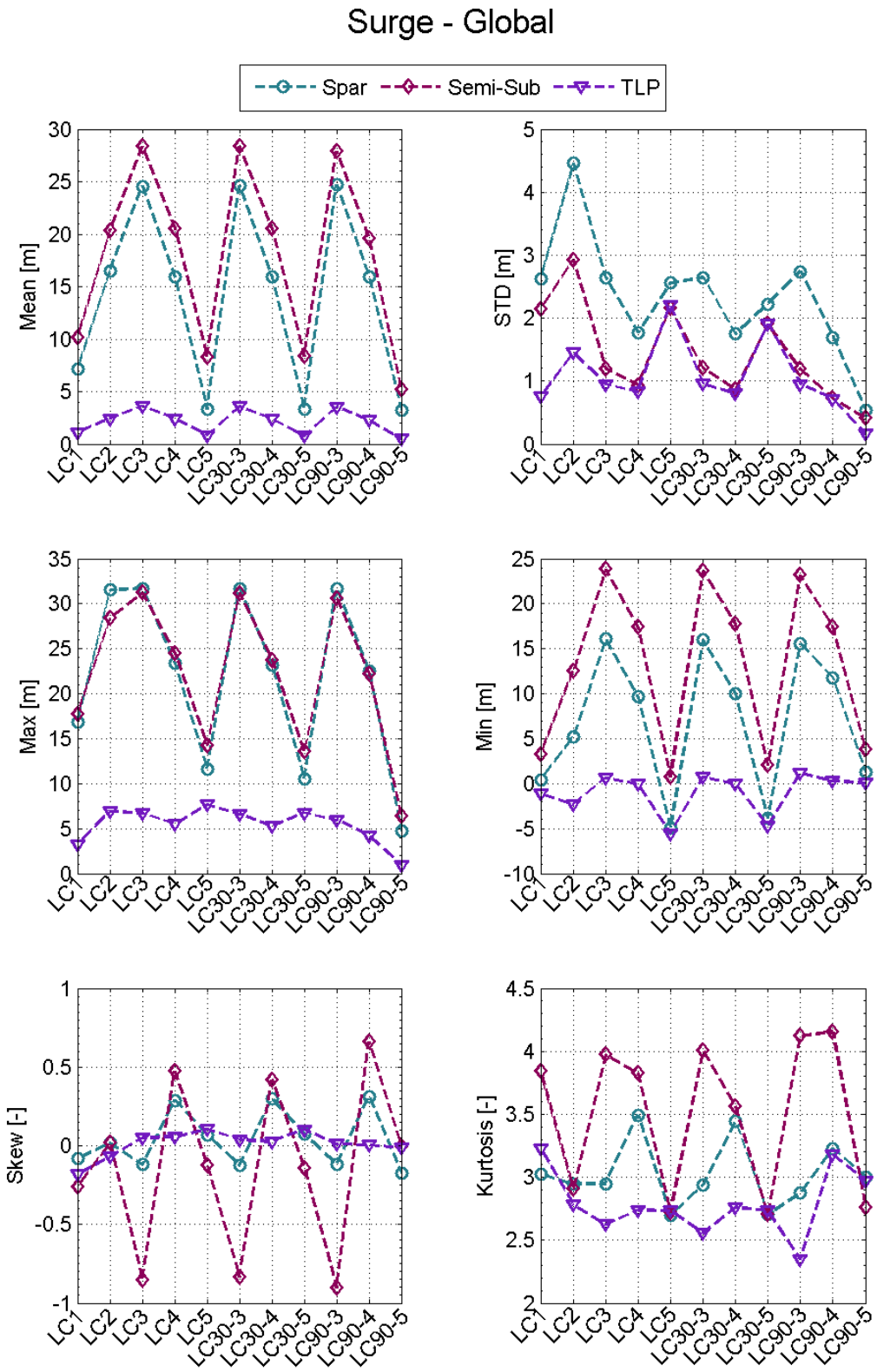

Sway in the waterline:

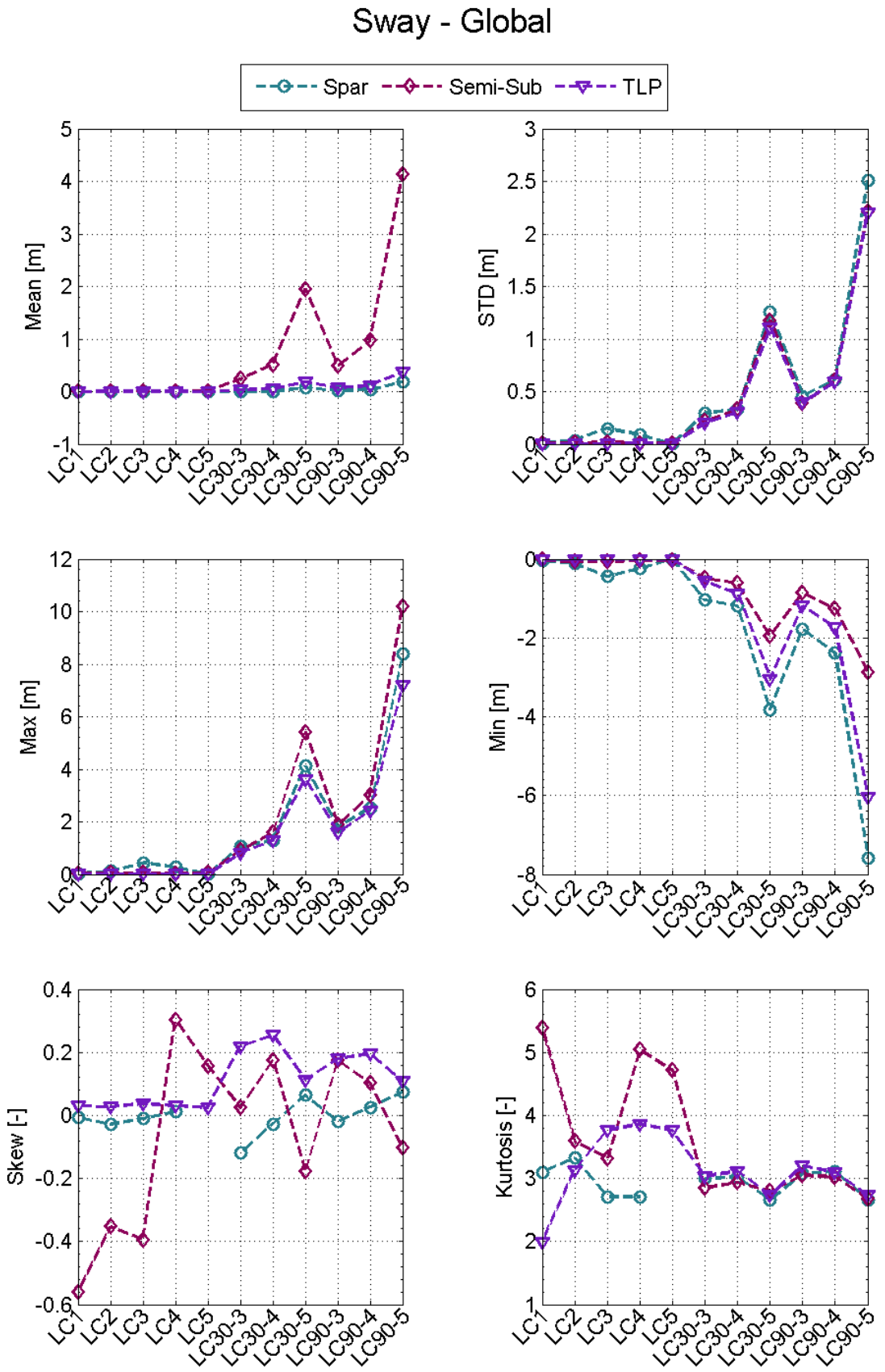

Heave in the waterline:

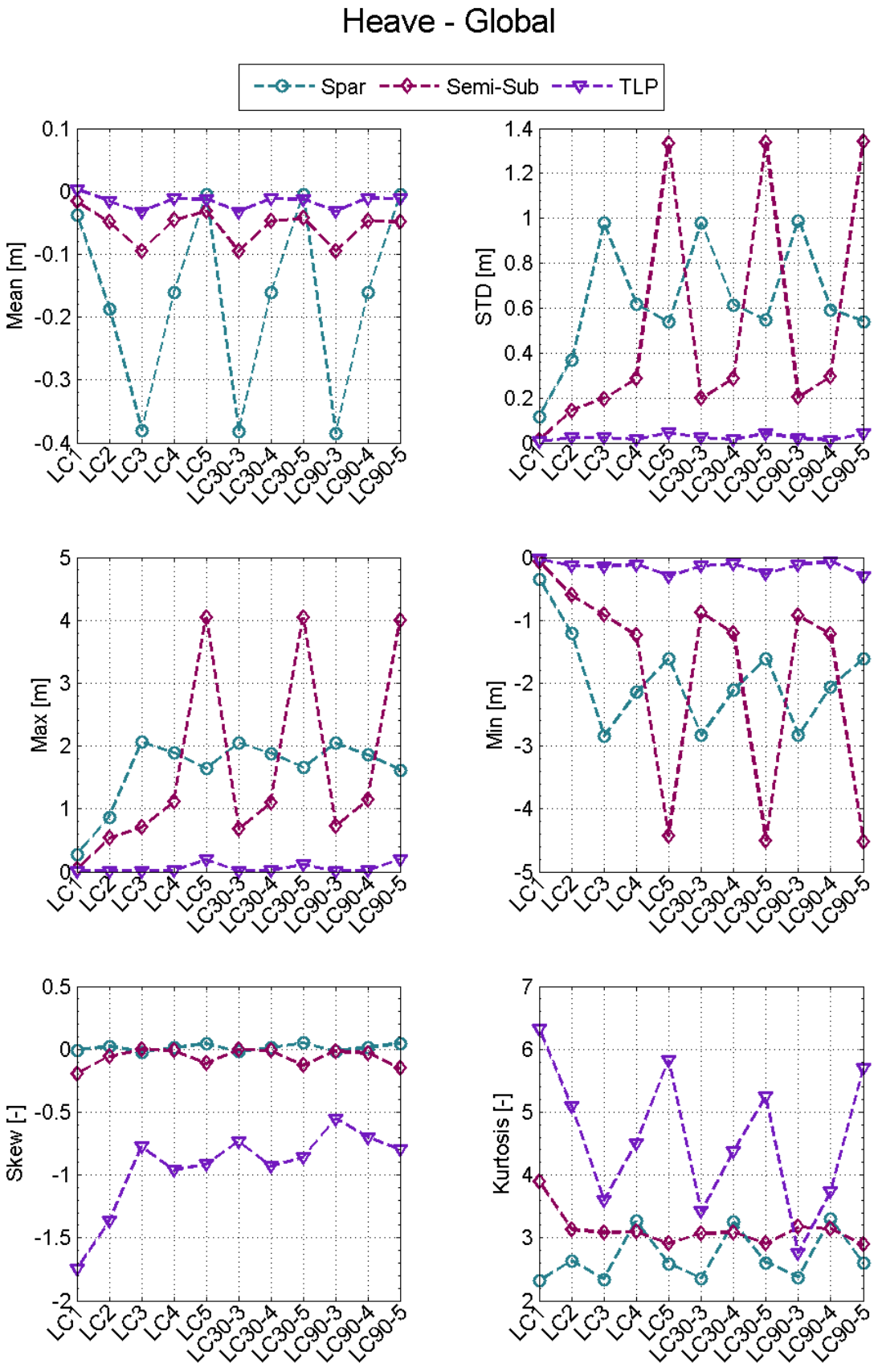

Roll:

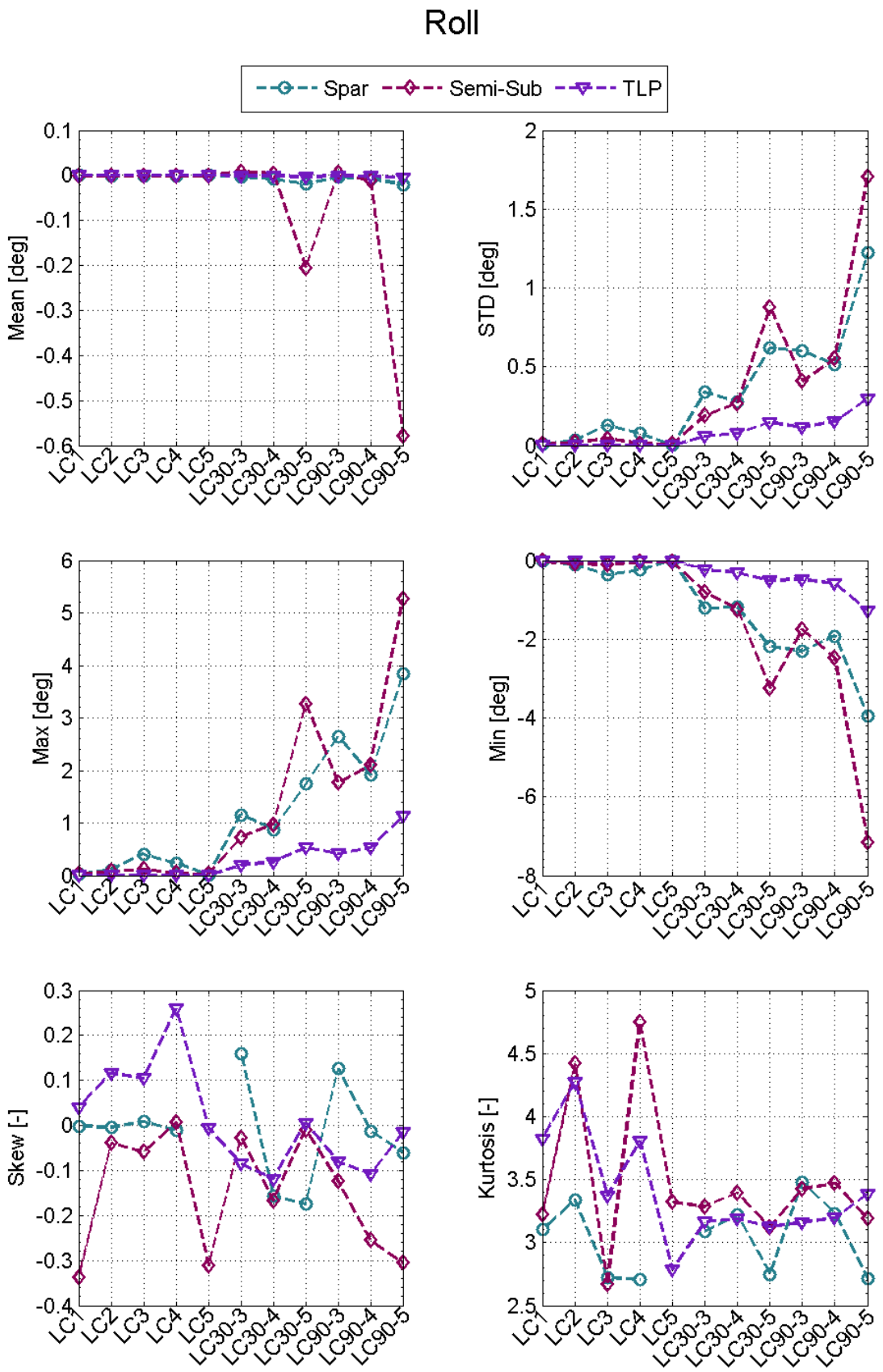
Roll
Spar
Semi-Sub
TLP
Mean [deg]
STD [deg]
Max [deg]
Min [deg]
Skew [-]
Kurtosis [-]
LC1
LC2
LC3
LC4
LC5
LC30-3
LC30-4
LC30-5
LC90-3
LC90-4
LC90-5

Pitch:

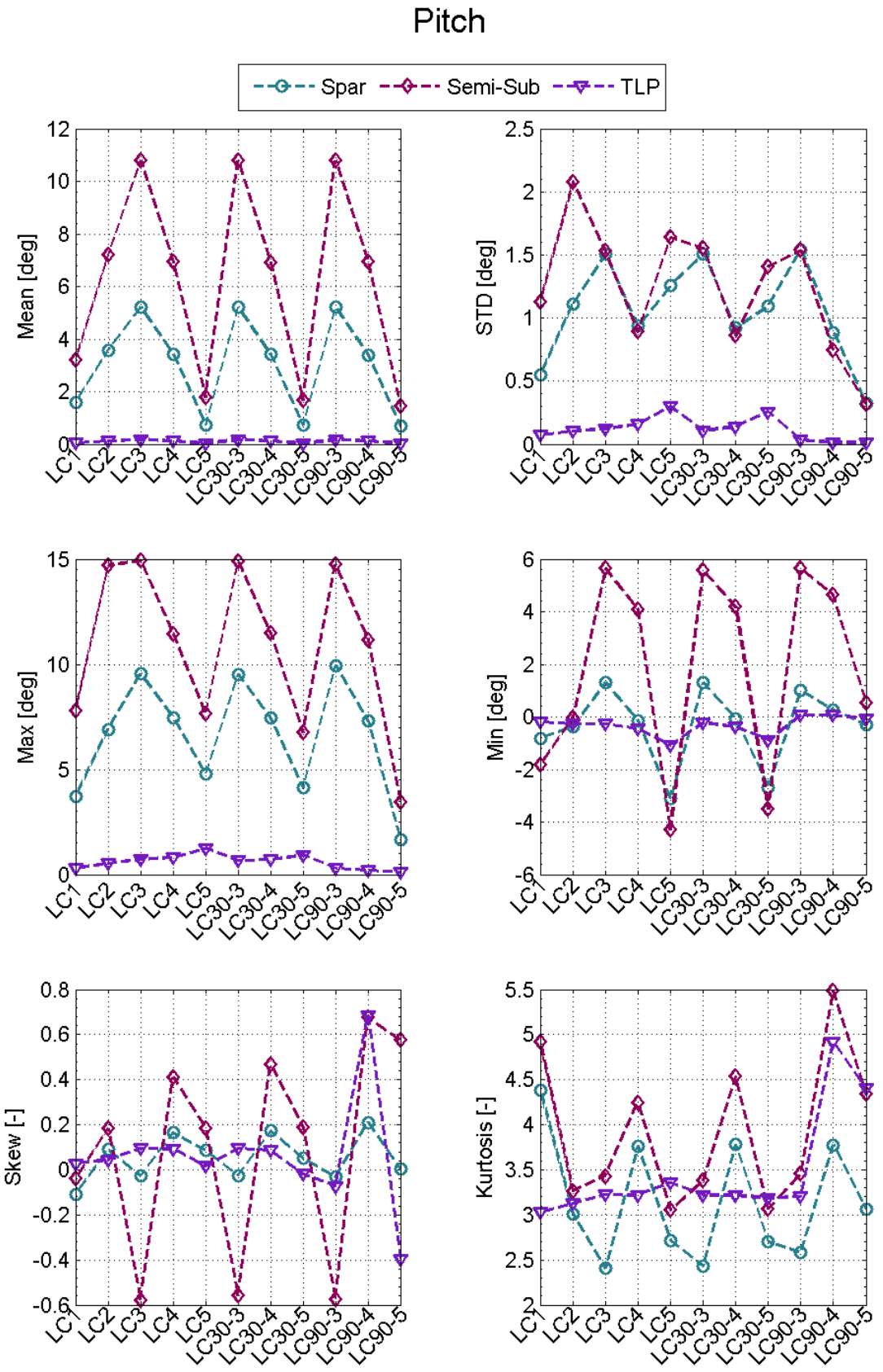
Pitch
Spar
Semi-Sub
TLP
Mean [deg]
STD [deg]
Max [deg]
Min [deg]
Skew [-]
Kurtosis [-]
LC1
LC2
LC3
LC4
LC5
LC30-3
LC30-4
LC30-5
LC90-3
LC90-4
LC90-5

Yaw:

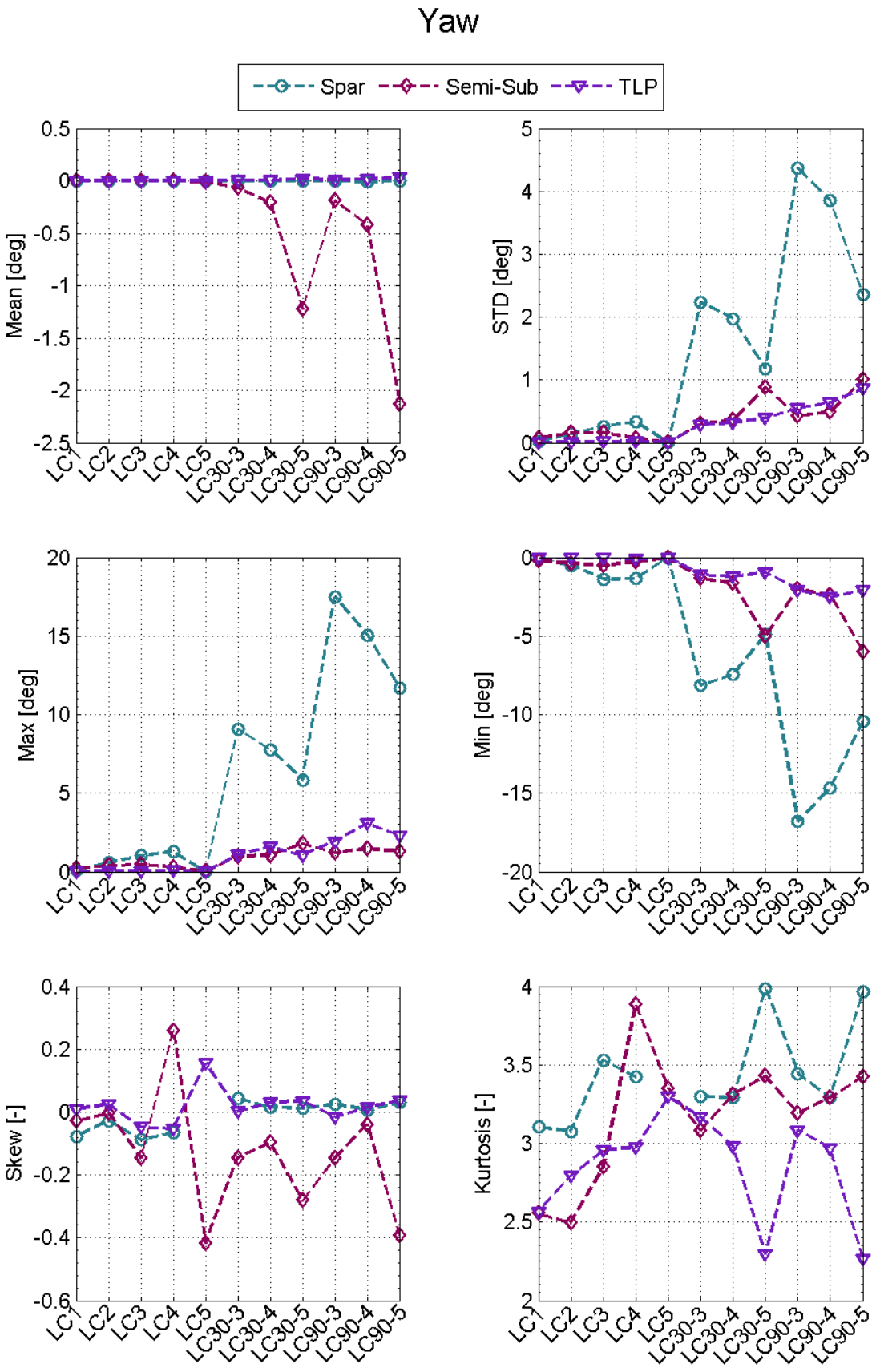
Yaw
Spar
Semi-Sub
TLP
Mean [deg]
STD [deg]
Max [deg]
Min [deg]
Skew [-]
Kurtosis [-]
LC1
LC2
LC3
LC4
LC5
LC30-3
LC30-4
LC30-5
LC90-3
LC90-4
LC90-5

Surge motion at nacelle:

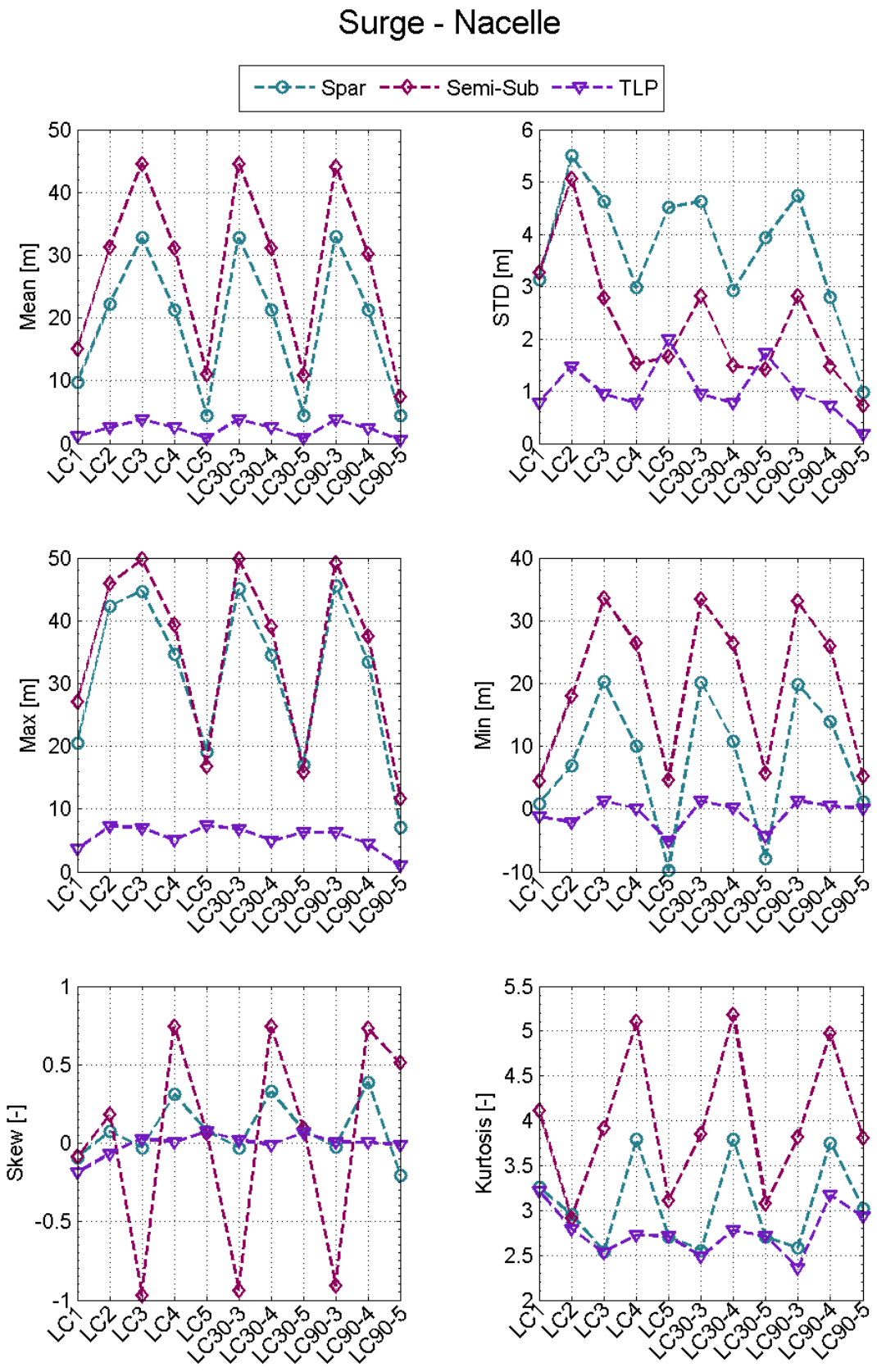

Sway motion at nacelle:

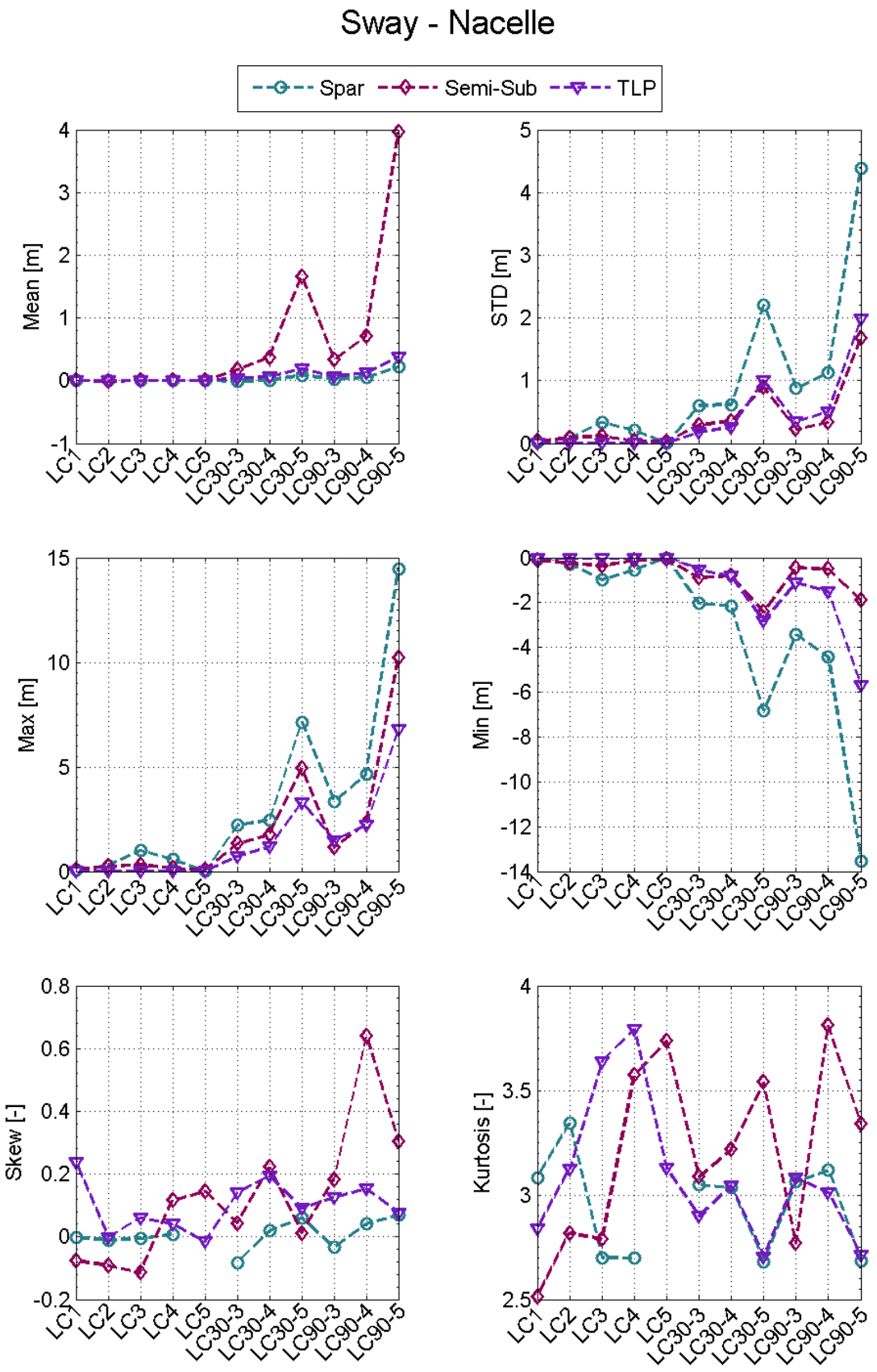

Surge acceleration at nacelle:

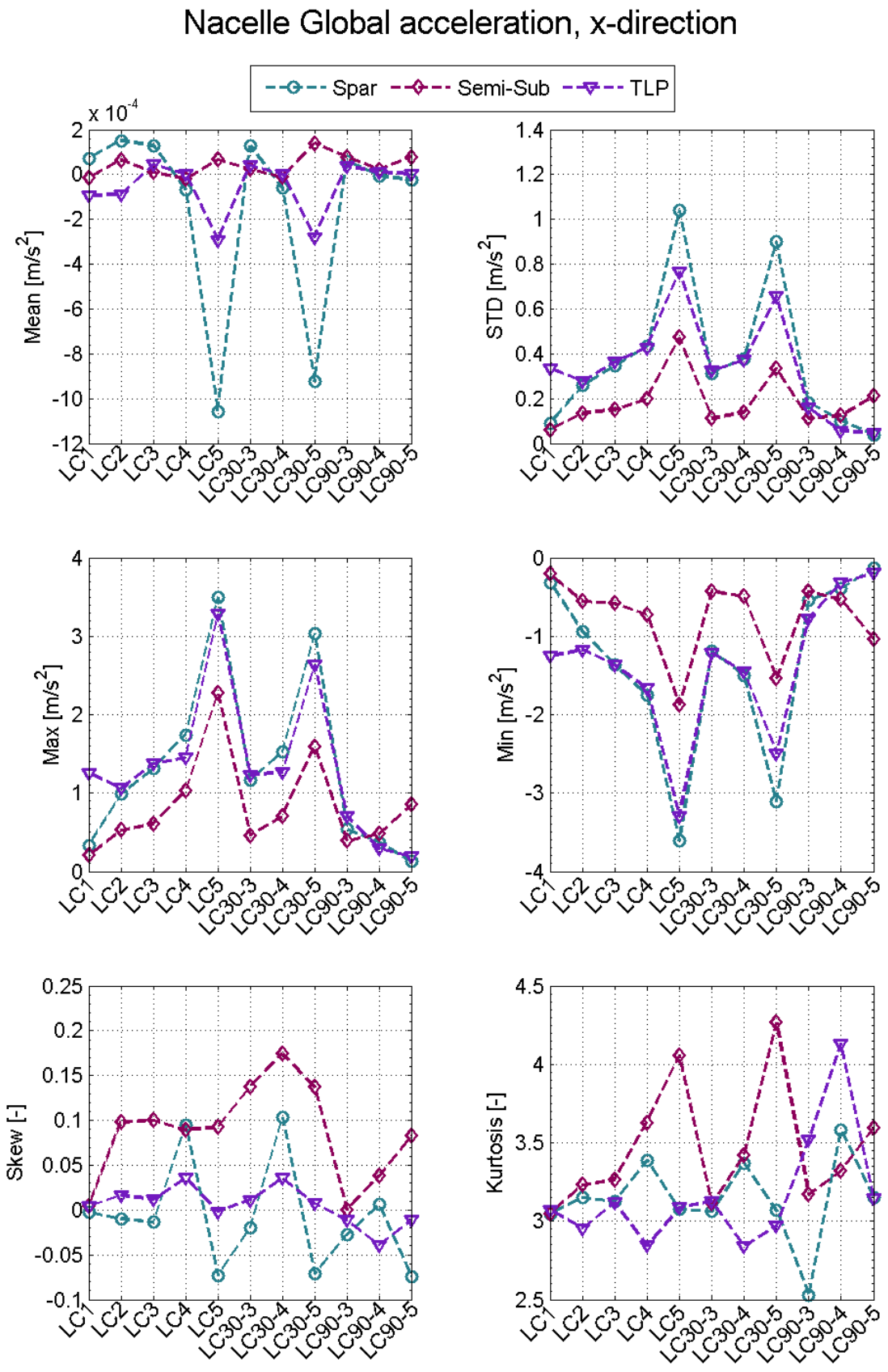

Sway acceleration at nacelle:

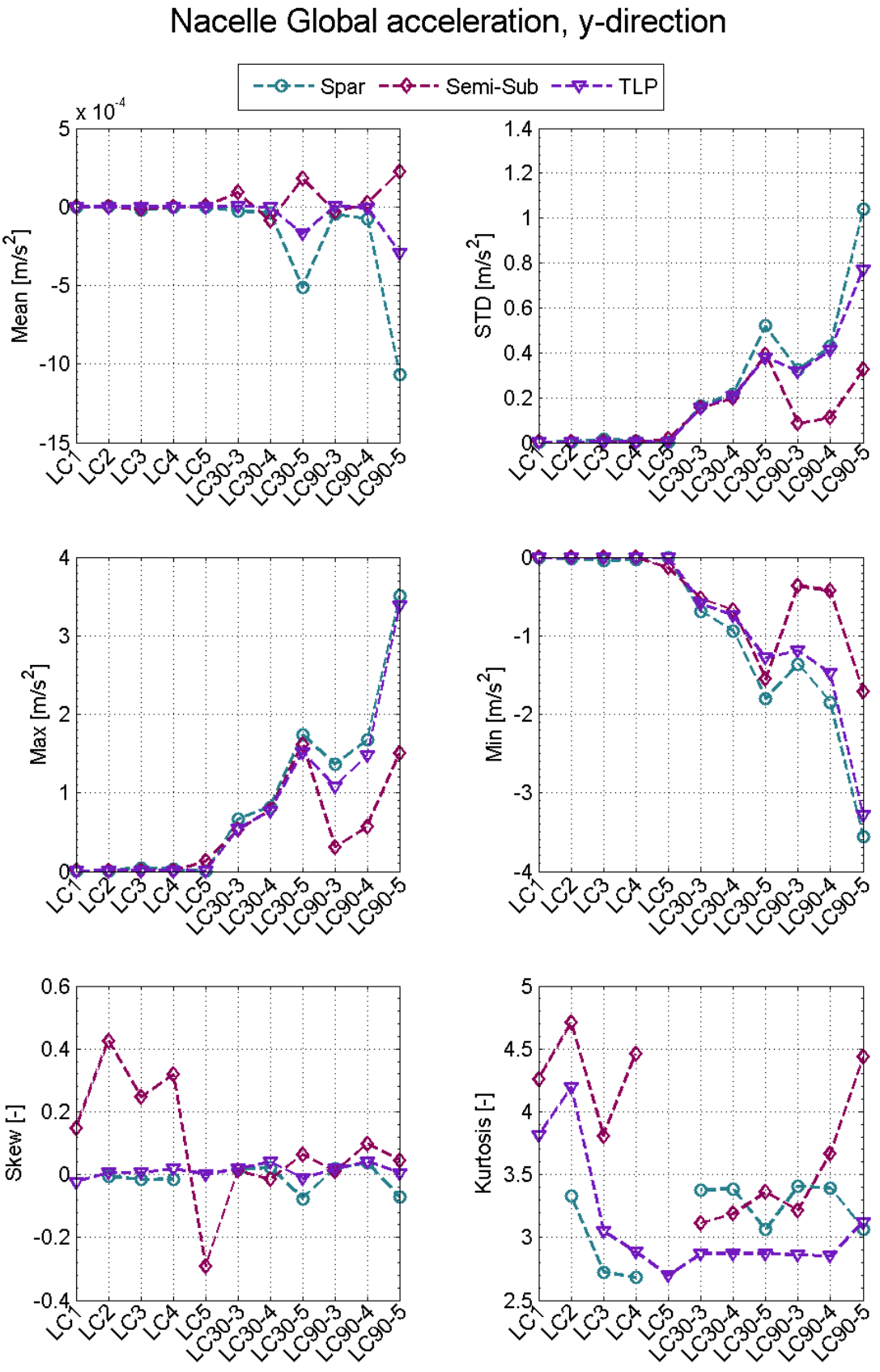

Thrust force:

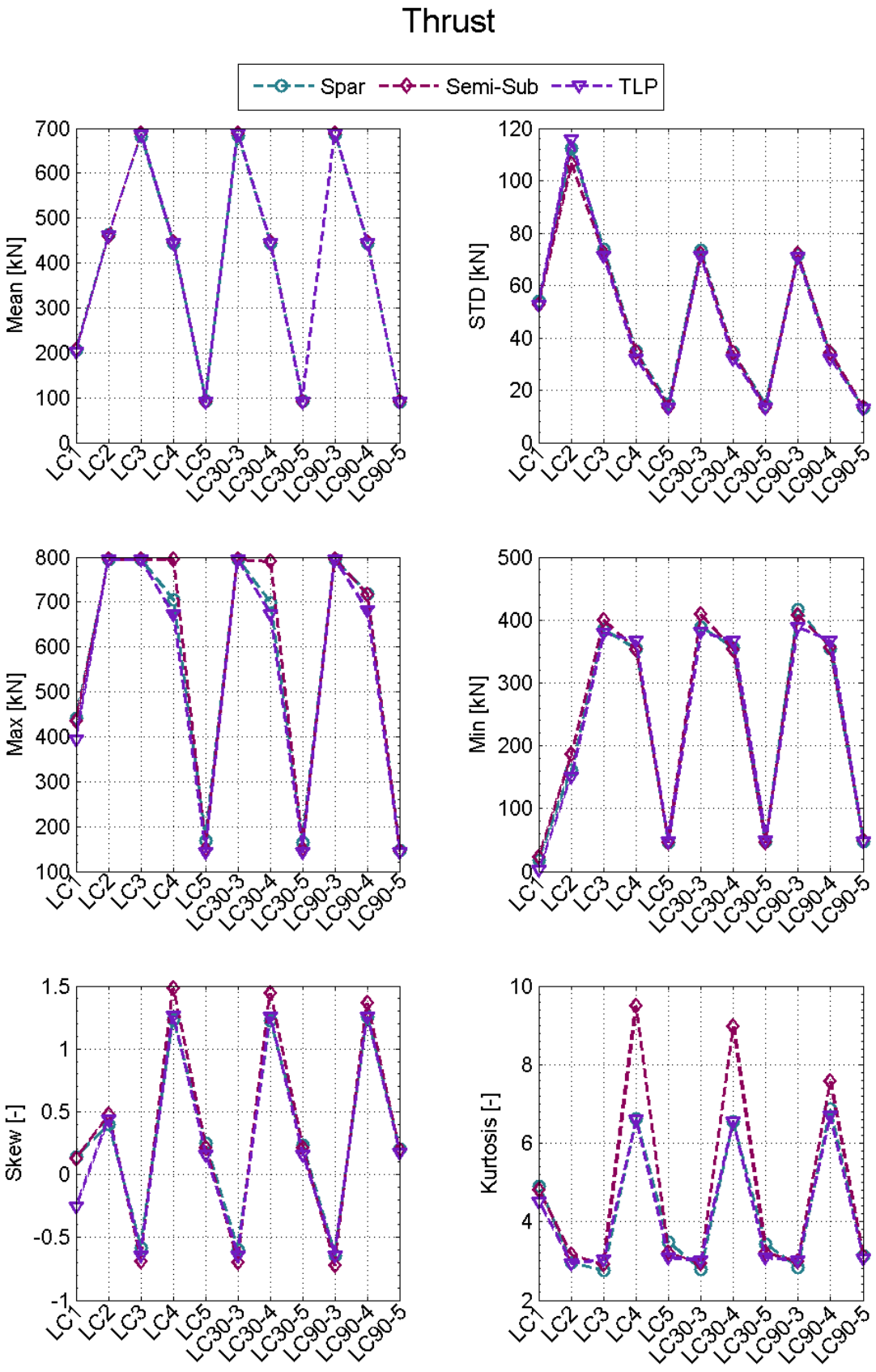

Power:

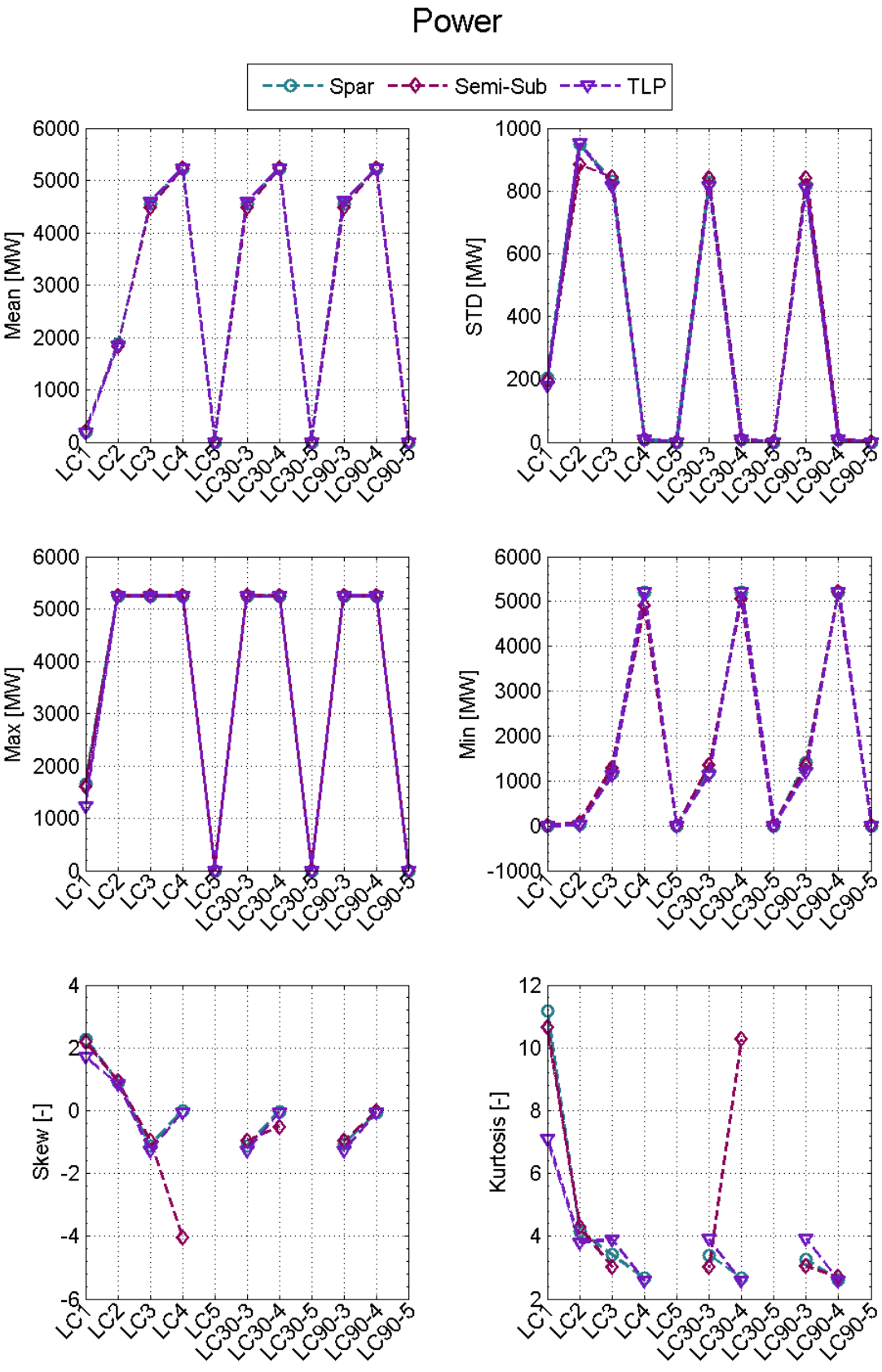
Power
Spar
Semi-Sub
TLP
Mean [MW]
STD [MW]
Max [MW]
Min [MW]
Skew [-]
Kurtosis [-]
LC1
LC2
LC3
LC4
LC5
LC30-3
LC30-4
LC30-5
LC90-3
LC90-4
LC90-5

Tension in mooring line #1:

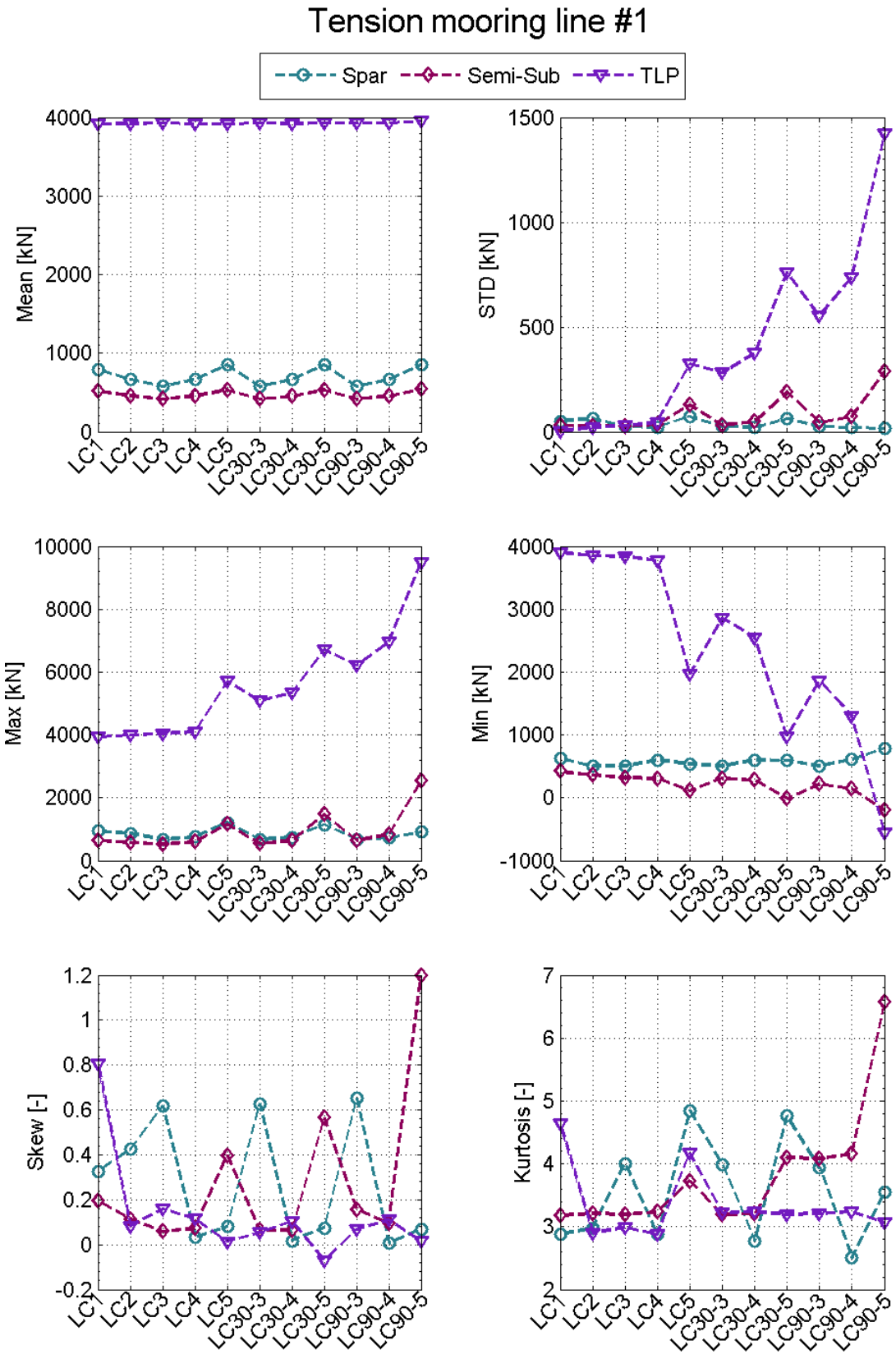

Tension in mooring line #2:

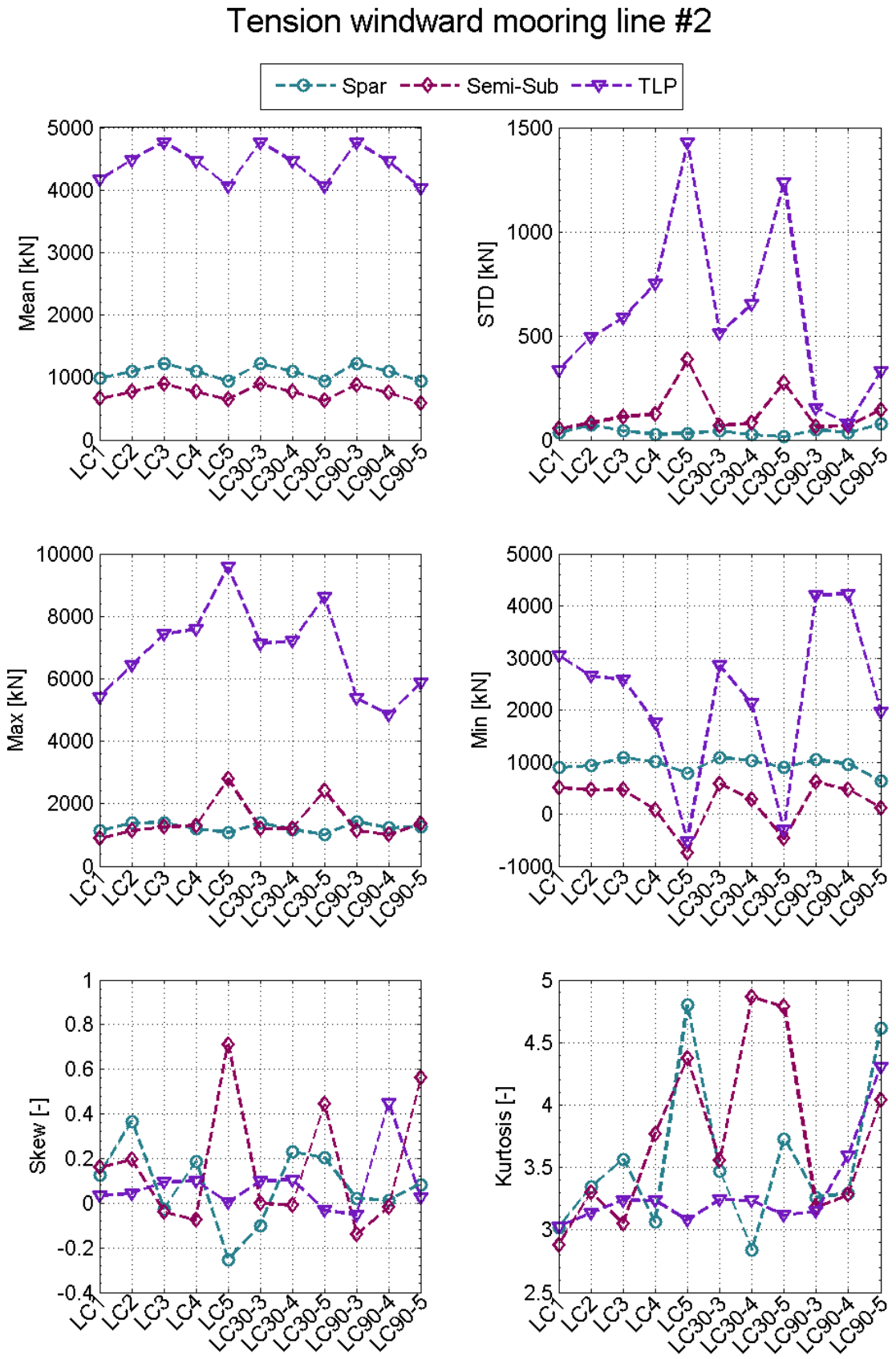

Wind speed:

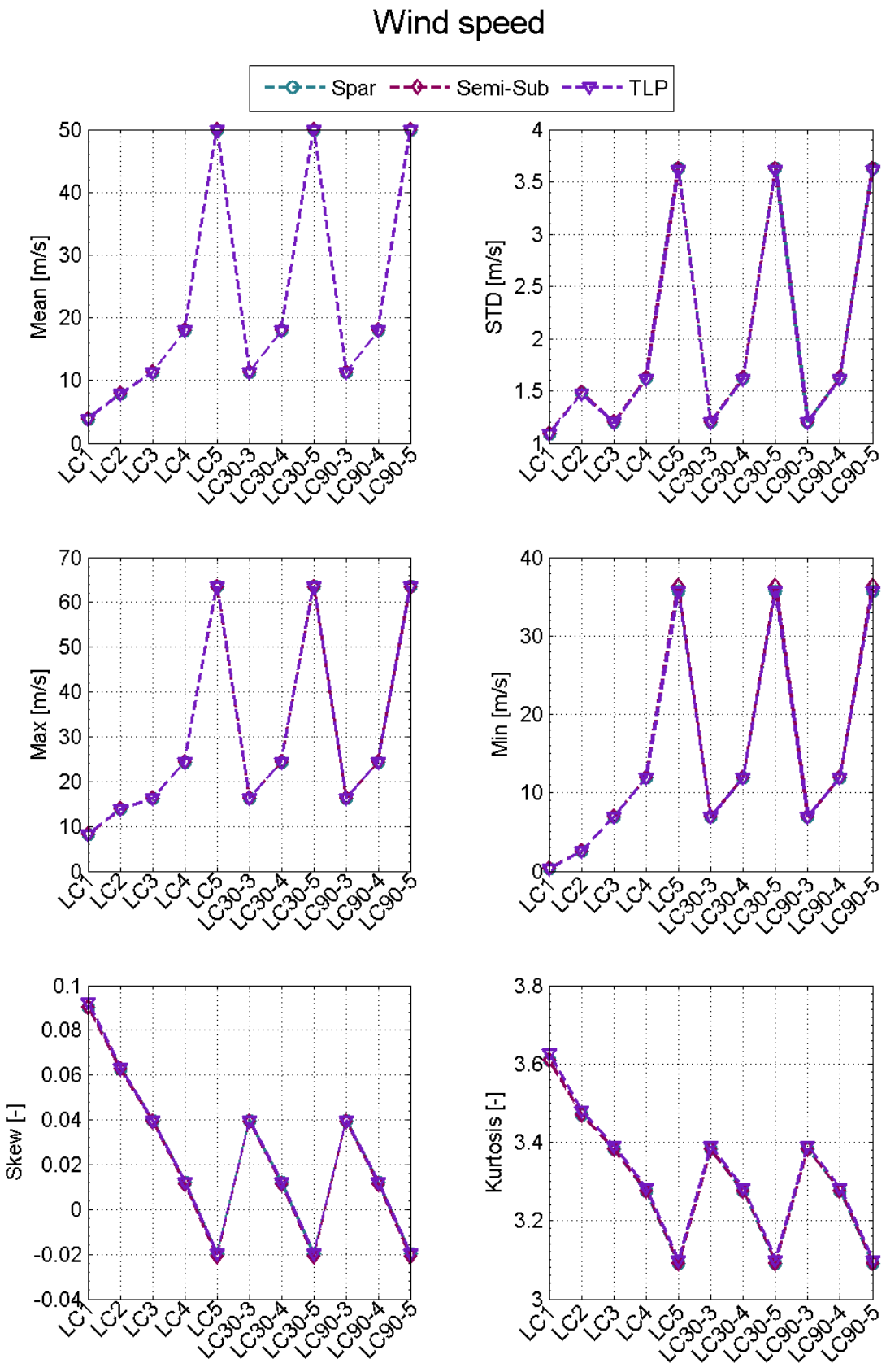
Wind speed
Spar
Semi-Sub
TLP
Mean [m/s]
STD [m/s]
Max [m/s]
Min [m/s]
Skew [-]
Kurtosis [-]
LC1
LC2
LC3
LC4
LC5
LC30-3
LC30-4
LC30-5
LC90-3
LC90-4
LC90-5

Relative wind speed:

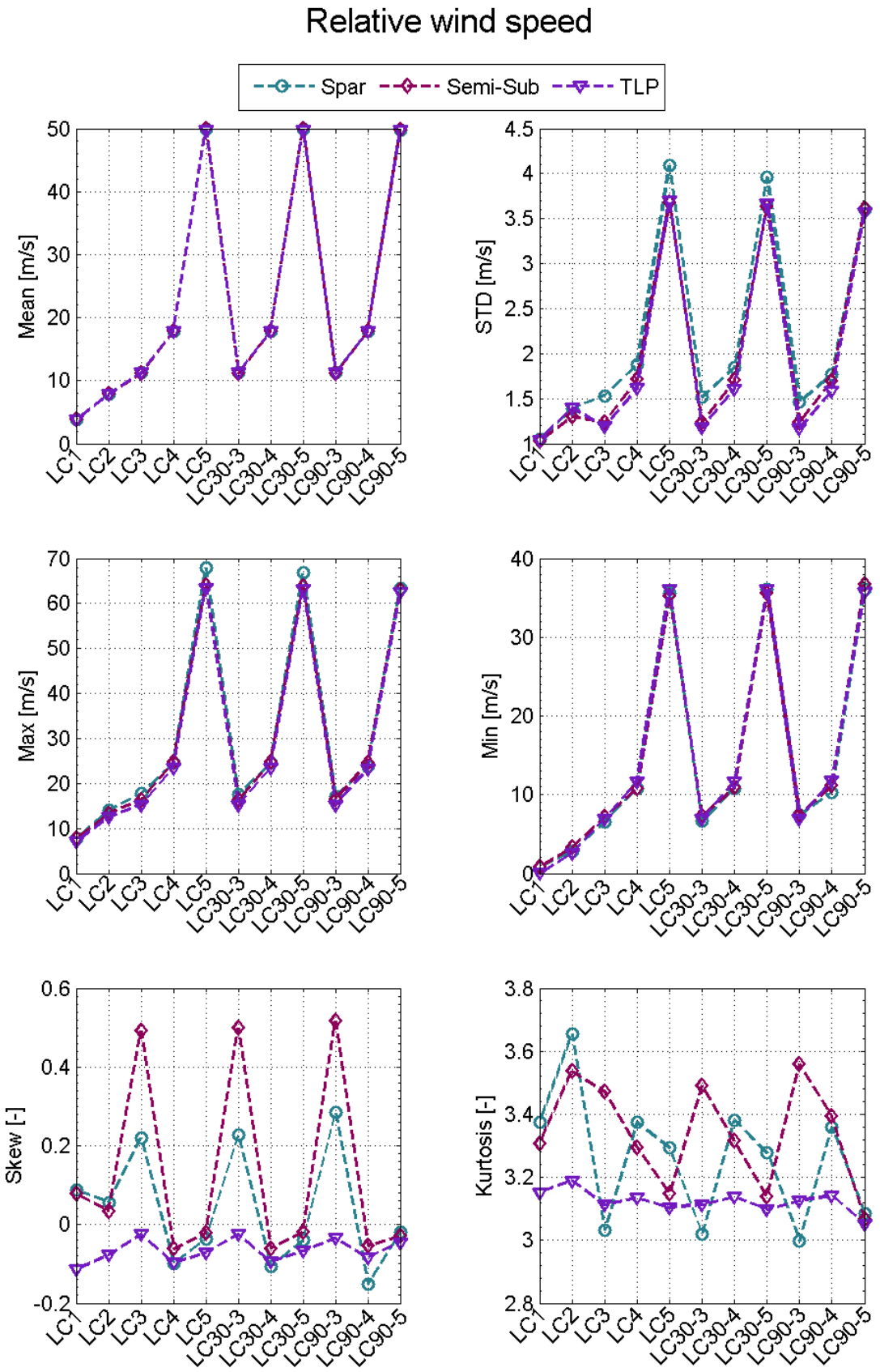

Notch filtered relative wind speed:

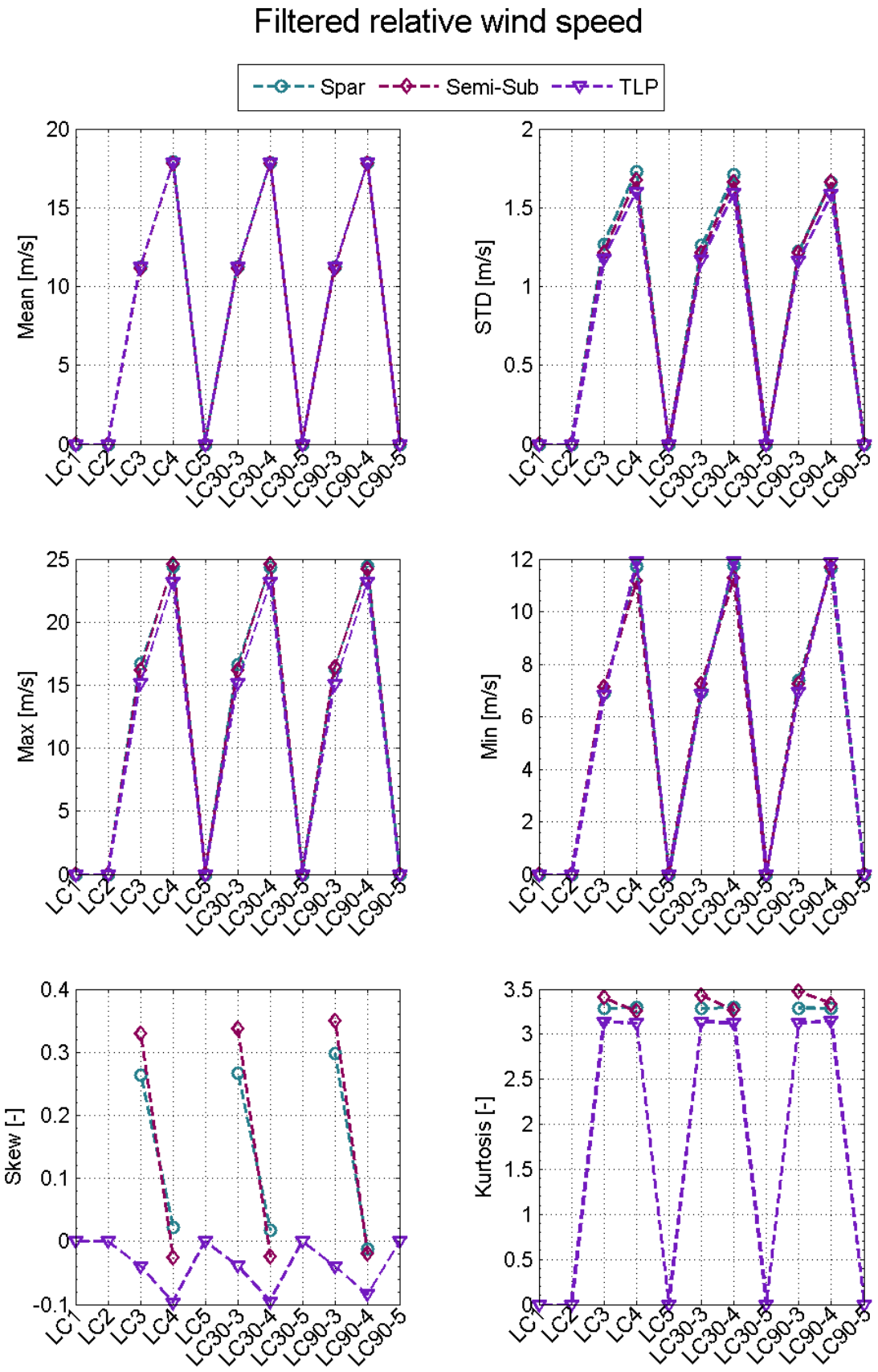

Appendix E: Cumulative averages of TLP statistics

E.1 LC0-3:

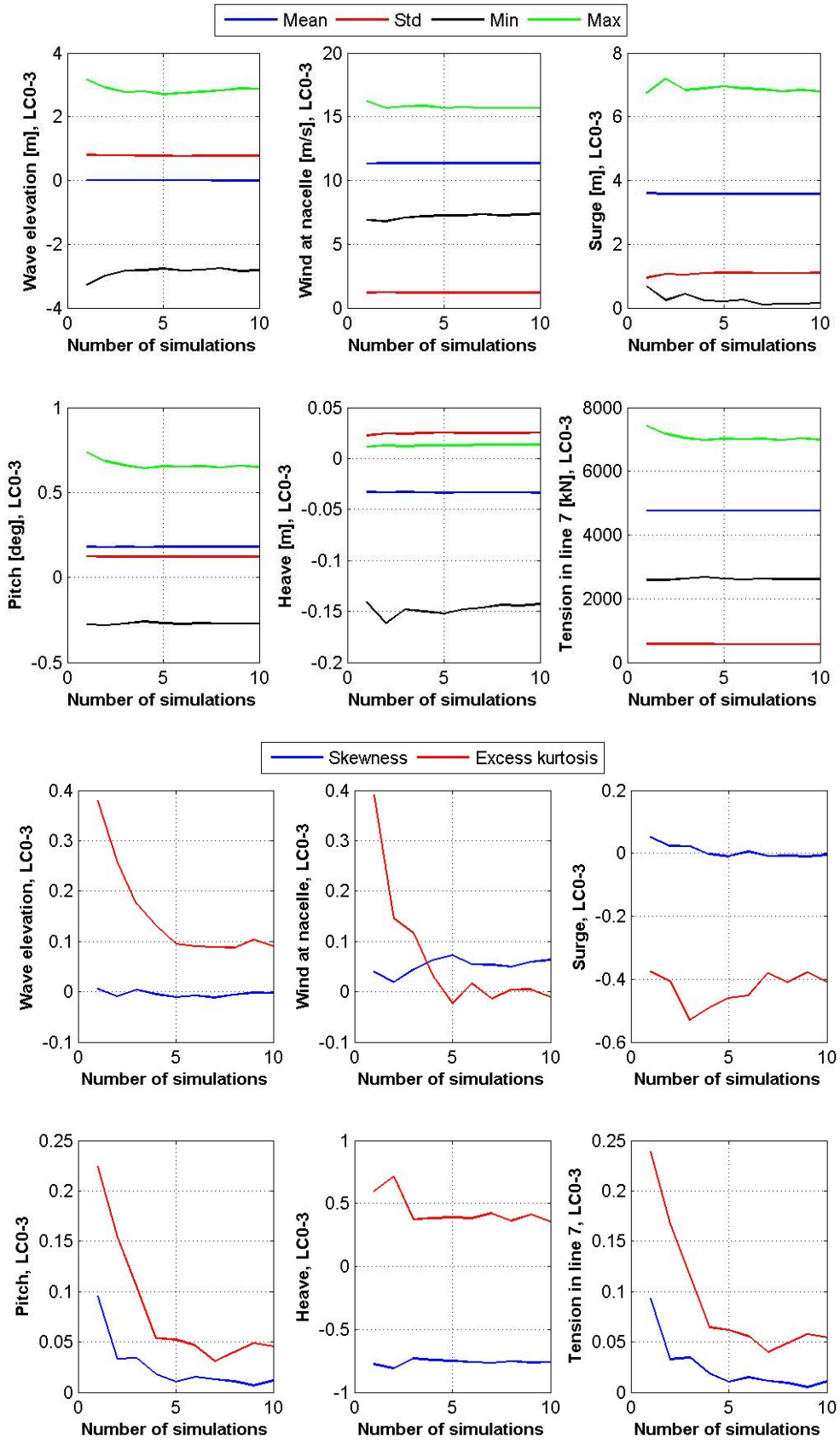

E.2 LC0-4:

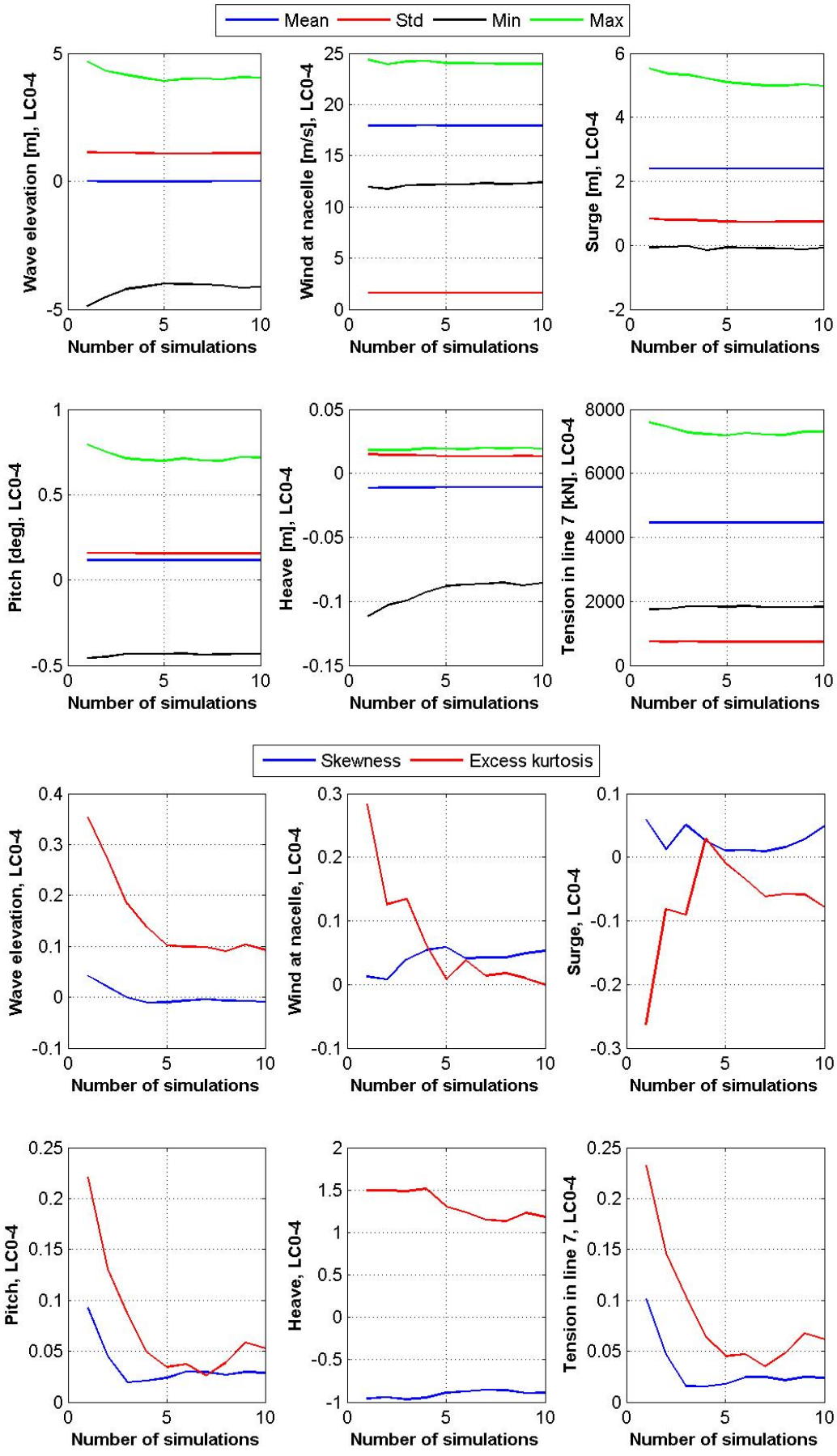
Mean
Std
Min
Max
Wave elevation [m], LC0-4
Wind at nacelle [m/s], LC0-4
Surge [m], LC0-4
Pitch [deg], LC0-4
Heave [m], LC0-4
Tension in line 7 [kN], LC0-4
Number of simulations
Skewness
Excess kurtosis
Wave elevation, LC0-4
Wind at nacelle, LC0-4
Surge, LC0-4
Pitch, LC0-4
Heave, LC0-4
Tension in line 7, LC0-4

Appendix F: Statistics of the TLP at 120 and 200 m water depths

Presented here are the mean values, standard deviations, minimum and maximum values of different response parameters at 120 m and 200 m water depths. LC0-1 to 5 are considered.

Surge in the waterline:

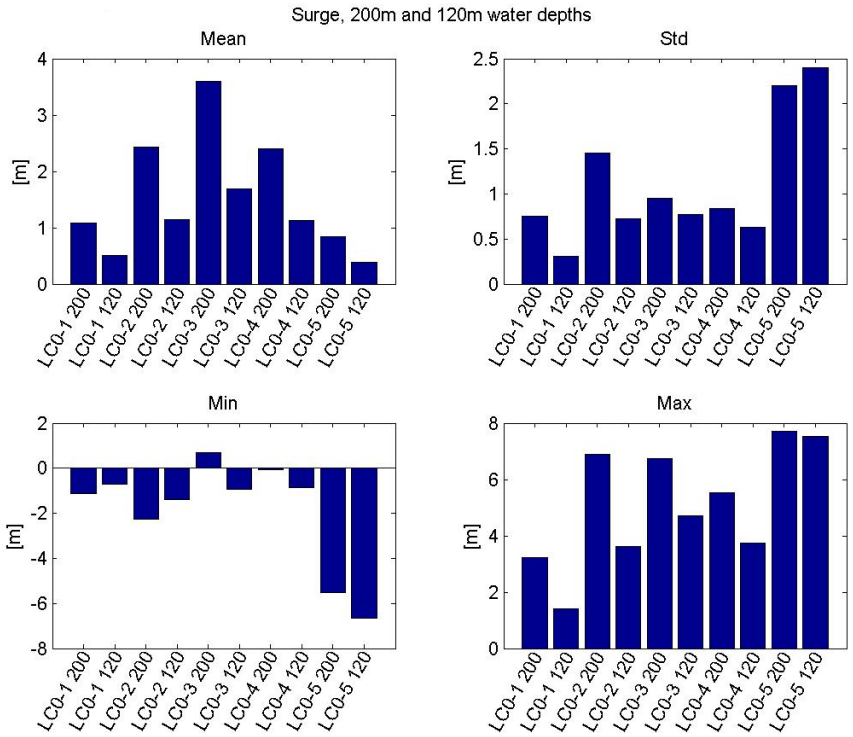

Heave in the waterline:

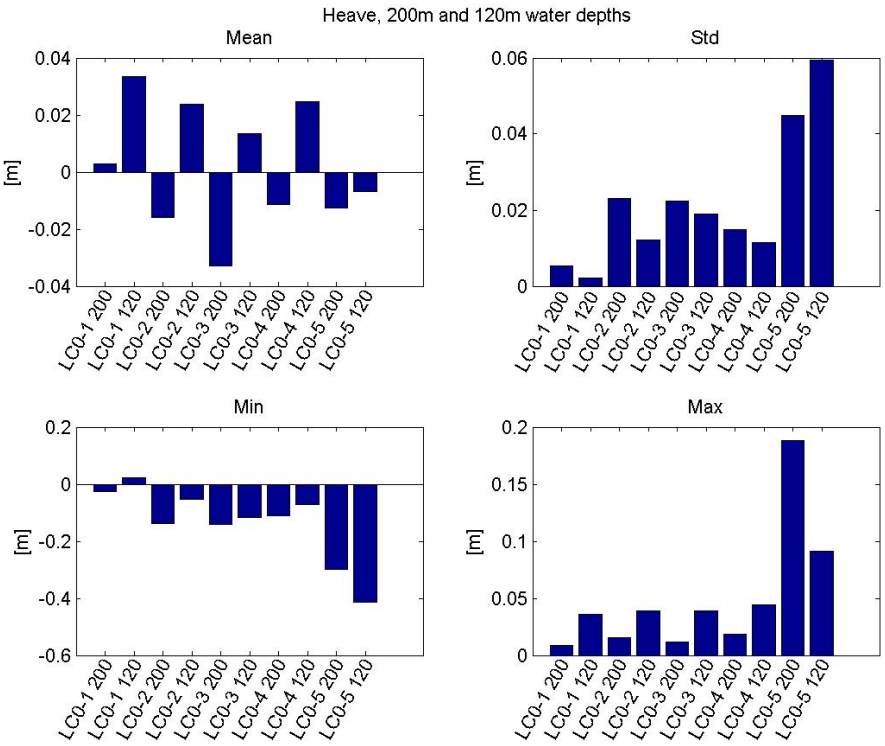

Pitch:

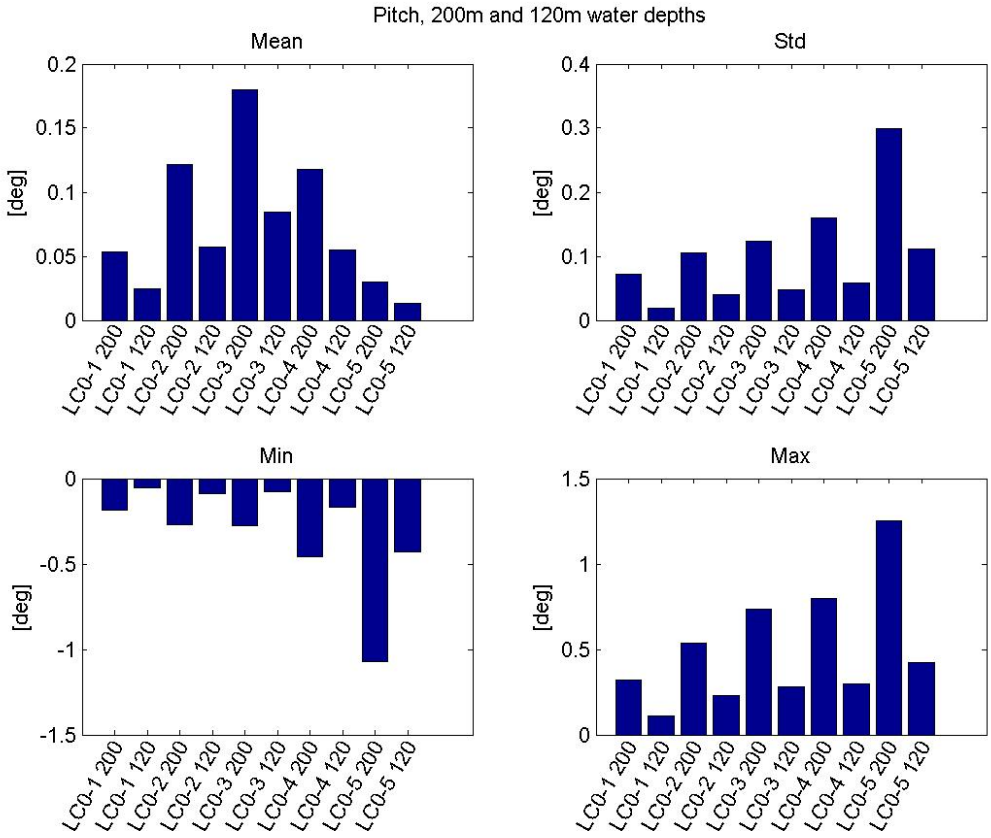

Nacelle acceleration in x-direction at nacelle:

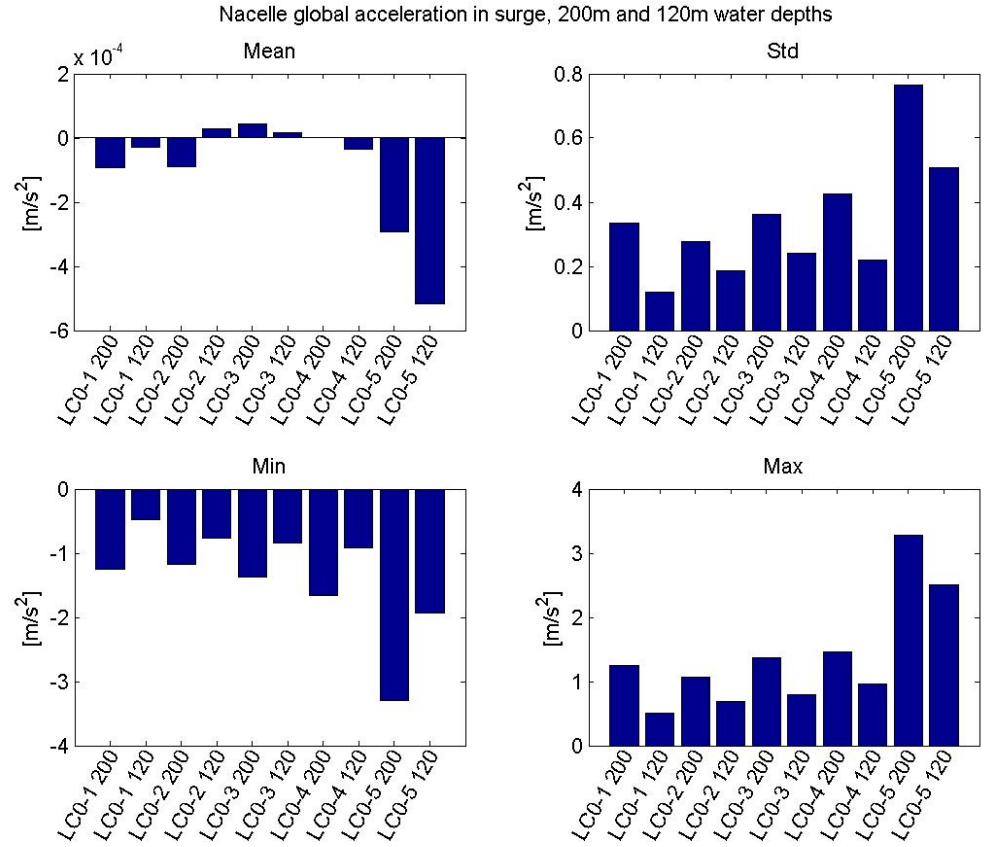

Tension in line number 3:

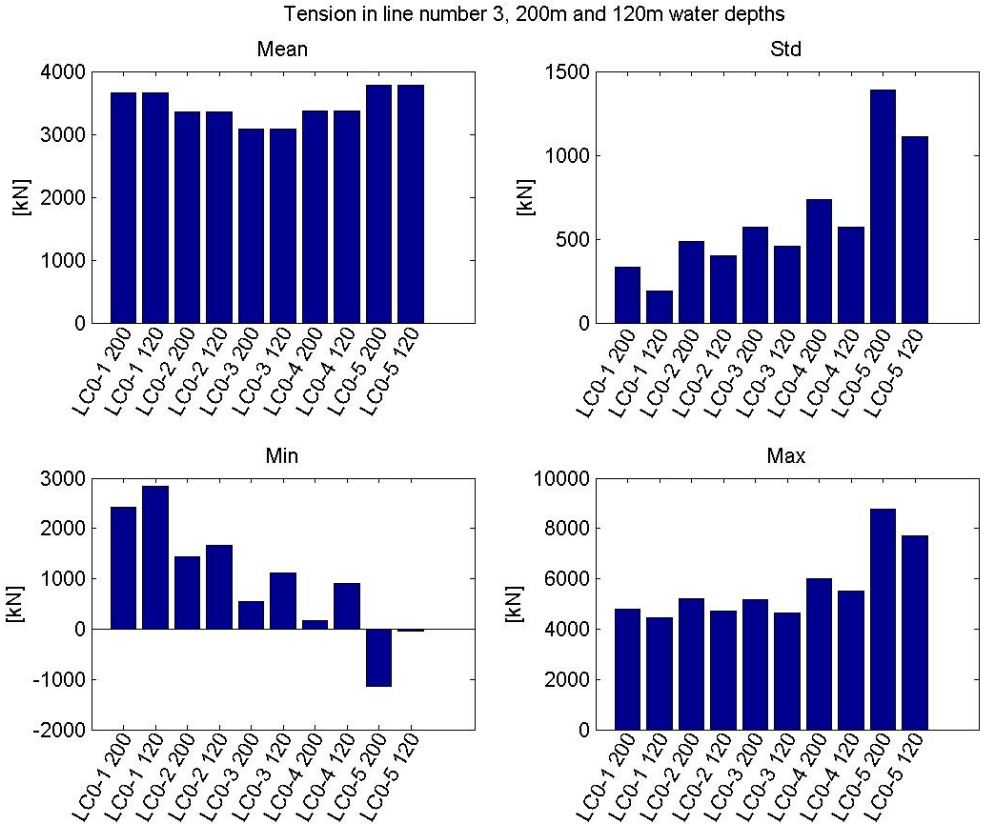

Tension in line number 7: